

Southern Methodist University

SMU Scholar

---

Chemistry Theses and Dissertations

Chemistry

---

Fall 12-16-2017

## Quantum Chemical Studies of Noncovalent Interactions and Multicenter Bonds Utilizing Local Vibrational Modes

Vytor Oliveira

*Southern Methodist University*, [voliveira@smu.edu](mailto:voliveira@smu.edu)

Follow this and additional works at: [https://scholar.smu.edu/hum\\_sci\\_chemistry\\_etds](https://scholar.smu.edu/hum_sci_chemistry_etds)

 Part of the [Physical Chemistry Commons](#)

---

### Recommended Citation

Oliveira, Vytor, "Quantum Chemical Studies of Noncovalent Interactions and Multicenter Bonds Utilizing Local Vibrational Modes" (2017). *Chemistry Theses and Dissertations*. 1.

[https://scholar.smu.edu/hum\\_sci\\_chemistry\\_etds/1](https://scholar.smu.edu/hum_sci_chemistry_etds/1)

This Dissertation is brought to you for free and open access by the Chemistry at SMU Scholar. It has been accepted for inclusion in Chemistry Theses and Dissertations by an authorized administrator of SMU Scholar. For more information, please visit <http://digitalrepository.smu.edu>.

QUANTUM CHEMICAL STUDIES OF  
NONCOVALENT INTERACTIONS AND MULTICENTER BONDS  
UTILIZING LOCAL VIBRATIONAL MODES

Approved by:

---

Dr. Elfriede Kraka  
Professor

---

Dr. Thomas R. Cundari  
Professor

---

Dr. Isaac Garcia-Bosch  
Assistant Professor

---

Dr. Peng Tao  
Assistant Professor

QUANTUM CHEMICAL STUDIES OF  
NONCOVALENT INTERACTIONS AND MULTICENTER BONDS  
UTILIZING LOCAL VIBRATIONAL MODES

A Dissertation Presented to the Graduate Faculty of the  
Dedman College

Southern Methodist University

in

Partial Fulfillment of the Requirements

for the degree of

Doctor of Philosophy

with a

Major in Theoretical and Computational Chemistry

by

Vytor Pinheiro Oliveira

B.S., Universidade de Brasília, Brasília, 2010

M.S., Universidade de Brasília, Brasília, 2013

December 16, 2017

Copyright (2017)

Vytor Pinheiro Oliveira

All Rights Reserved

## ACKNOWLEDGMENTS

I thank my mentors, Dr. Kraka and Dr. Cremer. It was a great honor and privilege to be able to learn from your classes, seminars, and workshops during these last four years. I am grateful for all the effort and patience you invested in my education, on the discussion of my projects, and on the corrections of my manuscripts. I thank Dr. Wenli Zhou for giving great advice and support on Cfour calculations, Molden2AIM script, and the local mode program; Dr. Marek Freindorf for teaching me how to use ORCA, Molpro, and Datagraph; Dr. Dani Setiawan for introducing me to the analysis of noncovalent interactions and for being a great friend; Dr. Thomas Sexton for patiently answering many questions related and unrelated to chemistry; Dr. Terutaka Yoshizawa for helping me with NESC relativistic calculations and for being my practice partner in table tennis; Alan for the many fruitful discussions we had and the many rides he gave me; Yunwen, for helping me with the standalone local modes program, and also for inspiring me with his creativity and hard. Sally, Niraj and Seth for the great time we shared together in room 321B. I also thank all the support I received from my family and from my girlfriend Bruna – especially Bruna, for giving me the strength I needed to pursue this PhD. I thank Dr. Rob Kalescky for all the technical support he gave me on the supercomputers Mane Frame 1 and 2. Last but not least, I thank Brazil’s Science without Borders program for providing me financial support (BEX 9534-13-0), and SMU for all the computational resources made available to me.

Pinheiro Oliveira, Vytor

B.S., Universidade de Brasília, Brasília, 2010

M.S., Universidade de Brasília, Brasília, 2013

Quantum Chemical Studies of  
Noncovalent Interactions and Multicenter Bonds  
Utilizing Local Vibrational Modes

Advisor: Dr. Elfriede Kraka

Doctor of Philosophy degree conferred December 16, 2017

Dissertation completed November 27, 2017

The specificity and directionality of certain noncovalent interactions can be explored for the design of novel drugs, better catalysts, synthesis of complex supramolecular structures, and so on. For this purpose, a well-founded knowledge of how to control the strength of these interactions is desirable. Despite the many investigations on noncovalent interactions done so far, a quantitative assessment of the intrinsic strength of most of these interactions is still missing. Recently and for the first time, the Konkoli-Cremer local modes analysis was successfully used to probe the intrinsic strength of hydrogen and pnictogen bonds. In order to extend these investigations to other types of noncovalent interactions and to obtain a complete picture of how their strength could be tuned, more than 300 complexes have been studied in this work. High accuracy CCSD(T) calculations were performed to investigate the strength and nature of 36 neutral and anionic halogen bonded complexes and to compare them with 8 hydrogen, pnictogen, and chalcogen bonded complexes. Halogen bonding is found to arise from electrostatic and covalent contributions, which can be further strengthened if lone pair delocalization effects are possible. Phosphines turn out to lead to relatively strong halogen bonds, provided electronegative substituents increase covalent contributions in the form of 3c-4e bonding. Halogen bonds are found to be highly tunable, with binding energies varying from 1 to 45 kcal/mol. They are stronger than comparable interactions involving pnictogens and chalcogens. In a subsequent study, 202 halogen bonded

complexes were investigated. Ten different electronic effects were found to contribute to the halogen bond and are responsible for the large variation in their strength. Based on these effects, a strategy for the design of new materials was provided. The possibility of forming halogen bonds with metal centers (Cu, Ag, Au, Pt and Hg) was also investigated using all-electron Dirac-exact relativistic calculation to reliably account for scalar relativistic effects in Au, Pt and Hg. A continuous transition from halogen bond to 3c-4e bond and finally to a complete covalent metal-halide bond was found to exist for these systems. Dimethylaurate forms stronger halogen bonds than its lighter congeners due to the strong relativistic expansion of the d-orbitals in gold. In another investigation, chalcogen bonds which are closely related to halogen bonds but less explored, were thoroughly investigated by considering 100 different chalcogen bonded systems, including neutral, cationic, and anionic complexes, and  $sp^2$  and  $sp^3$  hybridized chalcogens. A new type of chalcogen bond involving homodimers of  $sp^2$  hybridized chalcogens was discovered. Covalency in chalcogen bonds was found to involve different charge transfer mechanisms, depending on the hybridization of the chalcogen involved. Chalcogen bonds tend to be less covalent and to have a smaller 3c-4e character compared to halogen bonds. The striking similarities between halogen and chalcogen bonding mechanism led us to investigate the existence of a general bonding mechanism to describe noncovalent interactions involving pnictogens, chalcogens, and halogens. Highly accurate CCSD(T) calculations was done for 32 different complexes and from the analysis of these complexes, a conformationally driven bonding mechanism is suggested. It was shown that some complexes cannot be strictly defined as a chalcogen or pnictogen bonded but are the result of an admixture of both interactions. In addition to the study of noncovalent interactions, the stability of planar gold clusters was investigated and an aromaticity index based on local stretching force constants was derived to measure the  $\sigma$ -aromaticity of these clusters. The stability of the planar gold clusters was explained on the basis of the 3c-2e character of  $Au_3$  subunits. The results discussed in this dissertation provide an wide view on how noncovalent interactions and multicenter bonds can be tuned, serving as a starting point for the design of novel materials.

## TABLE OF CONTENTS

LIST OF FIGURES .....	viii
LIST OF TABLES .....	x
CHAPTER	
1. INTRODUCTION .....	1
2. COMPUTATIONAL TOOLS .....	4
2.1. Quantifying the strength of an interaction .....	4
2.2. Determining the nature of a noncovalent interaction: .....	6
2.3. A general protocol for the analysis of noncovalent interactions .....	9
3. THE INTRINSIC STRENGTH OF HALOGEN BONDS .....	11
3.1. Halogen bond definition .....	11
3.2. Importance of using an accurate computational method .....	12
3.3. Summary of results.....	14
4. A BROAD VIEW OF HALOGEN BONDING .....	18
4.1. Introduction .....	18
4.2. A dual computational level approach .....	18
4.3. Summary of results.....	19
4.4. Strategies for material design .....	21
5. FROM METAL-LIGAND TO HALOGEN BONDING .....	22
5.1. Halogen bonding involving a metal center .....	22
5.2. Scalar relativistic effects .....	23
5.3. Summary of results.....	24
6. CHALCOGEN BONDING .....	26
6.1. Introduction .....	26

6.2. Chalcogen bonding mechanism .....	26
6.3. Electrostatic versus covalent contributions .....	27
6.4. Summary of results.....	28
6.5. Strategies for the design of new materials .....	30
7. NONCOVALENT INTERACTIONS INVOLVING HALOGENS, CHALCOGENS AND PNICOGENS .....	31
7.1. Introduction .....	31
7.2. Summary of results.....	31
8. $\sigma$ -AROMATICITY IN SMALL GOLD CLUSTERS .....	35
8.1. Introduction .....	35
8.2. Assessment of $\sigma$ -aromaticity .....	35
8.3. Summary of results.....	38
9. CONCLUSION, OUTLOOK AND CONTRIBUTION ACCOUNT.....	39
REFERENCES .....	44
10. PUBLICATIONS.....	60
Paper I. The intrinsic strength of the halogen bond: Electrostatic and covalent contributions described by coupled cluster theory .....	61
Paper II. Quantitative assessment of halogen bonding utilizing vibrational spectroscopy .....	78
Paper III. Transition from metal-ligand bonding to halogen bonding involving a metal as halogen acceptor a study of Cu, Ag, Au, Pt, and Hg complexes .....	94
Paper IV. The many facets of chalcogen bonding: Described by vibrational spectroscopy .....	103
Paper V. A systematic coupled cluster study of noncovalent interactions involving halogens, chalcogens and pnicoGENS .....	122
Paper VI. The peculiar role of the Au <sub>3</sub> unit in Au <sub>m</sub> clusters: $\sigma$ -aromaticity of the Au <sub>5</sub> Zn <sup>+</sup> ion .....	136

## LIST OF FIGURES

Figure	Page
2.1	Flow chart of how local modes are obtained from normal vibrational modes. . . . . 5
3.1	Schematic representation of a XB. . . . . 11
3.2	Recognition of T3 by human thyroid hormone receptor [65]. XBs are shown by dotted lines. . . . . 12
3.3	Color coded electrostatic potential mapped on the 0.001 e/Bohr <sup>3</sup> electron density surface of FCl and NH <sub>3</sub> . The electrostatic potential varies from positive (blue) to negative (red) . . . . . 15
3.4	A) Orbital interaction diagram of the FCl⋯NH <sub>3</sub> B) Electron difference density distribution for FCl⋯NH <sub>3</sub> complex. Electron density increase in blue, decrease in red. . . . . 15
3.5	Comparison of the 3c-4e bond % character of FCl⋯NR <sub>m</sub> (in red) and FCl⋯PR <sub>m</sub> (in green). . . . . 17
5.1	Electron difference density distributions between NESC-TPSS-D3 scalar relativistic density and the non-relativistic density plotted for an electron density of 0.0015 e/Bohr <sup>3</sup> . Blue regions indicate an increase in the electron density, red regions a decrease relative to the non-relativistic density. . . . . 23
6.1	Frontier molecular orbitals of FNTe. . . . . 27
6.2	Electrostatic potential of F <sub>2</sub> CSe plotted on the 0.001 e/Bohr <sup>3</sup> electron density surface (a) Lowest unoccupied molecular orbital (LUMO) of F <sub>2</sub> CSe (b) F <sub>2</sub> CSe⋯NH <sub>3</sub> (c) F <sub>2</sub> CSe⋯Cl <sup>-</sup> (d). . . . . 28
7.1	The two common conformations found for halogen⋯halogen, chalcogen⋯chalcogen, and pnictogen⋯pnictogen interactions. . . . . 32
7.2	Charge transfer and electrostatic attraction in type I and II conformations of (FCl <sub>2</sub> ) <sub>2</sub> . . . . . 33
7.3	Electrostatic potential of F <sub>2</sub> CSe plotted on the 0.001 e/Bohr <sup>3</sup> electron density surface (a) Lowest unoccupied molecular orbital (LUMO) of F <sub>2</sub> CSe (b) F <sub>2</sub> CSe⋯NH <sub>3</sub> (c) F <sub>2</sub> CSe⋯Cl <sup>-</sup> (d). . . . . 34

8.1	Comparison of the geometry of the Jahn Teller unstable $\text{Au}_3$ ( $D_{3h}$ symmetry), stable $\text{Au}_3$ ( $C_s$ symmetry), and $\text{Au}_3^{2+}$ ( $D_{3h}$ symmetry). Distances in Å and number of valence electrons in parenthesis. ....	36
8.2	Comparison of the geometry of $\text{Au}_6$ ( $D_{3h}$ symmetry) and $\text{Au}_5\text{Zn}^+$ ( $C_{2v}$ symmetry). Bond distances are given in Å . ....	38

## LIST OF TABLES

Table		Page
3.1	Percent deviation in the XB distances.....	13
3.2	Percent deviation in the $k^a(XA)$ values.....	13
3.3	Comparison of XB, hydrogen, chalcogen, and pnictogen bonds. <sup>a</sup> .....	17

This dissertation is dedicated to my beloved family.

## Chapter 1

### INTRODUCTION

Different from covalent bonds, which are responsible for holding atoms together within a molecule, noncovalent interactions are generally weaker and easily reversible, being largely responsible for the properties of condensed phases [1] and for the stabilization of the tertiary structures of DNA, RNA, and proteins. Noncovalent interactions incorporate a wide variety of different types of interactions, ranging from weak nonspecific dispersive to strong and highly directional interactions. By far the most studied directional noncovalent interaction is the hydrogen bond (HB), which has already been successfully exploited by synthetic chemists for diverse applications. In catalysis, HBs can lower the activation barrier by stabilizing the transition state, and can induce stereo and enantioselectivity [2]. In supramolecular chemistry and crystal engineering, building blocks are created in a way that HBs can direct self-assembly of complex supramolecular architectures [3]. In pharmaceutical design, they are used to guide ligand-receptor recognition [4]. In the last few decades, the investigation of other possible directional noncovalent interactions led to the discovery that halogen, chalcogen and pnictogen atoms could replace the hydrogen in a HB, forming a halogen bond (XB), chalcogen bond (ChB), and pnictogen bond (PnB). These interactions are strong enough to compete with HBs [5,6] and can also direct self-assembly of supramolecular structure [7,8], participate in the stabilization of tertiary structure of proteins [9], and aid in ligand-receptor recognition of several biomolecules [10]. The realization of the importance of these less explored noncovalent interactions led to intensive research efforts to learn how to control them by elucidating their nature and quantifying their strength [6,11].

Standard procedures to analyze the strength of noncovalent interactions are mostly based on structural parameters (e.g. interatomic distances) or binding energies. These parameters are useful to discuss specific electronic effects. However, shorter interactions are not necessary

stronger [6, 12] and binding energies account for all interactions between the monomers, making it difficult to single out the energy associated with a specific noncovalent interaction. Cremer and co-workers showed that vibrational spectroscopy provides a reliable parameter to measure the intrinsic strength of a chemical bond [13, 14]. They also demonstrated that it is always possible to derive, from calculated or experimental frequencies, the local stretching force constant ( $k^a$ ) of a chemical bond [15, 16], which as proven by Zhou and Cremer [14] is directly related to the intrinsic strength of the chemical bond. Over the last ten years the local vibrational modes developed by Cremer, Konkoli and Zou [15, 16] have proven to be a powerful and dynamic tool, being successfully applied for diverse studies. Including the investigation of the strength of long C-C bonds [17], carbon-halogen bonds, carbon-chalcogen bonds [18, 19], and used to identify the strongest bond in chemistry [20]. The local modes were also applied for the investigation of noncovalent interactions, for example, to measure the strength of HBs and PnBs based on either experimental or calculated vibrational frequencies [21–27], and also to explain why warm water freezes faster than cold water [28]. Another invaluable application of local modes is to derive more reliable electronic parameters to quantify important molecular properties, for example to obtain a more general and more reliable metal-ligand parameter than the Tolman electronic parameter [29, 30], and to quantify aromaticity in organic molecules [31, 32].

In this thesis we discuss recent results that further expand the applicability of the local modes. By combining the analysis of the intrinsic strength of a bond based on  $k^a$  values of a systematic series of XBs, ChBs and PnBs with analysis of electronic effects based on binding energies, geometric parameters, charge transfer, dipole moments, electrostatic potentials, energy and electron density distribution, a clear picture of the interplay between electronic effects and bond strength is obtained. These are used to answer the following questions:

- i. Can we derive a general protocol to systematize the analysis of the strength and nature of noncovalent interactions?
- ii. How strong are the XB compared to other noncovalent interactions?

- iii. Can one determine the covalent and/or electrostatic character of halogen and chalcogen bonds? When do electrostatics and when do covalent contributions prevail?
- iv. How strong are XBs formed with metal center? Can relativistic effects influence the strength of these interactions?
- v. Does the hybridization of the chalcogen affect the ChB mechanism?
- vi. Is there a general bonding mechanism to describe XB, ChB, and, PnB?
- vii. How does the intrinsic strength of the noncovalent interactions relate to other properties such as binding energies, interatomic distances, energy and electron density, and electrostatic potential?

We also combined the analysis of local modes and other properties to investigate what role  $\sigma$ -aromaticity plays in the stability of small planar gold cluster. These questions are addressed in the next chapters as follows. In chapter 2, we briefly discuss the computational tools used and propose a protocol to investigate noncovalent interactions. In chapter 3, the bonding mechanism, nature, and strength of XBs are discussed. A new electronic parameter to measure 3c-4e electron character of XBs is derived and the strength of XBs is compared to PnBs, ChBs and HBs (Paper I) [5]. In chapter 4, a series of electronic effects related to the strength of more than two hundred XBs is discussed and useful strategies for the design of new XB materials are suggested (Paper II) [33]. In chapter 5, we utilize the Normalized Elimination of the Small Component (NESC) [34], an all-electrons Diract-exact scalar relativistic method to investigate scalar relativistic effects in halogen-metal bonds (Paper III) [35]. In chapter 6, we investigate one hundred ChBs. A new type of ChB is described and material design strategies are suggested (Paper IV) [36]. In Chapter 7, we derive a general description of XB, ChB and PnB based on the conformation adopted by the complexes (paper V). In chapter 8, we discuss the stability of small planar gold clusters based on the  $\sigma$ -aromaticity of three membered Au ring subunits (Paper VI) [37]. In chapter 9 we present a summary of the answers to questions i-viii, and future perspectives. In chapter 10 all peer-review publications (paper I-VI) are provided.

## Chapter 2

### COMPUTATIONAL TOOLS

A brief summary of the properties used to access the strength and nature of noncovalent interactions is given. Rather than providing a detailed mathematical derivation of each property used, we clarify their meaning, as well as advantages and limitations. At the end of this chapter a general protocol for the investigation of noncovalent interactions developed during this thesis work is discussed.

#### 2.1. Quantifying the strength of an interaction

**Binding energies:** The energy required to completely dissociate a complex into its constituting monomers is called binding energy ( $\Delta E$ ). If a complex is dissociated but the monomer geometries are kept frozen, we speak of interaction energies ( $E_{int}$ ). These quantities are useful to discuss the overall gain in stability with the complex formation, but they give limited information about the strength of a specific bond.  $\Delta E$  and  $E_{int}$  are cumulative properties; they include, besides the strength of the interaction, the energy required for the electron density reorganization of the fragments upon dissociation. They also account for all possible interactions between the monomers, which means that it is not possible to single out the fraction of these quantities related to a specific atom-atom interaction. Experimentally, one measures binding enthalpy  $\Delta H$ , which is obtained theoretically by including the zero-point energy and temperature-dependent enthalpy terms derived from the partition functions.

**Local vibrational modes:** Vibrational spectroscopy provides an alternative to the dissociative process of  $\Delta E$ . The stretching vibration of a bond, given by an infinitesimally small displacement of the atoms involved, can be used to probe the strength of a bond while preserving the electronic structure. However, normal vibrational modes are not suited for this purpose. Due to mode-mode coupling, the normal vibrational modes delocalize through-

out the whole molecular framework. Konkoli and Cremer [15] obtained local vibrational modes (free from mode-mode coupling) by solving a local equivalent of Wilson vibration equation [15,38]. A description of how mode-mode coupling is solved and a comparison of the normal stretching modes and local stretching modes of  $F_3^-$  is provided on Figure 2.1. Recently, Zou and Cremer proved that these local modes are the only local equivalent of the normal modes [16]. The local stretching force constant ( $k^a$ ) measures the curvature of the potential energy surface relative to an infinitesimally small increase of the bond length [39]. A large  $k^a$  value indicates a strong curvature, thus a strong bond [14].

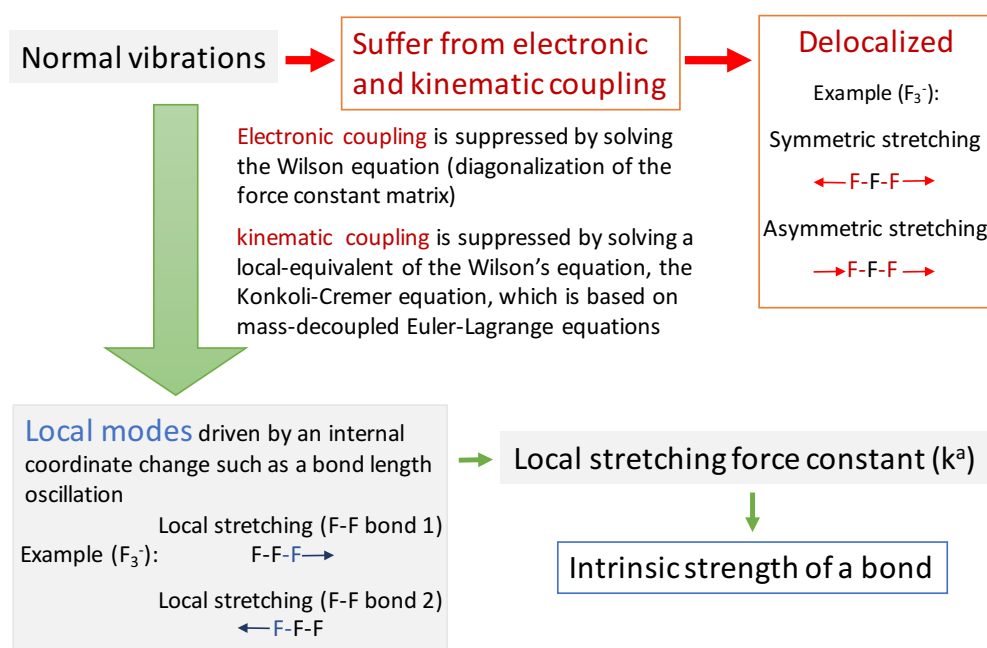


Figure 2.1. Flow chart of how local modes are obtained from normal vibrational modes.

Local vibrational frequencies are measurable quantities. McKean could isolate a single C-H stretching vibration in organic molecules by replacing all hydrogen but one with deuterium [40]. In this case, mode-mode coupling is suppressed due to the large mass difference of H compared to D, resulting in a localized C-H stretching vibration [41]. Local mode information can also be obtained from the fifth or higher-order overtone of CH stretching modes [42]. Kraka, Larsson, and Cremer [43] showed that in organic complexes, there is

a linear correlation ( $R^2 = 0.99$ ) between experimentally determined overtone frequencies of CH bond and the corresponding calculated local harmonic frequencies; thus confirming the local nature of high order overtones of CH bonds.

Local mode frequencies can be obtained either by a set of experimental or calculated normal mode frequencies [44]. Experimentally derived local modes have the advantage of accounting for anharmonicity, whereas calculated frequencies are usually obtained using the harmonic approximation due to the high computational cost associated with the inclusion of anharmonic corrections. In all studies described here, we exclusively used calculated harmonic frequencies and their associated force constants. It is important to mention that in contrast to local stretching frequencies, the  $k^a$  values do not depend on the masses of the vibrating atoms; therefore, they are better suited descriptors of the intrinsic strength of a bond.

**Bond strength order:** The analysis of the intrinsic strength of a bond can be facilitated by converting  $k^a$  into bond strength order (BSO). This is done by using a power relationship based on the generalized Badger rule [43] derived by Kraka, Larsson and Cremer (Eq. 2.1):

$$BSO\ n = a(k^a)^b \tag{2.1}$$

Constants  $a$  and  $b$  are determined from the  $k^a$  reference values of well-known bond order (Wiberg or Mayer bond order can also be used in this context), and by assuming that for a  $k^a$  equal zero, the BSO  $n$  is also zero. The most suitable references are obtained from bonds formed by atoms of the same period as the bonds of interest. However, to compare various bonds involving different combinations of atoms across the periodic table, a single power equation must be used.

## 2.2. Determining the nature of a noncovalent interaction:

There are four major approaches to investigate the nature of noncovalent interactions. The first approach is based on a completely electrostatic point of view. According to the Hellman-Feynman theorem, [45] once the electron density (obtained quantum-mechanically)

is known, all forces exerted on the nuclei by the electrons in a complex can be considered to be classical Coulombic forces. The electrostatic model of noncovalent interactions put forward by Clark, Politzer, and Murray [46–50] basically associates the attraction of regions of opposite electrostatic potential between monomers to the formation of noncovalent interactions. The second approach is based on the donor-acceptor model, first proposed by Mulliken [51]. The donor-acceptor model associates the stability of the complexes to a charge transfer from one monomer (electron donor) to the other (electron acceptor). This model uses molecular orbitals and orbital interaction diagrams to describe the charge transfer mechanism in noncovalent interactions [52–54]. The third approach is based on the analysis of electron and energy densities. These properties account for both the kinetic and potential contributions of a noncovalent interaction. The fourth approach uses a model dependent energy decomposition schemes to decompose the interaction energy into physically sounded terms [6, 55, 56]. In our work, we combined the strong points of each model to formulate a protocol of general applicability for the description of the nature of noncovalent interactions. We made use of the following properties:

**Electrostatic potential:** The electrostatic potential  $V(\mathbf{r})$  is an observable quantity given by the potential that all the nuclei and electrons of a molecule create at any point  $\mathbf{r}$  in space. The electrostatic potential mapped onto the van der Waals surface of the monomers (commonly assumed to be given by 0.001 e/Bohr<sup>3</sup> molecular electron density contour [57]) provides the anisotropic representation of the charge distribution, which cannot be obtained from an atomic charge analysis. Regions of positive  $V(\mathbf{r})$  reflect a dominant nuclear contribution, and are usually associated with regions of low electron density. These regions are attracted to the negative site, associated with region of high electron density, such as lone pairs and  $\pi$  bonds.

The analysis of the unperturbed molecular electrostatic potentials of the monomers provides information about positively and negatively charged sites. A comparison of the electrostatic attractive capabilities of different monomers is done based on the analysis of the maximum electrostatic potentials at positive sites ( $V_{max}$ ) and the minimum value at nega-

tive sites ( $V_{min}$ ). However, this analysis serves only as a first approximation since it does not account for polarization effects. In the complex, the mutual polarization between the monomers substantially changes the electron density distribution and electrostatic potential [49].

It is also important to emphasize that the electrostatic view oversimplifies the description of the noncovalent interaction, especially when charge transfer contribution is relevant. An important component in the stabilization of a chemical bond is the lowering of the kinetic energy due to an increase in the electron delocalization [58, 59]. If a model based only on the potential energy is used, the role of the lowering of the kinetic energy in the formation of noncovalent interactions is neglected.

**Charge transfer:** A quantification of covalent effects (i.e. charge transfer) can be obtained from a natural bond orbital (NBO) analysis [60]. The NBO method transforms non-local canonical orbitals into orbitals, localized in one (lone pair) or two (bond pair) centers, forming a Lewis-like molecular bonding pattern of electron pairs. Intermolecular charge transfer energies are then obtained from a second order perturbation analysis usually involving the delocalization of a lone pair orbital of one monomer (electron donor) into an empty  $\sigma^*$  or  $\pi^*$  orbital of the other monomer (electron acceptor). Orbital interaction diagrams are also useful to rationalize possible charge transfer mechanisms.

**Difference electron densities:** The difference between the electron densities of the complex and the monomers (obtained using the frozen geometry of the complex) results in a three-dimensional map showing shifts in the electron density upon complex formation. Electron density accumulation in the intermonomer region and electron density depletion in the antibonding region of the electron acceptor are usually associated with charge transfer. However, electron density shifts also account for other contributions such as polarization and exchange repulsion.

**Energy and electron densities:** Based on the analysis of a variety of different bonds, Cremer and Kraka [61] suggested two criteria for determining the covalent character of a bond: i) there must be a minimum electron density path connecting the interacting atoms

(necessary condition) ii) At the density critical point of the bond  $\mathbf{r}_b$ , there must be a predominance of the local potential energy  $V(\mathbf{r}_b)$  (always negative, i.e. stabilizing) over the local kinetic energy  $G(\mathbf{r}_b)$  (always positive, i.e. destabilizing), indicating that an accumulation of electronic charge at  $\mathbf{r}_b$  has a stabilizing effect. In other words, the energy density  $H(\mathbf{r}_b) = H_b = V(\mathbf{r}_b) + G(\mathbf{r}_b)$  has to be negative (sufficient condition). These criteria can also be applied for noncovalent interactions to distinguish between interactions of dominant electrostatic character ( $H_b \geq 0$ ) and interactions of partial covalent character ( $H_b < 0$ ).

**Energy decomposition:** In general, it is useful to decompose interaction energies into physically meaningful components such as dispersion, electrostatic, induction, exchange-repulsion, and polarization [55,56]. However, energy decomposition schemes suffer from two shortcomings, i) they are based on interaction energies, and therefore it is not possible to obtain specific atom-atom contributions and ii) The many contributions considered are not orthogonal. Consequently, the definition of each component is somewhat arbitrary.

### 2.3. A general protocol for the analysis of noncovalent interactions

We developed a general protocol for the analysis of noncovalent interactions based on the systematic study of XB, ChB, and PnB based on five steps:

1. All complexes are ordered according to the intrinsic strength of the noncovalent interaction from the weakest to the strongest with the help of BSO *versus*  $k^a$  plots. If a large variety of complexes are involved, these can be divided into small subgroups where only an atom or a molecular group varies.
2. The energy density value ( $H_b$ ) is used to differentiate interactions of dominant electrostatic character ( $H_b > 0$ ) from interactions of partial covalent character ( $H_b < 0$ ).
3. The strength of the electrostatic interactions is explained on the basis of monomers properties, such as the extreme values of the electrostatic potential, dipole moments, multipole moments, and polarizabilities.
4. Interactions of partial covalent character also require the analysis of electron delocaliza-

tion energies and charge transfer values obtained from the NBO analysis, which can be rationalized on the basis of orbital diagrams. In most complexes, the covalent contribution involves a charge transfer from the highest occupied molecular orbital (HOMO) of one monomer into the lowest unoccupied molecular orbital (LUMO) of the other monomer. Therefore, the first vertical ionization energy can be used to evaluate the HOMO energy. However, vertical electron affinities are not suitable to investigate the LUMO. Different from ionization potentials of neutral molecules, the electron affinities do not involve charge separation, which results in values that are too small. Hartree Fock orbital energies calculated with small basis sets provide a qualitatively simple alternative for evaluating LUMO energies.

5. The correlation of BSO with  $\Delta E$  is used to identify secondary contributions to the complex stabilization. BSO values in a series of similar complexes that are inversely proportional to  $\Delta E$  values indicate the presence of secondary interactions or strong electronic reorganization. Electron difference densities and energy decomposition analysis can also help to identify secondary contributions (see paper IV).

## THE INTRINSIC STRENGTH OF HALOGEN BONDS

**3.1. Halogen bond definition**

According to the International Union of Pure and Applied Chemistry (IUPAC) conventions [62], halogen bonding (XB) is a noncovalent interaction, where a halogen atom in a molecular entity functions as an electrophilic site able to form an attractive interaction with a nucleophilic site in the same molecular entity or with another molecule or atom. The XB (schematically represented on Figure 3.1) is denoted by three dots  $\cdots$  and forms a near linear interaction between a halogenated moiety called halogen donor (YX) and a Lewis base ( $\text{AR}_m$ ) called halogen acceptor (Figure 3.1).



Figure 3.1. Schematic representation of a XB.

First reports of XB systems date back approximately two centuries [11]. However, it was only about 15 years ago that XB started gaining the attention of the scientific community. The recognition of the importance of XB was triggered by the discoveries that they could serve as effective tools to direct self-assembly phenomena in crystal engineering [63] and that XB plays a major role in the ligand recognition mechanisms of important biological processes such as the recognition of the 3,5,3'-triiodothyroxine (T3) by human thyroid hormone receptor [64, 65], which occur via two XB between iodines and carbonyl oxygens (Figure 3.2).

Over the last 15 years, quantum chemical studies were made to support experimental findings and to provide a theoretical description of the nature and strength of the XB. Despite the many investigations done, there is a scarce number of high accuracy studies on XBs, and no reliable quantitative assessments of their strength. Therefore, we combined high accuracy coupled cluster calculations to the analysis of the local stretching force constant associated with the XB ( $k^a(XA)$ ) to investigate the strength of 36 complexes, and to compare these complexes to eight hydrogen, chalcogen, and pnictogen bonded complexes.

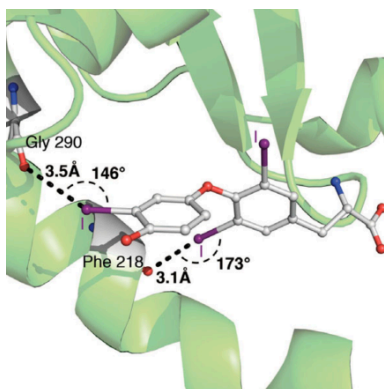


Figure 3.2. Recognition of T3 by human thyroid hormone receptor [65]. XBs are shown by dotted lines.

### 3.2. Importance of using an accurate computational method

The requirement of high accuracy calculations for a quantitative study of a diverse set of XBs was investigated by comparing CCSD(T) results to the less accurate MP2, DFT, and double hybrid DFT methods. Tables 3.1 and 3.2 show the percent deviation in distances and in local stretching force constant values ( $k^a(XA)$ ) for a selection of five complexes. Although all methods reproduced the XB distances reasonably well (within a 5% deviation from CCSD(T) results), deviations of up to 71% were found for the  $k^a(XA)$  values. Confirming that highly accurate quantum chemical methods are needed for a reliable quantitative description of the halogen bond strength. Especially if second order properties such as vibrational frequencies are needed.

Table 3.1. Percent deviation in the XB distances.

	$F_3^-$	$FCl\cdots NFH_2$	$FCl\cdots NH_3$	$FCl\cdots NH_2CH_3$
B3LYP	-	4	2	-1
$\omega$ B97X-D	2	1	1	-1
M06-2X	4	-2	0	0
MP2	1	5	4	4
B2PLYPD	-1	5	3	1
mPW2PLYPD	0	4	3	1
ref. CCSD(T)	1.739	2.4	2.32	2.193

<sup>a</sup> reference values (ref.) are given in Å.

Table 3.2. Percent deviation in the  $k^a(XA)$  values.

	$F_3^-$	$FCl\cdots NFH_2$	$FCl\cdots NH_3$	$FCl\cdots NH_2CH_3$
B3LYP	-	-65	-44	-13
$\omega$ B97X-D	28	-20	-4	0
M06-2X	70	31	23	0
MP2	-45	-23	-30	-41
B2PLYPD	3	-71	-54	-27
mPW2PLYPD	2	-60	-45	-21
ref. CCSD(T)	1.376	0.197	0.311	0.497

<sup>a</sup> reference values (ref.) are given in mdyn/Å.

### 3.3. Summary of results

The XB is highly tunable, having binding energies that vary from 1 to 13 kcal/mol for neutral complexes, and reaching up to 45 kcal/mol for charged 3-center 4-electron (3c-4e) bonded systems. The comparison of the halogen bond strength order (BSO(XA)) and energy densities indicates that halogen bonds vary from weak electrostatic to strong covalent. By ordering the halogen bonds according to their strength with the help of BSO(XA) *versus*  $k^a(\text{XA})$  diagrams, several strength trends related to the halogen atom (X), the halogen-donor bond YX, and the halogen acceptor  $\text{AR}_m$  are observed. These trends can only be understood by considering both covalent and electrostatic parts of the XB mechanism.

The electrostatic part is a result of the anisotropic charge distribution of a covalently bonded halogen X. Whenever a halogen atom X forms a covalent  $\sigma$ -bond with an atom (or molecular group) Y, the effective atomic radius of X along the extension of the Y-X bond axis becomes smaller than in the direction perpendicular to it. This effect is called polar flattening, and the region of depleted electron density collinear to the  $\sigma$ -bond but at the opposite end of the halogen atom is called  $\sigma$ -hole [49, 50]. If the Y substituent is electronegative enough to effectively polarize X, a positive electrostatic potential is formed at the  $\sigma$ -hole, which interacts attractively with the negative electrostatic potential of the lone pair region of a heteroatom A. The electrostatic attraction in  $\text{FCl}\cdots\text{NH}_3$  is shown on Figure 3.3, where the positive potential at the  $\sigma$ -hole of FCl molecule interacts with the negative electrostatic potential in the lone pair of ammonia (lp(N)). Electrostatic attraction increases with the increase in the polarizing power of A, polarity of the YX bond, or polarizability of X.

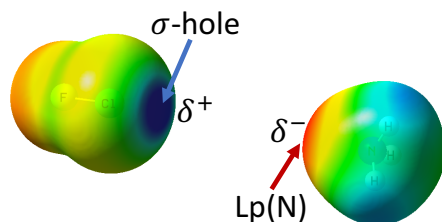


Figure 3.3. Color coded electrostatic potential mapped on the  $0.001 \text{ e}/\text{Bohr}^3$  electron density surface of FCl and  $\text{NH}_3$ . The electrostatic potential varies from positive (blue) to negative (red) .

The covalent part can be rationalized on the basis of a simple orbital diagram as shown in Figure 3.4A for  $\text{FCl}\cdots\text{NH}_3$ . In this complex, the lone pair of the nitrogen  $\text{lp}(\text{N})$  is delocalized into the  $\sigma^*(\text{FCl})$  orbital, leading to an accumulation of electron density in the intermonomer region and a depletion of electron density in the YX bond region (Figure 3.4B). The covalent contribution is proportional to the  $\text{lp}(\text{N})-\sigma(\text{FCl})$  orbital overlap and inversely proportional to the orbital energy gap.

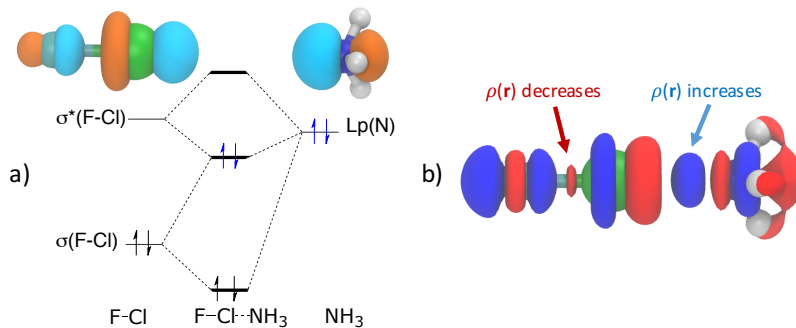


Figure 3.4. A) Orbital interaction diagram of the  $\text{FCl}\cdots\text{NH}_3$  B) Electron difference density distribution for  $\text{FCl}\cdots\text{NH}_3$  complex. Electron density increase in blue, decrease in red.

The charge transfer from  $\text{lp}(\text{A})$  to a  $\sigma^*(\text{YX})$  orbital results in an electron density depletion at the YX bond region, which generally leads to an elongation of the YX bond and a red shift in its frequency. However, in  $\text{O}_2\text{NCl}\cdots\text{NH}_3$  the N-Cl bond becomes shorter and the N-Cl frequency is blue shifted. We used local modes and the local mode decomposition into

normal modes [15, 16] to identify the shift in the local N-Cl stretching vibration and the normal mode with the highest local N-Cl stretching character in the complexes as well as in the  $\text{O}_2\text{NCl}$  monomer. The local N-Cl stretching vibration shift is of  $32\text{ cm}^{-1}$ , compared to only  $13\text{ cm}^{-1}$  in the normal mode frequency with the highest NCl stretching character. The larger shift in the local stretching vibration highlights the advantages of carrying this analysis in terms of local modes. The blue shift in  $\text{O}_2\text{NCl}$  occurs because the  $\sigma^*(\text{NCl})$  orbital is already partially occupied due to an anomeric interaction involving the  $\text{lp}(\text{O})$  and the  $\sigma^*(\text{NCl})$  orbitals. As the complex is formed exchange repulsion between the electrons in the  $\sigma^*(\text{NCl})$  and  $\text{lp}(\text{N})$  orbitals strengthens the N-Cl bond by pushing charge from  $\sigma^*(\text{NCl})$  orbital back to the  $\text{NO}_2$  group.

Halogen bonds strongly depend on the halogen acceptor ( $\text{AR}_m$ ). This is clearly seen from the comparison of the halogen bond strength in  $\text{FCl} \cdots \text{AR}_m$  complexes, where  $\text{AR}_m$  is a series of amines or phosphines. For the amines the BSO values vary from 0.101 to 0.242 depending on the substituents. Electronegative substituents weaken the halogen bond by withdrawing charge from the nitrogen, whereas electron donating groups strengthen it. An even stronger and more complex dependence on the substituents is found for the phosphines. The BSO in these complexes varies from 0.087 to 0.396. Electronegative ligands withdraw charge, weakening the electrostatic part of the interaction. However, they also contribute to an effective contraction of the  $\text{lp}(\text{P})$  orbital, which improves the overlap with the  $\sigma^*(\text{YX})$  orbital, and thus increasing charge transfer. The strong charge transfer in phosphine complexes leads to a substantial weakening of the YX bond, resulting in complexes with partial 3c-4e bond character. This can be quantified based on the ratio of the BSO values of the YX bond and  $\text{X} \cdots \text{A}$  interaction. If this ratio leads to unity (as it is found for  $\text{F}_3^-$ ), a complete 3c-4e bond is formed. Figure 3.5 shows a comparison of the 3-4e character of XBs in phosphine and amine complexes. Compared to amines, where 3c-4e character reaches up to 40%, phosphines have considerably higher 3c-4e character reaching up to 90%.

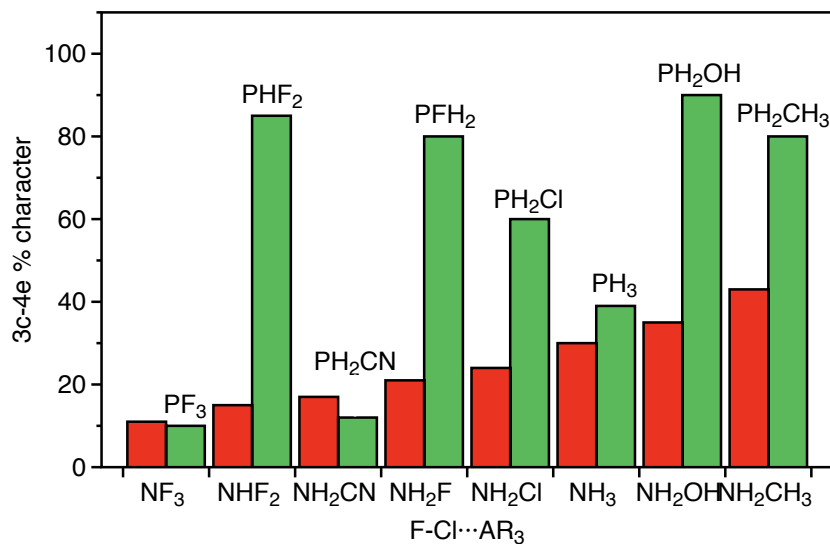


Figure 3.5. Comparison of the 3c-4e bond % character of  $\text{FCl} \cdots \text{NR}_m$  (in red) and  $\text{FCl} \cdots \text{PR}_m$  (in green).

Table 3.3 shows a comparison of the  $\Delta E$ ,  $k^a(\text{XA})$ , and BSO values for interactions involving halogens, pnictogens, chalcogens, and hydrogen with ammonia and chloride Lewis bases. XB is stronger than hydrogen, pnictogen, chalcogen bonds for neutral and anionic systems. A clear advantage of XBs over hydrogen bonds is the possibility of tuning the strength of the interaction by varying the halogen involved, as shown on Table 3.3. Although  $\text{FCl} \cdots \text{NH}_3$  forms a weaker bond than  $\text{FH} \cdots \text{NH}_3$ , the more polarizable Br in  $\text{FBr} \cdots \text{NH}_3$  is able to form a stronger interaction.

Table 3.3. Comparison of XB, hydrogen, chalcogen, and pnictogen bonds.<sup>a</sup>

Neutral	$\Delta E$	$k^a(\text{XA})$	BSO(XA)	Anionic	$\Delta E$	$k^a(\text{XA})$	BSO(XA)
$\text{FCl} \cdots \text{NH}_3$	9.39	0.311	0.216	$\text{FCl} \cdots \text{Cl}^-$	28.98	0.855	0.382
$\text{FHS} \cdots \text{NH}_3$	7.58	0.194	0.166	$\text{FHS} \cdots \text{Cl}^-$	22.48	0.443	0.264
$\text{FH}_2\text{P} \cdots \text{NH}_3$	6.10	0.144	0.140	$\text{FH}_2\text{P} \cdots \text{Cl}^-$	18.62	0.307	0.214
$\text{FH} \cdots \text{NH}_3$	12.11	0.353	0.232	$\text{FH} \cdots \text{Cl}^-$	22.80	0.415	0.254
$\text{FBr} \cdots \text{NH}_3$	14.10	0.479	0.276				

<sup>a</sup> Calculated at CCSD(T)/aug-cc-pVTZ level.  $\Delta E$  values are given in kcal/mol and.

## Chapter 4

### A BROAD VIEW OF HALOGEN BONDING

#### 4.1. Introduction

Previously we showed that halogen bond (XB) is a highly tunable interaction (chapter III and papers I and II). Therefore, to better understand how to control the strength of the halogen bond we decided to do an extensive investigation of a set of 202 XB complexes. This set consists of 148 complexes of the type  $YX \cdots AR_m$  ( $Y, X = F, Cl, Br, I, At$ ;  $A = O, S, N, P$ ; and  $R = H, F, Cl, CH_3, SiH_3, CN, OH$ ) where the halogen donor  $Y$ , the halogen  $X$ , the acceptor atom  $A$  and its substituents  $R_m$  were varied systematically to determine decisive electronic effects necessary to describe the XB strength. The other 52 complexes are halomethanes, halotetragenes, and organoiodines used to define strategies for the design of new materials based on XB.

#### 4.2. A dual computational level approach

A complete analysis based solely on high accuracy CCSD(T) calculations can only be carried out for a set of very small complexes. The computational cost of CCSD(T) scales to the seventh power of the size of the systems (e.g., a molecule  $X$ , which is twice as large as molecules  $Y$  has a computational cost of approximately 128 times larger than  $Y$ ). Recent approximations for CCSD(T) were able to reduce the exponential scaling of CCSD(T) to near linear scaling with minimal loss in accuracy [66, 67]. However, analytical gradient and Hessian, which are required for accurate calculations of geometries and frequencies, are not available yet. To obtain a reliable description of local vibrational modes with a less computationally demanding method, we compared XB distances and local stretching force constants ( $k^a(XA)$ ) for a set of 28 complexes obtained at CCSD(T)/aug-cc-pVTZ with

several DFTs.  $\omega$ B97X-D led to the smallest deviations (paper II). Binding energies were computed also using CCSD(T) energies to estimate the accuracy of  $\omega$ B97X-D for the entire set of molecules.

### 4.3. Summary of results

Eleven different electronic effects were found to play a decisive role in the XB. These can be separated into two groups; orbital based effects (1-5) and other effects (6-11) as follows:

1. **Lp(A)- $\sigma^*(XY)$  orbital overlap effect.** An efficient orbital overlap is obtained by having: i) a linear lp(A)- $\sigma^*(XY)$  arrangement and a short X...A distance ii) X...A atoms of close periods iii) A substituent Y more electronegative than X (by this the X coefficient in  $\sigma(XY)$  is decreased and due to orbital orthogonality, the X coefficient in  $\sigma^*(XY)$  is increased). iv) Electronegative substituents that can effectively contract the diffuse lp(A) orbital of third period heteroatoms.
2. **Electronegativity of A and substituent effects on lp(A) orbital energies.** Charge transfer is inversely proportional to the lp(A)- $\sigma^*(XY)$  orbital energy gap. This energy gap is decreased by raising the lp(A) energy in the following ways: i) having a less electronegative A (e.g. using third row heteroatoms such as P and S) or ii) by an electron donating substituent (e.g.  $\text{CH}_3$ ). Noteworthy is that electronegative substituents have a smaller impact over the lp(A) orbital energy of heteroatoms of the third period (A = P and S) compared to second period elements (A = N and O).
3. **Electronegativity of Y and X.** A more electronegative substituent Y and halogen X leads to lower  $\sigma(XY)$  and  $\sigma^*(XY)$  orbital energies. However, this effect has to be contrasted with effect 1, since a lower electronegativity difference between X and Y reduces the X orbital coefficient at  $\sigma^*(XY)$  (see effect 1), thus decreasing the lp(A)- $\sigma^*(XY)$  orbital overlap.
4. **Relativistic effects.** Relativistic contraction of s and p orbitals of heavy elements (I and At), lowers the electronegativity of X but weakens the electrostatic potential at the  $\sigma$ -hole.

5. **Formation of a 3c-4e bond.** As the XB becomes stronger and more covalent, the YX bond tends to become weaker, leading to the formation of a 3c-4e bonds as is found for trihalides (e.g.  $\text{F}_3^-$ ). This effect is especially pronounced for the YX-phosphine (Y and X are halogens) complexes.
6. **Halogen transfer and ion interaction.** For  $\text{YX}\cdots\text{P}(\text{CH}_3)_3$  complexes the XA bond strength can surpass that of XY, leading to the formation of inverted 3c-4e bonds and ion pair complexes of the  $\text{Y}^- \cdots \text{XP}(\text{CH}_3)_3^+$  type.
7. **Charge attraction/repulsion.** A Coulomb attraction between a negatively charged X and a positively charged A leads to stabilization. However, strong XBs are observed even in complexes where X and A adopt positive atomic charges (see effect 8).
8. **Anisotropic charge distribution at X and A.** Atomic charges do not describe the anisotropy of the electron density distribution. The negative charge in the YX  $\sigma$ -bond direction screens the X nucleus less than in the  $\pi$  direction, leading to a positive electrostatic potential ( $\sigma$ -hole). On the other hand, the A atom is better screened in the  $\text{lp}(\text{A})$  region, leading to a negative electrostatic potential.
9. **Dipole-dipole interactions.** The electrostatic attraction between the monomers can be enhanced or weakened according to the orientation of their dipole moment.
10. **Mutual polarization of the monomers.** As the halogen donor YX approaches the halogen acceptor  $\text{AR}_m$ , the negative electrostatic potential at  $\text{lp}(\text{A})$  polarizes the positive potential at the YX  $\sigma$ -hole. This effect is proportional to the polarizability of the monomers.
11. **Cooperative effect.** XB strength can be augmented by the cooperative effect of a hydrogen bond. This is found for  $\text{FCl}\cdots\text{PH}_2\text{OH}$  and  $\text{FCl}\cdots\text{NH}_2\text{OH}$ , where the H of the hydroxyl group can form a weak electrostatic interaction with the  $\pi$ -density of the Cl.

Orbital related effects are relevant to describe the covalent part of the XB, whereas the other effects play a more prominent role in the electrostatic part of the interaction. These

effects play an important role in connection of possible strategies that can be adopted for the design of new materials based on XBs, summarized in the following section.

#### 4.4. Strategies for material design

Halocarbons are the most common compounds used in the design of materials based on XB. These are used to synthesize liquid crystals, gels, fluorescent materials, and supramolecular compartments for example [11, 68–71]. The lower electronegativity of carbon compared to that of the halogens leads to higher  $\sigma(\text{YX})$  and  $\sigma^*(\text{YX})$  orbital energies (effect 3) and to a reduced  $\text{lp}(\text{A})-\sigma^*(\text{YX})$  orbital overlap (effect 1), thus to a reduced charge transfer. As a result, halocarbons form weak electrostatic interactions which can be strengthened by increasing the positive electrostatic potential at the  $\sigma$ -hole of the halogen as well as the polarizability of the molecules. This can be accomplished by: i) increasing the polarizability of the halogen and the halogen donor ii) increasing the effective electronegativity of C iii) modifying the Lewis base. Therefore, iodo-carbon molecules with a highly polarizable framework are suitable halogen donors. Some examples already used in supramolecular materials are perfluorinated iodobenzene and iodopolyalkyne [72–75]. We suggest as a possible new strategy the 1,3 dipolar cycloaddition of I-substituted derivatives of 1,3 dipolar molecules (e.g. I–NNN, ICNI, I<sub>2</sub>CNN) and diaminopolyalkynes or diaminoperfluorinated polyalkenes. This reaction could lead to a stable network of bonds that could be explored for the synthesis of new XBed polymers.

### 5.1. Halogen bonding involving a metal center

Halogen bonding (XB) is not restricted to main element chemistry but can also involve metals as halogen donor groups [76, 77], or as halogen acceptors [78–80]. Koten and co-workers [81] were the first to report late transition metal complexes where  $I_2$  coordinates to a square planar  $d^8$  metal ( $M = Pt$  or  $Pd$ ) in a linear fashion ( $I-I-M \approx 180^\circ$ ). They suggested that the  $I_2$  ligand would be stabilized by a charge transfer from the  $d_{z^2}$  lone pair of the metal to the  $\sigma^*(I-I)$  of  $I_2$ , which is typical of a XB. This hypothesis was confirmed by Rogachev and Hoffmann [82] who showed that when  $I_2$  acts as an electron acceptor, a metal-iodine linear coordination is formed and when  $I_2$  acts as an electron donor a bent iodine-metal coordination is formed. They also showed that the binding energies of the XBed complexes were stronger for the heavier metal Pt compared to the lighter congener metals Ni and Pd. Although, it was not investigated by the authors, the scalar relativistic expansion of the 5d orbitals of Pt could be responsible for the higher binding energies involving Pt complexes. To better comprehend how strong the XB with metal centers can be and the role of relativistic effects, we studied the XBs in complexes of the type  $YX \cdots MR_n$ , where  $YX =$  dihalogens, interhalogens, and halocarbons, and  $MR_n =$  neutral (Pt, Hg) and anionic metal complexes (Cu, Ag and Au). The all-electron Dirac-exact Normalized Elimination of the Small Component (NESC) method developed by Cremer and co-workers [34, 83] was used to obtain an accurate description of scalar relativistic effects.

## 5.2. Scalar relativistic effects

The NESC method provides a way to determine the magnitude of scalar relativistic effects. This is done by taking the difference between the relativistic and the non-relativistic electron densities. Figure 5.1 shows this difference for  $I_2$ ,  $I_2 \cdots Cu(CH_3)_2^-$ ,  $I_2 \cdots Ag(CH_3)_2^-$ , and  $I_2 \cdots Au(CH_3)_2^-$ .

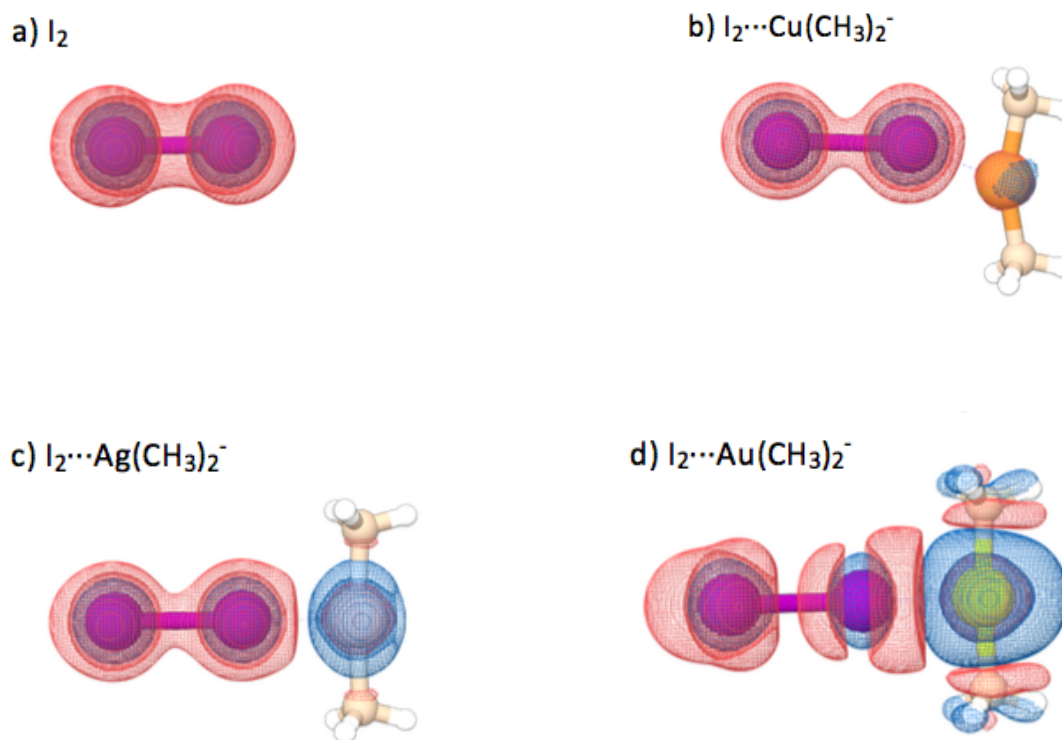


Figure 5.1. Electron difference density distributions between NESC-TPSS-D3 scalar relativistic density and the non-relativistic density plotted for an electron density of  $0.0015 \text{ e/Bohr}^3$ . Blue regions indicate an increase in the electron density, red regions a decrease relative to the non-relativistic density.

Relativistic contraction of 5s and 5p in  $I_2$  leads to a depletion of electron density far from the nuclei (in red) and an increase of electron density close to the nuclei (in blue), thus it leads to a more compact (less polarizable) electron density at the  $I_2$ . At the metal center it is possible to see that relativistic effects increase substantially from Cu to Ag to Au, with

negligible effects for Cu. Due to the 4d (Ag) and 5d (Au) expansion, electrons density close to Au (in red) is shifted to an outer region (in blue) increasing the polarizability of Au.

### 5.3. Summary of results

In this work (Paper III) we presented for the first time a quantitative description of the intrinsic strength of XBs with metal centers based on local stretching force constants and the analysis of binding energies, geometric parameters, electron and energy distributions, and electrostatic potentials. All of these quantities were calculated using NESC to obtain an accurate description of scalar relativistic effects. The following conclusions were reached:

Small changes in the halogen, halogen donor, metal center, and its substituents can lead to changes in the nature of the XBs, which varies from classical XB, to non-classical 3c-4e bonds (NC and i-NC), and finally to covalent metal-halogen bonds (i-XB-M). The change in the bond type from XB to i-XB-M is accompanied by an increase in the strength and covalent character of the halogen-metal interaction and by a decrease in the strength of the halogen-donor (YX) bond. Gold is able to form stronger XBs than Cu and Ag due to the better availability of  $lp(Au)$ , which is a result of the scalar relativistic contraction of 6s and expansion of 5d orbitals.

XBs with metal centers share several common features with the XBs involving main elements (chapter 3 and 4; papers I and II). In both cases, halotrifluoromethanes form weaker and less covalent XBs compared to dihalogens and interhalogens. This is due to the lower electronegativity of carbon compared to the halogens. Another common feature is the unusual strength trend found for the complexes formed by dimethylaurates and trimethylphosphines with dihalogens and interhalogens. In these complexes, the less polarizable interhalogen FCl forms a stronger interaction than the more polarizable FI. Similarly  $Cl_2$  establishes a stronger bond than  $I_2$ . The reason for the stronger Cl-metal and Cl-P bond in these complexes is due the lower electronegativity of Cl compared to I, resulting in lower  $\sigma(YX)$  and  $\sigma^*(YX)$  orbital energies and a stronger  $lp-\sigma^*(YX)$  charge transfer. These complexes already have strong covalent character and are better described as 3c-4e nonclassical bonds.

Although extreme values of the electrostatic potential in the monomers showed only a limited qualitative correlation with the XB strength, they correctly showed that  $\text{Au}(\text{CH}_3)_2^-$  is a stronger halogen acceptor than  $\text{Ag}(\text{CH}_3)_2^-$  and  $\text{Cu}(\text{CH}_3)_2^-$ , and that  $\text{AuF}_2^-$  is a better halogen acceptor than  $\text{AuCl}_2^-$ . Future work should focus on possible ways to control the oxidative addition of dihalogens to planar transition metal pincer complexes. Since the halogen-halogen and metal-halogen bonds are very sensitive to small changes in the metal ligands, oxidative addition of a dihalogen to metal centers could be facilitated, for example, by small modification of metal pincer complexes. Another topic to be explored is the possibility of forming long strands where a halogen donor such as diiodo-acetylene or 1,4-diiodobenzene interact by frontside and backside of a planar transition metal complex, which could lead to the formation of metal-XB polymeric structures.

## Chapter 6

### CHALCOGEN BONDING

#### 6.1. Introduction

Similar to halogen bonding (XB), chalcogen bonding (ChB) is defined as an attractive interaction between the electrophilic region of a chalcogen atom ( $E = S, Se, Te$ ) and a nucleophilic region in another, or the same, molecule [8]. The ChB complex is denoted by  $X(Y)E \cdots AR_n$ , where  $E \cdots A$  is the ChB,  $X$  is the chalcogen substituent collinear to the ChB,  $Y$  is the substituent orthogonal to the ChB,  $AR_n$  is the chalcogen acceptor.

Since chalcogens are well known to have a rich chemistry [84] and to play an important role in biochemical [9, 85–87] and material science [8, 88–91], we decided to investigate in detail the bonding mechanism of the ChB and to compare it with XB. For this purpose, a set of one hundred different ChB systems including neutral, cationic, anionic, and  $sp^3$  and  $sp^2$  hybridized chalcogens were analyzed. Different from our previous investigations on XB, in this study we shifted our focus from describing the major electronic effects related to ChB to the identification of the essential effects required to explain the ChB geometry and strength dependence with the chalcogen atoms ( $sp^3$  and  $sp^2$  hybridized), the substituents  $X$  and  $Y$ , and the chalcogen acceptor  $AR_n$ . A new type of ChB is found and strategies to obtain new material based on ChB are described.

#### 6.2. Chalcogen bonding mechanism

The ChB mechanism has both electrostatic and covalent parts, similar to the XB mechanism (described on chapter 3 and papers I and II), but with few important differences. First, the electrostatic potential of a  $sp^3$  chalcogen can have two  $\sigma$ -holes, one collinear to the Y-E bond and the other collinear to the X-E bond. In the case of a  $sp^2$  chalcogen the

$\sigma$ -hole is still collinear to the X-E double bond. Second, the covalent part of the ChB is related to two different charge transfer mechanisms, which depend on the hybridization of the chalcogen. Charge transfer occurs either from the lone pair A ( $\text{lp(A)}$ ) to the  $\sigma^*(\text{EX})$  orbital of an  $\text{sp}^3$  chalcogen or to the  $\pi^*(\text{EX})$  orbital of an  $\text{sp}^2$  chalcogen. Both covalent and electrostatic contributions are maximized when X is the most electronegative substituent.

A slightly different bonding mechanism is found for the symmetric homodimer complexes  $(\text{F(H)E})_2$ . In these complexes both monomers donate and accept charge via the  $\text{lp(E')} \rightarrow \sigma^*(\text{EX})$  and the  $\text{lp(E)} \rightarrow \sigma^*(\text{E'X})$  charge transfer mechanisms. To maximize the  $\text{lp(E')}-\sigma^*(\text{EX})$  and  $\text{lp(E)}-\sigma^*(\text{E'X})$  orbital overlaps and minimize the  $\text{lp(E')}-\text{lp(E)}$  exchange-repulsion, the monomers adopt a skewed conformation. The stronger covalent contribution of these interactions compensates for the weaker electrostatic attraction resulted from the poorer alignment between the positive electrostatic potential in the X-E  $\sigma$ -hole and the negative electrostatic potential in the  $\text{lp(E')}$  region. We found that a symmetric homodimer can also be held by the charge transfer from the  $\text{lp(E')}$  to the  $\pi^*(\text{EX})$  orbital as in  $(\text{FNTe})_2$  (Figure 6.1). The binding energy of  $(\text{FNTe})_2$  is 7.9 kcal/mol and the bond strength order (BSO) is 0.2. This new kind of interaction may be relevant for the design of novel material.

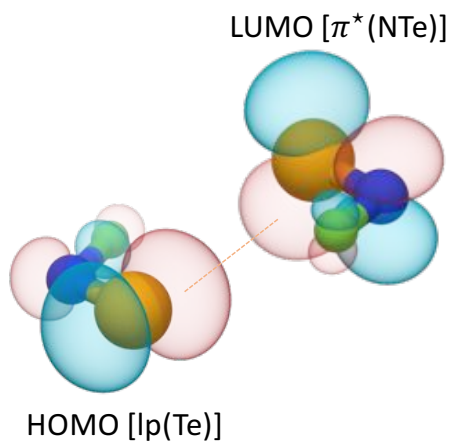


Figure 6.1. Frontier molecular orbitals of FNTe.

### 6.3. Electrostatic versus covalent contributions

Different from  $sp^3$  chalcogen donors, where the  $\sigma$ -hole and the lowest unoccupied molecular orbital ( $\sigma^*(EX)$ ) are collinear, in  $sp^2$  chalcogens the  $\sigma$ -hole is still collinear to the EX double bond (Figure 6.2 a) but the lowest unoccupied orbital ( $\pi^*(EX)$ ) is orthogonal to the  $\sigma$ -hole (Figure 6.2). Because of this, the charge transfer and electrostatic contributions are maximized for different geometries. As a result, weak electrostatic complexes adopt different geometries compared to stronger and partially covalent complexes. The former lead to close to linear interactions (Figure 6.2 c), whereas the latter leads to bent interactions (Figure 6.2 d).

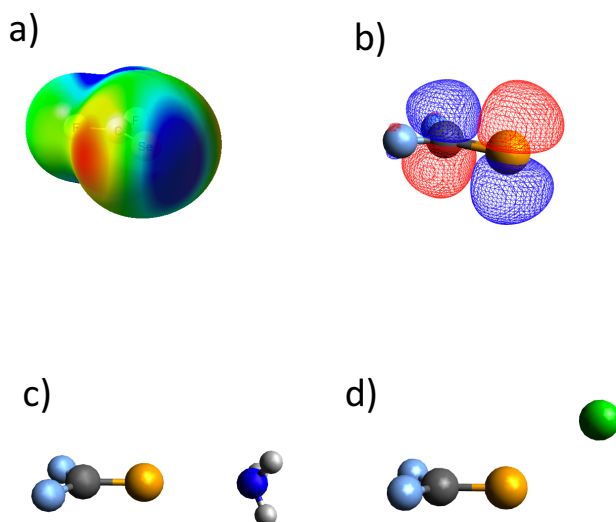


Figure 6.2. Electrostatic potential of F<sub>2</sub>CSe plotted on the 0.001 e/Bohr<sup>3</sup> electron density surface (a) Lowest unoccupied molecular orbital (LUMO) of F<sub>2</sub>CSe (b) F<sub>2</sub>CSe...NH<sub>3</sub> (c) F<sub>2</sub>CSe...Cl<sup>-</sup> (d).

### 6.4. Summary of results

We found that the ChB strength systematically increases with:

1. The polarizability of the chalcogen atom ( $E = S < Se < Te$ ). Te is more easily

polarized by the substituents X and Y than the other chalcogens, leading to a more positive electrostatic potential at the  $\sigma$ -hole.

2. The decrease in the electronegativity of the acceptor heteroatom A ( $A = F < O < N$ ). Nitrogen has a more negative electrostatic potential at the lp(N) region and is also a better electron donor than other heteroatoms of the second period.
3. Increased electronegativity of X ( $X = CF_3 < NF_2 < OF < F$ ). The higher electronegativity of F leads to a  $\sigma^*(FE)$  orbital which is lower in energy (closer to the  $\sigma^*(XE)$ ), thus increasing lp(A) $\rightarrow\sigma^*(XE)$  charge transfer. The stronger polarizing power of X also leads to a more positive electrostatic potential at the  $\sigma$ -hole.
4. Electron withdrawing capability of Y ( $Y = CH_3 < CF_2H < CF_3 < CN$ ). A stronger electron withdrawing substituent Y leads to a more positive electrostatic potential at E.
5. Lower exchange repulsion between lp(A) and Y. A stronger ChB is found by rotating  $CH_3$ ,  $CF_2H$ , and  $CF_3$  to positions where the exchange repulsion between lp(A) and Y is minimized.
6. Electron donor ability of the chalcogen acceptor ( $AR_m = P(CH_3)_3 > N(CH_3)_3 > As(CH_3)_3$ ). The lp(P) orbital in the trimethylphosphine has a higher energy than the lp(N) and is not as diffuse as lp(As).

The binding energy ( $\Delta E$ ) of neutral ChB complexes were found to reach up to 28.0 kcal/mol for  $F(PMe_2)Te)_2$ , a complex where two ChBs are simultaneously formed, whereas charged complexes could reach  $\Delta E$  values up to 47.5 kcal/mol. The ChB strength depends mostly on the chalcogen donor, the chalcogen, and the X ligand collinear to the ChB. Even though the Y ligand has a smaller impact on the ChB, it can still be used to fine tune the strength of the interaction. In general, ChB involves a smaller charge transfer and has a lower 3c-4e bond character compared to XB. The lower covalent character of ChBs is due to the lower electronegativity of chalcogens compared to halogens, and also due to the slightly bent X-E-A angle of these complexes, which results in a less effective lp(A)- $\sigma^*(XE)$  overlap.

## 6.5. Strategies for the design of new materials

Based on the analysis of strength trends, we concluded that an efficient strategy for the development of new ChB materials is the use of monomers that can make multiple ChBs, such as 1,2,5-telluradiazoles. This can be improved by fusing ring structures and increasing the number of possible ChBs.

## Chapter 7

# NONCOVALENT INTERACTIONS INVOLVING HALOGENS, CHALCOGENS AND PNICOGENS

### 7.1. Introduction

Halogen···halogen interactions, commonly found on crystallographic structures, are usually associated with two types of conformations (Figure 7.1). The halogen···halogen type I conformation is characterized by angles of approximately the same magnitude between the X and Y halogens and their substituents W and Z, whereas type II conformation is characterized by a close to linear angle between the intermolecular interaction and the substituent W and a close to right angle between the substituent Z and the intermolecular interaction. An inspection of complexes commonly discussed in the literature showed that complexes involving chalcogen···chalcogen and pnicoген···pnicoген interactions also adopt two conformations (Figure 7.1). Despite the clear similarities between these complexes, no comparisons based on type I and II conformations were attempted. Moreover, complexes involving a pnicoген···chalcogen interaction were also found in two different conformations, which closely resemble type I and II. These observations, together with our previous experience on halogen bonds (XBs) and chalcogen bonds (ChBs), let us to hypothesize that a general conformational based description of the bonding mechanism of noncovalent interactions of halogens, chalcogens, and pnicoгенs was feasible.

### 7.2. Summary of results

To confirm our hypothesis, high accuracy CCSD(T) calculations were done for 32 weak noncovalent interactions ( $\Delta E < 10\text{kcal/mol}$ ) involving halogens, chalcogens, and pnicoгенs. We found that charge transfer in these complexes could be explained on the basis of a

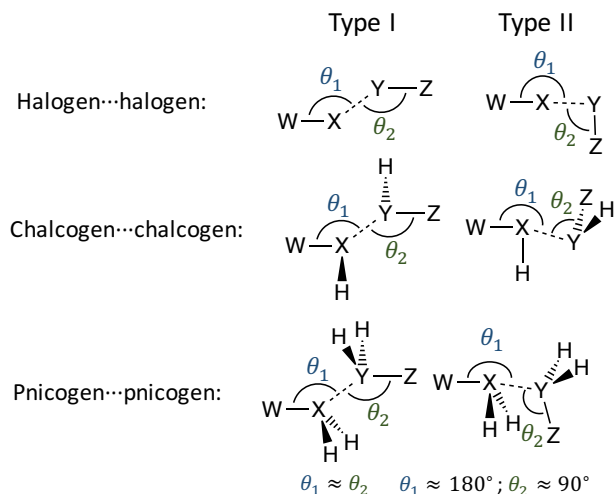


Figure 7.1. The two common conformations found for halogen···halogen, chalcogen···chalcogen, and pnictogen···pnictogen interactions.

simple orbital diagram (paper V), which depends only on the conformation adopted by the complex. Type I complexes adopt a skewed conformation allowing both monomers to donate and receive electron charge via two charge transfer mechanisms, while minimizing lone pair repulsion between the heteroatoms involved. In type II conformation each monomer acts as an electron donor or electron acceptor, resulting in a head on interaction between the lone pair of the nucleophile and a  $\sigma^*$  orbital of the electrophile. These interactions also have an electrostatic component. In type II complexes the positive electrostatic potential in the  $\sigma$ -hole region of a halogen, chalcogen, or pnictogen faces the negative electrostatic potential in the lone pairs of the nucleophile. Electrostatics play a smaller role in type I complexes, since the  $\sigma$ -hole of one monomer does not face the lone pairs of the other monomer. Orbitals involved in the charge transfer mechanisms of type I and II are depicted for FCl···ClF complex on Figure 7.2, together with the electrostatic potential of the unperturbed monomer.

Although most complexes of type I are held by charge transfer contributions, electrostatic contributions are still important. An example is the  $(\text{FH}_2\text{N})_2$  complex, where the electrostatic attraction between the lone pairs of the nitrogen of one monomer and the positive charge at the hydrogen of the other monomer contributes to a relatively strong N···N

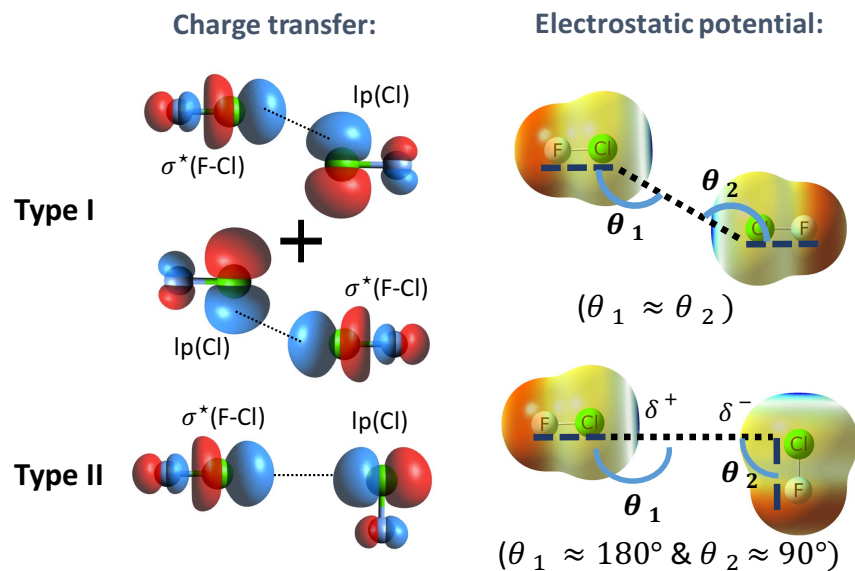


Figure 7.2. Charge transfer and electrostatic attraction in type I and II conformations of  $(\text{FCl}_2)_2$

interaction. Noteworthy is that type I interactions are not restricted to homodimers. As long as the monomers have compatible orbital energies and sizable overlap between the lone pair and the  $\sigma^*$  orbitals, heterodimers of type I can be formed. An interesting example is the complex  $\text{FHS}\cdots\text{PH}_2\text{F}$  which has three different minima involving. Two minima refer to type II conformations, one with a ChB and the other with a pnictogen bond (PnB), and the third minimum has a type I conformation held by an admixture of a pnictogen and a chalcogen bond. Type I interactions can be easily distinguished from type II by an analysis of the difference density, such as the ones shown in Figure 7.3 for the three minima of  $\text{FHS}\cdots\text{PH}_2\text{F}$ . Type II complexes are characterized by a spherical shaped increase of electron density in the intermonomer region (in blue), whereas, in type I complexes the electron density increase adopts an elongated shape (prolate) due the two charger transfer mechanisms involved.

This study brought also a better understanding of the strength dependence of the various complexes studied. In our previous study on XBs covering only type II interaction (paper I), we showed that XB is stronger than ChB or PnB. In this study we showed that type I inter-

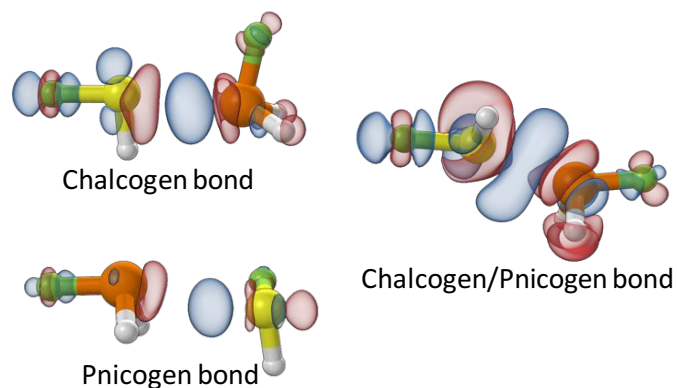


Figure 7.3. Electrostatic potential of  $F_2CSe$  plotted on the  $0.001 \text{ e/Bohr}^3$  electron density surface (a) Lowest unoccupied molecular orbital (LUMO) of  $F_2CSe$  (b)  $F_2CSe \cdots NH_3$  (c)  $F_2CSe \cdots Cl^-$  (d).

actions follow the opposite strength trends; PnBs are found to be stronger than comparable ChBs or XBs. We also measured the angular distortion sensitivity by stepwise bending the noncovalent interactions of seven complexes. The type I conformation of XBs complexes was found to be a point of maximum energy in the potential energy surface (confirmed by the existence of one imaginary frequency associated with a bending vibrational mode) if these complexes are bent to a type II conformation a point of minimum energy is found. There is a small energy difference between type I and type II XBs (inferior to 1 kcal/mol), which can be easily overcome by crystal packing forces. This is the reason why both type I and type II halogen $\cdots$ halogen contacts are observed in crystal structures. On the other hand, type I pnicogen and chalcogen homodimers are minimum points in the potential energy surface and no stable type II complexes are found. In general, the angular sensitivity of type I and II increases with the strength and covalent character of the interaction.

## Chapter 8

### $\sigma$ -AROMATICITY IN SMALL GOLD CLUSTERS

#### 8.1. Introduction

Small gold clusters have been the subject of intense research due to their unique catalytic, electronic and optical properties [92–96], which can be controlled by changing the number of gold atoms, the shape of the cluster, the support, and additives used [93–95,97]. Compared to the lighter congeners (Ag and Cu), Au is able to form relatively short and strong bonds, which is due to the strong scalar relativistic contraction of the 6s orbital and expansion of the 5d orbitals of Au [98,99]. In this work, we propose a simple structural principle to explain the preferred planar geometry of small gold clusters ( $\text{Au}_m$ ;  $m < 8$ ) based on the aggregation of  $\text{Au}_3$  three membered ring units (3-rings). The 3-rings structure is stabilized due to  $\sigma$ -aromaticity, i.e., the (3c-2e) delocalization of  $\sigma$ -electrons in the surface of the 3-rings. Apart from this the  $\text{Au}_6$  cluster was compared with the valence isoelectronic  $\text{Au}_5\text{Zn}^+$  cluster, a potential  $\sigma$ -aromatic cluster. [100]

#### 8.2. Assessment of $\sigma$ -aromaticity

Although aromaticity cannot be directly measured, it manifests in different molecular properties:

**Energy-based properties:** The electron deficient cation  $\text{Au}_3^+$  forms a stable equilateral triangle structure of  $D_{3h}$  symmetry, where the highest occupied molecular orbital (HOMO) is the fully delocalized ( $a_1'$ -symmetrical) 3c orbital formed by the bonding combination of the 6s orbitals of the Au atoms. Hence,  $\text{Au}_3^+$  can be considered to be a  $\sigma$ -aromatic 2e system (Figure 8.1). The addition of an electron to this system leads to the Jahn-Teller unstable  $\text{Au}_3(3e)$ , which distorts from the  $D_{3h}$  cyclic symmetry to an acyclic  $C_{2v}$  symmetry

to regain stability(Figure 8.1). Compared to  $\text{Au}_3^+(2e)$ , the  $\text{Au}_3(3e)$  system is considerably less stable as is shown by its lower atomization energy ( $\text{AE} = 127.6$  compared to  $73.3$  kcal/mol). Furthermore if the normalized atomization energies ( $\text{NAE} = \text{AE}/N$ , where  $N$  is the number of Au atoms) of the cyclic and polycyclic  $\text{Au}_m$  clusters  $\text{Au}_3^+$ ,  $\text{Au}_4$  ( $D_{2h}$ ),  $\text{Au}_5$ ,  $\text{Au}_6$ , and  $\text{Au}_7$  are compared to the NAE of the acyclic clusters  $\text{Au}_2$  and  $\text{Au}_4$  ( $C_{2h}$ ), it becomes clear that the formation of 3-ring structures similar to the one in  $\text{Au}_3^+$  grants extra stability for polycyclic gold clusters.

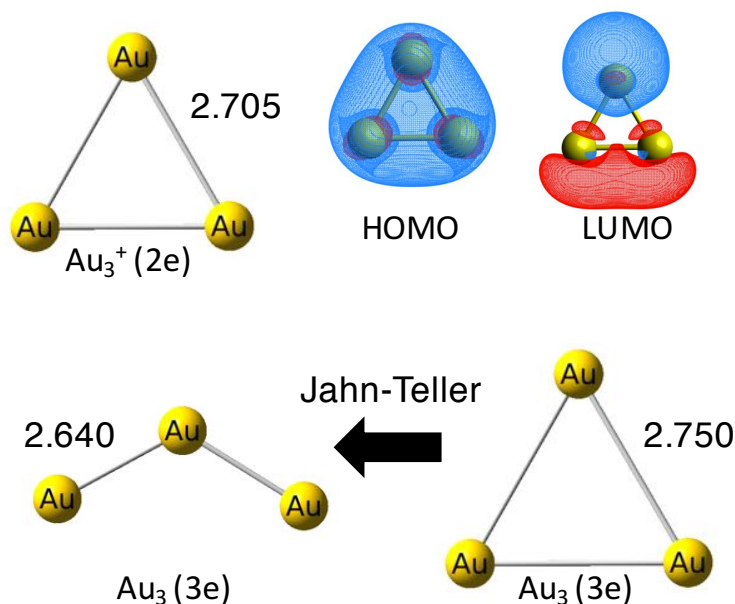


Figure 8.1. Comparison of the geometry of the Jahn Teller unstable  $\text{Au}_3$  ( $D_{3h}$  symmetry), stable  $\text{Au}_3$  ( $C_s$  symmetry), and  $\text{Au}_3^{2+}$  ( $D_{3h}$  symmetry). Distances in Å and number of valence electrons in parenthesis.

**Magnetic properties:** Nucleus-independent chemical shifts calculated at 1 Å above the rings centroid (NICS(1)), indicate the existence of a diatropic ring current characteristic of an aromatic system.  $\text{Au}_3^+$  has the most negative NICS(1) in line with its optimal  $2e$  delocalization. For the 3-rings in  $\text{Au}_5$ ,  $\text{Au}_6$  and  $\text{Au}_7$  the delocalization decreases with the number of shared edges of each 3-ring, suggesting a decrease of aromatic  $\sigma$ -delocalization in the inner rings.

**Vibrational properties:** The local stretching force constant ( $k^a$ ) of Au-Au bonds in the classical 2c-2e bond of  $\text{Au}_2$  and in the 3c-2e bonds of  $\text{Au}_3^+$  were used to derive a relative bond strength order (BSO) and an aromaticity index (AI). The latter was obtained by extending the definition of Cremer and co-workers originally defined for  $\pi$ -aromatic ring systems to describe  $\sigma$ -aromaticity in  $\text{Au}_m$  clusters. For this purpose, an AI = 1 is chosen to indicate the fully delocalized 3-ring system in  $\text{Au}_3^+$ , whereas values inferior to 1 indicate a decrease in  $\sigma$ -delocalization and an AI = 0 is chosen to indicate the classical 2c-2e covalent bond found in  $\text{Au}_2$ . The AI description was complemented with the estimation of electron deficiency of each 3-ring unit, obtained by rescaling BSO values so that the sum of all BSO of a given  $\text{Au}_m$  cluster adds up to the total number of electrons. The electron counting of each 3-ring is given by dividing the rescaled BSO values of bonds shared between two 3-ring units by two and then summing up the three rescaled BSO values referent to each Au-Au bond in a specific 3-ring unit. The electron counting from rescaled BSO values and the AI values show that outer 3-ring units have both stronger  $\sigma$ -delocalization and an electron counting closer to 2e (similar to  $\text{Au}_3^+$ ), whereas inner 3-ring units tend to have lower AI values and to be more electron deficient. This is in line with NICS(1) values.

**Electron density properties:** Surface delocalization was calculated from the ratio of the density at the ring critical point ( $\rho(\text{RCP})$ ) by the magnitude of the laplacian at the direction orthogonal to the ring plane ( $\nabla^2\rho(z)$ ) using the formula:  $\eta = |\rho(\text{RCP})/\nabla^2\rho(z)|$ . A larger  $\eta$  value indicates electron localization, whereas a lower  $\eta$  accompanied by a more negative  $\nabla^2\rho(z)$  indicates stronger surface delocalization. The decrease in surface delocalization agreed qualitatively with NICS(1) and AI values.

**Aromaticity in  $\text{Au}_5\text{Zn}^+$  cluster:** We confirmed that the molecule  $\text{Au}_5\text{Zn}^+$  is also stabilized by  $\sigma$ -delocalization. Both the large AI and the negative NICS(1) values confirm the strong delocalization character of  $\text{Au}_5\text{Zn}^+$ . Furthermore, the Au-Zn bonds in this cation are shorter and stronger than the Au-Au bonds in the valence isoelectronic  $\text{Au}_6$  molecules (Figure 8.2). This is a result of the higher electronegativity of Zn as well as the positive charge of the complex, thus leading to a more stable structure (NAE = 49.4 compared to

43.1 kcal/mol of  $\text{Au}_6$ ).

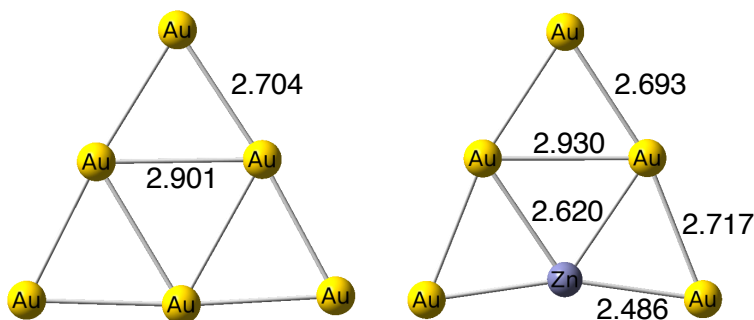


Figure 8.2. Comparison of the geometry of  $\text{Au}_6$  ( $D_{3h}$  symmetry) and  $\text{Au}_5\text{Zn}^+$  ( $C_{2v}$  symmetry). Bond distances are given in Å .

### 8.3. Summary of results

The most stable  $\text{Au}_m$  planar structures are the ones able to form the largest number of 3-ring units with dominant 3-center 2-electron character (as it is in  $\text{Au}_3^+$ ). The different types of properties analyzed led to different manifestations of aromaticity. Energy properties reveal the impact of aromaticity on the stability of the cluster in an unspecific way. Therefore, other properties are required to better comprehend the electronic changes responsible for this stabilization. Magnetic properties help to elucidate the aromatic character of each 3-ring unit. However NICS(1) is a hypersensitive measure of magnetic anisotropy and potential orbital current and can only give qualitative insight on the higher aromaticity of the outer 3-ring units compared to the inner units. Vibrational properties combined with the analysis of atomic charge and contrasted with local properties of the electron density provide detailed and reliable quantitative description of 3-ring  $\sigma$ -aromaticity and surface delocalization. Future studies should use the principles described here to elucidate the stability of larger gold clusters and also to investigate whether these principles could be generalized to describe different metal clusters.

## Chapter 9

### CONCLUSION, OUTLOOK AND CONTRIBUTION ACCOUNT

**Conclusions:** For the first time, the strength of more than 300 noncovalent interactions, including halogen, chalcogen, and pnictogen bonds in neutral, cationic, and anionic systems was determined quantitatively utilizing local stretching force constants, which measure the strength of a bond without changing its electronic structure. The stretching force constant can be directly related to measured or calculated frequencies. This analysis was complemented by the investigation of binding energies, geometries, NBO charges, charge transfer values, dipole moments, electrostatic potentials, electron and energy density distributions, difference density distributions. As a result, a detailed description of the many electronic effects responsible for the strength of these noncovalent interactions was obtained. Leading to important new insights, and to the following conclusions:

1. Halogen bonds are highly tunable interactions. By varying the polarizability of the halogen, the polarity of the halogen donor bond and the electron donor ability of the Lewis base, binding energies ranging from 1 to 45 kcal/mol are obtained. Halogen bonds can be stronger than hydrogen chalcogen and pnictogen bonds for both neutral and charged complexes.
2. Halogen, chalcogen and pnictogen bonds are found to vary from weak electrostatic to strong and covalent. The strength of these interactions increases in a way that three-center four-electron bonding becomes possible.
3. The covalent character of halogen, chalcogen, and pnictogen bonds is usually characterized by the charge transfer from the lone pair of the heteroatom of a Lewis base to the  $\sigma^*(YX)$  orbital, X is a halogen, chalcogen or pnictogen and Y is a substituent covalently bond to X. However, in  $sp^2$  hybridized chalcogens the charge transfer involves a

$\pi^*(\text{YX})$  orbital instead of a  $\sigma^*(\text{YX})$ . A new type of chalcogen bonded homodimer was found by exploring the charge transfer mechanism characteristic of  $\text{sp}^2$  chalcogens.

4. Halogen bonds formed with metal halogen acceptor are found to be sensitive to small changes in the electronic structure of the complex. Different substituent at the halogen donor or acceptor can make the metal-halogen interaction changes from a typical halogen bond into a nonclassical 3c-4e bonding, or even into a metal-halide bond. Scalar relativistic expansion of d orbitals of gold favors the formation of stronger halogen bonds. This is also likely to occur for Pt and Ir complexes.
5. A bonding mechanism based on the two most common conformations adopted halogen, chalcogen and pnictogen bonded complex was derived. This mechanism correctly predicts the possible formation of noncovalent interactions that are neither chalcogen bonds or pnictogen bonds but an admixture of both bond types.
6. The intrinsic strength of a series of noncovalent interactions, given by  $k^a$  or BSO values, was related to other quantities, such as interatomic distances, binding energies, interaction energies, energy and electron density values at the electron density critical point, and electrostatic potentials [5, 33, 35, 36]. Qualitative correlations are observed only for a small set of similar complexes. If a diverse set of complexes is considered, the correlations become much too scattered. Although these quantities are useful to discuss specific electronic effects, they do not reflect the intrinsic strength of the noncovalent interactions.
7. Based on the systematic study of more than three hundred XB, ChB, and PnB complexes described in this thesis, a general protocol for the analysis of noncovalent interactions was formulated (chapter 2). This protocol not only systematizes the analysis of the strength and nature of noncovalent interactions but also facilitates the identification of electronic effects that contributes to their strength.

In addition to the study of noncovalent interactions, we also investigated the stability of small planar gold clusters. In this study we derived a new quantitative parameter to

measure  $\sigma$ -delocalization in metal clusters by extended the definition of Cremer and coworkers aromaticity index (AI) [31, 32]. We also suggested a general building principle to explain the preferred conformation adopted by small planar gold cluster based on the formation of the structure with the highest number of  $\text{Au}_3$  subunits with dominant 3c-2e character.

**Impact of this study:** The new insights presented on this thesis, and the results presented on papers I-VI are expected to have a positive impact on:

1. The understanding of the role of electrostatic and covalent contributions involved in the formation of various types of noncovalent interactions and how the strength of these interactions can be fine tuned.
2. Development of new halogen, chalcogen, pnictogen bonded materials. The detailed analysis of the strength of noncovalent interactions presented on papers I-V can contribute to a more rational design of new materials held by stronger noncovalent interactions. The new type of interaction describe on paper IV can also lead to novel material with unique electronic and structural features.
3. Strategies for the design of novel materials. The bonding mechanism derived on paper V, not only leads to a more general description of different types of noncovalent interactions formed by halogen, chalcogen, and pnictogen atoms but can also be exploited for a conformationally driven design of new materials.
4. The development of more reliable DFTs and force field parameters. These can take advantage of the high accurate data provided on papers I and V and the large and systematic amount of data on halogen and chalcogen bonds provided on paper II, IV.
5. Experimental detection of noncovalent interactions. On paper I, II and IV, the normal vibrational frequencies with the highest local stretching character are provided to help experimentalist identifying the peaks associated to these noncovalent interaction in the experimental vibrational spectra. These can only be measured by modern spectroscopic

methods such as depolarized Raman scattering and Terahertz spectroscopy, which can measure vibrational frequencies down to  $50\text{ cm}^{-1}$ .

6. The understanding of the role of  $\sigma$ -delocalization in the formation of stable metal clusters.

**Future perspectives:** In addition to the suggestions of new materials provided at the end of chapters 4, 5, and 6. Future studies should use the protocol proposed on chapter 2 to investigate tetrel bonds [101], aerogen bonds [102], aurophilic interactions [103], beryllium and magnesium bonds [104, 105], agostic and anagostic interactions [106], and cation- $\pi$  interactions [107]. A detailed description of these noncovalent interactions could lead to the development of new materials, better catalysts, new insight on biochemical processes, improved parameters for molecular mechanic force fields, and to a general understanding of noncovalent interactions. The protocol discussed on chapter 2, together with the analysis of 3c-4e character of a bond could also be used to investigate hypervalent iodine reagents, which can lead to the development of improved oxidizing agents. Future studies should also investigate cooperative, effects in noncovalent interactions. In our studies we saw that a secondary hydrogen bond could enhance the strength of the halogen bond in  $\text{FCl}\cdots\text{NH}_2\text{OH}$  and  $\text{FCl}\cdots\text{PH}_2\text{OH}$  complex. Similar effects are found in other systems. Cooperative effects are found also in halogen, chalcon, pnictogen bonded polymers [108]. The local stretching force constant is an ideal tool to investigate how the intrinsic strength of these noncovalent interactions changes as the size of the polymer increases.

**Ongoing projects:** Currently, three projects are still being pursued (most calculations are finished and a manuscript for each project is being prepared): i) The oxidative addition of dihalogens to 16  $d^8$  transition metal pincer complexes are being analyzed. ii) The strength and 3c-4e bond character in 36 hypervalent iodine complexes are being analyzed. iii) The strength of agostic bonds, involving early (Ti, Zr, Hf) and late transition metals (Co, Rh, Ir, Ni, Pd, Pt) in 46 complexes are being investigated.

**Contribution account:** All calculations, tables and figures reported on papers I - VI were

done by me. The only exceptions are the NICS, ELF, and energy gap values and the figures and tables related to these properties on paper VI. I also draft the manuscript of papers I - V, and on paper VI, I helped with part of the discussion of the results related to energy-based, vibrational, and electron density properties.

**Calculations done:** During this thesis a total of 17,670 single calculations were performed, which added up to a total CPU-time of approximately 147.8 CPU years (time required to run all calculations sequentially in a single-core CPU). These calculations involved the study of about 685 different molecular systems. This work also involved the use of 13 different software packages and a variety of different quantum mechanical methods as follows:

Highly accurate CCSD(T)/aug-cc-pVTZ [109–111] calculations of energies, geometries and harmonic frequencies of 76 different complexes, plus 38 monomers were carried out with CFOUR [112] (papers I and V). In addition, single-point energies necessary for the calculation of binding energies involving 315 complexes, plus 145 monomers were done at CCSD(T)/aug-cc-pVTZ level utilizing CFOUR, Gaussian [113], and MolPro [114] softwares. The 8 largest complexes of paper II was calculated with DLPNO-CCSD(T) [66, 67] approximation on ORCA [115] software. Less computationally demanding DFT and MP2 [116] calculations were carried out in Gaussian 09. These comprises the calculation of energies, geometries and frequencies of more than 330 complexes.

A series of exchange-correlation functionals were tested to guide our choice of the most appropriated functional for each study (paper II - IV): i) for noncovalent interactions  $\omega$ B97X [117, 118],  $\omega$ B97XD, M06-2X [119], B3LYPD [120, 121] and B2PLYPD [122] were tested. ii) for studies involving Au and other metals  $\omega$ B97XD, M06-2X, M06 [119], PBE [123], TPSS [124] and B3LYP were tested. All DFT calculation were done with an ultrafine or superfine integration grid [125]. Calculations involving relativistic atom (I, At, Te, Sn, Au) were carried out with relativistic effect core potentials [126–128] (ECPs) in papers II, IV and VI. In paper III, we utilized, for the first time, the normalized elimination of the small component (NESC) [34], an all-electron Diract-exact relativistic method, for the study of halogen bonds. This comprised of 29 metal halogen bonded complexes. Although ECPs

can give qualitatively correct energetic and vibrational properties for these complexes, the calculation of difference densities to evaluate relativistic effects required the NESC method.

**Molecular properties investigated:** Several other software packages were employed for the calculation of molecular properties. Local vibrational mode analysis was carried out with COLOGNE [129], natural bond orbital analysis was done with NBO 6 [60]. Topological electronic density analysis was done with AIMAll [130] and Multiwfn [131]. Electron densities and electrostatic potentials were generated with Multiwfn. Energy decomposition utilizing symmetry-adapted perturbation theory [55] (SAPT) was done in MolPro. The Molden2AIM script [132], was used to transform the molecular wavefunctions written in MOLDEN file format obtained from CFOUR into WFN file format. Electron difference density plots were generated with Chimera [133] and VMD [134], Hartree-Fock orbitals and natural localized molecular orbital (NLMOs) were plotted with Avogadro [135], and electrostatic potentials were mapped onto electron density surfaces with Gaussview.

## REFERENCES

- [1] Steve Scheiner. *Noncovalent Forces*, pages 1–11. Springer International Publishing, 2015.
- [2] Robert R. Knowles and Eric N. Jacobsen. Attractive noncovalent interactions in asymmetric catalysis: Links between enzymes and small molecule catalysts. *Proc. Natl. Acad. Sci.*, 107(48):20678–20685, 2010.
- [3] M. Morgan Conn and Julius Rebek. Self-assembling capsules. *Chem. Rev.*, 97(5):1647–1668, 1997. PMID: 11851461.
- [4] Caterina Bissantz, Bernd Kuhn, and Martin Stahl. A medicinal chemist’s guide to molecular interactions. *J. Med. Chem.*, 53(14):5061–5084, 2010.
- [5] Vytor Oliveira, Elfi Kraka, and Dieter Cremer. The intrinsic strength of the halogen bond: Electrostatic and covalent contributions described by coupled cluster theory. *Phys. Chem. Chem. Phys.*, 18:33031–33046, 2016.
- [6] Steve Scheiner. Detailed comparison of the pnictogen bond with chalcogen, halogen, and hydrogen bonds. *Int. J. Quantum Chem.*, 113(11):1609–1620, 2013.
- [7] Pierangelo Metrangolo, Hannes Neukirch, Tullio Pilati, and Giuseppe Resnati. Halogen bonding based recognition processes: A world parallel to hydrogen bonding. *Acc. Chem. Res.*, 38(5):386–395, 2005.
- [8] Kamran T. Mahmudov, Maximilian N. Kopylovich, M. Fatima C. Guedes da Silva, and Armando J. L. Pombeiro. Chalcogen bonding in synthesis, catalysis and design of materials. *Dalton Trans.*, 46:10121–10138, 2017.
- [9] Michio Iwaoka, Shinya Takemoto, and Shuji Tomoda. Statistical and theoretical investigations on the directionality of nonbonded S···O interactions. Implications for molecular design and protein engineering. *J. Am. Chem. Soc.*, 124(35):10613–10620, 2002.

- [10] Rainer Wilcken, Markus O. Zimmermann, Andreas Lange, Andreas C. Joerger, and Frank M. Boeckler. Principles and applications of halogen bonding in medicinal chemistry and chemical biology. *J. Med. Chem.*, 56(4):1363–1388, 2013.
- [11] Gabriella Cavallo, Pierangelo Metrangolo, Roberto Milani, Tullio Pilati, Arri Priimagi, Giuseppe Resnati, and Giancarlo Terraneo. The halogen bond. *Chem. Rev.*, 116(4):2478–2601, 2016.
- [12] D. Setiawan, E. Kraka, and D. Cremer. Reevaluation of the bond length - bond strength rule: The stronger bond is not always the shorter bond. *J. Comput. Chem.*, 37:130–142, 2016.
- [13] Dieter Cremer and Elfi Kraka. From molecular vibrations to bonding, chemical reactions, and reaction mechanism. *Current Organic Chemistry*, 14(15):1524–1560, 2010.
- [14] W. Zou and D Cremer.  $C_2$  in a box: Determining its intrinsic bond strength for the  $X^1\Sigma_g^+$  ground state. *Chem. Eur. J.*, 22:4087–4089, 2016.
- [15] Z. Konkoli and D. Cremer. A new way of analyzing vibrational spectra I. Derivation of adiabatic internal modes. *Int. J. Quantum. Chem.*, 67:1–11, 1998.
- [16] W. Zou, R. Kalescky, E. Kraka, and D. Cremer. Relating normal vibrational modes to local vibrational modes with the help of an adiabatic connection scheme. *J. Chem. Phys.*, 137:084114, 2012.
- [17] Alan Humason, Wenli Zou, and Dieter Cremer. 11,11-dimethyl-1,6-methano[10]annulene - an annulene with an ultralong cc bond or a fluxional molecule? *J. Phys. Chem. A*, 119(9):1666–1682, 2015.
- [18] Kalescky, R. and Zou, W. and Kraka, E. and Cremer, D. Quantitative Assessment of the Multiplicity of Carbon-Halogen Bonds: Carbenium and Halonium Ions with F, Cl, Br, I. *J. Phys. Chem. A*, 118:1948–1963, 2014.
- [19] Elfi Kraka and Dieter Cremer. Characterization of cf bonds with multiple-bond character: Bond lengths, stretching force constants, and bond dissociation energies. *ChemPhysChem*, 10(4):686–698, 2009.

- [20] R. Kalescky, E. Kraka, and D. Cremer. Identification of the strongest bonds in chemistry. *J. Phys. Chem. A*, 117:8981–8995, 2013.
- [21] Marek Freindorf, Elfi Kraka, and Dieter Cremer. A comprehensive analysis of hydrogen bond interactions based on local vibrational modes. *Int. J. Quantum Chem.*, 112(19):3174–3187, 2012.
- [22] R. Kalescky, E. Kraka, and D. Cremer. Local vibrational modes of the formic acid dimer - the strength of the double hydrogen bond. *Mol. Phys.*, 111:1497–1510, 2013.
- [23] R. Kalescky, W. Zou, E. Kraka, and D. Cremer. Local vibrational modes of the water dimer - comparison of theory and experiment. *Chem. Phys. Lett.*, 554:243–247, 2012.
- [24] R. Kalescky, W. Zou, E. Kraka, and D. Cremer. Vibrational properties of the isotopomers of the water dimer derived from experiment and computations. *Aust. J. Chem.*, 67:426–434, 2014.
- [25] Dani Setiawan, Elfi Kraka, and Dieter Cremer. Strength of the pnictogen bond in complexes involving group va elements n, p, and as. *J. Phys. Chem. A*, 119(9):1642–1656, 2015.
- [26] Dani Setiawan and Dieter Cremer. Super-pnictogen bonding in the radical anion of the fluorophosphine dimer. *Chem. Phys. Lett.*, 662:182 – 187, 2016.
- [27] X. Zhang, H. Dai, H. Yan W. Zou, and D Cremer. B-H $\cdots\pi$  interaction: A new type of nonclassical hydrogen bonding. *J. Am. Chem. Soc.*, 138:4334–4337, 2016.
- [28] Yunwen Tao, Wenli Zou, Junteng Jia, Wei Li, and Dieter Cremer. Different ways of hydrogen bonding in water - Why does warm water freeze faster than cold water? *J. Chem. Theory Comput.*, 13(1):55–76, 2017.
- [29] Robert Kalescky, Elfi Kraka, and Dieter Cremer. New approach to tolmans electronic parameter based on local vibrational modes. *Inorg. Chem.*, 53(1):478–495, 2014.

- [30] Dani Setiawan, Robert Kalescky, Elfi Kraka, and Dieter Cremer. Direct measure of metal-ligand bonding replacing the tolman electronic parameter. *Inorg. Chem.*, 55(5):2332–2344, 2016.
- [31] Dani Setiawan, Elfi Kraka, and Dieter Cremer. Quantitative assessment of aromaticity and antiaromaticity utilizing vibrational spectroscopy. *J. Org. Chem.*, 81(20):9669–9686, 2016.
- [32] R. Kalescky, E. Kraka, and D. Cremer. Description of aromaticity with the help of vibrational spectroscopy: Anthracene and phenanthrene. *J. Phys. Chem. A*, 118:223–237, 2014.
- [33] Vytor Oliveira, Elfi Kraka, and Dieter Cremer. Quantitative assessment of halogen bonding utilizing vibrational spectroscopy. *Inorg. Chem.*, 56(1):488–502, 2017.
- [34] W. Zou, M. Filatov, and D. Cremer. An Improved Algorithm for the Normalized Elimination of the Small-Component Method. *Theor. Chem. Acc.*, 130:633–644, 2011.
- [35] Vytor Oliveira and Dieter Cremer. Transition from metal-ligand bonding to halogen bonding involving a metal as halogen acceptor a study of cu, ag, au, pt, and hg complexes. *Chem. Phys. Lett.*, 681:56 – 63, 2017.
- [36] Vytor Oliveira, Dieter Cremer, and Elfi Kraka. The many facets of chalcogen bonding: Described by vibrational spectroscopy. *J. Phys. Chem. A*, 121(36):6845–6862, 2017.
- [37] Yanle Li, Vytor Oliveira, Chunmei Tang, Dieter Cremer, Chunyan Liu, and Jing Ma. The peculiar role of the  $\text{Au}_3$  unit in  $\text{au}_m$  clusters:  $\sigma$ -aromaticity of the  $\text{Au}_5\text{Zn}^+$  ion. *Inorg. Chem.*, 56(10):5793–5803, 2017.
- [38] E. B. Wilson, J. C. Decius, and P. C. Cross. *Molecular vibrations. The theory of infrared and Raman vibrational spectra*. McGraw-Hill, New York, 1955.
- [39] Dieter Cremer and Elfi Kraka. Generalization of the tolman electronic parameter: The metal-ligand electronic parameter and the intrinsic strength of the metal-ligand bond. *Dalton Trans.*, 46:8323–8338, 2017.

- [40] D. C. McKean. Individual CH Bond Strengths in Simple Organic Compounds: Effects of Conformation and Substitution. *Chem. Soc. Rev.*, 7:399–422, 1978.
- [41] J. A. Larsson and D. Cremer. Theoretical verification and extension of the McKean relationship between bond lengths and stretching frequencies. *J. Mol. Struct.*, 485:385–407, 1999.
- [42] Bryan R. Henry. The Local Mode Model and Overtone Spectra: A Probe of Molecular Structure and Conformation. *Acc. Chem. Res.*, 20:429–435, 1987.
- [43] Elfi Kraka, J. Andreas Larsson, and Dieter Cremer. Generalization of the badger rule based on the use of adiabatic vibrational modes in vibrational modes in computational IR spectroscopy. In Jörg Grunenberg, editor, *Computational spectroscopy: Methods, experiments and applications*, pages 105–149. Wiley, New York, 2010.
- [44] D. Cremer and E. Kraka. From Molecular Vibrations to Bonding, Chemical Reactions, and Reaction Mechanism. *Curr. Org. Chem.*, 14:1524–1560, 2010.
- [45] R. P. Feynman. Forces in molecules. *Phys. Rev.*, 56:340–343, Aug 1939.
- [46] Peter Politzer, Jane S. Murray, and Timothy Clark. Halogen bonding and other  $\sigma$ -hole interactions: a perspective. *Phys. Chem. Chem. Phys.*, 15:11178–11189, 2013.
- [47] T. Clark, P. Politzer, and Jane S. Murray. Correct electrostatic treatment of noncovalent interactions: the importance of polarization. *WIREs Comp. Mol. Sci.*, 5:169–177, 2015.
- [48] Jane S. Murray and Peter Politzer. Molecular electrostatic potentials and noncovalent interactions. *WIREs Comput. Mol. Sci.*, pages n/a–n/a.
- [49] Timothy Clark. Polarization, donor-acceptor interactions, and covalent contributions in weak interactions: A clarification. *J. Mol. Model.*, 23(10):297, Sep 2017.
- [50] Timothy Clark. Halogen bonds and  $\sigma$ -holes. *Faraday Discuss.*, pages –, 2017.
- [51] Robert S. Mulliken. Structures of complexes formed by halogen molecules with aromatic and with oxygenated solvents. *J. Am. Chem. Soc.*, 72(1):600–608, 1950.

- [52] Lando P. Wolters, Patric Schyman, Mariela J. Pavan, William L. Jorgensen, F. Matthias Bickelhaupt, and Sebastian Kozuch. The many faces of halogen bonding: a review of theoretical models and methods. *WIREs Comput. Mol. Sci.*, 4(6):523–540, 2014.
- [53] Marcin Palusiak. On the nature of halogen bond - the kohn-sham molecular orbital approach. *J. Mol. Struct. THEOCHEM*, 945(1-3):89 – 92, 2010.
- [54] Balazs Pinter, Nick Nagels, Wouter A. Herrebout, and Frank DeProft. Halogen bonding from a hard and soft acids and bases perspective: Investigation by using density functional theory reactivity indices. *Chem. Europ. J.*, 19(2):519–530, 2013.
- [55] Krzysztof Szalewicz. Symmetry-adapted perturbation theory of intermolecular forces. *WIREs Comput. Mol. Sci.*, 2(2):254–272, 2012.
- [56] Anthony J. Stone. Are halogen bonded structures electrostatically driven? *J. Am. Chem. Soc.*, 135(18):7005–7009, 2013.
- [57] Richard F. W. Bader, Marshall T. Carroll, James R. Cheeseman, and Cheng Chang. Properties of atoms in molecules: atomic volumes. *J. Am. Chem. Soc.*, 109(26):7968–7979, 1987.
- [58] K. Ruedenberg. The Physical Nature of the Chemical Bond. *Rev. Mod. Phys.*, 34:326–352, 1962.
- [59] Michael W. Schmidt, Joseph Ivancic, and Klaus Ruedenberg. Covalent bonds are created by the drive of electron waves to lower their kinetic energy through expansion. *J. Chem. Phys.*, 140(20):204104, 2014.
- [60] F. Weinhold and C. R. Landis. *Valency and bonding: A natural bond orbital donor-acceptor perspective*. Cambridge University Press, Cambridge, UK, 2003.
- [61] E. Kraka and D. Cremer. Chemical Implication of Local Features of the Electron Density Distribution. In Z.B. Maksic, editor, *Theoretical models of chemical bonding. The concept of the chemical bond, Vol 2*, pages 453–542. Springer Verlag, Heidelberg, Germany, 1990.

- [62] Desiraju, Gautam R. and Ho, P. Shing and Kloo, Lars and Anthony C. Legon and Roberto Marquardt and Metrangolo, Pierangelo and Politzer, Peter and Resnati, Giuseppe and Rissanen, Kari . Definition of the halogen bond (iupac recommendations 2013), 2013.
- [63] Rosa Bailey Walsh, Clifford W. Padgett, Pierangelo Metrangolo, Giuseppe Resnati, T. W. Hanks, and William T. Pennington. Crystal engineering through halogen bonding: Complexes of nitrogen heterocycles with organic iodides. *Cryst. Growth Des.*, 1(2):165–175, 2001.
- [64] Pascal Auffinger, Franklin A. Hays, Eric Westhof, and P. Shing Ho. Halogen bonds in biological molecules. *Proc. Natl. Acad. Sci. U.S.A*, 101(48):16789–16794, 2004.
- [65] Matthew R. Scholfield, Crystal M. Vander Zanden, Megan Carter, and P. Shing Ho. Halogen bonding (x-bonding): A biological perspective. *Protein Science*, 22(2):139–152, 2013.
- [66] Christoph Riplinger and Frank Neese. An efficient and near linear scaling pair natural orbital based local coupled cluster method. *J. Chem. Phys.*, 138(3), 2013.
- [67] Christoph Riplinger, Barbara Sandhoefer, Andreas Hansen, and Frank Neese. Natural triple excitations in local coupled cluster calculations with pair natural orbitals. *J. Chem. Phys.*, 139(13), 2013.
- [68] Gilles Berger, Jalal Soubhye, and Franck Meyer. Halogen bonding in polymer science: from crystal engineering to functional supramolecular polymers and materials. *Polym. Chem.*, 6:3559–3580, 2015.
- [69] Dominik Cincic, Tomislav Friscic, and William Jones. Isostructural materials achieved by using structurally equivalent donors and acceptors in halogen-bonded cocrystals. *Chem. Eur. J.*, 14(2):747–753, 2008.
- [70] Lydia C. Gilday, Sean W. Robinson, Timothy A. Barendt, Matthew J. Langton, Benjamin R. Mullaney, and Paul D. Beer. Halogen bonding in supramolecular chemistry. *Chem. Rev.*, 115(15):7118–7195, 2015.

- [71] Oliver Dumele, Nils Trapp, and François Diederich. Halogen bonding molecular capsules. *Angew. Chem. Int. Ed. Engl.*, 54(42):12339–12344, 2015.
- [72] Catherine Perkins, Stefano Libri, Harry Adams, and Lee Brammer. Diiodoacetylene: compact, strong ditopic halogen bond donor. *Cryst. Eng. Comm.*, 14:3033–3038, 2012.
- [73] Liang Luo, Christopher Wilhelm, Aiwu Sun, Clare P. Grey, Joseph W. Lauher, and Nancy S. Goroff. Poly(diiododiacetylene): Preparation, isolation, and full characterization of a very simple poly(diacetylene). *J. Am. Chem. Soc.*, 130(24):7702–7709, 2008.
- [74] Nancy S. Goroff, Sean M. Curtis, Jeffrey A. Webb, Frank W. Fowler, , and Joseph W. Lauher. Designed cocrystals based on the pyridine-iodoalkyne halogen bond. *Org. Lett.*, 7(10):1891–1893, 2005.
- [75] Oliver Dumele, Dino Wu, Nils Trapp, Nancy Goroff, and François Diederich. Halogen bonding of (iodoethynyl)benzene derivatives in solution. *Org. Lett.*, 16(18):4722–4725, 2014.
- [76] Lee Brammer, Guillermo Minguez Espallargas, and Stefano Libri. Combining metals with halogen bonds. *CrystEngComm.*, 10:1712–1727, 2008.
- [77] Roberta Bertani, Paolo Sgarbossa, Alfonso Venzo, Francesco Lejl, Mario Amati, Giuseppe Resnati, Tullio Pilati, Pierangelo Metrangolo, and Giancarlo Terraneo. Halogen bonding in metal-organic-supramolecular networks. *Coord. Chem. Rev.*, 254(5-6):677 – 695, 2010. A Tribute to Fausto Calderazzo on the Occasion of his 80th Birthday.
- [78] Daniil M. Ivanov, Alexander S. Novikov, Ivan V. Ananyev, Yulia V. Kirina, and Vadim Yu. Kukushkin. Halogen bonding between metal centers and halocarbons. *Chem. Commun.*, 52:5565–5568, 2016.
- [79] Bo Lu, Xueying Zhang, Ling Peng Meng, and Yanli L. Zeng. The Pt (II)···Cl Interactions: Nature and Strength. *ChemistrySelect*, 1(18):5698–5705, 2016.

- [80] Meng Gao, Qingzhong Li, Hai-Bei Li, Wenzuo Li, and Jianbo Cheng. How do organic gold compounds and organic halogen molecules interact? comparison with hydrogen bonds. *RSC Adv.*, 5:12488–12497, 2015.
- [81] Johannus A. M. Van Beek, Gerard. Van Koten, Wilberth J. J. Smeets, and Anthony L. Spek. Model for the initial stage in the oxidative addition of I<sub>2</sub> to organoplatinum(II) compounds. X-ray structure of square-pyramidal [Pt<sup>II</sup>IC<sub>6</sub>H<sub>3</sub>(CH<sub>2</sub>NMe<sub>2</sub>)<sub>2</sub>-o,o'(η<sup>1</sup> - I<sub>2</sub>)] containing a linear Pt-I-I arrangement. *J. Am. Chem. Soc.*, 108(16):5010–5011, 1986.
- [82] Andrey Yu. Rogachev and Roald Hoffmann. Iodine (I<sub>2</sub>) as a janus-faced ligand in organometallics. *J. Am. Chem. Soc.*, 135(8):3262–3275, 2013.
- [83] D. Cremer, W. Zou, and M. Filatov. Dirac-exact relativistic methods: The normalized elimination of the small component method. *WIREs Comput. Mol. Sci.*, 4:436–467, 2016.
- [84] Francesco Devillanova and Wolf-Walther Du Mont, editors. *Handbook of chalcogen chemistry*. The Royal Society of Chemistry, 2013.
- [85] Brett R. Beno, Kap-Sun Yeung, Michael D. Bartberger, Lewis D. Pennington, and Nicholas A. Meanwell. A survey of the role of noncovalent sulfur interactions in drug design. *J. Med. Chem.*, 58(11):4383–4438, 2015.
- [86] Yoshimitsu Nagao, Terukage Hirata, Satoru Goto, Shigeki Sano, Akikazu Kakehi, Kinji Iizuka, and Motoo Shiro. Intramolecular nonbonded s · · · o interaction recognized in (acylimino)thiadiazoline derivatives as angiotensin ii receptor antagonists and related compounds. *J. Am. Chem. Soc.*, 120(13):3104–3110, 1998.
- [87] Sajesh P Thomas, K Satheeshkumar, Govindasamy Mugesh, and T N Guru Row. Unusually short chalcogen bonds involving organoselenium: Insights into the Se-N Bond cleavage mechanism of the antioxidant ebselen and analogues. *Chem. Eur. J.*, 21(18):6793–6800, 2015.

- [88] Rolf Gleiter and Daniel B Werz. Elastic cycles as flexible hosts: How tubes built by cyclic chalcogenaalkynes individually host their guests. *Chem. Lett.*, 34(2):126–131, 2005.
- [89] Anthony F. Cozzolino, Qin Yang, and Ignacio Vargas-Baca. Engineering second-order nonlinear optical activity by means of a noncentrosymmetric distortion of the [te-n]<sub>2</sub> supramolecular synthon. *Cryst. Growth Des.*, 10(11):4959–4964, 2010.
- [90] Anthony F. Cozzolino, Philip J.W. Elder, and Ignacio Vargas-Baca. A survey of tellurium-centered secondary-bonding supramolecular synthons. *Coord. Chem. Rev.*, 255(11-12):1426 – 1438, 2011.
- [91] Tristram Chivers and Risto S Laitinen. Tellurium: A maverick among the chalcogens. *Chem. Soc. Rev.*, 44(7):1725–1739, 2015.
- [92] Haruta Masatake, Kobayashi Tetsuhiko, Sano Hiroshi, and Yamada Nobumasa. Novel gold catalysts for the oxidation of carbon monoxide at a temperature far below 0°. *Chem. Lett.*, 16(2):405–408, 1987.
- [93] Steeve Chretien, Steven K. Buratto, and Horia Metiu. Catalysis by very small au clusters. *Curr. Opin. Solid State Mater. Sci.*, 11(5):62 – 75, 2007.
- [94] Peter Johnston, Nicholas Carthey, and Graham J. Hutchings. Discovery, development, and commercialization of gold catalysts for acetylene hydrochlorination. *J. Am. Chem. Soc.*, 137(46):14548–14557, 2015.
- [95] Luis M. Molina and Julio A. Alonso. Chemical properties of small au clusters: An analysis of local site reactivity. *J. Phys. Chem. C*, 111(18):6668–6677, 2007.
- [96] Satyender Goel, Kirill A. Velizhanin, Andrei Piryatinski, Sergei A. Ivanov, and Sergei Tretiak. Ligand effects on optical properties of small gold clusters: A tddft study. *J. Phys. Chem. C*, 116(5):3242–3249, 2012.
- [97] Pyykko Pekka. Magic nanoclusters of gold. *Nat. Nanotechnol.*, 2:273–274, 2007.

- [98] J.P. Desclaux and P. Pyykko. Dirac-fock one-centre calculations. the molecules  $\text{CuH}$ ,  $\text{AgH}$  and  $\text{AuH}$  including p-type symmetry functions. *Chemical Physics Letters*, 39(2):300 – 303, 1976.
- [99] Pekka Pyykko. Theoretical chemistry of gold. *Angew. Chem. Int. Ed.*, 43(34):4412–4456, 2004.
- [100] Hiromasa Tanaka, Sven Neukermans, Ewald Janssens, Roger E. Silverans, and Peter Lievens.  $\sigma$  aromaticity of the bimetallic  $\text{Au}_5\text{Zn}^+$  cluster. *J. Am. Chem. Soc.*, 125(10):2862–2863, 2003.
- [101] Antonio Bauzá, Tiddo J. Mooibroek, and Antonio Frontera. Tetrel-bonding interaction: Rediscovered supramolecular force? *Angew. Chem. Int. Ed.*, 52(47):12317–12321, 2013.
- [102] Antonio Bauzá and Antonio Frontera. Aerogen bonding interaction: A new supramolecular force? *Angew. Chem. Int. Ed.*, 54(25):7340–7343, 2015.
- [103] Hubert Schmidbaur and Annette Schier. Auophilic interactions as a subject of current research: an up-date. *Chem. Soc. Rev.*, 41:370–412, 2012.
- [104] Otilia Mó, Manuel Yáñez, Ibon Alkorta, and José Elguero. Modulating the strength of hydrogen bonds through beryllium bonds. *J. Chem. Theory Comput.*, 8(7):2293–2300, 2012.
- [105] Rizalina Tama, Otilia Mó, Manuel Yáñez, and M. Merced Montero-Campillo. Characterizing magnesium bonds: main features of a non-covalent interaction. *Theor. Chem. Acc.*, 136(3):36, Feb 2017.
- [106] Maurice Brookhart, Malcolm L. H. Green, and Gerard Parkin. Agostic interactions in transition metal compounds. *Proc. Natl. Acad. Sci.*, 104(17):6908–6914, 2007.
- [107] Dennis A. Dougherty. The cation- $\pi$  interaction. *Acc.Chem. Res.*, 46(4):885–893, 2013.

- [108] Dario J.R. Duarte, Emilio L. Angelina, and Nelida M. Peruchena. Physical meaning of the qtain topological parameters in hydrogen bonding. *J. of Mol. Model.*, 20(11), 2014.
- [109] III Purvis, G. D. and R. J. Bartlett. A Full Coupled-Cluster Singles and Doubles Model: The Inclusion of Disconnected Triples. *J. Chem. Phys.*, 76(4):1910–1918, 1982.
- [110] T.H. Dunning Jr. Gaussian Basis Sets for Use in Correlated Molecular Calculations. I. The Atoms Boron Through Neon and Hydrogen. *J. Chem. Phys.*, 90:1007–1023, 1989.
- [111] D.E. Woon and T.H. Dunning Jr. Gaussian Basis Sets for Use in Correlated Molecular Calculations. III. The Atoms Aluminum Through Argon. *J. Chem. Phys.*, 98:1358–1371, 1993.
- [112] J. F. Stanton, J. Gauss, M. E. Harding, and P. G. Szalay. CFOUR, A quantum chemical program package, 2010. see <http://www.cfour.de> (accessed Nov 10, 2017).
- [113] M. J. Frisch, G. W. Trucks, H. B. Schlegel, G. E. Scuseria, M. A. Robb, J. R. Cheeseman, G. Scalmani, V. Barone, B. Mennucci, G. A. Petersson, and et al. Gaussian 09 revision C. 1, 2010. Gaussian Inc., Wallingford, CT.
- [114] H. J. Werner, P. J. Knowles, G. Knizia, F. R. Manby, M. Schütz, P. Celani, T. Korona, R. Lindh, A. Mitrushenkov, G. Rauhut, and et al. MOLPRO, Version 2010. 1. A package of ab initio programs, 2010. see <http://www.molpro.net> (accessed Nov 10, 2017).
- [115] Frank Neese. The orca program system. *Wiley Interdisciplinary Reviews: Computational Molecular Science*, 2(1):73–78, 2012.
- [116] Chr. Møller and M. S. Plesset. Note on an approximation treatment for many-electron systems. *Phys. Rev.*, 46:618–622, Oct 1934.
- [117] Head-Gordon M. Chai J. D. Long-range corrected hybrid density functionals with damped atom-atom dispersion corrections. *Phys. Chem. Chem. Phys.*, 10:6615, 2008.

- [118] Head-Gordon M. Chai J. D. Systematic optimization of long-range corrected hybrid density functionals. *J. Chem. Phys.*, 128:084106, 2008.
- [119] Yan Zhao and Donald G. Truhlar. The m06 suite of density functionals for main group thermochemistry, thermochemical kinetics, noncovalent interactions, excited states, and transition elements: Two new functionals and systematic testing of four m06-class functionals and 12 other functionals. *Theor. Chem. Acc.*, 120(1):215–241, 2008.
- [120] A. D. Becke. Density-functional thermochemistry. III. The role of exact exchange. *J. Chem. Phys.*, 98:5648–5652, 1993.
- [121] P. J. Stevens, F. J. Devlin, C. F. Chabrowski, and M. J. Frisch. Ab initio calculation of vibrational absorption and circular dichroism spectra using density functional force fields. *J. Phys. Chem.*, 98:11623–11627, 1994.
- [122] Stefan Grimme and Frank Neese. Double-hybrid density functional theory for excited electronic states of molecules. *J. of Chem.Phys.*, 127(15):154116, 2007.
- [123] C. Adamo and V. Barone. Toward reliable density functional methods without adjustable parameters: The PBE0 model. *J. Chem. Phys.*, 110:6158–6169, 1999.
- [124] Jianmin Tao, John P. Perdew, Viktor N. Staroverov, and Gustavo E. Scuseria. Climbing the density functional ladder: Nonempirical meta-generalized gradient approximation designed for molecules and solids. *Phys. Rev. Lett.*, 91:146401, Sep 2003.
- [125] Cremer D. Grafenstein J. Efficient dft integrations by locally augmented radial grids. *J. Chem. Phys.*, 127:164113, 2007.
- [126] Kirk A. Peterson, Benjamin C. Shepler, Detlev Figgen, and Hermann Stoll. On the spectroscopic and thermochemical properties of clo, bro, io, and their anions. *J. Phys. Chem. A*, 110(51):13877–13883, 2006.
- [127] Kirk A. Peterson. Systematically convergent basis sets with relativistic pseudopotentials. i. correlation consistent basis sets for the post-d group 13-15 elements. *J. Chem. Phys.*, 119(21):11099–11112, 2003.

- [128] Kirk A. Peterson, Detlev Figgen, Erich Goll, Hermann Stoll, and Michael Dolg. Systematically convergent basis sets with relativistic pseudopotentials. ii. small-core pseudopotentials and correlation consistent basis sets for the post-d group 16-18 elements. *J. Chem. Phys.*, 119(21):11113–11123, 2003.
- [129] E. Kraka, W. Zou, M. Filatov, J. Grafenstein, D. Izotov, J. Gauss, Y. He, A. Wu, Z. Konkoli, V. Polo, L. Olsson, Z. He, and D. Cremer. COLOGNE2016, 2016. see <http://www.smu.edu/catco> (accessed Nov 10, 2017).
- [130] T.A. Keith. TK Gristmill Software ([aim.tkgristmill.com](http://aim.tkgristmill.com)), 2011. Overland Park KS, USA.
- [131] T. Lu and F. Chen. Multiwfn: A multifunctional wavefunction analyzer. *J. Comput. Chem.*, 33:580–592, 2012.
- [132] W. Zou, D. Nori-Shargh, and J. E. Boggs. On the covalent character of rare gas bonding interactions: A new kind of weak interaction. *J. Phys. Chem. A*, 117:207–212, 2013.
- [133] Eric F. Pettersen, Thomas D. Goddard, Conrad C. Huang, Gregory S. Couch, Daniel M. Greenblatt, Elaine C. Meng, and Thomas E. Ferrin. Ucsf chimera -a visualization system for exploratory research and analysis. *J. Comput. Chem.*, 25(13):1605–1612, 2004.
- [134] William Humphrey, Andrew Dalke, and Klaus Schulten. VMD – Visual Molecular Dynamics. *J Mol Graph Model*, 14:33–38, 1996.
- [135] Marcus D. Hanwell, Donald E. Curtis, David C. Lonie, Tim Vandermeersch, Eva Zurek, and Geoffrey R. Hutchison. Avogadro: an advanced semantic chemical editor, visualization, and analysis platform. *J. Cheminform*, 4(1):17, Aug 2012.
- [136] Chérif F. Matta, Norberto Castillo, and Russell J. Boyd. Extended weak bonding interactions in dna:  $\pi$ -stacking (base-base), base-backbone, and backbone-backbone interactions. *J. of Phys. Chem. B*, 110(1):563–578, 2006.

- [137] A.K. Wilson, D.E. Woon, K.A. Peterson, and T.H. Dunning Jr. Gaussian Basis Sets for Use in Correlated Molecular Calculations. IX. The Atoms Gallium through Krypton. *J. Chem. Phys.*, 110:7667–7676, 1999.
- [138] Changwei Wang, David Danovich, Yirong Mo, and Sason Shaik. On the nature of the halogen bond. *J. Chem. Theor. Comp.*, 10(9):3726–3737, 2014.
- [139] D. Cremer and E. Kraka. A description of the chemical bond in terms of local properties of electron density and energy. *Croat. Chem. Acta*, 57(6):1259–1281, 1984.
- [140] Pierangelo Metrangolo and Giuseppe Resnati. Type II halogen···halogen contacts are halogen bonds. *IUCrJ*, 1(1):5–7, Jan 2014.
- [141] J. P. Perdew, K. Burke, and M. Ernzerhof. *Phys. Rev. Lett.*, 77:3865, 1996.
- [142] Stefan Grimme, Jens Antony, Stephan Ehrlich, and Helge Krieg. A consistent and accurate ab initio parametrization of density functional dispersion correction (DFT-D) for the 94 elements H-Pu. *J. of Chem. Phys.*, 132(15):154104, 2010.
- [143] Stefan Grimme, Stephan Ehrlich, and Lars Goerigk. Effect of the damping function in dispersion corrected density functional theory. *J. of Comput. Chem.*, 32(7):1456–1465, 2011.

Chapter 10  
PUBLICATIONS

- Paper I** The intrinsic strength of the halogen bond: Electrostatic and covalent contributions described by coupled cluster theory; Vytor Oliveira, Elfi Kraka, and Dieter Cremer; *Phys. Chem. Chem. Phys.*, 18:33031-33046, 2016.
- Paper II** Quantitative assessment of halogen bonding utilizing vibrational spectroscopy; Vytor Oliveira, Elfi Kraka, and Dieter Cremer; *Inorg. Chem.*, 56(1):488-502, 2017.
- Paper III** Transition from metal-ligand bonding to halogen bonding involving a metal as halogen acceptor a study of Cu, Ag, Au, Pt, and Hg complexes; Vytor Oliveira and Dieter Cremer; *Chem. Phys. Lett.*, 681:56 - 63, 2017.
- Paper IV** The many facets of chalcogen bonding: Described by vibrational spectroscopy; Vytor Oliveira, Dieter Cremer, and Elfi Kraka; *J. Phys. Chem. A*, 121(36):6845-6862, 2017.
- Paper V** A systematic coupled cluster study of noncovalent interactions involving halogens, chalcogens and pnictogens; Vytor Oliveira and Elfi Kraka. Submitted.
- Paper VI** The peculiar role of the Au<sub>3</sub> unit in Au<sub>m</sub> clusters:  $\sigma$ -aromaticity of the Au<sub>5</sub>Zn<sup>+</sup> ion; Yanle Li, Vytor Oliveira, Chunmei Tang, Dieter Cremer, Chunyan Liu, and Jing Ma; *Inorg. Chem.*, 56(10):5793-5803, 2017.

Paper I.        The intrinsic strength of the halogen bond: Electrostatic and covalent contributions described by coupled cluster theory


 Cite this: *Phys. Chem. Chem. Phys.*,  
2016, 18, 33031

# The intrinsic strength of the halogen bond: electrostatic and covalent contributions described by coupled cluster theory†

Vytor Oliveira, Elfi Kraka and Dieter Cremer\*

36 halogen-bonded complexes  $YX \cdots AR_m$  ( $X$ : F, Cl, Br;  $Y$ : donor group;  $AR_m$  acceptor group) have been investigated at the CCSD(T)/aug-cc-pVTZ level of theory. Binding energies, geometries, NBO charges, charge transfer, dipole moments, electrostatic potential, electron and energy density distributions, difference density distributions, vibrational frequencies, local stretching and bending force constants, and relative bond strength orders  $n$  have been calculated and used to order the halogen bonds according to their intrinsic strength. Halogen bonding is found to arise from electrostatic and strong covalent contributions. It can be strengthened by H-bonding or lone pair delocalization. The covalent character of a halogen bond increases in the way 3c-4e (three-center-four-electron) bonding becomes possible. One can characterize halogen bonds by their percentage of 3c-4e bonding. FCl-phosphine complexes can form relatively strong halogen bonds provided electronegative substituents increase the covalent contributions in form of 3c-4e halogen bonding. Binding energies between 1 and 45 kcal mol<sup>-1</sup> are calculated, which reflects the large variety in halogen bonding.

 Received 27th September 2016,  
Accepted 17th November 2016

DOI: 10.1039/c6cp06613e

[www.rsc.org/pccp](http://www.rsc.org/pccp)

## 1 Introduction

Halogen bonding (XB; in the following also used for halogen bond and halogen-bonded) is a non-covalent interaction formed between an electrophilic halogen atom  $X$  in  $XY$  (dihalogens, interhalogens; or halogenated molecules) and a nucleophilic heteroatom  $A$  (*i.e.*  $A$  with lone-pair (lp) electrons) where XB can take place in the gas phase, solution, or the solid state. Due to its unique features, XB is increasingly used in medicinal,<sup>1–3</sup> supramolecular, and materials chemistry,<sup>4–10</sup> apart from its role in structural chemistry,<sup>11–14</sup> synthesis<sup>8,15,16</sup> or catalysis.<sup>14,16,17</sup> Therefore, XB has been the topic of several recent reviews.<sup>2,5,10,13,16,18–22</sup> In this connection, the excellent review by Metrangolo and co-workers<sup>10</sup> and the earlier work of these authors on XB<sup>23–25</sup> deserves special attention. XB was already observed 200 years ago<sup>10</sup> and ever since played some role in synthetic chemistry.<sup>10</sup> However, its nature was only understood in the last two decades when quantum chemical studies focused on XB.<sup>20,26–36</sup> It became soon clear that high-accuracy quantum chemical methods are

needed to reliably describe XB, especially when involving fluorine. Nevertheless, the number of high accuracy studies on XB is still limited.<sup>33–40</sup>

Karpfen<sup>36</sup> analyzed XBs between  $X_2$  or  $XY$  ( $F_2$ ,  $Cl_2$ ,  $Br_2$ ,  $ClF$ ,  $BrCl$ ) and  $NH_3$  utilizing CCSD(T). He found that binding energies do not follow the trends in the  $XY$  dipole moments or  $XY$  polarizabilities. Legon<sup>33</sup> and Hill and Hu<sup>35</sup> performed CCSD(T)-F12 calculations pointing out the relationship between various complex properties and the complex binding energy. Hiberty and co-workers<sup>37</sup> compared the bonding features of trihalides  $X_3^-$  ( $X = F, Cl, Br, I$ ) utilizing valence bond and CCSD(T) theory. Other authors carried out benchmark calculations on neutral and charged XB-complexes at the CCSD(T)/CBS (complete basis set limit) level to obtain reliable XB distances, binding energies and interaction energies (complex binding energies for frozen geometries of the monomers).<sup>32,34,38,41</sup>

Other quantum chemical investigations on XB were based on less accurate methods such as DFT (density functional theory),<sup>38,41–48</sup> or second order Møller-Plesset perturbation theory.<sup>12,49–59</sup> Symmetry-adapted perturbation theory<sup>15,51,57,60–64</sup> or other energy decomposition methods<sup>52,54,64</sup> were used to partition the XB binding energy into electrostatic, exchange, dispersion, *etc.* contributions. Since the nature of XB is reflected by the charges of the atoms involved ( $A$  and  $X$ ), the charge transfer from  $R_m A$  to  $XY$ , charge polarization of the monomers, the electron density distribution  $\rho(\mathbf{r})$ , its Laplacian, the energy density distribution  $H(\mathbf{r})$ , or the electrostatic potential  $V(\mathbf{r})$  were analyzed.<sup>44,50,51,53,55,62,65–74</sup>

Computational and Theoretical Chemistry Group (CATCO),  
Department of Chemistry, Southern Methodist University, 3215 Daniel Ave, Dallas,  
Texas 75275-0314, USA. E-mail: [dcremer@smu.edu](mailto:dcremer@smu.edu)

† Electronic supplementary information (ESI) available: It contains calculated geometries and energies for all molecules calculated in this work (PDF). Also, NBO charges, dipole moments and polarizabilities of the monomers, the correlation of the intrinsic XB strength with binding energies, bond lengths and density values is shown. See DOI: 10.1039/c6cp06613e

XB should lead to a change in the covalent bond XY. Jemmis<sup>75,76</sup> analyzed changes in the XY distances to explained red/blue-shifted XB-complexes. XY elongation occurs due to the lone pairs of the acceptor atom lp(A) been donated to the antibonding orbital  $\sigma^*(XY)$ , whereas XY shortening occurs due to a negative hyperconjugation mechanism. Del Bene and co-workers have investigated the spin–spin coupling constants affected by XB.<sup>49,56,77</sup>

A comparison of XB with other non-covalent interactions was carried out by several authors.<sup>12,46,78–83</sup> For example, Mo and co-workers<sup>82</sup> used BLWs (Block-Localized Wavefunctions) to analyze the directionality of non-covalent interactions for halogen, pnictogen, and chalcogen bonding. Scheiner,<sup>80</sup> as well as Elguero and co-workers,<sup>78</sup> reviewed the similarities and differences between halogen, chalcogen, pnictogen, and hydrogen bonding. Grabowski<sup>79</sup> compared the mechanism of hydrogen with halogen bonding.

XB is characterized by three common features: (i) the distance  $X \cdots A$  between halogen X and nucleophile (Lewis base) A is shorter than the sum of the van der Waals radii. (ii) The covalent XY distance in the XB complex tends to be longer than in the monomer XY (for exceptions, see Section 3). (iii) The angle YXA is close to  $180^\circ$ .<sup>10</sup> These structural features are electronically related to an interplay of electrostatic and covalent interactions, which results in the strength, tunability, and amphoteric character of XB. The anisotropy of the electron density distribution at X in a singly bonded X–Y causes unique electrostatic features as reflected by a  $\sigma$ -hole (positive electrostatic potential  $V$  in the non-bonded direction)<sup>84–86</sup> that is surrounded in the  $\pi$ -direction by a belt of negative charge (negative  $V$ ). For a  $\sigma$ -hole, the electron density distribution is tightly bonded to the nucleus X so that a nucleophile A with an into space extending lp can dock with the tail density of the lp into the  $\sigma$ -hole of halogen X.<sup>84–86</sup> The  $\sigma$ -hole and the electrostatic attraction should increase with the atomic number of X in the series  $F < Cl < Br < I < At$  where  $F_2$  should be the weakest halogen donor in complexes  $XX \cdots AR_m$ .<sup>10</sup>  $\pi$ -Systems such as benzene can also function as a Lewis base (instead of a heteroatom) and interact with an electrophilic halogen *via* XB.<sup>10,87,88</sup>

Despite the many investigations of XB carried out so far, there is no quantitative assessment of the XB bond strength. Complex binding energies and interaction energies can provide only a qualitative insight as they include, besides the intrinsic XB strength, all changes in the monomers upon dissociation of a XB dimer. A quantitative and reliable strength parameter is the local XB stretching force constant  $k^a$  that probes the intrinsic strength of the XB without changing the electronic structure of the complex as the force constant always refers to an infinitesimally small change in the complex geometry.<sup>89</sup> In general, a stretching force constant (derived, *e.g.*, from the normal mode frequencies or directly from the Hessian of the energy) cannot be used for this purpose as it is always contaminated by mode–mode coupling.<sup>89–91</sup> However, force constants of the local vibrational modes, which are derived from the mass-decoupled Wilson equation<sup>91,92</sup> of vibrational spectroscopy, are no longer

flawed by mode–mode coupling and provide a reliable measure of the intrinsic bond strength.<sup>89,93–96</sup> Using local vibrational modes calculated with CCSD(T)<sup>97</sup> as an accurate quantum chemical tool, we will for the first time provide reliable data on the intrinsic strength of XB. In this connection, we will pursue the following objectives and provide answers to the following questions.

(i) The intrinsic bond strength of XB varies. How large can this variation be and how does it depend on donor and acceptor of the XB complex? (ii) What bonding mechanism is responsible for the strength XB? When do electrostatic and when do covalent interactions dominate the bonding mechanism? Can the  $\sigma$ -hole attraction mechanism rationalize the intrinsic strength of XB? (iii) Is the XY bond strength related to the XB strength so that the latter can be anticipated by the former? (iv) Does the YXA bending force constant reflect the XB strength? (v) How does the negative charge of an anion change the strength of a XB? (vi) In the case of the trihalides  $[Y \cdots X \cdots Y]^-$  (X, Y: halogen), one obtains ions, which are valence isoelectronic with  $XeF_2$  and, therefore should be characterized by 3c-4e (3-center-4-electron) bonding. These ions should represent systems with covalent XBs. How can one quantify the covalent character of these bonds and the 3c-4e bonding mechanism?

These questions will be answered by investigating 36 neutral and anionic halogen bonded complexes as well as eight complexes with hydrogen, pnictogen, or chalcogen bonding (Fig. 1). Apart from presenting an order of XB according to its intrinsic strength, we will analyze the strength of the XB using two models. The first is based on orbital theory and the second on electron density theory. Whenever one uses a model one has to point out its limitations in connection to the five basic interactions determining the strength of XB: exchange repulsion, covalent, electrostatic, inductive, and dispersion interactions. Recently, Politzer and co-workers<sup>98–100</sup> have put forward the idea that non-covalent interactions such as XB might be described purely on the basis of Coulomb interactions, which have a physical basis. However, to learn about the mechanistic details of non-covalent interactions it is useful to refer to quantum chemical models. In this sense, we will use orbital theory to describe the covalent interactions between the monomers and single out the charge transfer between specific orbitals of the monomers as a reflection of these covalent interactions although part of this charge transfer can be due to other than covalent interactions. In a similar way, we will use the energy density to distinguish between covalent and electrostatic interactions where the former will include all interactions leading to stabilization and a negative energy density whereas the latter lead to destabilization and a positive energy density.

The results of this investigation will be presented in the following way. In Section 2, we will shortly describe the quantum chemical methods and tools used in this work. The nature of the XB will be discussed in Section 3 where the focus is on the role of the XB donor and acceptor. Also, we will investigate the influence of the charge in anionic XB complexes and

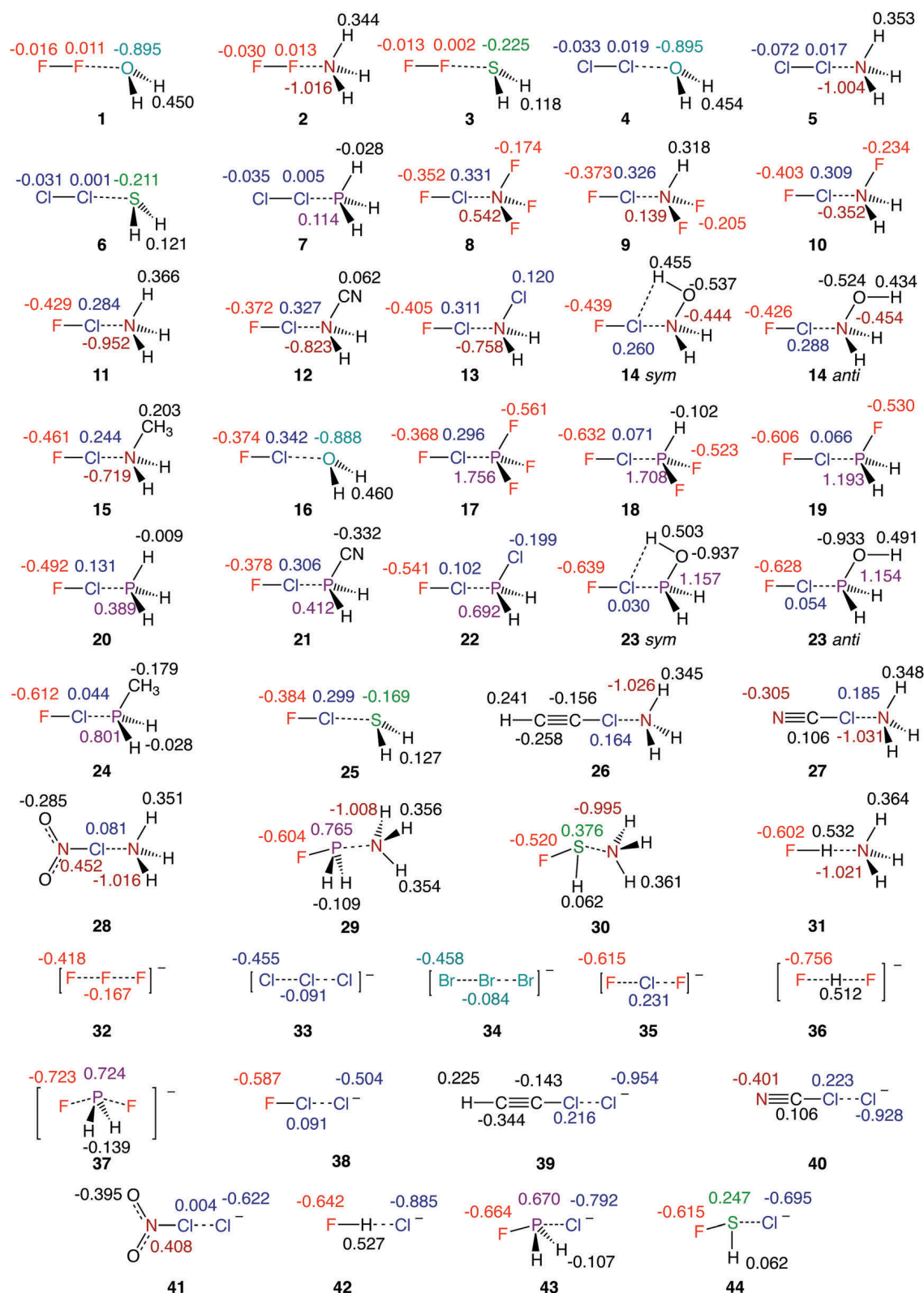


Fig. 1 Schematic representation of complexes **1–44** with selected NBO atomic charges calculated at CCSD(T)/aug-cc-pVTZ. Color is used to relate charges to atoms.

compare XB with other non-covalent bonds. In Section 4, we will analyze how different XB properties commonly used in the literature reflect the strength of XB. Finally, in Section 5, we will

draw the conclusions of this investigation and provide an outlook on how the results of this work can be used in the future.

## 2 Computational methods

The geometries of all complexes investigated were fully optimized at the coupled cluster level using CCSD(T) (all single, double, and perturbative triple excitations are included)<sup>97</sup> and augmented triple zeta basis sets aug-cc-pVTZ,<sup>101–103</sup> which contain diffuse basis functions to describe the charge distribution of heteroatoms or anions and the dispersion interactions in non-covalently bonded complexes. For the geometry optimizations, a convergence criterion of  $10^{-7}$  Hartree Bohr<sup>-1</sup> was used and for the SCF (self-consistent field) iterations and the iterations of the CC amplitudes a threshold of  $10^{-9}$ .

Each stationary point obtained in the geometry optimizations was identified as a minimum with the help of the analytical frequencies. The normal modes obtained by solving the Wilson equation<sup>92</sup> were used to calculate the local stretching modes and their properties according to the procedures described by Konkoli and Cremer.<sup>89–91,93</sup> Apart from this, all normal modes calculated were characterized in terms of local modes to identify those with strong XB stretching or bending character.<sup>104</sup>

There is a one to one relationship between normal and local vibrational modes,<sup>93</sup> which implies that there are just six local intermonomer vibrations. One of them is the local XB stretching mode characterized by the local stretching frequency  $\omega^a(\text{XB})$  and the local stretching force constant  $k^a(\text{XB})$ . As was demonstrated by Zou and Cremer, there is a direct relationship between the local stretching force constant of a bond and its intrinsic strength.<sup>105</sup> Accordingly, the intrinsic strength of the XB was determined by its  $k^a(\text{XB})$  value the analysis of which was simplified by converting local stretching force constants into bond strength orders (BSOs)  $n(\text{XB})$  according to

$$n = a(k^a)^b \quad (1)$$

with  $a = 0.418$  and  $b = 0.564$ . Eqn (1) is based on the generalized Badger rule derived by Cremer and co-workers.<sup>96,106</sup> Constants  $a$  and  $b$  were determined by assuming an  $n$  value of 1.00 for the FF bond in F<sub>2</sub> and  $n = 0.50$  for the 3c-4e bond in [F · · F · · F]<sup>-</sup>, which according to the Rundle–Pimentel model of bonding has two electrons in a bonding and two electrons in a non-bonding orbital. For  $k^a = 0$ , an  $n$  value of zero was enforced.

Binding energies  $\Delta E$  were calculated at the CCSD(T) level after applying the counterpoise correction of Boys and Bernardi<sup>107</sup> to determine the corrections for the basis set superposition errors (BSSE). The atomic charges and the charge transfer between the monomers were calculated with the help of the NBO (natural bond orbital) population analysis<sup>108</sup> using CCSD(T) response densities. Local properties of the electron density distribution,  $\rho(\mathbf{r})$ , and energy density distribution,  $H(\mathbf{r})$ , were also computed at the CCSD(T) level of theory. The Cremer–Kraka criteria for covalent bonding were applied.<sup>109–111</sup> These associate a stabilizing energy density at the bond critical point  $\mathbf{r}_b$  ( $H(\mathbf{r}_b) = H_b < 0$ ) with dominating covalent character, whereas a destabilizing energy density ( $H_b > 0$ ) indicates bonding due to electrostatic interactions. The electrostatic character of the interactions was also investigated by using the maximum value of the electrostatic potential  $V(\mathbf{r})$  on the van der Waals surface (modeled by the 0.001 e Bohr<sup>-3</sup> electron

density surface) of the halogen donor monomers. The halogen acceptor ability of a monomer AR<sub>*m*</sub> was assessed by calculating the most negative value of  $V(\mathbf{r})$  in the lp(A) region (Table 2).

Beside calculating the charge transfer between the interacting monomers, we also calculated the difference density distribution  $\Delta\rho(\mathbf{r}) = \rho(\text{Complex},\mathbf{r}) - \rho(\text{Monomer1},\mathbf{r}) - \rho(\text{Monomer2},\mathbf{r})$ , which was determined and plotted for the complex enveloping surface of an electron density distribution of 0.001 e Bohr<sup>-3</sup>. A positive difference density in the XB region is an alternative measure for its covalent character.

All local mode calculations were performed with COLOGNE-2016.<sup>112</sup> The CCSD(T) energy, energy gradient, and Hessian were calculated with CFOUR.<sup>113</sup> For the NBO analysis, NBO 6<sup>108</sup> was used whereas the electron (energy) density distribution was investigated with the program AIMALL.<sup>114</sup> Correlated electron and energy density distributions were analyzed with the programs Molden2AIM, and MOLBO of Zou and co-workers.<sup>115</sup> The CCSD(T) electrostatic potential  $V(\mathbf{r})$  were calculated with Multiwfn.<sup>116</sup>

## 3 Results and discussion

Table 1 lists the distances  $r(\text{XY})$  between the halogen atom X and the donor group or atom Y, the XB distance  $r(\text{XA})$  between X and heteroatom A of the acceptor of the XB, the counterpoise corrected binding energy  $\Delta E$ , the electron density  $\rho_b$  and the energy density  $H_b$  at the density critical point associated with XB, the intermonomer charge transfer obtained from the NBO analysis, the local bending force constant  $k^a(\text{YXA})$ , the local stretching force constant  $k^a(\text{XY})$ , the percentage of 3c-4e XB given by the ratio  $n(\text{AX})/n(\text{XY})$ , the local stretching force constant  $k^a(\text{XA})$ , the BSO  $n$  of the XB, and the local frequency  $\omega^a(\text{XA})$ . The last column shows the frequency, the normal mode number  $m$  and the percentage of XB stretching character contained in mode  $m$ . Calculated NBO atomic charges are given in Fig. 1. Additional properties (dipole moments, static polarizabilities, *etc.*) are given in the ESI.†

In Table 2, the CCSD(T) values of the electrostatic potential, which are used to characterize either the  $\sigma$ -hole or the lp(A) of the monomers are summarized. The BSO values of the XB of all complexes investigated are given as a function of the local X · · A stretching force constant in Fig. 2.

In previous work, experimentalist used the halogen stretching force constant as a measure for the intrinsic strength of the XB. Legon and co-workers<sup>33</sup> measured the rotational spectra and the centrifugal constants of XB complexes to determine the intermonomer stretching force constant  $k_\sigma$ , which differs from the local XB stretching force constant  $k^a(\text{XB})$  because the former is contaminated by coupling effects with other vibrational modes. Since the coupling effects are small in the case of a complex, one can expect that  $k_\sigma$  values are related to the  $k^a(\text{XA})$  values. This expectation is confirmed by the data points of ten representative complexes shown in Fig. 3.

### The nature of halogen bonding

There is a covalent and an electrostatic contribution to XB.<sup>10</sup> The covalent contribution is the result of a charge transfer from

Table 1 Geometry, energy, electron density, energy density, and vibrational data for complexes 1–44<sup>a</sup>

#	Complexes ( <i>sym.</i> )	<i>r</i> (XY)	<i>r</i> (XA)	$\Delta E$	$\rho_b$	$H_b$	CT	$k^a$ (YXA)	$k^a$ (XY)	<i>n</i> (XY)	$k^a$ (XA)	<i>n</i> (XA)	3c-4e (%)	$\omega^a$ (XA)	$\omega_\mu$ (% $\omega^a$ )
<b>Dihalogens</b>															
1	F <sub>2</sub> ···OH <sub>2</sub> ( <i>C<sub>s</sub></i> )	1.423	2.662	1.15	0.010	0.003	0.005	0.027	4.488	0.974	0.057	0.083	9	105	88(3;99.2)
2	F <sub>2</sub> ···NH <sub>3</sub> ( <i>C<sub>3v</sub></i> )	1.432	2.615	1.69	0.014	0.004	0.017	0.051	3.821	0.890	0.062	0.087	10	114	96(3;100)
3	F <sub>2</sub> ···SH <sub>2</sub> ( <i>C<sub>s</sub></i> )	1.425	3.092	0.89	0.008	0.002	0.011	0.027	4.238	0.943	0.034	0.062	7	70	58(3;99.3)
4	Cl <sub>2</sub> ···OH <sub>2</sub> ( <i>C<sub>s</sub></i> )	2.027	2.808	2.62	0.015	0.003	0.014	0.088	2.896	0.761	0.097	0.112	15	123	107(3;99.7)
5	Cl <sub>2</sub> ···NH <sub>3</sub> ( <i>C<sub>3v</sub></i> )	2.047	2.664	4.43	0.025	0.001	0.055	0.165	2.370	0.680	0.132	0.133	20	150	131(3;100)
6	Cl <sub>2</sub> ···SH <sub>2</sub> ( <i>C<sub>s</sub></i> )	2.032	3.209	2.23	0.013	0.001	0.030	0.078	2.715	0.734	0.069	0.092	13	84	73(3;100)
7	Cl <sub>2</sub> ···PH <sub>3</sub> ( <i>C<sub>3v</sub></i> )	2.034	3.220	2.22	0.014	0.001	0.030	0.064	2.612	0.718	0.062	0.087	12	80	69(3;100)
<b>Interhalogen FCl</b>															
8	FCl···NF <sub>3</sub> ( <i>C<sub>3v</sub></i> )	1.650	2.784	1.41	0.017	0.002	0.021	0.076	4.220	0.941	0.081	0.101	11	117	66(3;100)
9	FCl···NHF <sub>2</sub> ( <i>C<sub>s</sub></i> )	1.660	2.575	3.47	0.028	0.001	0.047	0.166	3.865	0.896	0.131	0.133	15	149	62(2;3.4) 108(3;95.7)
10	FCl···NH <sub>2</sub> F ( <i>C<sub>s</sub></i> )	1.680	2.400	6.22	0.044	-0.004	0.094	0.279	3.156	0.799	0.197	0.167	21	183	149(2;98.9)
11	FCl···NH <sub>3</sub> ( <i>C<sub>3v</sub></i> )	1.703	2.320	9.39	0.053	-0.009	0.145	0.434	2.687	0.729	0.311	0.216	30	230	207(3;100)
12	FCl···NH <sub>2</sub> CN ( <i>C<sub>s</sub></i> )	1.662	2.594	3.88	0.028	0.000	0.045	0.196	3.759	0.882	0.155	0.146	17	162	132(3;98.2) 173(4;1.5)
13	FCl···NH <sub>2</sub> Cl ( <i>C<sub>s</sub></i> )	1.685	2.379	6.90	0.046	-0.005	0.094	0.320	3.042	0.782	0.234	0.184	24	199	157(3;97.3) 254(4;2.4)
14	FCl···NH <sub>2</sub> OH ( <i>C<sub>s</sub></i> ) <i>syn</i>	1.712	2.223	9.84	0.068	-0.016	0.179	0.451	2.472	0.696	0.379	0.242	35	254	208(3;98.6) 348(5;1.2)
	FCl···NH <sub>2</sub> OH ( <i>C<sub>s</sub></i> ) <i>anti</i>	1.700	2.300	8.59	0.056	-0.010	0.138	0.430	2.697	0.731	0.285	0.206	28	220	182(3;97.8) 298(4;1.12) 87(1;1.0)
15	FCl···NH <sub>2</sub> CH <sub>3</sub> ( <i>C<sub>s</sub></i> )	1.736	2.193	12.80	0.073	-0.019	0.217	0.551	2.239	0.658	0.497	0.281	43	290	239(3;92.5) 335(5;7.1)
16	FCl···OH <sub>2</sub> ( <i>C<sub>s</sub></i> )	1.660	2.566	4.75	0.024	0.002	0.032	0.178	3.967	0.909	0.170	0.154	17	162	145(3;99.9)
17	FCl···PF <sub>3</sub> ( <i>C<sub>3v</sub></i> )	1.659	2.953	1.85	0.023	0.000	0.072	0.106	3.552	0.854	0.062	0.087	10	80	55(3;100)
18	FCl···PHF <sub>2</sub> ( <i>C<sub>s</sub></i> )	1.887	2.057	7.15	0.147	-0.087	0.561	0.242	1.209	0.465	0.909	0.396	85	306	228(3;95.0) 372(5;3.5) 432(6;1.4)
19	FCl···PH <sub>2</sub> F ( <i>C<sub>s</sub></i> )	1.883	2.104	7.88	0.133	-0.072	0.540	0.093	1.097	0.440	0.730	0.350	80	275	218(3;94.6) 383(4;5.3)
20	FCl···PH <sub>3</sub> ( <i>C<sub>3v</sub></i> )	1.785	2.360	5.42	0.080	-0.026	0.361	0.361	0.654	0.329	0.121	0.127	39	112	106(1;100)
21	FCl···PH <sub>2</sub> CN ( <i>C<sub>s</sub></i> )	1.670	2.852	2.83	0.029	-0.002	0.073	0.147	2.857	0.755	0.069	0.092	12	85	73(2;100)
22	FCl···PH <sub>2</sub> Cl ( <i>C<sub>s</sub></i> )	1.840	2.195	5.44	0.110	-0.049	0.439	0.195	1.022	0.423	0.417	0.255	60	207	164(3;98.3) 325(4;1.7)
23	FCl···PH <sub>2</sub> OH ( <i>C<sub>s</sub></i> ) <i>syn</i>	1.916	2.100	13.11	0.135	-0.076	0.609	0.286	1.095	0.440	0.905	0.395	90	306	283(4;99.1)
	FCl···PH <sub>2</sub> OH ( <i>C<sub>s</sub></i> ) <i>anti</i>	1.904	2.102	10.12	0.134	-0.074	0.574	0.377	1.073	0.435	0.799	0.368	85	287	250(4;95.7) 352(5;4.3)
24	FCl···PH <sub>2</sub> CH <sub>3</sub> ( <i>C<sub>s</sub></i> )	1.902	2.157	12.15	0.120	-0.060	0.567	0.383	1.039	0.427	0.701	0.342	80	269	244(4;95.5) 294(5;4.5)
25	FCl···SH <sub>2</sub> ( <i>C<sub>s</sub></i> )	1.673	2.863	4.31	0.027	-0.001	0.085	0.206	3.237	0.810	0.128	0.131	16	114	105(1;100)
<b>NH<sub>3</sub> acceptor</b>															
26	HCCCl···NH <sub>3</sub> ( <i>C<sub>3v</sub></i> )	1.652	3.072	2.45	0.011	0.002	0.009	0.049	5.072	1.044	0.073	0.095	9	111	97(3;100)
27	NCCL···NH <sub>3</sub> ( <i>C<sub>3v</sub></i> )	1.648	2.964	4.10	0.013	0.002	0.014	0.074	4.976	1.033	0.103	0.116	11	132	115(3;100)
28	O <sub>2</sub> NCl···NH <sub>3</sub> ( <i>C<sub>s</sub></i> )	1.839	2.772	3.83	0.021	0.001	0.037	0.117	1.592	0.543	0.114	0.123	23	139	117(4;100)
29	FH <sub>2</sub> P···NH <sub>3</sub> ( <i>C<sub>s</sub></i> )	1.644	2.663	6.10	0.025	-0.002	0.057	0.317	3.794	0.886	0.144	0.140	16	159	139(2;98.1) 148(3;1.9)
30	FHS···NH <sub>3</sub> ( <i>C<sub>s</sub></i> )	1.670	2.512	7.58	0.035	-0.003	0.081	0.410	3.309	0.820	0.194	0.166	20	184	163(3;99.9)
31	FH···NH <sub>3</sub> ( <i>C<sub>3v</sub></i> )	0.953	1.695	12.11	0.053	-0.018	0.069	0.096	6.340	1.184	0.353	0.232	20	798	273(3;99.7)
<b>Ionic systems</b>															
32	[F···F···F] <sup>-</sup> ( <i>D<sub>∞h</sub></i> )	1.739	1.739	22.86	0.113	-0.027	0.584	0.367	1.376	0.500	1.376	0.500	100	496	398(3;28.5) 548(4;71.5)
33	[Cl···Cl···Cl] <sup>-</sup> ( <i>D<sub>∞h</sub></i> )	2.328	2.328	23.43	0.080	-0.022	0.546	0.465	0.701	0.342	0.701	0.342	100	261	260(3;90.3) 262(4;9.7)
34	[Br···Br···Br] <sup>-</sup> ( <i>D<sub>∞h</sub></i> )	2.594	2.594	26.21	0.062	-0.015	0.542	0.416	0.730	0.350	0.730	0.350	100	177	161(3;15.7) 184(4;84.3)
35	[F···Cl···F] <sup>-</sup> ( <i>D<sub>∞h</sub></i> )	1.875	1.875	45.01	0.121	-0.054	0.384	0.744	1.486	0.522	1.486	0.522	100	453	447(3;19.9) 455(4;80.1)
36	[F···H···F] <sup>-</sup> ( <i>D<sub>∞h</sub></i> )	1.140	1.140	43.21	0.178	-0.264	0.244	0.351	0.848	0.380	0.848	0.380	100	1226	1271(2;99.0)
37	[F···PH <sub>2</sub> ···F] <sup>-</sup> ( <i>C<sub>2v</sub></i> )	1.836	1.836	41.69	0.097	-0.068	0.277	0.812	1.257	0.475	1.257	0.475	100	308	413(3;20.0) 431(4;80.0)
38	FCl···Cl <sup>-</sup> ( <i>C<sub>∞v</sub></i> )	1.883	2.316	28.98	0.081	-0.024	0.496	0.590	1.212	0.465	0.855	0.382	82	288	283(3;99.9)
39	HCCCl···Cl <sup>-</sup> ( <i>C<sub>∞v</sub></i> )	1.657	3.025	8.11	0.018	0.001	0.046	0.138	4.599	0.988	0.166	0.152	15	127	114(3;100)
40	NCCL···Cl <sup>-</sup> ( <i>C<sub>∞v</sub></i> )	1.659	2.883	16.59	0.024	0.000	0.072	0.190	4.126	0.929	0.247	0.190	20	155	140(3;100)
41	O <sub>2</sub> NCl···Cl <sup>-</sup> ( <i>C<sub>2v</sub></i> )	1.957	2.455	20.47	0.062	-0.013	0.378	0.474	0.732	0.350	0.487	0.278	79	217	214(3;98.5) 241(4;1.5)
42	FH···Cl <sup>-</sup> ( <i>C<sub>∞v</sub></i> )	0.971	1.915	22.82	0.048	-0.017	0.115	0.186	5.355	1.076	0.415	0.254	24	848	255(1;99.5)
43	FH <sub>2</sub> P···Cl <sup>-</sup> ( <i>C<sub>s</sub></i> )	1.725	2.649	18.62	0.039	-0.009	0.208	0.531	2.136	0.641	0.307	0.214	33	178	166(1;100)
44	FHS···Cl <sup>-</sup> ( <i>C<sub>s</sub></i> )	1.790	2.493	22.48	0.056	-0.014	0.305	0.581	1.466	0.518	0.443	0.264	51	212	204(1;99.4)
<b>Donors</b>															
#	Complexes ( <i>sym.</i> )	<i>r</i>	$k^a$	<i>n</i>	$\omega^a$	<i>V</i>	#	Complexes ( <i>sym.</i> )	<i>r</i>	$k^a$	<i>n</i>	$\omega^a$	<i>V</i>		
45	F <sub>2</sub>	1.418	4.700	1.000	916	16.5	50	HCCCl	1.649	5.227	1.062	996	34.2		
46	FCl	1.646	4.326	0.954	772	40.4	51	NCCL	1.644	5.209	1.060	995	36.8		
47	Cl <sub>2</sub>	2.019	3.025	0.780	542	25.4	52	H <sub>2</sub> FP	1.577	5.791	1.125	914	36.6		
48	Br <sub>2</sub>	2.313	2.340	0.675	317	28.5	53	HFS	1.626	4.569	0.984	807	40.3		
49	O <sub>2</sub> NCl	1.864	1.403	0.506	488	21.9	54	FH	0.921	9.594	1.496	4125	68.3		

<sup>a</sup> Computed at CCSD(T)/aug-cc-pVTZ. Bond distances  $r(\text{XY})$  and  $r(\text{XA})$  in Å,  $\Delta E$  in kcal mol<sup>-1</sup>, density at the XA critical point  $\rho_b$  in e Bohr<sup>-3</sup>, energy density at XA critical point  $H_b$  in Hartree Bohr<sup>-3</sup>, NBO intermonomer charge transfer (CT), local YXA bending force constant in mdyÅ rad<sup>-2</sup>, local XY and XB stretching force constant in mdyÅ<sup>-1</sup>, local stretching frequency  $\omega^a$  in cm<sup>-1</sup>, bond strength order *n*, 3c-4e% character calculated from  $n(\text{XA})/n(\text{XY})$ , normal mode frequencies related to XA stretching  $\omega_\mu$  in cm<sup>-1</sup> (normal mode number; % $\omega^a$ : % of local XA stretching character). In case of the X-donor monomers, the maximum electrostatic potential *V* computed on the 0.001 e Bohr<sup>-3</sup> electron density surface for the  $\sigma$ -hole of X (*V* in kcal mol<sup>-1</sup>) is also given.

Table 2 Minimum electrostatic potential  $V$  at  $lp(A)^a$ 

X-Acceptor	$V(r)$	X-Acceptor	$V(r)$
NR <sub>3</sub>		PR <sub>3</sub>	
NF <sub>3</sub>	-2.2	PF <sub>3</sub>	2.6
NH <sub>3</sub>	-37.3	PH <sub>3</sub>	-15.7
NHF <sub>2</sub>	-16.1	PHF <sub>2</sub>	-6.0
NH <sub>2</sub> F	-27.9	PH <sub>2</sub> F	-11.2
NH <sub>2</sub> CH <sub>3</sub>	-36.6	PH <sub>2</sub> CH <sub>3</sub>	-21.0
NH <sub>2</sub> OH	-26.5	PH <sub>2</sub> OH	-14.6
NH <sub>2</sub> CN	-11.8	PH <sub>2</sub> CN	-1.3
NH <sub>2</sub> Cl	-27.1	PH <sub>2</sub> Cl	-8.5
AR <sub>2</sub>		Anions	
OH <sub>2</sub>	-32.3	F <sup>-</sup>	-168.6
SH <sub>2</sub>	-16.5	Cl <sup>-</sup>	-139.5
		Br <sup>-</sup>	-131.6

<sup>a</sup> Minimum electrostatic potential  $V$  (kcal mol<sup>-1</sup>) computed on the 0.001 e Bohr<sup>-3</sup> electron density surface at  $lp(A)$ . CCSD(T)/aug-cc-pVTZ.

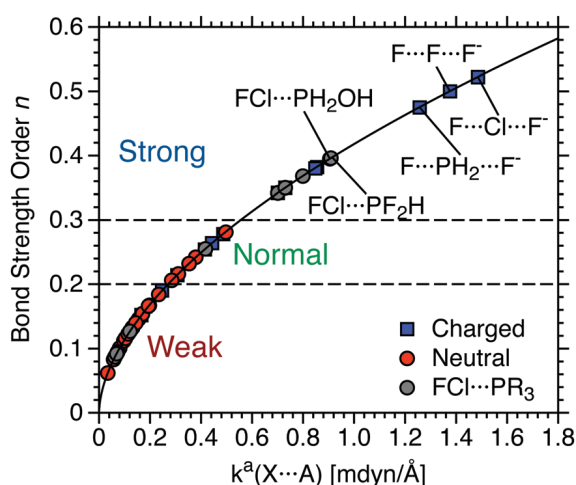


Fig. 2 Power relationship between the relative bond strength order (BSO)  $n$  and the local stretching force constants  $k^a$  of XB (halogen), HB (hydrogen), PB (pnictogen), and CB (chalcogen) bonding in complexes 1–44. CCSD(T)/aug-cc-pVTZ calculations. See also Table 1 and Fig. 1.

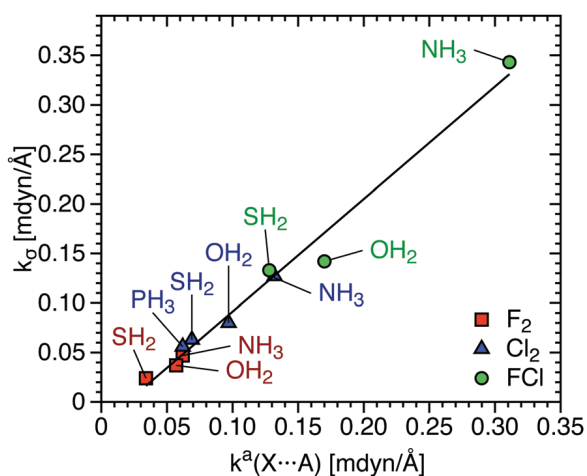


Fig. 3 Linear relationship between intermonomer stretching force constant  $k_p$ , measured by microwave spectroscopy<sup>33</sup> and local XB stretching force constants  $k^a$  calculated at CCSD(T)/aug-cc-pVTZ.  $R^2 = 0.983$ .

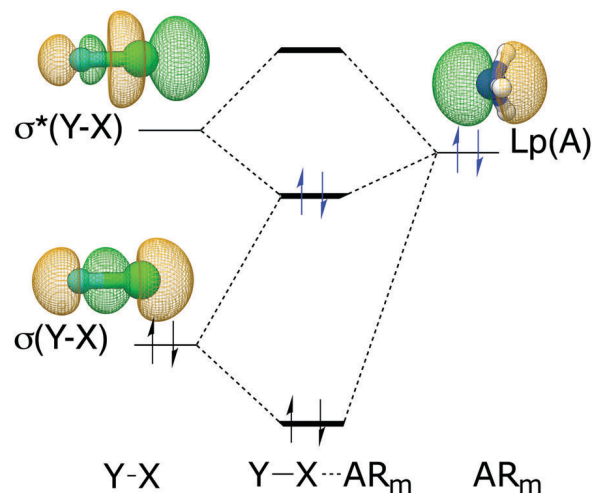


Fig. 4 Orbital interaction diagram showing the 2e-delocalization of an electron lone pair at the halogen acceptor (A) into the  $\sigma^*(XY)$  orbital of the halogen donor XY.

$lp(A)$  to the  $\sigma^*(XY)$  orbital (Fig. 4) thus leading to 2e-delocalization and stabilization of  $lp(A)$ . The magnitude of the 2e-delocalization is proportional to the orbital overlap and inversely proportional to the energy gap  $\Delta\epsilon(2e)$  between the energies of the  $lp(A)$  and the  $\sigma^*(XY)$  orbital. As shown in Fig. 4, the 2e-stabilization effect is always accompanied by a 4e-destabilization effect involving  $lp(A)$  and the bonding  $\sigma(XY)$  orbital. The 2e-stabilization increases and the 4e-destabilization decreases when increasing the electronegativity of Y because this (i) lowers the energies of  $\sigma(XY)$  and  $\sigma^*(XY)$  orbital (decrease of  $\Delta\epsilon(2e)$  and increase of  $\Delta\epsilon(4e)$ ) and (ii) increases the overlap between  $lp(A)$  and  $\sigma^*(XY)$  (decreases the overlap between  $lp(A)$  and  $\sigma(XY)$  as the lower electronegativity of X leads to a smaller X coefficient. Because of orbital orthogonality, the X coefficient becomes larger in the  $\sigma^*(XY)$  orbital). As a consequence of the charge transfer from  $lp(A)$  to  $\sigma^*(XY)$  and the formation of the XB, the Y–X single bond is weakened (for exceptions, see Section 3).

The electrostatic part of the halogen bond depends on (i) the mutual polarization of the monomers and (ii) on the Coulomb attraction between a negatively charged heteroatom A and the  $\sigma$ -hole of X. The latter effect is relevant when Y has a larger electronegativity than X thus withdrawing  $\sigma$  charge from X and contracting the  $\sigma$  density at X and generating a  $\sigma$ -hole.<sup>84,85</sup> Dispersive contributions are smaller than the other contributions, but still non-negligible, especially for weak halogen bonds.<sup>80</sup>

We have determined the covalent character of the monomer interactions in complexes 1–44 (Fig. 1) utilizing the energy density  $H_b$  at the density critical point  $r_b$  between X and A (Fig. 5). There is a continuous transition from electrostatic ( $H_b$  close to zero) to covalent XB with negative  $H_b$  values indicating that electron density accumulation in the interaction region is stabilizing the complex. Utilizing the BSO values in Fig. 2, one can distinguish between weak predominantly electrostatic halogen bonds ( $0.05 < n(XA) \leq 0.2$ ), normal halogen bonds ( $0.2 < n(XA) \leq 0.3$ ), and strong, predominantly covalent halogen bonds ( $0.3 < n(XA) < 0.6$ ). As shown in Fig. 2, XB

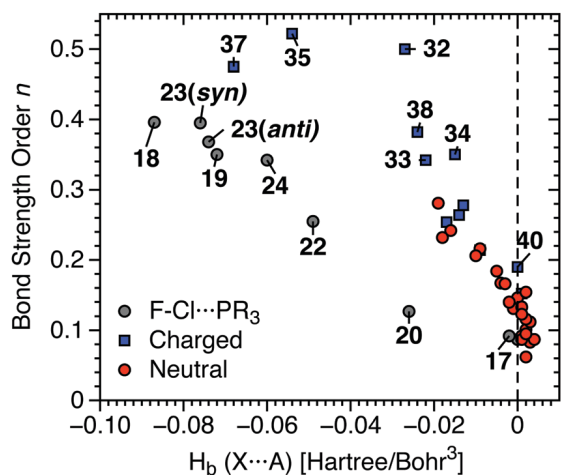


Fig. 5 Comparison of the bond strength order  $n$  with the energy density  $H_b$  at the density critical point of XB (halogen bonding), HB (hydrogen bonding), PB (pnictogen bonding), or CB (chalcogen bonding).  $H_b$  values close to zero indicate electrostatic and negative  $H_b$  values covalent bonding.<sup>109,110</sup> CCSD(T)/aug-cc-pVTZ. For the numbering of complexes, see Fig. 1.

varies over a BSO range larger than 0.5, which is significantly larger than found in the case of hydrogen bonding<sup>95</sup> and pnictogen bonding.<sup>117,118</sup>

### Halogen bonding leading to a blue shift

There are cases of XB that lead to a shortening rather than lengthening of the XY bond.<sup>75,76</sup> For example, in complex **28** ( $\text{O}_2\text{NCl} \cdots \text{NH}_3$ ) the NCl bond becomes shorter by 0.025 Å (reduction from 1.864 Å in the monomer to 1.839 Å in the complex; Table 1 and Table S3 in the ESI†). This leads to a blue shift in the NCl stretching frequency by 32  $\text{cm}^{-1}$  (from 488  $\text{cm}^{-1}$  in the monomer to 520  $\text{cm}^{-1}$  in the XB-complex), which has to be compared with a blue shift of just 13  $\text{cm}^{-1}$  in the normal mode frequencies that have strong N–Cl stretching character (monomer: 378  $\text{cm}^{-1}$  (98.2% NCl stretching character); complex: 391  $\text{cm}^{-1}$  (99.9%)). This underlines the advantages of carrying out the analysis in terms of local rather than normal modes. The cause of the strengthening of the NCl bond upon XB formation with  $\text{NH}_3$  is a result of exchange repulsion between the monomers upon complex formation. The Lewis base  $\text{NH}_3$  is a weak lp-density donor (charge transfer of just 0.037  $e$  compared to 0.378  $e$  of  $\text{Cl}^-$  in **41** ( $\text{O}_2\text{NCl} \cdots \text{Cl}^-$ ); Table 1). Hence, exchange repulsion is a dominant force when the monomers are approaching. The electron density of the monomer  $\text{O}_2\text{NCl}$  is polarized, the NCl bond becomes more polar, and the NCl antibonding orbital is lowered in energy (see Fig. S5 in the ESI† for perspective drawings of the MOs). This leads to a stronger interaction with the ONO lp-orbitals in the sense of an anomeric interaction so that lp(O) density is transferred into the NCl bond (Jemmis has used the term “negative hyperconjugation” in this connection<sup>75,76</sup>). Normally, this would lead to bond weakening but due to the increased polarity of the NCl bond, the NCl antibonding character is decreased, and bond shortening rather than lengthening results during XB-complex formation with the

Lewis base  $\text{NH}_3$  as is nicely documented by the habitus of the XB-complex HOMO (see ESI†). Hence, exchange repulsion is the actual cause for the blue shift in the XY frequency.<sup>119,120</sup> The anion of Cl has a much more diffuse charge distribution that leads to less exchange repulsion, less polarization, and a larger charge transfer. Accordingly a lengthening of the N–Cl bond in **41** and a red shift of 136  $\text{cm}^{-1}$  in the local NCl frequency is the consequence.

### Halogen bonding in dihalogens and interhalogens

Fig. 6 gives the relative strength of the XB for a series of halogen donors Y in Y–X ( $\text{F}_2$ ,  $\text{Cl}_2$ , FCl) and halogen acceptors  $\text{AR}_m$  ( $\text{OH}_2$ ,  $\text{NH}_3$ ,  $\text{SH}_2$ ,  $\text{PH}_3$ ). A stable halogen bonded  $\text{F}_2 \cdots \text{PH}_3$  complex could not be found at the CCSD(T) level because of the weakness of  $\text{F} \cdots \text{P}$  interactions. All but complex **11** ( $\text{FCl} \cdots \text{NH}_3$ ) of complexes 1–11 shown in Fig. 6 are weak and dominated by electrostatic interactions as is documented by the small BSO values and the positive (or weakly negative)  $H_b$ -values (Table 1).

Dihalogen  $\text{F}_2$  leads to weak interactions with a Lewis base as the  $\sigma^*(\text{FF})$  orbital is strongly contracted. Therefore, it provides insufficient overlap with orbital lp(A). The corresponding XBs are relatively weak with  $n$ -values smaller than 0.1 (red squares in Fig. 6). Hence, it depends on the polarizing power of the acceptor  $\text{AR}_m$  and the electrostatic interactions between the monomers to establish a XB. The electrostatic potential values  $V$  at lp(A) are useful to explain trends in the calculated BSO(XB) values ( $V(\text{NH}_3)$ :  $-37.3 \text{ kcal mol}^{-1} < V(\text{OH}_2)$ :  $-32.3 \text{ kcal mol}^{-1} \ll V(\text{SH}_2)$ :  $-16.5 < V(\text{PH}_3)$ :  $-15.7 \text{ kcal mol}^{-1}$ , Table 2).  $\text{Cl}_2$  can be better polarized than  $\text{F}_2$  and has a more positive  $\sigma$ -hole ( $V(\text{F}_2)$ : 16.5;  $V(\text{Cl}_2)$ : 25.4  $\text{kcal mol}^{-1}$ , Table 2), which leads to stronger but still dominantly electrostatic XBs ( $n < 0.15$ , blue triangles in Fig. 6).

Significantly stronger XBs are obtained in the case of an interhalogen such as FCl (green dots in Fig. 6). The electrostatic part of the interactions is enlarged due to the dipole moment of FCl (0.93 Debye, CCSD(T)), which increases the attraction

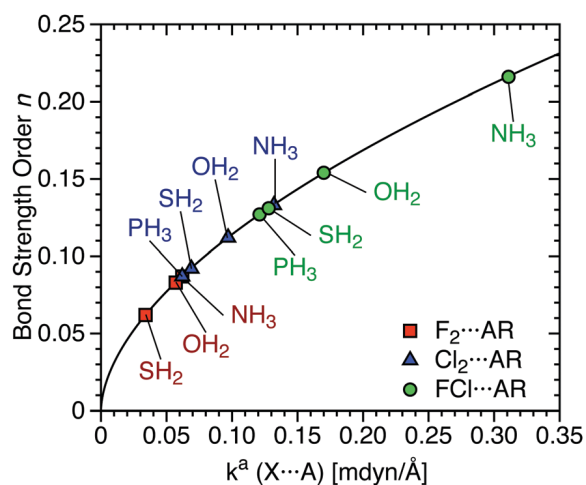


Fig. 6 Power relationship between the relative BSO  $n$  and the local XB stretching force constant  $k^a$  for XB complexes involving  $\text{F}_2$ ,  $\text{Cl}_2$  and FCl halogen donors and various acceptors. Calculated at CCSD(T)/aug-cc-pVTZ.

between the halogen X (partially positively charged) and the Lewis-base A (partially negatively charged). Additional covalent interactions lead to a larger variation in the BSO values ( $0.13 < n < 0.22$ ). The antibonding FCl orbital is sufficiently low in energy to support a stronger charge transfer of 145  $m_e$  (milli-electron) for **11** (Table 1). This becomes possible because of an enlarged Cl orbital coefficient in the  $\sigma^*(\text{FCl})$  orbital (Allred-Rochow electronegativities:  $\chi(\text{F}) = 4.10 < \chi(\text{Cl}) = 2.83^{121}$ ) and a larger overlap with the lp(A) orbital of the acceptor.

The charge transfer does not necessarily relate to the strength of a XB. For example, the BSO values of the complexes  $\text{FCl} \cdots \text{PH}_3$  (**20**) and  $\text{FCl} \cdots \text{NH}_3$  (**11**) are 0.127 and 0.216, respectively, whereas the corresponding charge transfer values are 361 and 145  $m_e$ . The 2e-stabilizing interaction in **20** is largely offset by electrostatic repulsion between the positively charged Cl atom (131  $m_e$ ) and the positively charged P atom (389  $m_e$ ). Hence, the electrostatic part of the XB decides on the ordering of the BSO values in the case of the FCl complexes.

### Influence of the acceptor

The nature of the XB strongly depends on the availability of the lp(A) electrons, the polarizing power, and the negative charge of the acceptor atom A. This is demonstrated for the 8 amine and 8 phosphine  $\cdots \text{ClF}$  complexes shown in Fig. 7. The XB strength increases in the series  $\text{NF}_3 < \text{NHF}_2 < \text{NH}_2\text{CN} < \text{NH}_2\text{F} < \text{NH}_2\text{Cl} < \text{NH}_3 < \text{NH}_2\text{OH} < \text{NH}_2\text{CH}_3$  whereas for the phosphine complexes the order is changed to  $\text{PF}_3 \leq \text{PH}_2\text{CN} < \text{PH}_3 \ll \text{PH}_2\text{Cl} \ll \text{PH}_2\text{CH}_3 \leq \text{PH}_2\text{F} < \text{PH}_2\text{OH} \leq \text{PHF}_2$ . The BSO values of the amine complexes vary from 0.10 to 0.28 and those of the phosphine complexes from 0.09 to 0.40 thus revealing that XB is more variable in the case of the phosphines.

The trend observed for the amines can be easily explained using the electrostatic description of XB, but considering in a few cases covalent contributions. Electronegative substituents such as F lower the negative charge at N and thereby the attraction between the positively charged Cl and atom A. Considering the number of electronegative substituents and their electronegativity

(in the case of CN, the group electronegativity) one can explain the BSO (intrinsic strength) values of all amine complexes with  $n$  smaller or equal to that of  $\text{NH}_3$ . Unusually large are only the BSO value of  $\text{F-Cl} \cdots \text{NH}_2\text{OH}$  (0.242) and that of  $\text{F-Cl} \cdots \text{NH}_2\text{CH}_3$  (0.281). In the latter case, the hyperconjugative effect of the methyl group increases the electron-donor ability of N thus leading to a larger charge transfer and a stronger admixture of covalent bonding.

In the case of the  $\text{NH}_2\text{OH}$  partner of FCl, one should expect an electrostatic effect and a BSO value larger than that of  $\text{NH}_2\text{F}$  (0.167) but smaller than that of  $\text{NH}_2\text{Cl}$  (0.184). The actual increase to the value of 0.242 can only be rationalized by analyzing the calculated equilibrium geometry. The OH group is placed in the mirror plane of the complex and *syn* with regard to the Cl atom. Although the  $\text{H} \cdots \text{Cl}$  distance is 2.579 Å, a weak, electrostatic H-bond is established (stretching  $k^a = 0.088 \text{ mdyn } \text{Å}^{-1}$ ; BSO value: 0.111), which stabilizes the complex, leads to a relative short ClN distance of 2.223 Å (for  $\text{NH}_3$ : 2.320 Å), and the increase in the BSO value. If the OH group is forced into the *anti* position the BSO value is decreased to 0.206 which is slightly higher than one would expect from the electrostatic model.

XB in the phosphine complexes suffers from two electronic deficiencies both caused by the lp(P) orbital (lp(P) is too diffuse to make P a strongly polarizing atom; insufficient overlap with the  $\sigma^*(\text{FCl})$  orbital) so that charge cannot be transferred effectively and a more covalent interaction becomes possible. If the positive charge of P increases for example because of electronegative substituents, then the lp(P) is contracted, the polarizing power of P is increased, and a better overlap with the  $\sigma^*(\text{FCl})$  orbital leads to a better charge transfer. However, the latter effect will be limited because of increased P, Cl repulsion, a decrease of the orbital energy of lp(P), an increase of  $\Delta\epsilon(2e)$ , and a reduction of the 2e-stabilization effect. In connection with the electrostatic effect, one has to consider that the partially positive charge of P is shielded to some extent by the lp(P) density in the direction of the Cl atom as is indicated by the negative electrostatic potential of the monomers ( $V(\text{PH}_3)$ :  $-15.7$ ,  $V(\text{PFH}_2)$ :  $-11.2$ ;  $V(\text{PHF}_2)$ :  $-6.0 \text{ kcal mol}^{-1}$ ; Table 2)

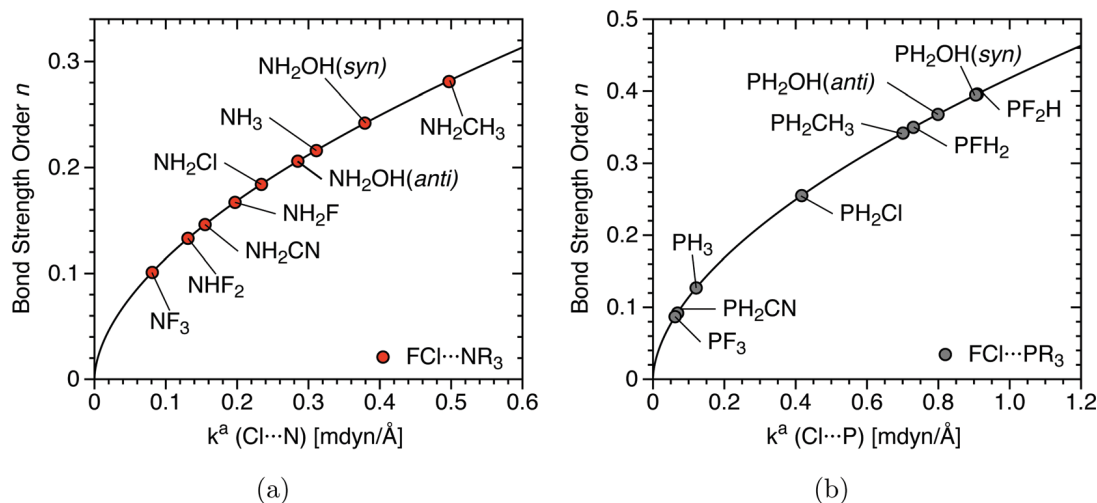


Fig. 7 Relationship between the relative BSO  $n$  and the local XB stretching force constant  $k^a$ , calculated at CCSD(T)/aug-cc-pVTZ. (a)  $\text{Cl} \cdots \text{N}$  halogen bonding between FCl and eight amines. (b)  $\text{Cl} \cdots \text{P}$  halogen bonding between FCl and eight phosphines.

with the only exception being  $V(\text{PF}_3)$ : 2.55 kcal mol<sup>-1</sup>; Table 2). There must be a compromise between the contraction of  $\text{lp}(\text{P})$  (due to the electronegative substituents at P) and the enlargement of  $\Delta\epsilon(2e)$  (reduction of 2e-stabilization).

For the XB-complex **17** ( $\text{FCl}\cdots\text{PF}_3$ ), one might think of a  $\sigma$ -hole,  $\sigma$ -hole interaction and a mutual transfer of charge from the P to the Cl and from the Cl back to P in the sense of a mixed halogen–pnictogen bond. The calculated charge transfer of 0.072  $e$  from Lewis base to X-donor suggests a dominance of XB. A pnictogen bond would lead to a lengthening of the PF bonds<sup>117,118</sup> whereas the calculated geometries indicate a reduction of the PF bonds from 1.580 (monomer) to 1.573 Å (complex) as it is typical of XB. Furthermore, one has to emphasize that the description in terms of  $\sigma$ -hole,  $\text{lp}$  interactions is in itself a model that excludes the effects of the kinetic energy and, therefore should not be pushed too far.

The charge transfer values of Table 1 and the difference density distributions shown in Fig. 8 provide an insight where the best compromise is achieved. For three F substituents as in  $\text{PF}_3$ , the increase in  $\Delta\epsilon$  is too large, 2e-stabilization and charge transfer are strongly reduced (72  $m_e$ ) compared to  $\text{PH}_3$  (361  $m_e$ ) so that electrostatic interactions dominate XB. The difference density distributions confirm this in so far as for  $\text{PF}_3$  just a small region of density increase between Cl and P (blue ball in Fig. 8) and a similar increase at the F atom is visible whereas for the  $\text{PH}_3$  complex regions of charge increase and decrease alternate throughout the complex from the nonbonding region of the PH bonds to the  $\text{lp}(\text{F})$  region, which is in line with charge transfer and charge polarization.

For the  $\text{PHF}_2$ , a clear increase in charge transfer (561  $m_e$ , Table 1) and charge polarization is documented by the difference density distribution in Fig. 8. The charge transfer leads to a lengthening of the FCl bond from 1.785 ( $\text{PH}_3$ ) to 1.887 Å ( $\text{PHF}_2$ ), the ClP distance is reduced from 2.360 to 2.057 Å and the charge

at the F(Cl) atom increases from 492  $m_e$  ( $\text{PH}_3$ ) to 632  $m_e$ . The BSO value of the XB is 0.396 ( $\text{PHF}_2$ ) whereas that of the FCl bond is reduced from 0.954 to 0.465 suggesting that the real structure is a superposition of the halogen-bonded complex and the ion pair  $\text{F}^-\cdots\text{Cl}-\text{PHF}_2^+$ . Such structures were first discussed by Alkorta and co-workers<sup>49</sup> and called chlorine shared bonds. It is more appropriate to consider them as a superposition of XB and 3c-4e-bonds (in short: 3c-4e XBs), which can be identified *via* (i) the large charge at the interhalogen F, (ii) the BSO values of F–Cl and Cl $\cdots$ P which are similar or inverted, (iii) the difference density distributions with an increase in the XB and at the interhalogen F (Fig. 8), and (iv) delocalization of the  $\text{lp}(\text{Cl})$  electrons into the  $\sigma^*(\text{PR})$  orbitals, especially into those of the PF bonds.

We quantify the amount of 3c-4e XB with the help of the calculated BSO(XY) and BSO(XB) values. If the latter is zero, there is no XB. If they are equal, there will be 100% 3c-4e XB. In general, the percentage of 3c-4e XB is given by the expression  $100 \times n(\text{AX})/n(\text{XY})$ . For amines these values are up to 40% ( $\text{NH}_2\text{CH}_3$ : 43%, Table 1). However, for the phosphines, they can increase to 90%:  $\text{PH}_2\text{OH}$  (90; 0.395)  $\approx$   $\text{PHF}_2$  (85%;  $n(\text{XB}) = 0.396$ )  $>$   $\text{PH}_2\text{CH}_3$  (80)  $\approx$   $\text{PH}_2\text{F}$  (79)  $>$   $\text{PH}_2\text{Cl}$  (60)  $>$   $\text{PH}_3$  (39).

3c-4e XBs are found for  $\text{PH}_2\text{OH}$  ( $n(\text{ClP}) = 0.395$ ), which, as in the case of the corresponding amine complex, forms an electrostatic H-bond with Cl ( $r = 2.889$  Å,  $k^a = 0.098$  mdyne Å<sup>-1</sup>, BSO value: 0.113;  $\text{PH}_2\text{F}$ :  $n(\text{ClP}) = 0.350$ ;  $\text{PH}_2\text{CH}_3$ :  $n(\text{ClP}) = 0.342$ ;  $\text{PH}_2\text{Cl}$ :  $n(\text{ClP}) = 0.255$ ). Interesting is the  $\text{PH}_2\text{CH}_3$  value as one could argue that in this case the hyperconjugative effect of a methyl group increases the Lewis-base character of the phosphine. Hyperconjugation also strengthens the electrostatic contribution. Even though the electronegativity of C (or the Me group) is larger than that of P ( $\chi(\text{C}) = 2.50 > \chi(\text{P}) = 2.06^{121}$ ), leading to an increase of the positive charge at P (801 compared to 389  $m_e$  in **20** and 0.358 in  $\text{PH}_2\text{CH}_3$  compared to 0.108 in  $\text{PH}_3$ )

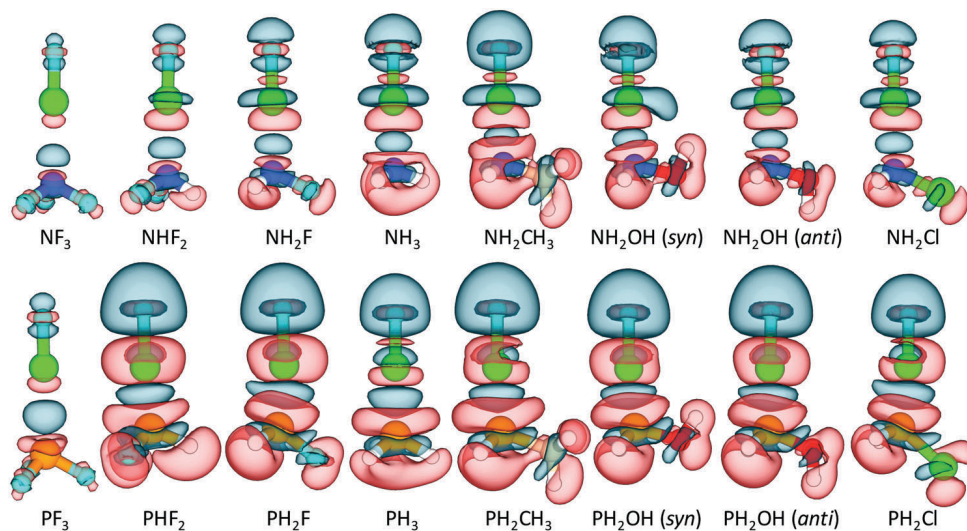


Fig. 8 CCSD(T)/aug-cc-pVTZ electron difference density distributions  $\Delta\rho(\mathbf{r})$  given for  $\text{FCl}\cdots\text{NR}_3$  and  $\text{FCl}\cdots\text{PR}_3$  complexes.  $\Delta\rho(\mathbf{r})$  is plotted for an electron density surface with a constant density value of 0.001 a.u. Blue regions indicate an increase in the electron density, red regions a density decrease relative to the superimposed density of the monomers.

there is a decrease of the electrostatic potential in the lone pair region ( $V(\text{PH}_3)$ :  $-15.7$ ;  $V(\text{PH}_2\text{CH}_3)$ :  $-21.0$  kcal mol $^{-1}$ ; Table 2).

### Halogen bonding in anions

The ideal 3c-4e XB with 100% electron delocalization and therefore covalent nonclassical bonding ( $H_b < 0$ , Table 1) is realized for  $[\text{F}\cdots\text{F}\cdots\text{F}]^-$  (32), which we have used as suitable reference with a BSO of 0.500. Anions  $[\text{Cl}\cdots\text{Cl}\cdots\text{Cl}]^-$  (33) and  $[\text{Br}\cdots\text{Br}\cdots\text{Br}]^-$  (34) have also 100% 3c-4e XB, but their BSO decreases to 0.342 and 0.350. The decrease is due to an increase of the  $\sigma$  orbital energies (because of decreasing electronegativity) and increased lp-repulsion between the  $p\pi$  electrons of the halogen atoms. The latter becomes less destabilized with increasing X-X distance so that  $[\text{Br}\cdots\text{Br}\cdots\text{Br}]^-$  has a somewhat larger BSO value (0.350) than  $[\text{Cl}\cdots\text{Cl}\cdots\text{Cl}]^-$  (0.342). Since the negative charge is accumulated at the terminal atoms, the inclusion of a less electronegative atom such as Cl leads to an increase in the BSO to 0.522 (35), which is also reflected in its binding energy  $\Delta E$  of 45.0 kcal mol $^{-1}$  (Table 1). Such an increase is also found when H occupies the central position (36), but since H does not possess a  $2p\sigma$ -orbital its BSO is just 0.380 ( $\Delta E = 43.2$  kcal mol $^{-1}$ ).

An unexpectedly strong 3c-4e bond is obtained if  $\text{PH}_2$  is in the center of the anion (BSO: 0.475;  $\Delta E = 41.7$  kcal mol $^{-1}$ ) as in  $[\text{F}\cdots\text{PH}_2\cdots\text{F}]^-$  (37). The complex has a butterfly form with long PF bonds (1.838 compared to the 1.577 Å of the PF bond in the monomer  $\text{PFH}_2$ ). The molecule should be a suitable ligand for transition metal complexes or suitable for fluorination. Bonding in  $\text{F}_3^-$  and related halogen systems correspond to covalent (delocalized) XB, in  $[\text{F}\cdots\text{H}\cdots\text{F}]^-$  to covalent (delocalized) H-bonding, and, accordingly, in  $[\text{F}\cdots\text{PH}_2\cdots\text{F}]^-$  to covalent (delocalized) pnictogen bonding although the latter term is actually reserved for the non-covalent interactions of two pnictogens. One could also speak of hypervalent bonding as  $\text{PF}_2\text{H}_2^-$  or  $\text{PF}_4^-$  are isoelectronic with the corresponding sulfur analogues difluorodihydrogen and tetrafluoro sulfurane. Compared to the axial SF bonds in these molecules (1.646 Å), the axial PF bonds are lengthened by 0.2 Å, which is due to the negative charge in the axial positions (see Fig. 1) entering the third and antibonding PPF orbital.

The local bending force constants  $k^a(\text{YXA})$  provide an indirect indicator for the strength of the covalent 3c-4e bonds. A stiffer linear arrangement reflects a stronger covalent XB:  $[\text{Br}\cdots\text{Br}\cdots\text{Br}]^-$  ( $k^a(\text{YXA})$  mdyn Å rad $^{-2}$ ): (0.416; BSO: 0.350)  $\approx$   $[\text{Cl}\cdots\text{Cl}\cdots\text{Cl}]^-$  (0.465; 0.342)  $<$   $[\text{F}\cdots\text{F}\cdots\text{F}]^-$  (0.367; 0.500)  $<$   $[\text{F}\cdots\text{Cl}\cdots\text{F}]^-$  (0.744; 0.522)  $<$   $[\text{F}\cdots\text{PH}_2\cdots\text{F}]^-$  (0.812; 0.475)  $<$   $[\text{F}\cdots\text{H}\cdots\text{F}]^-$  (0.351; 0.380). The comparison with the BSO values reveals that the bending force constants are useful, but do not provide a quantitative measure of the 3c-4e bond strength as the different size of the central atom (group) can lead to an increase of the bending force constant, which disguises the stiffness caused by 4e-delocalization in YXA.

3c-4e XB is partly lost if the symmetry of the complex is reduced by substituting one of the terminal halogens by another group. Table 1 reveals that in the series  $\text{O}_2\text{NCl}\cdots\text{Cl}^-$  (79% of 3c-4e bonding;  $n(\text{XA}) = 0.278$ )  $>$   $\text{FCl}\cdots\text{Cl}^-$  (82%; 0.382)  $>$   $\text{FSH}\cdots\text{Cl}^-$  (51%; 0.264)  $>$   $\text{FH}_2\text{P}\cdots\text{Cl}^-$  (33%; 0.214)  $>$   $\text{FH}\cdots\text{Cl}^-$

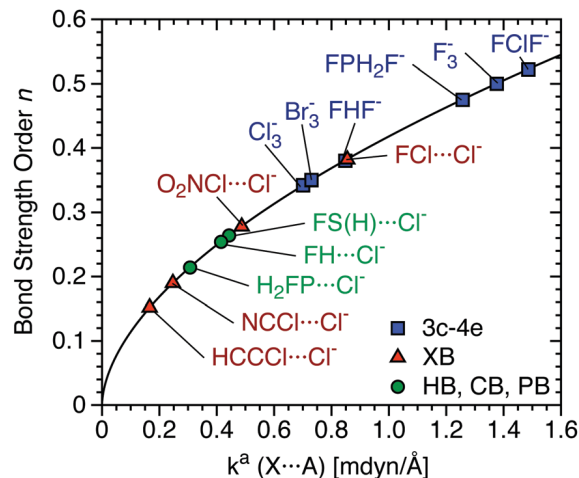


Fig. 9 Relationship between the relative BSO  $n$  and the local XB stretching force constant  $k^a$  for ionic complexes. See text. CCSD(T)/aug-cc-pVTZ calculations.

(24%; 0.254)  $>$   $\text{NCCl}\cdots\text{Cl}^-$  (20%; 0.190)  $>$   $\text{HCCCl}\cdots\text{Cl}^-$  (15%; 0.152) the 3c-4e bonding is successively lost, which is (partly) in line with a weakening of the XA covalent interactions as reflected by BSO,  $H_b$ , and charge transfer values. Clearly, the higher the energy of the acceptor orbital  $\sigma^*(\text{XY})$  is (the lower the electronegativity of the donor Y), the weaker is the actual XB and the lower is the degree of 3c-4e delocalization. It is interesting to note that chalcogen bonding as in  $\text{F}(\text{H})\text{S}\cdots\text{Cl}^-$  (44) is stronger than pnictogen bonding in  $\text{FH}_2\text{P}\cdots\text{Cl}^-$  (43) or H-bonding in  $\text{FH}\cdots\text{Cl}^-$  (42). In Fig. 9, examples of stronger and weaker XBs are shown.

### Non-covalent interactions in neutral systems: comparison of halogen bonding with chalcogen, pnictogen, and H-bonding

Considering ammonia as a prototypical neutral acceptor, two series of complexes were compared: (i) XBs for different X-donors ( $\text{FCl}$ ,  $\text{Cl}_2$ ,  $\text{O}_2\text{NCl}$ ,  $\text{NCCl}$ ,  $\text{HCCCl}$ ) where a Cl atom

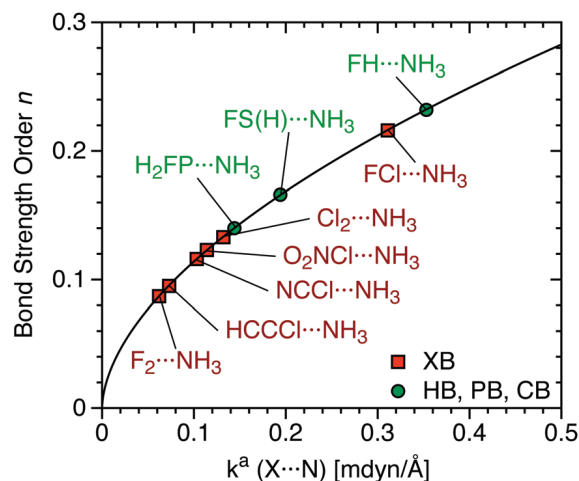


Fig. 10 Relationship between the relative BSO  $n$  and the local XB stretching force constant  $k^a$  for complexes between  $\text{NH}_3$  and a halogen (YX), pnictogen ( $\text{H}_2\text{FP}$ ), chalcogen ( $\text{F}(\text{H})\text{S}$ ) or hydrogen bonding partner (FH). CCSD(T)/aug-cc-pVTZ calculations.

interacts with the N atom of  $\text{NH}_3$ . (ii) The XB in  $\text{FCl} \cdots \text{NH}_3$  was compared with other types of non-covalent interactions such as H-bonding in  $\text{FH} \cdots \text{NH}_3$ , pnictogen-bonding in  $\text{H}_2\text{FP} \cdots \text{NH}_3$  and chalcogen bonding in  $\text{F(H)S} \cdots \text{NH}_3$ . In these complexes, electrostatic interactions can be complemented by a charge transfer from  $\text{lp(N)}$  to the  $\sigma^*$  orbital of the halogen, hydrogen, pnictogen, or chalcogen donor.

According to Fig. 10 the polarity of the Y-X bonds and the polarizability of X decide on the magnitude of the electrostatic interactions, which should increase in the series Y-X:  $\text{F-F}$  (0.087) <  $\text{HCCl}$  (0.095) <  $\text{NCCl}$  (0.116) <  $\text{O}_2\text{NCl}$  (0.123) <  $\text{Cl}_2$  (0.133) <  $\text{H}_2\text{FP}$  (0.140) <  $\text{F(H)S}$  (0.166) <  $\text{FCl}$  (0.216) <  $\text{FH}$  (0.232). There are also minor covalent interactions as is reflected by the charge transfer values especially in the case of  $\text{Cl}_2 \cdots \text{NH}_3$  (55  $m_e$ ) compared to  $\text{NCCl} \cdots \text{NH}_3$  (14  $m_e$ ), leading to a stronger XB even though  $\text{NCCl}$  has a more positive electrostatic potential ( $V(\text{NCCl})$ : 36.8;  $V(\text{Cl}_2)$ : 25.4 kcal mol<sup>-1</sup>). Larger charge transfer values are found for the chalcogen bond of  $\text{F(H)S} \cdots \text{NH}_3$  (81  $m_e$ ), the pnictogen bond of  $\text{H}_2\text{FP} \cdots \text{NH}_3$  (57  $m_e$ ), the H-bond of  $\text{FH} \cdots \text{NH}_3$  (69  $m_e$ ), and the XB in  $\text{FCl} \cdots \text{NH}_3$  (145  $m_e$ ). In all these cases, a lengthening of the charge acceptor bond is observed (from 1.626 to 1.670; 1.577 to 1.644, 0.921 to 0.953, and 1.646 to 1.703 Å, Table 1).

Clearly, the XB is stronger than the chalcogen or pnictogen bond if one compares the three non-covalent interactions  $\text{FCl} \cdots \text{NH}_3$ ,  $\text{F(H)S} \cdots \text{NH}_3$ , and  $\text{H}_2\text{FP} \cdots \text{NH}_3$ . This is the result of three electronic factors: (i) because Cl has a smaller covalent radius than S or P, FCl can establish a stronger interaction with larger orbital overlap. (ii) Due to the high electronegativity of both F and Cl, the energy of the  $\sigma^*(\text{XY})$  orbital is lower leading to a smaller  $\Delta\epsilon(2e)$  and a stronger 2e-destabilizing interaction. (iii) FCl forms a head-on interaction with  $\text{NH}_3$  thus maximizing charge transfer (covalent interactions because of 2e-delocalization and stabilization) and electrostatic interactions (*via* a  $\sigma$ -hole).

If the non-covalent interactions between the monomers have an increasing charge transfer contribution, orbital overlap  $S$  is maximized, and the geometry leading to a maximal  $S$  becomes less flexible. Hence, the rigidity of the YXA unit measured by the local bending force constant  $k^a(\text{YXA})$  increases for an increased covalent contribution to the  $\text{YX} \cdots \text{AR}$  interactions. The values of  $k^a(\text{YXA})$  listed in Table 1 reflect this: 0.434 ( $\text{FCl} \cdots \text{NH}_3$ ) > 0.410 ( $\text{F(H)S} \cdots \text{NH}_3$ ) > 0.317 ( $\text{H}_2\text{FP} \cdots \text{NH}_3$ ) > 0.096 mdyn Å rad<sup>-2</sup> ( $\text{FH} \cdots \text{NH}_3$ ). Important in this connection is that one compares non-covalent interactions of the same type. Clearly, the H-bonding interactions as a first row-second row interaction should not be compared with a third row-second row interaction. Exchange repulsion between  $\text{lp(X)}$ ,  $\text{lp(A)}$ , and AR bonding electrons is no longer present so that the H-bond in  $\text{FH} \cdots \text{NH}_3$  ( $n = 0.232$ , see above) becomes stronger than the other non-covalent interactions.

### Comparison of BSO values with other quantities

We have investigated whether the intrinsic strength of the XB is related to the distance  $r(\text{XA})$ , the binding energy, or the energy density at the critical point. The latter quantities are commonly discussed in the literature to assess the strength of the XB.<sup>10</sup>

However, there is no relationship for example between the XB strength and the binding energy  $\Delta E$  as the latter is a cumulative quantity that accounts not only for the intrinsic strength of the XB, but also for the energy required for the reorganization of the electronic structure of the monomer upon the formation of the complex and for contributions due to secondary inter-monomer interactions. Accordingly, a strong scattering of the data points is obtained when correlating BSO and  $\Delta E$  ( $r(\text{XA}), H_b$ ) values for a larger set of complexes as we have done in the ESI<sup>†</sup> (not always done in the literature<sup>49,72</sup>) thus indicating that none of the latter quantities reflects the strength of the XB and therefore cannot be used for a quantitative ordering of XBs according to their strength. Even qualitatively, these quantities are limited to the description of small groups of XB systems dominated by similar electronic effects. As the BSO values derived from the local X $\cdots$ A stretching force constants provide a measure of the intrinsic strength of the bond, it is possible to discuss the strength of XB in a comparative, quantitative manner.

## 4 Conclusions and outlook

In this work, we present for the first time a quantitative description of the intrinsic strength of XB based on accurate CCSD(T)/aug-cc-pVTZ calculations of the local stretching force constant and an accurate analysis of binding energies, geometries, NBO charges, charge transfer values, dipole moments, electrostatic potentials, electron and energy density distributions, difference density distributions, vibrational frequencies, local bending force constants, and relative BSO values  $n$  all calculated at the coupled cluster level. In this way, a clear picture of the bonding mechanism emerges. XB has been compared with hydrogen, chalcogen, and pnictogen bonding where the latter term has been extended to include the interaction between a pnictogen atom and a hetero atom other than a pnictogen.

(1) XB can emerge from weak electrostatic interactions (binding energies  $\Delta E < 10$  kcal mol<sup>-1</sup>) or from fully covalent 3c-4e interactions ( $\Delta E$  up to 45 kcal mol<sup>-1</sup>). The majority of XBs have both electrostatic and covalent interactions and therefore span a large range of binding energies and BSO values. Based on the local XB stretching force constant, we suggest to distinguish between weak electrostatic XBs ( $0.05 < n(\text{XA}) \leq 0.2$ ), normal XBs ( $0.2 < n(\text{XA}) \leq 0.3$ ), and strong, predominantly covalent XBs ( $0.3 < n(\text{XA}) < 0.6$ , Fig. 2).

(2) The mechanism of XB as it was repeatedly described in the literature<sup>10</sup> has been confirmed in this work. The covalent part can be rationalized by the orbital diagram of Fig. 4 and is characterized by charge transfer values or the difference density distribution of Fig. 8. We show that the 4e-destabilizing factor must not be overlooked when analyzing XB.

(3) The electrostatic part of XB increases with (i) the polarizing power of the hetero atom A, (ii) the polarity of the XY bond, and (iii) the polarizability of the halogen atom X. This implies that halogens  $\text{X}_2$  with higher atomic number form stronger XBs and that in turn interhalogens XY form stronger XBs than dihalogens  $\text{X}_2$  where the strongest bonds for a series of

interhalogens are found for  $Y = F$ . Deviations from these trends normally indicate covalent contributions to XB as in the case  $FCl \cdots NH_3$ .

(4) Electronegative substituents R attached to A can have opposing effects on the strength of the XB. The latter is reduced in the case of an amine because the negative charge at N is lowered and  $X \cdots N$  attraction is reduced (e.g., in  $FCl \cdots NH_mR_{3-m}$  ( $m = 1, 2, 3$ ) complexes). This effect is even stronger for phosphines. But in this case it is annihilated by a stabilizing covalent effect, which is based on the contraction of the  $lp(P)$  orbital and an improved overlap with the  $\sigma^*(XY)$  orbital. Comparison of the calculated BSO and charge transfer values reveals that an optimal covalent contribution is obtained for the complex  $FCl \cdots PHF_2$ .

(5) XB can be strengthened by H bonding as we have demonstrated for the complexes  $FCl \cdots NH_2OH$  and  $FCl \cdots PH_2OH$ . A *syn*-arrangement of the XB and the OH group leads to an electrostatic  $lp(Cl) \cdots H-O$  bond with BSO values of 0.111 and 0.113 which increases the strength of the XB significantly. In the *anti* position, the effect of the OH group is destabilizing for amines and moderately stabilizing for phosphines.

(6) XB in substituted phosphines (R being more electronegative than P) leads to partial 3c-4e character, which can be quantified with the help of the BSO values:  $PH_2OH$  (90% of 3c-4e bonding;  $BSO = 0.395$ )  $\approx$   $PHF_2$  (85%;  $n(AX) = 0.396$ )  $>$   $PH_2CH_3$  (80%)  $\approx$   $PH_2F$  (79%)  $>$   $PH_2Cl$  (60%)  $>$   $PH_3$  (39%).

(7) 3c-4e bonding implies covalent character, which is completely fulfilled for anions of the type  $Y \cdots X \cdots Y$  (X,Y: halogen):  $[Cl \cdots Cl \cdots Cl]^-$  ( $BSO: 0.342$ )  $<$   $[Br \cdots Br \cdots Br]^-$  (0.350)  $<$   $[F \cdots F \cdots F]^-$  (0.500)  $<$   $[F \cdots Cl \cdots F]^-$  (0.522). This trend of increasing bond strengths is due to increasing covalent interactions and better charge distributions.

(8) Halogen bonding is stronger than pnictogen, chalcogen, or H bonding in comparable complexes. One obtains for the following anions:  $[F \cdots Cl \cdots F]^-$  (0.522)  $>$   $[F \cdots PH_2 \cdots F]^-$  (0.475)  $>$   $[F \cdots H \cdots F]^-$  (0.380); neutral complexes:  $FCl \cdots NH_3$  (0.216)  $>$   $F(H)S \cdots NH_3$  (0.166)  $>$   $H_2FP \cdots NH_3$  (0.140). In the latter case H-bonding is stronger because of the lack of destabilizing exchange repulsion:  $FH \cdots NH_3$  (0.232). The strength of the XB is due to the smaller covalent radius of a halogen (compared to pnictogen, chalcogen), the larger overlap, the lower  $\sigma$ -orbital energies, and the larger 2e-stabilization effect.

(9) The intrinsic XB strength as measured by the BSO values is not reflected by the binding energies  $\Delta E$  or the distance  $r(AX)$  because these parameters contain other effects, which are not related to the XB strength. The Badger rule (relationship between  $k^a(AX)$  and  $r(AX)$ )<sup>106,122</sup> is only qualitatively fulfilled. The same holds for the charge transfer values, the density and energy distribution,  $\rho_b$  and  $H_b$  values, or the bending force constants  $k^a(YXA)$ . These are useful quantities when discussing special electronic effects, but in general they do not reflect the intrinsic bond strength.

(10) All systems investigated were also calculated with several XC functionals. In general, DFT can give a qualitative correct description of XB, with few exceptions found for the  $F_2$  complexes, and in those cases where strongly electronegative substituents and/or 3c-4e bonding are involved.

Future work has to show how XB changes with increasing atomic numbers for X and A to see how relativistic effects influence XB. One other topic, which deserves more attention is the description of XB *via* the  $\sigma$ -hole mechanism. Any form of bonding implies changes in both the potential and the kinetic energy as was demonstrated by Ruedenberg when investigating the  $H_2^+$  and  $H_2$  bond.<sup>123,124</sup> If one exclusively focuses on the potential energy, then the kinetic energy as an important component of bonding is neglected and conclusions just drawn on the existence of a  $V(r)$ -based " $\sigma$ -hole" become questionable. Clearly, this aspect deserves additional investigation.

## Acknowledgements

This work was financially supported by the National Science Foundation grants CHE 1152357 and CHE 1464906. We thank SMU for providing computational resources. The authors acknowledge financial support by CAPES (Brazil; fellowship grant BEX 9534-13-0).

## References

- 1 M. C. Ford and P. S. Ho, Computational Tools To Model Halogen Bonds in Medicinal Chemistry, *J. Med. Chem.*, 2016, **59**, 1655–1670.
- 2 P. Ho, in *Halogen*, ed. I. Bonding, P. Metrangolo and G. Resnati, Topics in Current Chemistry, Springer International Publishing, 2015, vol. 358, pp. 241–276.
- 3 R. Wilcken, M. O. Zimmermann, A. Lange, A. C. Joerger and F. M. Boeckler, Principles and Applications of Halogen Bonding in Medicinal Chemistry and Chemical Biology, *J. Med. Chem.*, 2013, **56**, 1363–1388.
- 4 A. Abate, M. Saliba, D. J. Hollman, S. D. Stranks, K. Wojciechowski, R. Avolio, G. Grancini, A. Petrozza and H. J. Snaith, Supramolecular Halogen Bond Passivation of Organic-Inorganic Halide Perovskite Solar Cells, *Nano Lett.*, 2014, **14**, 3247–3254.
- 5 L. C. Gilday, S. W. Robinson, T. A. Barendt, M. J. Langton, B. R. Mullaney and P. D. Beer, Halogen Bonding in Supramolecular Chemistry, *Chem. Rev.*, 2015, **115**, 7118–7195.
- 6 C. B. Aakeroy, C. L. Spartz, S. Dembowski, S. Dwyre and J. Desper, A systematic structural study of halogen bonding *versus* hydrogen bonding within competitive supramolecular systems, *IUCrJ*, 2015, **2**, 498–510.
- 7 C. B. Aakeroy, T. K. Wijethunga, J. Desper and M. Dakovic, Crystal Engineering with Iodoethynylbenzenes: A Group of Highly Effective Halogen-Bond Donors, *Cryst. Growth Des.*, 2015, **15**, 3853–3861.
- 8 O. Dumele, N. Trapp and F. Diederich, Halogen Bonding Molecular Capsules, *Angew. Chem., Int. Ed.*, 2015, **54**, 12339–12344.
- 9 G. Berger, J. Soubhye and F. Meyer, Halogen bonding in polymer science: from crystal engineering to functional supramolecular polymers and materials, *Polym. Chem.*, 2015, **6**, 3559–3580.

- 10 G. Cavallo, P. Metrangolo, R. Milani, T. Pilati, A. Priimagi, G. Resnati and G. Terraneo, The Halogen Bond, *Chem. Rev.*, 2016, **116**, 2478–2601.
- 11 O. Dumele, D. Wu, N. Trapp, N. Goroff and F. Diederich, Halogen Bonding of (Iodoethynyl)benzene Derivatives in Solution, *Org. Lett.*, 2014, **16**, 4722–4725.
- 12 N. Nagels, Y. Geboes, B. Pinter, F. DeProft and W. A. Herrebout, Tuning the Halogen/Hydrogen Bond Competition: A Spectroscopic and Conceptual DFT Study of Some Model Complexes Involving CHF<sub>2</sub>I, *Chem. – Eur. J.*, 2014, **20**, 8433–8443.
- 13 A. Bauzá, T. J. Mooibroek and A. Frontera, The Bright Future of Unconventional  $\sigma/\pi$ -Hole Interactions, *ChemPhysChem*, 2015, **16**, 2496–2517.
- 14 M. Saito, N. Tsuji, Y. Kobayashi and Y. Takemoto, Direct Dehydroxylative Coupling Reaction of Alcohols with Organosilanes through Si–X Bond Activation by Halogen Bonding, *Org. Lett.*, 2015, **17**, 3000–3003.
- 15 C. B. Aakeroy, T. K. Wjethunga, J. Desper and C. Moore, Halogen-Bond Preferences in Co-crystal Synthesis, *J. Chem. Crystallogr.*, 2015, **45**, 267–276.
- 16 S. Schindler and S. M. Huber, in *Halogen Bonding II*, ed. P. Metrangolo and G. Resnati, Topics in Current Chemistry, Springer International Publishing, 2015, vol. 359, pp. 167–203.
- 17 F. Kniep, S. H. Jungbauer, Q. Zhang, S. M. Walter, S. Schindler, I. Schnapperelle, E. Herdtweck and S. M. Huber, Organocatalysis by Neutral Multidentate Halogen-Bond Donors, *Angew. Chem., Int. Ed.*, 2013, **52**, 7028–7032.
- 18 W. T. Pennington, T. W. Hanks and H. D. Arman, in *Halogen Bonding*, ed. P. Metrangolo and G. Resnati, Structure and Bonding, Springer Berlin Heidelberg, 2008, vol. 126, pp. 65–104.
- 19 T. M. Beale, M. G. Chudzinski, M. G. Sarwar and M. S. Taylor, Halogen bonding in solution: thermodynamics and applications, *Chem. Soc. Rev.*, 2013, **42**, 1667–1680.
- 20 L. P. Wolters, P. Schyman, M. J. Pavan, W. L. Jorgensen, F. M. Bickelhaupt and S. Kozuch, The many faces of halogen bonding: a review of theoretical models and methods, *Wiley Interdiscip. Rev.: Comput. Mol. Sci.*, 2014, **4**, 523–540.
- 21 A. V. Jentzsch and S. Matile, in *Halogen Bonding I*, ed. P. Metrangolo and G. Resnati, Topics in Current Chemistry, Springer International Publishing, 2015, vol. 358, pp. 205–239.
- 22 M. H. Kolar and P. Hobza, Computer Modeling of Halogen Bonds and Other  $\sigma$ -Hole Interactions, *Chem. Rev.*, 2016, **116**, 5155–5187.
- 23 P. Metrangolo, F. Meyer, T. Pilati, G. Resnati and G. Terraneo, Halogen Bonding in Supramolecular Chemistry, *Angew. Chem., Int. Ed.*, 2008, **47**, 6114–6127.
- 24 E. Parisini, P. Metrangolo, T. Pilati, G. Resnati and G. Terraneo, Halogen Bonding in Halocarbon-Protein Complexes: A Structural Survey, *Chem. Soc. Rev.*, 2011, **40**, 2267–2278.
- 25 G. Terraneo, G. Resnati and P. Metrangolo, *Iodine Chemistry and Applications*, John Wiley and Sons, Inc., 2014, pp. 159–194.
- 26 A. C. Legon, Prereactive Complexes of Dihalogens XY with Lewis Bases B in the Gas Phase: A Systematic Case for the Halogen Analogue B···XY of the Hydrogen Bond B···HX, *Angew. Chem., Int. Ed.*, 1999, **38**, 2686–2714.
- 27 M. C. A. Aragoni, M. Devillanova, F. A. Garau, A. Isaia, F. Lippolis and V. M. Annalisa, The nature of the chemical bond in linear three-body systems: from I<sub>3</sub><sup>−</sup> to mixed chalcogen/halogen and trichalcogen moieties, *Bioinorg. Chem. Appl.*, 2007, **2007**, 1–46.
- 28 B. Braida and P. C. Hiberty, Application of the valence bond mixing configuration diagrams to hypervalency in trihalide anions: a challenge to the Rundle-Pimentel model, *J. Phys. Chem. A*, 2008, **112**, 13045–13052.
- 29 J. E. Del Bene, I. Alkorta and J. Elguero, Do Traditional, Chlorine-shared, and Ion-pair Halogen Bonds Exist? An ab Initio Investigation of FCl:CNX Complexes, *J. Phys. Chem. A*, 2010, **114**, 12958–12962.
- 30 J. E. Del Bene, I. Alkorta and J. Elguero, Do nitrogen bases form chlorine-shared and ion-pair halogen bonds?, *Chem. Phys. Lett.*, 2011, **508**, 6–9.
- 31 O. Donoso-tauda, P. Jaque, I. Alkorta, J. Elguero and I. Alkorta, Traditional and ion-pair halogen-bonded complexes between chlorine and bromine derivatives and a nitrogen-heterocyclic carbene, *J. Phys. Chem. A*, 2014, **118**, 9552–9560.
- 32 J. Rezac and P. Hobza, Benchmark Calculations of Interaction Energies in Noncovalent Complexes and Their Applications, *Chem. Rev.*, 2016, **116**, 5038–5071.
- 33 A. C. Legon, A reduced radial potential energy function for the halogen bond and the hydrogen bond in complexes B···XY and B···HX, where X and Y are halogen atoms, *Phys. Chem. Chem. Phys.*, 2014, **16**, 12415–12421.
- 34 A. O. de-la Roza, E. R. Johnson and G. A. DiLabio, Halogen Bonding from Dispersion-Corrected Density-Functional Theory: The Role of Delocalization Error, *J. Chem. Theory Comput.*, 2014, **10**, 5436–5447.
- 35 J. G. Hill and X. Hu, Theoretical Insights into the Nature of Halogen Bonding in Prereactive Complexes, *Chem. – Eur. J.*, 2013, **19**, 3620–3628.
- 36 A. Karpfen, *Halogen Bonding*, 2008, vol. 126, pp. 1–15.
- 37 B. Braida and P. C. Hiberty, Application of the Valence Bond Mixing Configuration Diagrams to Hypervalency in Trihalide Anions: A Challenge to the Rundle-Pimentel Model, *J. Phys. Chem. A*, 2008, **112**, 13045–13052.
- 38 S. Kozuch and J. M. L. Martin, Halogen Bonds: Benchmarks and Theoretical Analysis, *J. Chem. Theory Comput.*, 2013, **9**, 1918–1931.
- 39 J. Grant Hill, The halogen bond in thiirane···ClF: an example of a Mulliken inner complex, *Phys. Chem. Chem. Phys.*, 2014, **16**, 19137–19140.
- 40 J. Grant Hill and A. C. Legon, On the directionality and non-linearity of halogen and hydrogen bonds, *Phys. Chem. Chem. Phys.*, 2015, **17**, 858–867.
- 41 A. Forni, S. Pieraccini, S. Rendine and M. Sironi, Halogen bonds with benzene: an assessment of DFT functionals, *J. Comput. Chem.*, 2014, **35**, 386–394.
- 42 L. P. Wolters and F. M. Bickelhaupt, Halogen Bonding versus Hydrogen Bonding: A Molecular Orbital Perspective, *ChemistryOpen*, 2012, **1**, 96–105.

- 43 B. Pinter, N. Nagels, W. A. Herrebout and F. DeProft, Halogen Bonding from a Hard and Soft Acids and Bases Perspective: Investigation by Using Density Functional Theory Reactivity Indices, *Chem. – Eur. J.*, 2013, **19**, 519–530.
- 44 V. Tognetti and L. Joubert, Electron density Laplacian and halogen bonds, *Theor. Chem. Acc.*, 2015, **134**, 1–10.
- 45 C. Wang, D. Danovich, Y. Mo and S. Shaik, On The Nature of the Halogen Bond, *J. Chem. Theory Comput.*, 2014, **10**, 3726–3737.
- 46 J. George, V. L. Deringer and R. Dronskowski, Cooperativity of Halogen, Chalcogen, and Pnictogen Bonds in Infinite Molecular Chains by Electronic Structure Theory, *J. Phys. Chem. A*, 2014, **118**, 3193–3200.
- 47 A. J. Parker, J. Stewart, K. J. Donald and C. A. Parish, Halogen Bonding in DNA Base Pairs, *J. Am. Chem. Soc.*, 2012, **134**, 5165–5172.
- 48 M. Palusiak, On the nature of halogen bond – The Kohn–Sham molecular orbital approach, *THEOCHEM*, 2010, **945**, 89–92.
- 49 J. E. D. Bene, I. Alkorta and J. Elguero, Influence of Substituent Effects on the Formation of P···Cl Pnictogen Bonds or Halogen Bonds, *J. Phys. Chem. A*, 2014, **118**, 2360–2366.
- 50 M. Tawfik and K. J. Donald, Halogen Bonding: Unifying Perspectives on Organic and Inorganic Cases, *J. Phys. Chem. A*, 2014, **118**, 10090–10100.
- 51 E. V. Bartashevich and V. G. Tsirelson, Interplay between non-covalent interactions in complexes and crystals with halogen bonds, *Russ. Chem. Rev.*, 2014, **83**, 1181.
- 52 D. J. R. Duarte, N. M. Peruchena and I. Alkorta, Double Hole-Lump Interaction between Halogen Atoms, *J. Phys. Chem. A*, 2015, **119**, 3746–3752.
- 53 H. J. Jahromi, K. Eskandari and A. Alizadeh, Comparison of halogen bonds in M–X···N contacts (M = C, Si, Ge and X = Cl, Br), *J. Mol. Model.*, 2015, **21**, 1–9.
- 54 R. Lo and B. Ganguly, Revealing halogen bonding interactions with anomeric systems: an *ab initio* quantum chemical studies, *J. Mol. Graphics Modell.*, 2015, **55**, 123–133.
- 55 V. Sladek, P. Skorna, P. Poliak and V. Lukes, The *ab initio* study of halogen and hydrogen  $\sigma$ N-bonded *para*-substituted pyridine···(X<sub>2</sub>/XY/HX) complexes, *Chem. Phys. Lett.*, 2015, **619**, 7–13.
- 56 I. Alkorta, J. Elguero, O. Mo, M. Yanez and J. E. Del Bene, Using beryllium bonds to change halogen bonds from traditional to chlorine-shared to ion-pair bonds, *Phys. Chem. Chem. Phys.*, 2015, **17**, 2259–2267.
- 57 B. Nepal and S. Scheiner, Long-range behavior of non-covalent bonds. Neutral and charged H-bonds, pnictogen, chalcogen, and halogen bonds, *Chem. Phys.*, 2015, **456**, 34–40.
- 58 S. M. Huber, E. Jimenez-Izal, J. M. Ugalde and I. Infante, Unexpected trends in halogen-bond based noncovalent adducts, *Chem. Commun.*, 2012, **48**, 7708–7710.
- 59 I. Alkorta, F. Blanco, M. Solimannejad and J. Elguero, Competition of Hydrogen Bonds and Halogen Bonds in Complexes of Hypohalous Acids with Nitrogenated Bases, *J. Phys. Chem. A*, 2008, **112**, 10856–10863.
- 60 U. Adhikari and S. Scheiner, Substituent Effects on Cl···N, S···N, and P···N Noncovalent Bonds, *J. Phys. Chem. A*, 2012, **116**, 3487–3497.
- 61 K. E. Riley, J. S. Murray, J. Fanfrlík, J. Rezáč, R. J. Solá, M. C. Concha, F. M. Ramos and P. Politzer, Halogen bond tunability II: the varying roles of electrostatic and dispersion contributions to attraction in halogen bonds, *J. Mol. Model.*, 2013, **19**, 4651–4659.
- 62 A. J. Stone, Are Halogen Bonded Structures Electrostatically Driven?, *J. Am. Chem. Soc.*, 2013, **135**, 7005–7009.
- 63 R. Sedlak, M. H. Kolár and P. Hobza, Polar Flattening and the Strength of Halogen Bonding, *J. Chem. Theory Comput.*, 2015, **11**, 4727–4732.
- 64 W. Zierkiewicz, D. C. Bienko, D. Michalska and T. Zeegers-Huyskens, Theoretical investigation of the halogen bonded complexes between carbonyl bases and molecular chlorine, *J. Comput. Chem.*, 2015, **36**, 821–832.
- 65 K. Dyduch, M. P. Mitoraj and A. Michalak, ETS-NOCV description of  $\sigma$ -hole bonding, *J. Mol. Model.*, 2013, **19**, 2747–2758.
- 66 M. P. Mitoraj and A. Michalak, Theoretical description of halogen bonding – an insight based on the natural orbitals for chemical valence combined with the extended-transition-state method (ETS-NOCV), *J. Mol. Model.*, 2013, **19**, 4681–4688.
- 67 E. V. Bartashevich and V. G. Tsirelson, Atomic dipole polarization in charge-transfer complexes with halogen bonding, *Phys. Chem. Chem. Phys.*, 2013, **15**, 2530–2538.
- 68 D. Duarte, G. Sosa and N. Peruchena, Nature of halogen bonding. A study based on the topological analysis of the Laplacian of the electron charge density and an energy decomposition analysis, *J. Mol. Model.*, 2013, **19**, 2035–2041.
- 69 E. L. Angelina, D. R. Duarte and N. M. Peruchena, Is the decrease of the total electron energy density a covalence indicator in hydrogen and halogen bonds?, *J. Mol. Model.*, 2013, **19**, 2097–2106.
- 70 S. J. Grabowski, Non-covalent interactions – QTAIM and NBO analysis, *J. Mol. Model.*, 2013, **19**, 4713–4721.
- 71 D. Duarte, E. L. Angelina and N. Peruchena, Physical meaning of the QTAIM topological parameters in hydrogen bonding, *J. Mol. Model.*, 2014, **20**, 1–10.
- 72 A. Shahi and E. Arunan, Hydrogen bonding, halogen bonding and lithium bonding: an atoms in molecules and natural bond orbital perspective towards conservation of total bond order, inter- and intra-molecular bonding, *Phys. Chem. Chem. Phys.*, 2014, **16**, 22935–22952.
- 73 D. Kaur, R. Kaur and B. Shiekh, Effects of substituents and charge on the RCHO···X–Y X = Cl, Br, I; Y:–CF<sub>3</sub>, –CF<sub>2</sub>H, –CFH<sub>2</sub>, –CN, –CCH, –CCCN; R:–OH, –OCH<sub>3</sub>, –NH<sub>2</sub>, –O–halogen-bonded complexes, *Struct. Chem.*, 2015, 1–11.
- 74 D. J. R. Duarte, G. L. Sosa, N. M. Peruchena and I. Alkorta, Halogen bonding. The role of the polarizability of the electron-pair donor, *Phys. Chem. Chem. Phys.*, 2016, **18**, 7300–7309.
- 75 J. Joy, E. D. Jemmis and K. Vidya, Negative hyperconjugation and red-, blue- or zero-shift in X–Z···Y complexes, *Faraday Discuss.*, 2015, **177**, 33–50.

- 76 J. Joy, A. Jose and E. D. Jemmis, Continuum in the X–Z–Y weak bonds: Z = main group elements, *J. Comput. Chem.*, 2015, **37**, 270–279.
- 77 I. Alkorta, J. Elguero and J. E. D. Bene, Characterizing Traditional and Chlorine-Shared Halogen Bonds in Complexes of Phosphine Derivatives with ClF and Cl<sub>2</sub>, *J. Phys. Chem. A*, 2014, **118**, 4222–4231.
- 78 A. Bauzá, I. Alkorta, A. Frontera and J. Elguero, On the Reliability of Pure and Hybrid DFT Methods for the Evaluation of Halogen, Chalcogen, and Pnictogen Bonds Involving Anionic and Neutral Electron Donors, *J. Chem. Theory Comput.*, 2013, **9**, 5201–5210.
- 79 S. J. Grabowski, Hydrogen and halogen bonds are ruled by the same mechanisms, *Phys. Chem. Chem. Phys.*, 2013, **15**, 7249–7259.
- 80 S. Scheiner, Detailed comparison of the pnictogen bond with chalcogen, halogen, and hydrogen bonds, *Int. J. Quantum Chem.*, 2013, **113**, 1609–1620.
- 81 Y.-Z. Zheng, N.-N. Wang, Y. Zhou and Z.-W. Yu, Halogen-bond and hydrogen-bond interactions between three benzene derivatives and dimethyl sulphoxide, *Phys. Chem. Chem. Phys.*, 2014, **16**, 6946–6956.
- 82 C. Wang, L. Guan, D. Danovich, S. Shaik and Y. Mo, The origins of the directionality of noncovalent intermolecular interactions, *J. Comput. Chem.*, 2016, **37**, 34–45.
- 83 C. Trujillo, G. Sanchez-Sanz, I. Alkorta and J. Elguero, Halogen, chalcogen and pnictogen interactions in (XNO<sub>2</sub>)<sub>2</sub> homodimers (X = F, Cl, Br, I), *New J. Chem.*, 2015, **39**, 6791–6802.
- 84 T. Clark, M. Hennemann, J. Murray and P. Politzer, Halogen bonding: the  $\sigma$ -hole, *J. Mol. Model.*, 2007, **13**, 291–296.
- 85 P. Politzer, J. Murray and M. Concha, Halogen bonding and the design of new materials: organic bromides, chlorides and perhaps even fluorides as donors, *J. Mol. Model.*, 2007, **13**, 643–650.
- 86 P. Politzer, J. S. Murray and T. Clark, Halogen bonding: an electrostatically-driven highly directional noncovalent interaction, *Phys. Chem. Chem. Phys.*, 2010, **12**, 7748–7757.
- 87 A. Legon, *Halogen Bonding*, 2008, vol. 126, pp. 17–64.
- 88 S. V. Rosokha, I. S. Neretin, T. Y. Rosokha, J. Hecht and J. K. Kochi, Charge-transfer character of halogen bonding: Molecular structures and electronic spectroscopy of carbon tetrabromide and bromoform complexes with organic  $\sigma$ - and  $\pi$ -donors, *Heteroat. Chem.*, 2006, **17**, 449–459.
- 89 Z. Konkoli and D. Cremer, A New Way of Analyzing Vibrational Spectra I. Derivation of Adiabatic Internal Modes, *Int. J. Quantum Chem.*, 1998, **67**, 1–11.
- 90 D. Cremer, J. A. Larsson and E. Kraka, in *Theoretical and Computational Chemistry, Volume 5, Theoretical Organic Chemistry*, ed. C. Parkanyi, Elsevier, Amsterdam, 1998, pp. 259–327.
- 91 W. Zou and D. Cremer, Properties of Local Vibrational Modes: The Infrared Intensity, *Theor. Chem. Acc.*, 2014, **133**, 1451.
- 92 E. B. Wilson, J. C. Decius and P. C. Cross, *Molecular Vibrations. The Theory of Infrared and Raman Vibrational Spectra*, McGraw-Hill, New York, 1955.
- 93 W. Zou, R. Kalescky, E. Kraka and D. Cremer, Relating Normal Vibrational Modes To Local Vibrational Modes With The Help of an Adiabatic Connection Scheme, *J. Chem. Phys.*, 2012, **137**, 084114.
- 94 R. Kalescky, W. Zou, E. Kraka and D. Cremer, Local Vibrational Modes of the Water Dimer – Comparison of Theory and Experiment, *Chem. Phys. Lett.*, 2012, **554**, 243–247.
- 95 M. Freindorf, E. Kraka and D. Cremer, A comprehensive analysis of hydrogen bond interactions based on local vibrational modes, *Int. J. Quantum Chem.*, 2012, **112**, 3174–3187.
- 96 R. Kalescky, E. Kraka and D. Cremer, Identification of the Strongest Bonds in Chemistry, *J. Phys. Chem. A*, 2013, **117**, 8981–8995.
- 97 K. Raghavachari, G. W. Trucks, J. A. Pople and M. Head-Gordon, *Chem. Phys. Lett.*, 1989, **157**, 479–483.
- 98 T. Clark, P. Politzer and J. S. Murray, Correct electrostatic treatment of noncovalent interactions: the importance of polarization, *Wiley Interdiscip. Rev.: Comput. Mol. Sci.*, 2015, **5**, 169–177.
- 99 P. Politzer, J. S. Murray and T. Clark, Mathematical modeling and Physical Reality in Non-covalent Interactions, *J. Mol. Model.*, 2015, **21**, 52–61.
- 100 P. Politzer, J. S. Murray and T. Clark,  $\sigma$ -Hole Bonding: A Physical Interpretation, *Top. Curr. Chem.*, 2015, **358**, 19–42.
- 101 D. Woon and T. J. Dunning, Gaussian Basis Sets for Use in Correlated Molecular Calculations. IV. Calculation of Static Electrical Response Properties, *J. Chem. Phys.*, 1994, **100**, 2975–2988.
- 102 T. Dunning, Gaussian Basis Sets for Use in Correlated Molecular Calculations. I. The Atoms Boron Through Neon and Hydrogen, *J. Chem. Phys.*, 1989, **90**, 1007–1023.
- 103 D. Woon and T. Dunning, Gaussian Basis Sets for Use in Correlated Molecular Calculations. III. The Atoms Aluminum Through Argon, *J. Chem. Phys.*, 1993, **98**, 1358–1371.
- 104 Z. Konkoli and D. Cremer, A New Way of Analyzing Vibrational Spectra III. Characterization of Normal Vibrational Modes in Terms of Internal Vibrational Modes, *Int. J. Quantum Chem.*, 1998, **67**, 29–41.
- 105 W. Zou and D. Cremer, C<sub>2</sub> in a Box: Determining its Intrinsic Bond Strength for the X<sup>1</sup> $\Sigma_g^+$  Ground State, *Chem. – Eur. J.*, 2016, **22**, 4087–4099.
- 106 E. Kraka, J. A. Larsson and D. Cremer, *Generalization of the Badger Rule Based on the Use of Adiabatic Vibrational Modes in Vibrational Modes in Computational IR Spectroscopy*, Wiley, New York, 2010, pp. 105–149.
- 107 S. Boys and F. Bernardi, The Calculation of Small Molecular Interactions by The Differences of Separate Total Energies. Some Procedures with Reduced Errors, *Mol. Phys.*, 1970, **19**, 553–566.
- 108 F. Weinhold and C. R. Landis, *Valency and Bonding: A Natural Bond Orbital Donor – Acceptor Perspective*, Cambridge University Press, Cambridge, UK, 2003.
- 109 D. Cremer and E. Kraka, A Description of the Chemical Bond in Terms of Local Properties of Electron Density and Energy, *Croat. Chem. Acta*, 1984, **57**, 1259–1281.

- 110 D. Cremer and E. Kraka, Chemical Bonds without Bonding Electron Density – Does the Difference Electron Density Analysis Suffice for a Description of the Chemical Bond?, *Angew. Chem., Int. Ed. Engl.*, 1984, **23**, 627–628.
- 111 E. Kraka and D. Cremer, in *Theoretical Models of Chemical Bonding. The Concept of the Chemical Bond*, ed. Z. Maksic, Springer Verlag, Heidelberg, Germany, 1990, vol. 2, pp. 453–542.
- 112 E. Kraka, W. Zou, M. Filatov, J. Grafenstein, D. Izotov, J. Gauss, Y. He, A. Wu, Z. Konkoli and V. Polo, *et al.*, *COLOGNE2016*, 2014; see <http://www.smu.edu/catco>.
- 113 J. F. Stanton, J. Gauss, M. E. Harding and P. G. Szalay, *et al.*, *CFOUR, A Quantum Chemical Program Package*. 2010, see <http://www.cfour.de>.
- 114 T. Keith, *TK Gristmill Software*, Overland Park KS, USA, 2011, [aim.tkgristmill.com](http://aim.tkgristmill.com).
- 115 W. Zou, D. Nori-Shargh and J. E. Boggs, On the Covalent Character of Rare Gas Bonding Interactions: A New Kind of Weak Interaction, *J. Phys. Chem. A*, 2013, **117**, 207–212.
- 116 T. Lu and F. Chen, Multiwfn: A Multifunctional Wavefunction Analyzer, *J. Comput. Chem.*, 2012, **33**, 580–592.
- 117 D. Setiawan, E. Kraka and D. Cremer, Description of pnictogen bonding with the help of vibrational spectroscopy – the missing link between theory and experiment, *Chem. Phys. Lett.*, 2014, **614**, 136–142.
- 118 D. Setiawan, E. Kraka and D. Cremer, Strength of the Pnictogen Bond in Complexes Involving Group Va Elements N, P, and As, *J. Phys. Chem. A*, 2014, **119**, 1642–16562.
- 119 E. Kraka, W. Zou, M. Freindorf and D. Cremer, Energetics and Mechanism of the Hydrogenation of  $XH_n$  for Group IV to Group VII Elements X, *J. Chem. Theory Comput.*, 2012, **8**, 4931–4943.
- 120 R. Kalescky, E. Kraka and D. Cremer, Description of Aromaticity with the help of Vibrational Spectroscopy: Anthracene and Phenanthrene, *J. Phys. Chem. A*, 2014, **118**, 223–237.
- 121 W. W. Porterfield, *Inorganic Chemistry, A Unified Approach*, Academic Press, San Diego, 1993.
- 122 R. M. Badger, A Relation Between Internuclear Distances and Bond Force Constants, *J. Chem. Phys.*, 1934, **2**, 128–131.
- 123 K. Ruedenberg, The Physical Nature of the Chemical Bond, *Rev. Mod. Phys.*, 1962, **34**, 326–352.
- 124 K. Ruedenberg, in *Localization and Delocalization in Quantum Chemistry*, ed. O. Chalvet, R. Daudel, S. Diner and J. P. Malrieu, Reidel, Dordrecht, Netherlands, 1975, vol. I, pp. 223–245.

Paper II. Quantitative assessment of halogen bonding utilizing vibrational spectroscopy

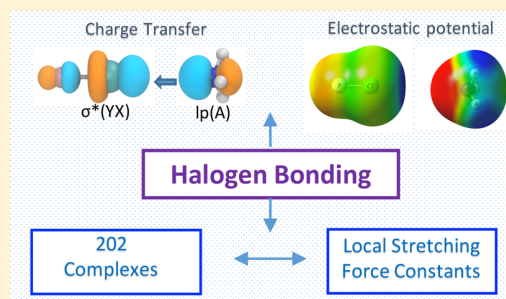
## Quantitative Assessment of Halogen Bonding Utilizing Vibrational Spectroscopy

Vytor Oliveira, Elfi Kraka,\*<sup>1</sup> and Dieter Cremer\*<sup>2</sup>

Computational and Theoretical Chemistry Group, Department of Chemistry, Southern Methodist University (SMU), 3215 Daniel Avenue, Dallas, Texas 75275-0314, United States

## Supporting Information

**ABSTRACT:** A total of 202 halogen-bonded complexes have been studied using a dual-level approach:  $\omega$ B97XD/aug-cc-pVTZ was used to determine geometries, natural bond order charges, charge transfer, dipole moments, electron and energy density distributions, vibrational frequencies, local stretching force constants, and relative bond strength orders  $n$ . The accuracy of these calculations was checked for a subset of complexes at the CCSD(T)/aug-cc-pVTZ level of theory. Apart from this, all binding energies were verified at the CCSD(T) level. A total of 10 different electronic effects have been identified that contribute to halogen bonding and explain the variation in its intrinsic strength. Strong halogen bonds are found for systems with three-center-four-electron (3c-4e) bonding such as chlorine donors in interaction with substituted phosphines. If halogen bonding is supported by hydrogen bonding, genuine 3c-4e bonding can be realized. Perfluorinated diiodobenzenes form relatively strong halogen bonds with alkylamines as they gain stability due to increased electrostatic interactions.



## INTRODUCTION

Halogen bonding has been the topic of many excellent reviews,<sup>1–11</sup> summarizing a large number of experimental and computational investigations. The importance of this kind of noncovalent interaction for materials chemistry,<sup>1,5,12–16</sup> structural chemistry,<sup>9,17–19</sup> synthesis,<sup>6,15,20</sup> catalysis,<sup>6,19,21,22</sup> or medicinal chemistry<sup>7,23</sup> is well-documented. Halogen bonding involves the interaction between a halogen (X) and a Lewis base (A). We will abbreviate halogen bonding in the following by XB, where this abbreviation is also used for the adjective “halogen-bonded”. It is generally accepted that quantum chemistry has been essential in understanding the various features of XB.<sup>4,10,24–35</sup> Most of the quantum-chemical investigations of the last years were based on density functional theory (DFT).<sup>36–44</sup> Other investigations used second-order Møller–Plesset perturbation theory<sup>18,24,45,46,48–54</sup> or more accurate methods.<sup>28,32–35,38,55,56</sup> In view of the many experimental and calculated data describing XB, it is safe to say that XB has many similarities with hydrogen bonding (HB):<sup>57–62</sup> Both involve a polarized H or X donor and a Lewis base with an occupied, relatively high-lying lone-pair (lp) orbital as the H or X acceptor A. Depending on the nature of the donor and acceptor, both HB and XB can vary from weakly electrostatic to strongly covalent interactions involving binding energies of 40 kcal/mol and more.<sup>1–10</sup> The strength of these interactions will depend on the complex geometry where a linear arrangement of HB or XB turns out to be energetically favorable. However, there is an important difference between HB and XB: The electronic nature of X should have a strong

influence on the XB strength, and because X can vary from F via Cl, Br, I, to At, more possibilities for designing XBs with specific properties should exist.

Standard procedures use, e.g., the binding energies of XB complexes or structural parameters such as the distance between X and A as a measure of the strength of the XB.<sup>2,63,64</sup> More sophisticated approaches have utilized symmetry-adapted perturbation theory<sup>20,47,52,65–70</sup> or other energy decomposition methods<sup>48,50,70</sup> to obtain insight into the nature of XB. One has determined the electrostatic, exchange, and dispersion interactions adding to XB within a given model. Alternatively, one has analyzed wave-function and molecular orbitals, electron density, magnetic properties, electrostatic potential, or other properties to describe XB.<sup>24,40,45–47,49,51,68,71–82</sup> However, none of these properties provides a reliable measure of the intrinsic XB strength, which is decoupled from other interactions between the monomers. For example, by determination of the binding energy  $\Delta E$ , all interactions between the monomers are included, and it is difficult to single out the energy associated with XB.<sup>83,84</sup> In this situation, vibrational spectroscopy helps because it is always possible to determine the local X...A stretching force constant, which provides a direct measure of the intrinsic bond strength.<sup>85–88</sup>

In previous investigations, we have used vibrational spectroscopy to determine the strength of the HB.<sup>83,89–94</sup> This was

Received: September 30, 2016

Published: December 14, 2016



investigation and provide an outlook on how the results of this work can be used in the future.

## ■ COMPUTATIONAL METHODS

A two-pronged strategy was pursued to obtain a reliable description of the local vibrational modes of the 202 XB complexes investigated in this work. For this purpose, a subset of 28 complexes was investigated employing CCSD(T) (coupled-cluster theory with all singles, doubles, and perturbative triple excitations)<sup>99</sup> and Dunning's augmented triple- $\zeta$  basis sets aug-cc-pVTZ,<sup>100–102</sup> which contain diffuse basis functions to describe the charge distribution of anions and heteroatoms and the dispersion interactions in noncovalently bonded complexes. For atoms Br, I, At, and Sn, scalar relativistic effects were assessed by using effective core potentials (ECPs) in combination with the Dunning basis sets.<sup>103</sup> The CCSD(T) calculations were carried out employing a convergence criterion of  $10^{-9}$  for the CC amplitudes. Various DFT methods were tested for their ability to reproduce the CCSD(T)/aug-cc-pVTZ results. All DFT calculations were performed with tight convergence criteria [self-consistent field,  $10^{-10}$ ; geometry iterations and forces,  $10^{-7}$  hartree/bohr] and an ultrafine grid.<sup>104</sup> It turned out that  $\omega$ B97X-D<sup>105,106</sup> leads to a better agreement with regard to the CCSD(T) results than, e.g., B3LYP,<sup>107,108</sup> PBE0,<sup>109,110</sup> or M06-2X.<sup>111</sup> However, even in the case of the  $\omega$ B97X-D/aug-cc-pVTZ calculations, significant differences with the CCSD(T)/aug-cc-pVTZ results were found. The data reflecting these differences are given in Table S2 and Figure S1. They reveal the following.

The largest discrepancies are found for XB complexes between F<sub>2</sub> or FCl and a Lewis base containing third-period atoms such as S or P. For F<sub>2</sub> complexes, the stability is underestimated by  $\omega$ B97X-D, whereas it is overestimated for the more stable FCl-amine and -phosphine complexes by maximally 2.9 kcal/mol. Percentage-wise deviations in the complex binding energies are generally not large and can be tolerated apart from the complexes mentioned. This holds also for the interaction distances  $r(XA)$  with the exception of F<sub>2</sub>...OH<sub>2</sub> and FCl...PF<sub>3</sub>. However, the more sensitive second-order response properties such as the local stretching force constants reveal the deficiencies of the  $\omega$ B97X-D/aug-cc-pVTZ description in half of the 28 complexes investigated. Especially problematic is the lack of accuracy of the  $k^a$  values in the cases of F<sub>2</sub> and F<sub>3</sub><sup>−</sup>, which were the first choice of reference molecules with defined bond orders (1.00 and 0.50; see below).

Clearly,  $\omega$ B97X-D is unable to describe F<sub>2</sub> and [F...F...F]<sup>−</sup> with the accuracy needed for this investigation. Therefore, we excluded these molecules and complexes containing F<sub>2</sub> from the DFT investigation. This implied that in this work FCl and [F...Cl...F]<sup>−</sup> were used as reference molecules (assumed bond orders 1.00 and 0.50; see below) to set up bond strength order (BSO) values. These are derived from the local stretching force constants, which were obtained utilizing the Konkoli–Cremer method that converts normal-mode frequencies  $\omega_\mu$  and force constants  $k_\mu$  of a quantum-chemical calculation into local-mode frequencies  $\omega_n^a$  and force constants  $k_n^a$  ( $\mu, n = 1, \dots, 3N - L$  with  $N$  = number of atoms and  $L$  = number of translations and rotations) using the local equivalent<sup>85–88</sup> of the Wilson equation of vibrational spectroscopy.<sup>112</sup>

According to the calculated Mayer bond orders<sup>113,114</sup> for FCl and [F...Cl...F]<sup>−</sup> (0.994 and 0.581, respectively), it is reasonable to assume that these are 1.00 and 0.50, where the latter is the result of 3c-4e delocalization and the occupation of all-bonding and nonbonding orbitals. By using these bond orders as reference BSO values and assuming that, for a stretching force constant  $k^a$  of zero, a zero BSO value results, the constants  $a$  and  $b$  in the power relationship<sup>91,115</sup>

$$n = a(k^a)^b \quad (1)$$

were determined to be 0.380 and 0.611, respectively. The corresponding CCSD(T) values are  $a = 0.387$  and  $b = 0.649$ , which confirms the usefulness of the  $\omega$ B97X-D/aug-cc-pVTZ calculations provided F<sub>2</sub> complexes are eliminated from the investigation. By determination of the BSO value  $n(X\cdots A) = n(XB)$  for each calculated

$k^a(X\cdots A)$ , an easy ordering and comparison of XBs according to their intrinsic strength becomes possible.

Because 3c-4e bonding can occur, its magnitude was assessed in percentage with the help of the ratio  $n(X\cdots A)/n(XY) \times 100$ . If this ratio leads to unity, 3c-4e bonding is fulfilled by 100% as in [F...Cl...F]<sup>−</sup>. Values below 40% indicate that 3c-4e bonding plays a minor role. Values above 100% suggest an inverse 3c-4e bond where the XA interactions (i.e., the XB) are stronger than the XY interactions. Values above 100% are listed in the tables to quickly identify inverted 3c-4e bonding but are compared with other values via their reciprocal. In addition to the BSO test, the XY and XA distances were compared with the corresponding values in the appropriate monomers.

Binding energies  $\Delta E$  were calculated at the  $\omega$ B97X-D/aug-cc-pVTZ level, where the counterpoise correction of Boys and Bernardi<sup>116</sup> was used to correct for basis set superposition errors (BSSEs). For each of the 202 complexes investigated, the BSSE-corrected CCSD(T)/aug-cc-pVTZ binding energy was also calculated to provide an estimate of the reliability of the  $\omega$ B97X-D/aug-cc-pVTZ calculations (see Table S1 and Figure S2). For this purpose, DLPNO-CCSD(T)<sup>117,118</sup> and the def2-TZVP basis sets<sup>119</sup> in conjunction with the Stuttgart–Dresden ECPs for iodine<sup>120</sup> were used.

The local properties of the electron density distribution,  $\rho(\mathbf{r})$ , and the energy density distribution,  $H(\mathbf{r}) = G(\mathbf{r}) + V(\mathbf{r})$  [ $G(\mathbf{r})$  = kinetic energy density (positive, destabilizing);  $V(\mathbf{r})$  = potential energy density (negative, stabilizing)], were computed at the  $\omega$ B97X-D/aug-cc-pVTZ level of theory. The Cremer–Kraka criteria for covalent bonding were applied.<sup>121–123</sup> These associate a negative and therefore stabilizing energy density at the bond critical point  $r_b$  [ $H(r_b) = H_b < 0$ ] with dominating covalent character, whereas a positive (destabilizing) energy density ( $H_b > 0$ ) is associated with predominant electrostatic interactions.

The covalent character of XB was also assessed by calculating the delocalization energy  $\Delta E(\text{del}) = \Delta E[\text{lp}(A) \rightarrow \sigma^*(XY)]$ , which is associated with CT from the lp(A) (Lewis base) to the antibonding  $\sigma^*(XY)$  orbital (halogen donor), thus leading to an increase of the electron density in the XB region. The magnitude of  $\Delta E(\text{del})$  was determined by second-order perturbation theory.<sup>124</sup> Detailed analysis of calculated atomic and monomer charges reveals that CT from the halogen acceptor to the halogen donor is largely dominated by the lp(A)  $\rightarrow \sigma^*(XY)$  transfer but is not the only CT. Also, there are other covalent contributions to XB according to the natural bond order (NBO) perturbation analysis. However,  $\Delta E(\text{del})$  turned out to be the most important contribution in line with frontier orbital theory, and therefore we considered the intermonomer CT calculated in this work as the “lp(A)  $\rightarrow \sigma^*(XY)$ ” CT for reasons of simplicity.

Electrostatic interactions were determined by investigating the electrostatic potential  $V(\mathbf{r})$  on the 0.001 e/bohr<sup>3</sup> electron density surface of the monomers listed in Tables S3 and S4. For halogen donors, the  $V(\mathbf{r})$  maximum in the nonbonding region in the  $\sigma$  direction ( $\sigma$ -hole-attracting negative charge) and, for halogen acceptors (Lewis bases), the  $V(\mathbf{r})$  minimum in the lp region were calculated. These values are given in the SI in kilocalories per mole and provide a measure for electrostatic attraction.<sup>125–128</sup>

Calculation of the local-mode properties was carried out with the program COLOGNE2016.<sup>129</sup> CCSD(T) energies were obtained with the packages CFOUR<sup>130</sup> and ORCA.<sup>131</sup> For NBO analysis, NBO 6<sup>124</sup> was used, whereas the electron (energy) density distribution was analyzed with the program AIMAll.<sup>132</sup> DFT calculations were performed with the package Gaussian09.<sup>133</sup>

## ■ RESULTS AND DISCUSSION

A schematic representation of the 202 molecules investigated in this work is given in Figure 1. They are separated into four groups (I–IV). Investigation of the FCl complexes of group I (1–22), which involve amines and phosphines, provides a possibility of studying the consequences of halogen acceptor substitution for the strength of XB. Group II (23–148) contains dihalogens X<sub>2</sub> and interhalogens XY interacting with acceptors AR<sub>m</sub> (R = F, H, CH<sub>3</sub>;  $m = 2, 3$ ), with A being an

atom of the second or third period (O and N or S and P). Group II is included to study the influence of the polarizability of X and the polarizing power of Y on XB. Groups III (149–180) and IV (181–202) contain the actual targets of this work: Simple halomethanes and halotetragenes interacting with amines, phosphines, or the Cl<sup>−</sup> anion are contained in group III. Group IV consists of organoiodine molecules interacting with Cl<sup>−</sup> or NH<sub>3</sub>.

In view of the large number of molecules investigated, the data for all monomers and XB complexes (see Figure 1) are summarized in Table S2, which contains bond lengths  $r(\text{YX})$  and  $r(\text{X}\cdots\text{A})$  in Å, binding energies  $\Delta E(\text{DFT})$  and  $\Delta E[\text{CCSD}(\text{T})]$  in kcal/mol, electron density  $\rho_b$  at the XB critical point in electron/bohr<sup>3</sup>, energy density  $H_b$  at the XB critical point in hartree/bohr<sup>3</sup>, delocalization energies  $\Delta E(\text{del}) = \Delta E(\text{lp} \rightarrow \sigma^*(\text{XY}))$  in kcal/mol, intermonomer CT dominated by the transition  $\text{lp}(\text{A}) \rightarrow \sigma^*(\text{XY})$  in electrons, local stretching force constants  $k^a(\text{XY})$  and  $k^a(\text{XB}) = k^a(\text{X}\cdots\text{A})$  in mdyn/Å, BSO values  $n(\text{XY})$  and  $n(\text{XB}) = n(\text{X}\cdots\text{A})$ , the degree of 3c-4e bonding in %, and the frequency of that normal mode, which has dominant XB stretching character. The latter is given to provide vibrational spectroscopy information, where the XB stretching band should be found when either IR or Raman spectra are recorded. Tables S3 and S4 contain molecular properties of the XB acceptors and donors, respectively. Figures S3–S5 provide a schematic representation of all complexes with NBO charges.

Rather than a discussion in detail of the data collected in the Supporting Information (SI), the most important results are given in the form of suitable diagrams. Figure 2 summarizes all

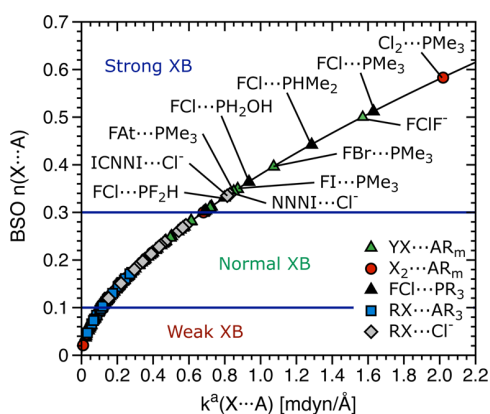


**Figure 2.** Power relationship between the relative BSO  $n$  and the local stretching force constants  $k^a$  of XB complexes 1–202 given according to eq 1 (solid black line). Weak, normal, and strong XB are separated by the horizontal blue lines.

results in a BSO diagram, which shows that XB can vary from very weak ( $n \leq 0.1$ ) to rather strong interactions ( $n \geq 0.3$ ), which are found for some phosphine complexes. The sequence of increasingly stronger XB shown in Figure 2 and given in more detail in Table S2 provides for the first time a quantitative comparison of the various types of XB.

In Figure 3, the nature of the XB is characterized with the help of the energy density  $H_b$  at the XB critical point. There is a variation from electrostatic ( $H_b$  values close to zero) to covalent bonding with distinctly negative  $H_b$  values that indicates stabilization of the electron density at the XB critical point and, by this, covalent interactions according to the

Cremer–Kraka criteria.<sup>121</sup> Analysis of the energy density is confirmed by the corresponding CT values from the  $\text{lp}(\text{A})$  orbital to the  $\sigma^*(\text{XY})$  orbital, and the corresponding delocalization energies are listed in Table S2.

Figure 4 provides analysis of FCl-amine and FCl-phosphine complexes, again based on the BSO values determined with eq 1. Figures 5 and 6 compare XB for various halogens and interhalogens (excluding the F<sub>2</sub> complexes for the reasons discussed above) in combination with second- and third-row heteroatoms A that characterize a given type of Lewis base. XBs for halomethanes, in general, and iodicarbons, specifically, are analyzed in Figures 7 and 8.

A possible relationship between the intrinsic bond strength of XB and the complex binding energy  $\Delta E$  (Figure 9) or the delocalization energy  $\Delta E(\text{lp} \rightarrow \sigma^*(\text{XY}))$  (Figure 10) is also investigated. In the SI, similar relationships with the electron density  $\rho_b$  and acceptor ionization potentials (IPs) are provided.

These results lead to a clear picture of the nature of XB, which can be rationalized by considering 10 different electronic effects. Most of them have been previously discussed in connection with XBs (orbital energy and overlap,<sup>36,37,44,53</sup> electrostatic effects and  $\sigma$ -hole influence,<sup>46,125–128,134–136</sup> and CT<sup>41,137</sup>). However, in this work we summarize these electronic effects in a compact way, applying vibrational spectroscopy and the local vibrational modes.

1. *Changes in the orbital energy of  $\text{lp}(\text{A})$  and the electronegativity of A.* Covalent contributions sensitively depend on the  $\text{lp}(\text{A})$  energy that influences the orbital energy difference  $\Delta\epsilon = \epsilon[\text{lp}(\text{A})] - \epsilon[\sigma^*(\text{XY})]$  with  $\epsilon[\text{lp}(\text{A})] < \epsilon[\sigma^*(\text{XY})]$ . The smaller  $\Delta\epsilon$  is, the larger are the CT and covalent contributions. Trends in  $\epsilon[\text{lp}(\text{A})]$  are reflected by the corresponding vertical IPs (see the SI) or, more directly, by the calculated  $\text{lp}(\text{A})$  orbital energies. For a third-row element like P, the  $\text{lp}$  orbital is lying higher in energy and by this the covalent contribution is larger, as confirmed by the BSO values of the phosphine and amine XB complexes shown in Figure 4.

1a. *Orbital energy of  $\text{lp}(\text{A})$  and  $\sigma$ -withdrawing/donating groups at A.* The  $\text{lp}(\text{A})$  orbital can be raised by suitable substituents to decrease  $\Delta\epsilon$ . As shown in Figure 4 (amines in red; phosphines in green), the XB strength ranges from BSO values  $n = 0.100$  for FCl $\cdots$ NF<sub>3</sub> to 0.270 for FCl $\cdots$ N(CH<sub>3</sub>)<sub>3</sub>, whereas for the phosphines, the bond strength varies from  $n = 0.064$  (FCl $\cdots$ PF<sub>3</sub>) to  $n = 0.512$  (FCl $\cdots$ P(CH<sub>3</sub>)<sub>3</sub>), thus revealing that the strength of the XBs formed with FCl largely depends on the halogen acceptor. For amines, the XB strength increases in the series NF<sub>3</sub> < NHF<sub>2</sub> < NH<sub>2</sub>CN < NH<sub>2</sub>F < NH<sub>2</sub>Cl  $\approx$  NH<sub>2</sub>SiH<sub>3</sub> < NH<sub>3</sub> < NH<sub>2</sub>OH < NH<sub>2</sub>CH<sub>3</sub> < NH(CH<sub>3</sub>)<sub>2</sub> < N(CH<sub>3</sub>)<sub>3</sub>. For phosphines, the intrinsic strength of XB increases as follows: PF<sub>3</sub>  $\approx$  PH<sub>2</sub>CN < PH<sub>3</sub> < PH<sub>2</sub>SiH<sub>3</sub> < PH<sub>2</sub>Cl < PH<sub>2</sub>F  $\approx$  PH<sub>2</sub>CH<sub>3</sub> < PHF<sub>2</sub> < PH<sub>2</sub>OH  $\ll$  PH(CH<sub>3</sub>)<sub>2</sub> < P(CH<sub>3</sub>)<sub>3</sub>. Electron-withdrawing substituents such as F in NF<sub>3</sub> lower  $\epsilon[\text{lp}(\text{A})]$  and thereby weaken XB, whereas electron-donating groups such as Me raise  $\epsilon[\text{lp}(\text{A})]$  and thereby strengthen the covalent contribution to XB.

1b. *Orbital energy of  $\text{lp}(\text{A})$  and  $\pi$ -withdrawing/donating groups at A.* Substituents, which lead to a potential delocalization of  $\text{lp}(\text{A})$  such as the cyano group in PH<sub>2</sub>CN, lower  $\epsilon[\text{lp}(\text{A})]$ , increase  $\Delta\epsilon$ , and thereby weaken XB (see 20 in Table S2).  $\pi$ -Donating substituents such as Cl in chlorinated phosphines have destabilizing  $p\pi, \text{lp}(\text{A})$  4e interactions that cause an increase of  $\epsilon[\text{lp}(\text{A})]$ . The latter effect can be stronger than the  $\sigma$ -electron-withdrawing effect so that the Lewis base becomes a

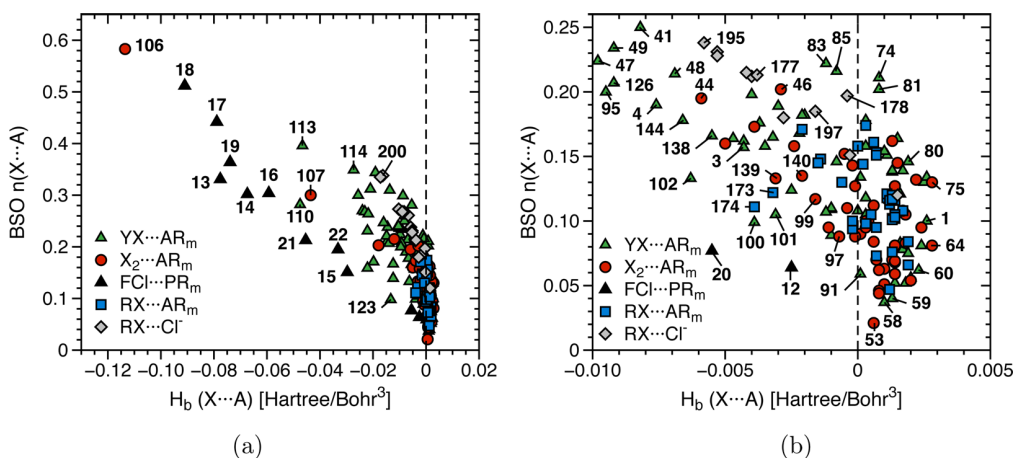


**Figure 3.** (a) Comparison of the BSO  $n$  with the energy density  $H_b$  at the density critical point of the XB for complexes 1–202. (b) Enlargement of the range  $0 < n < 0.026$ ;  $-0.010 < H_b < 0.005$  hartree/bohr<sup>3</sup>. Electrostatic XBs are indicated by  $H_b \geq 0$ , whereas negative  $H_b$  values are associated with covalent XB.<sup>121,122</sup> For the numbering of XB complexes, see Tables S2, S7, and S8.

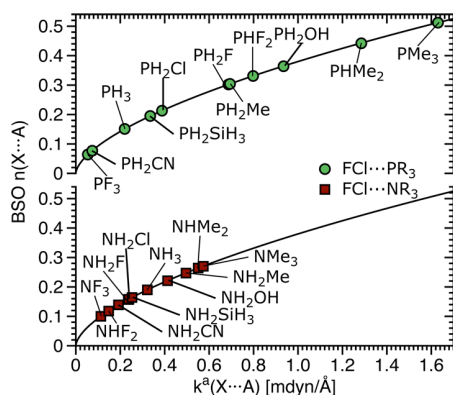


**Figure 4.** Relationship between the relative BSO  $n$  and the local XB stretching force constant  $k^a$  (eq 1; solid black lines) for XB complexes involving FCl as halogen donor and amines (lower curve, red squares) or phosphines (upper curve, green dots) as halogen acceptors.

stronger electron donor. For phosphines, these effects dominate, whereas for amines, the Cl substituent acts more as a  $\sigma$  acceptor rather than a  $\pi$  donor. The calculated strength

of XB in the FCl complexes of  $\text{NH}_3$  ( $n = 0.190$ ),  $\text{NH}_2\text{CN}$  (0.139),  $\text{NH}_2\text{Cl}$  (0.158) and  $\text{PH}_3$  (0.151),  $\text{PH}_2\text{CN}$  (0.077),  $\text{P}(\text{CN})_3$  (0.044),  $\text{PH}_2\text{Cl}$  (0.213), and  $\text{PCl}_3$  (0.096) confirms these effects (see Table S2 and Figure 4). Noteworthy is that the sensitivity of XB to substituent effects in the Lewis base is much larger for third rather than second period atoms A, which is especially obvious for the phosphines.

2. *Orbital overlap between X and A.* Covalent bonding requires an efficient overlap between the interacting orbitals, i.e., the  $\text{lp}(A)$  and  $\sigma^*(XY)$  orbitals. The latter depends on the geometry of the complex [a linear arrangement of the unit (A, centroid of lp, X, and Y) would be optimal as well as a short interaction distance  $r(X\cdots A)$ ], the nodal characteristics of the valence orbitals, and their diffuseness. The rule of thumb is that orbital overlap decreases when the principal quantum numbers of X and A increasingly differ and/or the electronegativity difference  $\Delta\chi(A, X) = \chi(A) - \chi(X)$  increases. Electronegative substituents at an atom A with a diffuse lp (e.g., P) can improve the overlap due to orbital contraction. The best overlap can be expected between atoms belonging to the same period and having similar  $\chi$  values. The overlap decreases in the series ClCl, ClBr, and ClI or in the series FF, FCl, FBr, FI, and FAT, as is in line with the

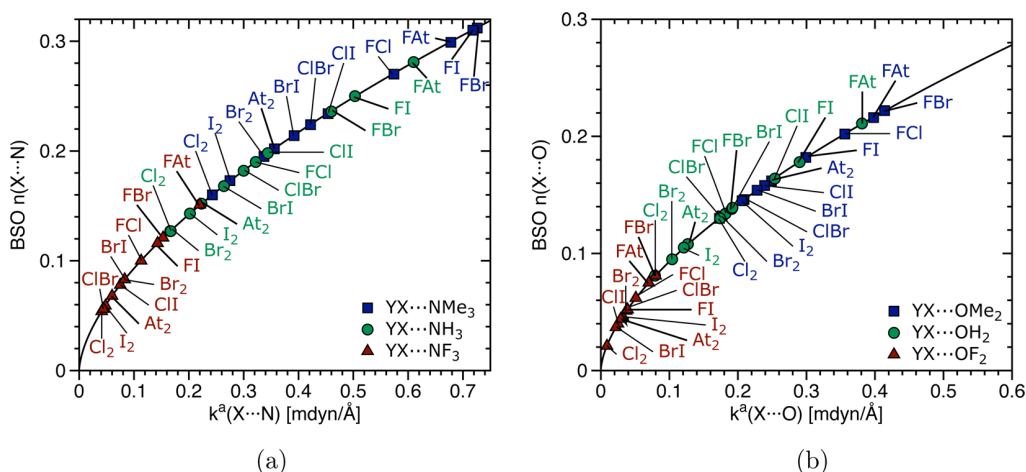


**Figure 5.** Relationship between the relative BSO  $n$  and the local XB stretching force constant  $k^a$  (eq 1; solid black lines) for dihalogens and interhalogens interacting with (a) amines  $\text{NF}_3$ ,  $\text{NH}_3$ , and  $\text{NMe}_3$  and (b)  $\text{OF}_2$ ,  $\text{OH}_2$ , or  $\text{OMe}_2$ .



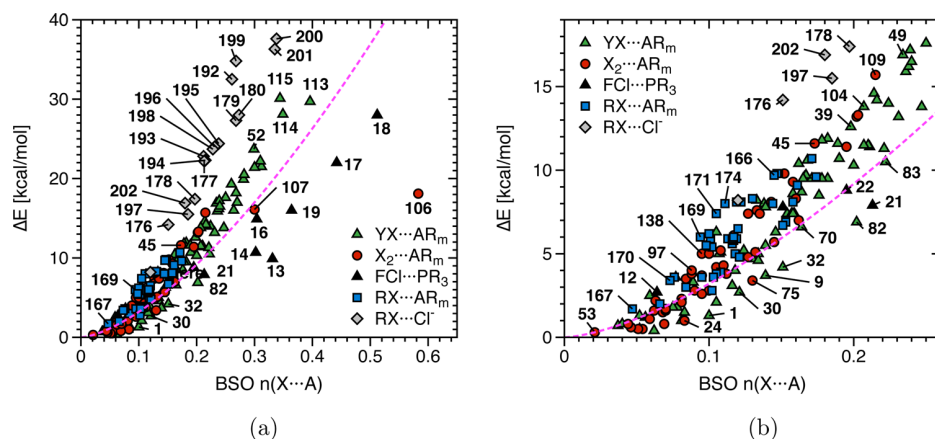


**Figure 9.** Comparison of the BSO  $n$  values and the binding energy  $\Delta E$  for (a) complexes 1–202. (b) Enlargement of the region  $0 < n < 0.026$ ;  $0 < \Delta E < 19$  kcal/mol. The purple line indicates the expected relationship between the two quantities. For the list of complex numbers, see Tables S2, S9, and S10.

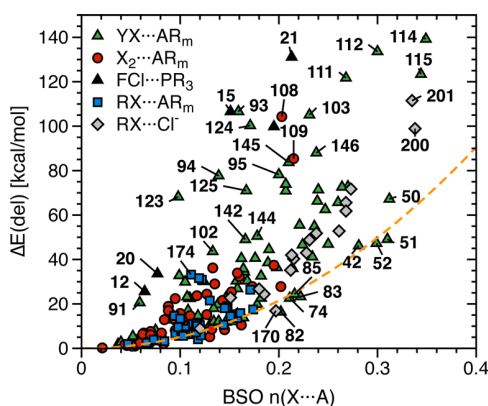


**Figure 10.** Comparison of the second-order CT stabilization energy  $\Delta E(\text{del}) = \Delta E[\text{lp}(A) \rightarrow \sigma^*(XY)]$  and the BSO  $n$  values. The yellow line provides a reference line (see the text). Complexes with 3c-4e bonding have large  $\Delta E(\text{del})$ . Complexes with strong 3c-4e bonding or phosphonium character are not included.

Because the phosphonium ion complexes also have 3c-4e bonding character (the percentages given in Table S2 are >100 and have to be inverted:  $100/115 = 87$ , 68, 43, and 81%), their PCl bond is labilized, and only  $\text{ClCl}\cdots\text{PMe}_3$  can be considered to be dominated by phosphonium character. In this work, the classification as an ion pair was first based on the YX and XA distance analysis using the corresponding monomer distances of di/interhalogens and phosphonium ions as reference (Table S5). Subsequently, it was revised by utilizing the corresponding BSO values (Table S6), which are more reliable. Accordingly,  $\text{Cl}^-\cdots\text{ClPMe}_3^+$  is the only system with sufficient ion-pair character, where bonding takes place in the form of noncovalent dihalogen interactions between the Cl anion and a positively charged Cl in the phosphonium ion. This situation is generally considered as XB and can be contrasted with fully delocalized 3c-4e systems such as  $[\text{F}\cdots\text{Cl}\cdots\text{F}]^-$  or  $\text{FCl}\cdots\text{PH}_2\text{OH}$  (19), which are also considered to be stabilized by XB.

**6. Charge attraction/repulsion between X and A.** Coulomb attraction between a negatively charged A and a positively charged X stabilizes XB. For an interhalogen XY, with Y being the more electronegative atom, CT from X to Y leads to bond polarity and a positively charged X atom. If the electronegativity difference  $\Delta\chi(Y,X) = \chi(Y) - \chi(X)$  increases (e.g., in the series

FCl to FAT), the charge of X increases and thereby X–A attraction exists. Similarly, the negative charge of A can be increased by electron-donating substituents so that Coulomb attraction increasingly supports XB. Noteworthy is that XB in FCl-phosphine complexes is relatively strong despite a charge repulsion between a positively charged X (because of the higher electronegativity of F) and a positively charged P (see Figure S3 and the following).

**7. Role of a  $\sigma$  hole at X and the electrostatic potential.** Charge repulsion between X and A, as suggested by the calculated NBO charges, does not consider the anisotropy of the electron density distribution. The negative charge of X screens the nucleus less in the XY bond ( $\sigma$  direction), thus leading to positive values of the electrostatic potential  $V$  when  $V$  is calculated outside the bond region for the  $0.001 \text{ e}/\text{bohr}^3$  electron density surface (henceforth called the van der Waals surface). This is generally interpreted as a  $\sigma$  hole. The importance of  $\sigma$ -hole,lp interactions is well-established.<sup>125–128</sup>

The  $\sigma$  hole of X in interhalogens XY increases with the polarity of the XY bond, which increases with increasing  $\Delta\chi(Y,X)$  [Allred–Rochow  $\chi$  values are 4.10 (F), 2.83 (Cl), 2.74 (Br), 2.21 (I), and 1.90 (At)<sup>141,142</sup>]. Similar trends can be found for the interhalogens (Table S4). Accordingly, XB is influenced by the  $\sigma$  hole of X in XY, as is reflected by an increase of the XB BSO values in the series  $X_2\cdots AR_m$  and  $\text{FX}\cdots AR_m$  ( $X = \text{Cl}, \text{Br}, \text{I}, \text{At}$ ;  $AR_m = \text{OH}_2, \text{NH}_3$ ; see Table S2).

**8. Dipole–dipole interactions between XY and  $AR_m$ .** Electrostatic attraction between X and A can be influenced if the molecular dipole moments are collinearly aligned as in  $\text{FCl}\cdots\text{NH}_3$ , whereas dipole–dipole repulsion in a complex influences the XB in  $\text{FCl}\cdots\text{PH}_3$ . Because of this, the dipole moments of the monomers are listed in the Tables S3 and S4. Noteworthy are the large dipole moments of  $\text{NH}_2\text{CN}$  (4.61 D, Table S2) and  $\text{PH}_2\text{CN}$  (3.70 D), which are arranged in a direction that leads to repulsion with the FCl dipole (0.86 D).

**9. Mutual polarization XY and  $AR_m$ .** Interaction between the multipole moments of the monomers (here only atomic charges and dipole moments are considered) is enhanced by induced electrostatic interactions. These depend on the polarizability of the monomers and their polarizing power. The first property is a tensor where for reasons of simplicity here just the isotropic polarizability  $\alpha_{\text{iso}}$  is considered (see Table S4), although a more detailed analysis might focus on the

$\sigma$  polarizability. The value of  $\alpha_{\text{iso}}$  increases steeply in the series  $F_2$  (8.2 bohr<sup>3</sup>),  $Cl_2$  (30.6),  $Br_2$  (45.4),  $I_2$  (71.6), and  $At_2$  (87.4), thus explaining why  $Cl_2$  and higher halogens are so easily polarized, which will lead also to an increase of the X  $\sigma$  hole by a Lewis base with sufficient polarizing power. This can be estimated by calculating  $V$  at a position on the van der Waals surface of A, which is next to X and gives a measure for the effect of the lp(A) electrons. The more negative  $V$  is for lp(A) (see Table S3), the stronger should be the polarizing power of the Lewis base. The negative value of  $V$  increases with (i)  $\chi(A)$  (amines have more negative values than phosphines) and (ii) the electron-donating power of R in  $AR_m$ . More positive values of  $V$  at the position of lp(A) are obtained if the lp electrons are delocalized as for CN substituents or when R has a much larger electronegativity than A (as in  $PF_3$ ).

10. *Augmentation of XB by HB.* There are some interesting exceptions to effects 1 and 2: An OH group does not lead to a weakening of the XB but to its strengthening ( $FCl \cdots PH_2OH$ :  $n = 0.364$  compared to  $n = 0.304$  for  $FCl \cdots PH_2CH_3$ ). Inspection of the geometry of  $FCl \cdots PH_2OH$  reveals that this unusual behavior of the OH group is due to HB with Cl, which increases the complex stability. If the HB is broken by rotation of the OH group, the hydroxyl group functions, as expected, as an electron-withdrawing group with a XB weakening effect.

Clearly, electronic effects 1–5 are relevant for the covalent part of XB, whereas effects 6–9 concern the electrostatic part. Additional electronic effects can augment either covalent or electrostatic XB. It is well-known that exchange repulsion and dispersion forces influence the strength of XB.<sup>68,143</sup> Furthermore, spin–orbit coupling plays a significant role for atoms such as Br, I, and At.<sup>144–146</sup> These additional effects were not explicitly calculated in this work but have to be considered in the following.

Before some classes of XB complexes are discussed in more detail, it is appropriate to differentiate between physically based observables and the model quantities used in this work. Clearly, the local mode frequency can be measured<sup>88</sup> and the local force constants can be derived from the former. This is also true for the electron density or the dipole moment, whereas NBO charges are orbital-based and therefore model quantities. A chemist wants to explain XB in terms of covalent, exchange, electrostatic, inductive, and dispersion interactions. Politzer and co-workers<sup>147–149</sup> have recently pointed out that according to the Hellmann–Feynman theorem<sup>150</sup> noncovalent interactions are purely Coulombic in nature and include polarization and dispersion. Therefore, noncovalent interactions such as XB may be described purely on the basis of Coulomb interactions. Although this is a valid view, it does not exclude that one uses model quantities such as NBO charges, CT values, or charge delocalization energies for a more detailed, model-based description of XB. We will use the CT values as an indicator of covalent bonding, where one has to realize that within the model used smaller contributions to CT might also arise from other than covalent interactions. In a similar way, we will use an energy-density-based model that distinguishes just between covalent and electrostatic forces.<sup>121–123</sup>

**XB with Phosphines.** Considering all effects, the strong covalency of XB in phosphine complexes (Table S2 and Figure 3) is noteworthy. This can lead to BSO values larger than 0.3 (1), where, as shown above, especially methyl substituents help to increase the intrinsic XB strength. For  $P(CH_3)_3$ , the lp(P) orbital energy is raised [CCSD(T): IP = 8.6 eV; IP( $PH_3$ ) = 10.5 eV; Table S3] via hyperconjugation and a lower electron-

withdrawing effect of the methyl group. The very low value of  $V$  [ $V(PMe_3) = -28.8$  kcal/mol;  $V(PH_3) = -16.9$  kcal/mol] and the high polarizability ( $PMe_3$ , 67.6 bohr<sup>3</sup>;  $\alpha_{\text{iso}}(PH_3)$ , 30.8 bohr<sup>3</sup>; Table S3) cause both the covalent and electrostatic parts of XB in, e.g.,  $FCl \cdots PMe_3$  ( $\Delta E = 28.0$  kcal/mol;  $n(XA) = 0.512$ ; Table S2), to be relatively large and the complex to take the character of a chlorophosphonium ion interacting with  $F^-$  via significant 3c-4e bonding (68%).

In the series  $Cl_2$ ,  $Br_2$ ,  $I_2$ , and  $At_2$  or  $FCl$ ,  $FBr$ ,  $FI$ , and  $FAt$ , the electrostatic interactions with  $P(CH_3)_3$  increase in a limited way because of an increasing  $\sigma$  hole and an increasing polarizability of X but an increased repulsion between positively charged X and P (Tables S3 and S4 and Figure S4). At the same time, the covalent contributions decrease because of an increase in the  $\sigma^*(XY)$  energy and a decrease of the orbital overlap, as is documented by the CT values in Table S2. Accordingly, for  $Cl_2$  and  $FCl$ , the strongest XB is found ( $n = 0.583$  for **106** and  $n = 0.512$  for **18**), indicating in the first case a phosphonium complex with 3c-4e character and in the second case inverted 3c-4e character.

Using the 10 electronic effects discussed above, the trends in the intrinsic strength of XB, as reflected by the BSO values shown in Figures 3–6, can be explained in detail. The insight provided by these values makes it possible to discuss XB for halogenated carbon molecules, which are directly relevant for polymer chemistry and materials science.

## ASSESSMENT OF XB INVOLVING TETRAGENES

The lower electronegativity of carbon compared to that of the halogens leads to higher orbital energies  $\sigma(XY)$  and  $\sigma^*(XY)$  and to reduced overlap between the latter and the lp(A) orbital. The polarity of the CX bond is inverted (compared to  $FCl$ ) and causes a larger (smaller) orbital coefficient of X in the  $\sigma(CX)$  bonding [ $\sigma^*(CX)$  antibonding] orbital. Hence, 4e repulsion between lp(A) and  $\sigma(CX)$  will be larger and 2e stabilization between lp(A) and  $\sigma^*(CX)$  lower. This can be directly verified by the reduced CT and  $\Delta E(\text{del})$  values of the halocarbons (Table S2). Halocarbons lead to weak electrostatic XB. To increase the intrinsic strength of the XB involving a halocarbon, the effective electronegativity of the C(X) carbon has to be increased, which is accomplished by halogenation. Apart from this, it is interesting to see how XB is changed when halomethanes are replaced by the corresponding silanes, germanes, and stannanes. For this purpose, a set of tetragenes interacting with  $NH_3$ ,  $NMe_3$ ,  $PMe_3$ , and the  $Cl^-$  anion as halogen acceptors were investigated. The calculated BSO values of the halomethanes are shown in Figure 7.

**XB for Halomethanes and Halotetragenes.** According to the calculated BSO values, both weak and normal XB are observed, where the largest BSO values are obtained for the  $Cl^-$  anion (0.120–0.273 corresponding to  $\Delta E$  values from 8.2 to 28.0 kcal/mol; Table S2), which indicates how anions as halogen acceptors significantly increase the strength of XB. Different from what was found for dihalogens and interhalogens, halocarbons form XB with phosphines and, in particular,  $P(CH_3)_3$ , which have slightly lower strength (0.047–0.122) than those formed with  $NH_3$  (0.066–0.153) and  $N(CH_3)_3$  (0.084–0.158; Table S2). This reflects the smaller covalent character of the XB involving tetragenes as X donors.  $P(CH_3)_3$  still leads to larger CT values (Table S2), but the corresponding XB strength is also influenced by electrostatic contributions such as X–A repulsion (attraction) determined by the

calculated atomic charges,  $\sigma$ -hole–lp(A) attraction as reflected by the calculated  $V$  values, and charge polarizability.

According to the BSO values,  $\sigma$ -hole–lp(A) attraction seems to be decisive, as suggested by  $V$  values of  $-37.7$ ,  $-30.9$ , and  $-28.8$  kcal/mol for the lp(A) in  $\text{NH}_3$ ,  $\text{N}(\text{CH}_3)_3$ , and  $\text{P}(\text{CH}_3)_3$ , respectively. Nevertheless, small covalent contributions remain to be important, as the BSO values of complexes with  $\text{H}_3\text{Cl}$ ,  $\text{F}_3\text{Cl}$ ,  $\text{Cl}_3\text{Cl}$ , and  $\text{Cl}_4$  reveal, where  $\text{Cl}_3\text{Cl}$  and  $\text{Cl}_4$  form stronger XB than  $\text{F}_3\text{Cl}$  for both  $\text{NH}_3$  and  $\text{Cl}^-$ . This can be related to a lowering of the lowest unoccupied molecular orbital (LUMO) of the halomethanes, as was already pointed out by Huber on the basis of binding energies.<sup>53</sup> The highest BSO values are obtained for  $\text{Cl}_3\text{C}-\text{I}$  as a halogen donor, which is because of its high polarizability (90.2 bohr<sup>3</sup>; Table S4) and a positive charge at I, which is more attracted by the negatively charged N in  $\text{NH}_3$  ( $-1.056$  e) and  $\text{N}(\text{CH}_3)_3$  ( $-0.500$  e) than the positively charged P (1.123 e; Figure S3) in  $\text{P}(\text{CH}_3)_3$ . Similar considerations apply to  $\text{F}_3\text{C}-\text{I}$  and  $\text{I}_3\text{C}-\text{I}$ , which lead with  $\text{N}(\text{CH}_3)_3$  to relatively strong XB complexes [ $\Delta E = 8.3$  and  $10.3$  kcal/mol (CCSD(T)].

When C is replaced with a less electronegative tetragene such as Si, Ge, or Sn [Allred–Rochow:  $\chi(\text{C}) = 2.50 > \chi(\text{Ge}) = 2.02 > \chi(\text{Si}) = 1.74 \approx \chi(\text{Sn}) = 1.72$ <sup>141,142</sup>], the strength of the XB decreases, where the BSO follows the changes in the  $\sigma$ -hole potential value (see Tables S2 and S4) and the fact that X becomes increasingly negatively charged. Again, the strongest values are found for the iodomethanes. This clarifies that once the interaction between  $R_m\text{CX}$  and a Lewis base is considered, it is limited to the moderate donor ability of the halocarbon, where an iodocarbon provides the best option. Therefore, stronger XB can only be provided by increasing the polarity of the C–I bond via an increase of the effective electronegativity of C, an increase of the polarizability of the halogen donor, and/or modification of the Lewis base. As the examples involving the chloride anion reveal, enlarged BSOs of up to 0.3 (in this work considered as the border to strong XB) result, where both increases of the covalent [higher lp(A) energies and stronger CT] and electrostatic contributions (higher polarizability of the Lewis base; Table S3) play a role.

**XB for Organoiodine Compounds.** Because iodocarbons provide the strongest XB (among the tetragenes), an increase of the perfluorinated iodoalkane chain might be one possibility (184, 185, 195, and 196) to strengthen the XB. However, the calculated BSO values reveal little improvement. The change in the effective electronegativity of C(I) is too small. A larger effect is obtained when *p*-diiodobenzene is perfluorinated. The BSO value increases from 0.105 (186) to 0.117 (187) and the binding energy from 3.8 to 6.0 kcal/mol where the increase of the  $\sigma$  hole from  $V = 22.0$  to 32.9 kcal/mol seems to be the most important change. Perfluorinated *p*-diiodobenzene materials are already widely used in gels, fluorescent materials, and others.<sup>16,151–153</sup>

A larger change in the electrostatic potential  $V$  is accomplished in the series difluorodiiodoethene (183,  $V = 32.3$  kcal/mol), diiodoacetylene (182; 37.6 kcal/mol), and iodocyanide (181; 51.8 kcal/mol; Table S4). If this is combined with increased covalent and electrostatic contributions, as provided by an anion such as  $\text{Cl}^-$ , then BSO values of 0.215, 0.212, and 0.261 can be obtained, where the switch in the order of the XB strengths is due to the covalent contributions and a relatively large CT of 0.188, 0.179, and 0.221 e (electron;  $\Delta E(\text{del}) = 40.3$ , 35.2, and 52.8 kcal/mol; Table S2) in line with the LUMO energies. The corresponding binding energies are

22.4, 22.9, and 31.6 kcal/mol [CCSD(T); Table S2]. Obviously, iodocyanide is too toxic to work with, but diiodoalkynes could be used as suitable compounds to form polymers based on XB, as is already known for some time.<sup>154–156</sup>

XB of similar or even larger strength than the one found in iodocyanide is observed for ONCI, ICNI, and NNNI complexes. In the first case, the nitroso substituent leads to an increase in the polarizability of the X donor (from 48.7 bohr<sup>3</sup> for NCI to 59.8 bohr<sup>3</sup> for ONCI), resulting in a slightly stronger bond (BSO value of 0.174 compared to 0.161 for  $\text{NCI}\cdots\text{NH}_3$ ), whereas for ICNI and NNNI, the higher electronegativity of N compared to C [ $\chi(\text{C}) = 2.50$ ;  $\chi(\text{N}) = 3.07$ ] lowers the energy of  $\sigma(\text{NI})$  and  $\sigma^*(\text{NI})$  and improves the lp(A)– $\sigma^*(\text{NX})$  overlap, which results in larger CT and  $\Delta E(\text{del})$  values compared to the ones found for iodocarbon complexes (Table S2). Although ICNI and NNNI have a lower electrostatic potential than NCI ( $V = 38.4$  and  $42.4$  kcal/mol compared to 51.8 kcal/mol), they are capable of forming XB of similar strength for  $\text{NH}_3$  (BSO values of 0.130 and 0.171 compared to 0.161) and stronger XB for  $\text{Cl}^-$  (BSO values of 0.335 and 0.368 compared to 0.261) with high 3c-4e character (101% and 88%).

## INTRINSIC XB STRENGTH AND COMPLEX BINDING ENERGIES

There is a tendency of considering the binding energy  $\Delta E$  of XB complexes as a direct result of the intrinsic strength of XB. This simplification overlooks that, even in the structurally simplest XB complex, the magnitude of  $\Delta E$  is determined by many factors rather than just the intrinsic strength of the XB. This also holds for dihalogens and interhalogens interacting with simple Lewis bases. The mutual polarization of the monomers leads in all cases to additional electronic effects, increasing the stability of the complex. Therefore,  $\Delta E$  is not a simple reflection of the intrinsic strength of XB.

If one correlates the two XB complex properties BSO  $n(\text{XA})$  and complex binding energy  $\Delta E$ , one obtains the diagram shown in Figure 9. The scattering of data points suggests that there is no direct relationship between the two quantities. However, as indicated by the purple curve, which gives largely a linear relationship between  $n$  and  $\Delta E$  based on the two reference molecules  $\text{Cl}_2\cdots\text{OF}_2$  (0.021) and  $\text{FCl}\cdots\text{OH}_2$  (0.134), three classes of XB complexes can be distinguished. The first class contains the phosphonium ion 106, which has a covalent Cl–P bond, some Cl $\cdots$ C interactions, and a BSO(XB) value that is larger than suggested by  $\Delta E$  (18.1 kcal/mol for  $\text{Cl}_2\cdots\text{PMe}_3$ ; however, 75.3 kcal/mol for  $\text{Cl}^-\cdots\text{ClPMe}_3^+$ ). In this class, one can also place systems 17, 18, or 107 with inverted 3c-4e character because they also have some (small) phosphonium character.

The second class contains complexes with strong 3c-4e bonding such as 7, 13–16, or 46–52, which also have larger BSO values than  $\Delta E$  values. Complex 19 belongs to this class but has a larger  $\Delta E$  due to a HB between XY and Lewis base. Complexes such as 113, 114, or 115 have much larger binding energies as a result of the large polarizabilities of the monomers, which leads to stabilizing attractions between FX and the methyl groups of the phosphine that do not enhance the direct interactions between X and A but  $\Delta E$ .

In the third class (to the left of the curve in Figure 9: larger  $\Delta E$  values than expected from the BSO values), there are complexes with electrostatic and moderately covalent XB.

Strong deviations from the expected  $\Delta E$  can be observed for the perfluorinated halogen donors **195** and **196**, which are strongly polarizable and therefore have significantly higher binding energies  $\Delta E$ . In this way, for each complex, additional stabilization effects can be quantitatively determined once a reasonable functional dependence has been established between  $n$  and  $\Delta E$  with the help of a few reference systems.

One can extend this approach by comparing delocalization energies  $\Delta E(\text{del})$  with BSO values  $n$  (Figure 10). Scattering is stronger in this case because the magnitude of  $\Delta E(\text{del})$  depends on the orbital energies of  $\text{lp}(\text{A})$  and  $\sigma^*(\text{XY})$  as well as their overlap. In the two previous sections, we have discussed the many effects determining orbital energies and overlap. On top of this, electrostatic interactions can increase the BSO value so that their magnitude becomes larger than expected from  $\Delta E(\text{del})$  (examples are **51** or **52**). By using  $\Delta E(\text{del})$  for analysis, one has to be aware that its calculation is based on the assumption of a specific Lewis structure, which in the case of nonclassical 3c-4e bonding leads to exaggerated delocalization energies. One can calculate with the perturbational molecular orbital approach 3c energies.<sup>124</sup> However, we have refrained from using this approach and have excluded complexes with strong 3c-4e bonding from the diagram in Figure 10 on which the analysis of the covalent contributions was based.

## CONCLUSIONS AND OUTLOOK

The strength of the XB of 202 complexes has been determined for the first time quantitatively using local stretching force constants, which reflect local features of the curvature of the potential energy surface and can be directly related to measured or calculated frequencies.<sup>86,89,90</sup> The current investigation is put into perspective with regard to other quantum-chemical investigations of the recent years in Table 1. On the basis of this comparison, a solid basis for future studies on more sophisticated XB complexes is laid in the current work. Our work has led to the following conclusions.

1. On the basis of the calculated BSO values, one can distinguish weak ( $n < 0.1$ ), normal ( $0.1 \leq n \leq 0.3$ ), and strong ( $n > 0.3$ ) XB. Complexes with  $n$  close to 0.5 benefit from nonclassical 3c-4e bonding. Complexes with  $n > 0.5$  result from a transfer of the halogen cation  $\text{X}^+$  from a polarized XY or XX to the halogen acceptor and the formation of an ion pair that itself is bonded by an inverted XB between the remaining halogen anion (as Lewis base) and the halogenated Lewis base as a new halogen donor. An example for such a  $\text{X}^+$  transfer is  $\text{Cl}_2 \cdots \text{PMe}_3 \rightarrow \text{Cl}^- \cdots \text{ClPMe}_3$ .

2. We have established 10 different electronic effects to analyze and explain the observed XB strength order of the 202 XB complexes.

3. The majority of the XB investigated has sizable covalent contributions. There is not a single XB with a strongly positive energy density in the bond region, which according to the Cremer–Kraka criteria would indicate dominant electrostatic bonding. Typically, the weak XB identified in this work possess energy densities close to zero and dominant electrostatic character.

4. Covalent contributions have been characterized by CT from  $\text{lp}(\text{A})$  to  $\sigma^*(\text{XY})$  and by the delocalization energy  $\Delta E(\text{del})$  associated with this process. In all cases, at least some covalent character of XB could be observed, which underlines that XB is, in general, more covalent than either HB or pnictogen bonding.<sup>83,97</sup>

**Table 1. Comparison of Quantum-Chemical Investigations of XB Complexes<sup>a</sup>**

XB complexes	method	properties and topics	ref
IV (6)	DFT-r4	ESP	20
I (22)	MP2	$\Delta E$ , $r$ , $J_{\text{coup}}$	30
II (76)	CCSD(T), microwave	$\Delta E$ , $r$ , $k_{\sigma}$	32
II (15)	CCSD(T)	$\Delta E$ , ED, $r$ , $\Theta$	34
III (18)	MP2	$\Delta E$ , $r$ , $\Delta\omega$ , IE	37
II (69)	CCSD(T)	benchmark $r$ , $\Delta E$	38
II, III (55)	DFT-r4 BLW	$\Delta E$ , IE, ED	41
III (100)	MP2	$\Delta E$ , $r$ , ESP	46
III (8)	MP2	$\Delta E$ , ESP, ED	54
II,III (28)	SAPT	$\Delta E$ , ED, $\Theta$ XB vs CB, PB	66, 67
I (15)	SAPT	$\Delta E$ , ED, $\Theta$	69
III (11)	DFT-r2	ESP, $\Delta E$ , $r$ , $\rho$	72
II (30)	DFT-r4	dipole, $\Delta E$	74
I (7)	MP2	$\Delta E$ , $r$ , ED, $\rho$ , $\Theta$	75
I (14)	MP2	$\rho$ , XB vs HB	76
I (16)	MP2	$\Delta E$ , $r$ , $J_{\text{coup}}$	83
III, IV (57)	DFT-r4, MP2	ESP, $\Delta E$ , $r$	123, 125
IV (12)	MP2	ESP, $\Delta E$ , $r$ , $\Theta$	130
II (7)	DFT-r4 BLW	$\Delta E$ , $r$ , ESP, ED, $\Delta\omega$ , $\Theta$ , XB vs HB, CB, PB	133
I, II, III, IV (202)	CCSD(T), DFT-r4	$\Delta E$ , $r$ , $\rho$ , ESP, $\omega^a$ , $k^b$ , BSO	this work

<sup>a</sup>Groups I–IV according to Figure 1 and the number of XB complexes studied given in parentheses. XC functionals of DFT are classified according to their rung in “Jacobs’s ladder” (r2, GGA; r4, hybrid XC). ESP = electrostatic potential,  $\Delta E$  = binding energy,  $J_{\text{coup}}$  = NMR spin–spin coupling constants, ED = energy decomposition,  $\rho$  = electron density,  $r$  = geometric parameters,  $k_{\sigma}$  = intermolecular force constant from microwave spectroscopy,  $\Delta\omega$  = frequency shifts,  $\Theta$  = angular distortion, CB = comparison with chalcogen bonding, and PB = with pnictogen bonding.

5. It is remarkable that, besides the covalent contributions, the  $\sigma$ -hole,  $\text{lp}(\text{A})$  interactions, as measured by the electrostatic potential  $V$ , are often decisive for the magnitude of the BSO because they directly influence the intrinsic bond strength. For example, the increasing intrinsic XB strength in the interactions of FCl, FBr, FI, and FAt with a Lewis base such as  $\text{PMe}_3$  can be predicted in this way. However, it is a simplification to explain XB just by  $\sigma$ -hole interactions because covalent contributions to XB always have to be considered.

6. Unusual are the relatively strong XB between dihalogens/halohalogen and phosphines, especially if these are carrying an electron-withdrawing substituent such as  $\text{Z} = \text{F}, \text{OH}, \text{Cl}, \text{CN}$ , etc. In these cases, 3c-4e bonding is established leading to an interaction of the type  $\text{Y} \cdots \text{X} \cdots \text{PR}_2\text{Z}$ . The degree of 3c-4e XB is quantitatively determined by the ratio  $\text{BSO}(\text{X} \cdots \text{A})/\text{BSO}(\text{Y} \cdots \text{X})$ . If the latter is close to 1.00, an ideal 3c-4e system is established. If it is larger than 1.00, then an inverted 3c-4e XB exists, with a stronger X–A interaction that in the extreme can lead to a new bond.

7. Relativistic effects both strengthen and weaken XB because of the  $s,p$ -orbital contraction for Br (small effect), I, and At. Orbital contraction increases somewhat the effective electronegativity, which causes a less steep decrease of the covalent contribution, as would be predicted by nonrelativistic orbital energies and the overlap with A. Second, they lead to a smaller  $\sigma$  hole (stronger shielding of the nucleus by orbital contraction)

for the higher halogens, as expected on the basis of their atomic number. Compared to the nonrelativistic effects, the relativistic effects are too small to change the overall trends in covalent or electrostatic XB.

8. It is remarkable that, because of the formation of a supporting HB, the otherwise destabilizing OH group can substantially increase the intrinsic strength of XB. In the case of  $\text{FCl}\cdots\text{PH}_2\text{OH}$ , a nonclassical complex is formed with ideal 3c-4e bonding. We suggest exploiting the combination of HB and XB systematically to generate new polymers and other materials.

9. Halomethanes and halotetragenes are limited in establishing strong covalent contributions to XB. This is actually a result of the relatively low electronegativity of C (and the higher tetragenesis) and the limited polarity of the C–X (Si–X, Ge–X, and Sn–X) bond. These limitations can be overcome by increasing the  $\sigma$  hole and polarizability of X, which is best accomplished by reverting to iodo-substituted carbon molecules. Essential is that the carbon framework is also highly polarizable, which is achieved if carbon molecules with multiple bonds are involved. This explains the stability of XB in connection with diiodoacetylene or diiodopolyalkyne and their frequent use in polymer chemistry.<sup>16,154–156</sup>

10. We suggest as new materials the use of perfluorinated diiodobenzene, which has relatively strong XB with alkylamines and gains stability by its large polarizability. Iodocyanide should be too poisonous to use, iodophosphaethyne ( $\text{I}-\text{C}\equiv\text{P}$ ) should only be stable at low temperatures, and diiododizomethane ( $\text{I}_2\text{CN}_2$ ) should be explosive, which limits the possibility of utilizing strong XB for systems with triple or multiple bonds. However, I-substituted derivatives of 1,3-dipolar molecules such as diazonium betaines (INN and  $\text{I}_2\text{CNN}$ ), nitrilium betaines (ICNO, ICNI, and  $\text{ICNCR}_2$ ), or azomethines should provide possibilities for polymers if reacted with diamino perfluorinated polyalkenes or diaminopolyalkynes. 1,3-dipolar cycloadditions would lead to a very stable network of bonds in such polymers.

11. Apart from providing for the first time a quantitative order of intrinsic XB strengths, we have developed a new method for analyzing complex binding energies  $\Delta E$ . This is based on two or three reference complexes that are used to establish a relationship between  $\Delta E$  and BSO  $n$ . Any deviation from the reference line can be analyzed in terms of the electronic effects, causing the deviation. This makes it possible to quantify the energetic consequences of the latter and get a better understanding of how the interplay of different electronic effects leads to the actual complex binding energy. Similarly, one can analyze the delocalization energies  $\Delta E(\text{del})$ , electron density  $\rho(\mathbf{r}_b)$ , or energy density  $H(\mathbf{r}_b)$  by comparing them with the BSO values and using suitable reference values.

Finally, a caveat has to be made with regard to the  $\sigma$ -hole,lp(A) interactions because one might consider them to be a covalent contribution in the sense that the “lp(A) orbital directly donates charge to the  $\sigma$ -hole”. However, covalent contributions always depend on both potential and kinetic energy. In this work, the energy density  $H(\mathbf{r}_b)$  was used to determine the covalency of XB. It was found that  $H(\mathbf{r})$  is not necessarily a minimum at the position of the  $\sigma$  hole, which indicates that analysis of the  $\sigma$  hole can provide some insight into the electrostatic but not the potential covalent character of XB. Additional covalent contributions, even if small, can change the intrinsic strength of XB.

## ■ ASSOCIATED CONTENT

### ● Supporting Information

The Supporting Information is available free of charge on the ACS Publications website at DOI: 10.1021/acs.inorgchem.6b02358.

Binding energies  $\Delta E$ , local stretching force constants  $k^a(\text{XA})$ , and bond distances  $r(\text{XA})$  obtained at CCSD-(T)/aug-cc-pVTZ and at  $\omega\text{B97X-D/aug-cc-pVTZ}$  for selected complexes (Table S1 and Figures S1 and S2), a summary of energetic, geometric, and vibrational data for all complexes (Table S2), selected properties of the XB donors (Table S3) and acceptors (Table S4), bond distances and bond ratios of complexes of high 3c-4e character (Table S5), the corresponding BSO ratios (Table S6), lists of complexes (Tables S7–S10), a comparison between  $\Delta E$  calculated at  $\omega\text{B97X-D/aug-cc-pVTZ}$  geometries using  $\omega\text{B97X-D/aug-cc-pVTZ}$  and CCSD(T)/aug-cc-pVTZ energies for all complexes (Figure S2), a schematic representation of all complexes with NBO charges (Figures S3–S5), a comparison of BSO  $n$  with the density  $\rho_b$  (Figure S6), and linear relationship between  $k^a(\text{XA})$  and the calculated vertical IPs for 11 Lewis bases (Figure S7) (PDF)

## ■ AUTHOR INFORMATION

### Corresponding Authors

\*E-mail: ekraka@gmail.com.

\*E-mail: dcremer@smu.edu.

### ORCID

Elfi Kraka: 0000-0002-9658-5626

Dieter Cremer: 0000-0002-6213-5555

### Notes

The authors declare no competing financial interest.

## ■ ACKNOWLEDGMENTS

This work was financially supported by National Science Foundation Grants CHE 1152357 and CHE 1464906. We thank SMU for providing computational resources. The authors acknowledge financial support by CAPES (Brazil; Fellowship Grant BEX 9534-13-0).

## ■ REFERENCES

- (1) Cavallo, G.; Metrangolo, P.; Milani, R.; Pilati, T.; Priimagi, A.; Resnati, G.; Terraneo, G. The Halogen Bond. *Chem. Rev.* **2016**, *116*, 2478–2601.
- (2) Pennington, W. T.; Hanks, T. W.; Arman, H. D. In *Halogen Bonding*; Metrangolo, P., Resnati, G., Eds.; Structure and Bonding; Springer: Berlin, 2008; Vol. 126; pp 65–104.
- (3) Beale, T. M.; Chudzinski, M. G.; Sarwar, M. G.; Taylor, M. S. Halogen bonding in solution: thermodynamics and applications. *Chem. Soc. Rev.* **2013**, *42*, 1667–1680.
- (4) Wolters, L. P.; Schyman, P.; Pavan, M. J.; Jorgensen, W. L.; Bickelhaupt, F. M.; Kozuch, S. The many faces of halogen bonding: a review of theoretical models and methods. *WIREs Comput. Mol. Sci.* **2014**, *4*, 523–540.
- (5) Gilday, L. C.; Robinson, S. W.; Barendt, T. A.; Langton, M. J.; Mullaney, B. R.; Beer, P. D. Halogen Bonding in Supramolecular Chemistry. *Chem. Rev.* **2015**, *115*, 7118–7195.
- (6) Schindler, S.; Huber, S. M. In *Halogen Bonding II*; Metrangolo, P., Resnati, G., Eds.; Topics in Current Chemistry; Springer International Publishing: Berlin, 2015; Vol. 359; pp 167–203.

- (7) Ho, P. In *Halogen Bonding I*; Metrangolo, P., Resnati, G., Eds.; Topics in Current Chemistry; Springer International Publishing: Berlin, 2015; Vol. 358; pp 241–276.
- (8) Jentzsch, A. V.; Matile, S. In *Halogen Bonding I*; Metrangolo, P., Resnati, G., Eds.; Topics in Current Chemistry; Springer International Publishing: Berlin, 2015; Vol. 358; pp 205–239.
- (9) Bauzá, T. J.; Mooibroek, T. J.; Frontera, A. The Bright Future of Unconventional  $\sigma/\pi$ -Hole Interactions. *ChemPhysChem* **2015**, *16*, 2496–2517.
- (10) Kolar, M. H.; Hobza, P. Computer Modeling of Halogen Bonds and Other  $\sigma$ -Hole Interactions. *Chem. Rev.* **2016**, *116*, 5155–5187.
- (11) Wang, H.; Wang, W.; Jin, W. J.  $\sigma$ -Hole Bond vs  $\pi$ -Hole Bond: A Comparison Based on Halogen Bond. *Chem. Rev.* **2016**, *116*, 5072–5104.
- (12) Abate, A.; Saliba, M.; Hollman, D. J.; Stranks, S. D.; Wojciechowski, K.; Avolio, R.; Grancini, G.; Petrozza, A.; Snaith, H. J. Supramolecular Halogen Bond Passivation of Organic-Inorganic Halide Perovskite Solar Cells. *Nano Lett.* **2014**, *14*, 3247–3254.
- (13) Aakeroy, C. B.; Spartz, C. L.; Dembowski, S.; Dwyre, S.; Desper, J. A systematic structural study of halogen bonding versus hydrogen bonding within competitive supramolecular systems. *IUCr* **2015**, *2*, 498–510.
- (14) Aakeroy, C. B.; Wijethunga, T. K.; Desper, J.; Dakovic, M. Crystal Engineering with Iodoethynylnitrobenzenes: A Group of Highly Effective Halogen-Bond Donors. *Cryst. Growth Des.* **2015**, *15*, 3853–3861.
- (15) Dumele, O.; Trapp, N.; Diederich, F. Halogen Bonding Molecular Capsules. *Angew. Chem., Int. Ed.* **2015**, *54*, 12339–12344.
- (16) Berger, G.; Soubhye, J.; Meyer, F. Halogen bonding in polymer science: from crystal engineering to functional supramolecular polymers and materials. *Polym. Chem.* **2015**, *6*, 3559–3580.
- (17) Dumele, O.; Wu, D.; Trapp, N.; Goroff, N.; Diederich, F. Halogen Bonding of (Iodoethynyl)benzene Derivatives in Solution. *Org. Lett.* **2014**, *16*, 4722–4725.
- (18) Nagels, N.; Geboes, Y.; Pinter, B.; DeProft, F.; Herrebout, W. A. Tuning the Halogen/Hydrogen Bond Competition: A Spectroscopic and Conceptual DFT Study of Some Model Complexes Involving CHF<sub>2</sub>I. *Chem. - Eur. J.* **2014**, *20*, 8433–8443.
- (19) Saito, M.; Tsuji, N.; Kobayashi, Y.; Takemoto, Y. Direct Dehydroxylative Coupling Reaction of Alcohols with Organosilanes through Si-X Bond Activation by Halogen Bonding. *Org. Lett.* **2015**, *17*, 3000–3003.
- (20) Aakeroy, C. B.; Wijethunga, T. K.; Desper, J.; Moore, C. Halogen-Bond Preferences in Co-crystal Synthesis. *J. Chem. Crystallogr.* **2015**, *45*, 267–276.
- (21) Kee, C. W.; Wong, M. W. In Silico Design of Halogen-Bonding-Based Organocatalyst for Diels-Alder Reaction, Claisen Rearrangement, and Cope-Type Hydroamination. *J. Org. Chem.* **2016**, *81*, 7459–7470.
- (22) Kniep, F.; Jungbauer, S. H.; Zhang, Q.; Walter, S. M.; Schindler, S.; Schnapperelle, I.; Herdtweck, E.; Huber, S. M. Organocatalysis by Neutral Multidentate Halogen-Bond Donors. *Angew. Chem., Int. Ed.* **2013**, *52*, 7028–7032.
- (23) Wilcken, R.; Zimmermann, M. O.; Lange, A.; Joerger, A. C.; Boeckler, F. M. Principles and Applications of Halogen Bonding in Medicinal Chemistry and Chemical Biology. *J. Med. Chem.* **2013**, *56*, 1363–1388.
- (24) Alkorta, I.; Elguero, J.; Mo, O.; Yanez, M.; Del Bene, J. E. Using beryllium bonds to change halogen bonds from traditional to chlorine-shared to ion-pair bonds. *Phys. Chem. Chem. Phys.* **2015**, *17*, 2259–2267.
- (25) Brea, O.; Mo, O.; Yanez, M.; Alkorta, I.; Elguero, J. Creating  $\sigma$ -Holes through the Formation of Beryllium Bonds. *Chem. - Eur. J.* **2015**, *21*, 12676–12682.
- (26) Legon, A. C. Prereactive Complexes of Dihalogens XY with Lewis Bases B in the Gas Phase: A Systematic Case for the Halogen Analogue B...XY of the Hydrogen Bond B...HX. *Angew. Chem., Int. Ed.* **1999**, *38*, 2686–2714.
- (27) Aragoni, M. C.; Arca, M.; Devillanova, M.; Garau, F. A.; Isaia, A.; Lippolis, F.; Mancini, A. The nature of the chemical bond in linear three-body systems: From I 3- to mixed chalcogen/halogen and trichalcogen moieties. *Bioinorg. Chem. Appl.* **2007**, *2007*, 1.
- (28) Braidia, B.; Hiberty, P. C. Application of the Valence Bond Mixing Configuration Diagrams to Hypervalency in Trihalide Anions: A Challenge to the Rundle-Pimentel Model. *J. Phys. Chem. A* **2008**, *112*, 13045–13052.
- (29) Del Bene, J. E.; Alkorta, I.; Elguero, J. Do Traditional, Chlorine-shared, and Ion-pair Halogen Bonds Exist? An ab Initio Investigation of FCl:CNX Complexes. *J. Phys. Chem. A* **2010**, *114*, 12958–12962.
- (30) Del Bene, J. E.; Alkorta, I.; Elguero, J. Do nitrogen bases form chlorine-shared and ion-pair halogen bonds? *Chem. Phys. Lett.* **2011**, *508*, 6–9.
- (31) Donoso-Tauda, O.; Jaque, P.; Elguero, J.; Alkorta, I. Traditional and ion-pair halogen-bonded complexes between chlorine and bromine derivatives and a nitrogen-heterocyclic carbene. *J. Phys. Chem. A* **2014**, *118*, 9552–9560.
- (32) Legon, A. C. A reduced radial potential energy function for the halogen bond and the hydrogen bond in complexes B...XY and B...HX, where X and Y are halogen atoms. *Phys. Chem. Chem. Phys.* **2014**, *16*, 12415–12421.
- (33) Otero de la Roza, A.; Johnson, E. R.; DiLabio, G. A. Halogen Bonding from Dispersion-Corrected Density-Functional Theory: The Role of Delocalization Error. *J. Chem. Theory Comput.* **2014**, *10*, 5436–5447.
- (34) Hill, J. G.; Hu, X. Theoretical Insights into the Nature of Halogen Bonding in Prereactive Complexes. *Chem. - Eur. J.* **2013**, *19*, 3620–3628.
- (35) Karpfen, A. *Halogen Bonding* **2008**, 126, 1–15.
- (36) Wolters, L. P.; Bickelhaupt, F. M. Halogen Bonding versus Hydrogen Bonding: A Molecular Orbital Perspective. *ChemistryOpen* **2012**, *1*, 96–105.
- (37) Pinter, B.; Nagels, N.; Herrebout, W. A.; DeProft, F. Halogen Bonding from a Hard and Soft Acids and Bases Perspective: Investigation by Using Density Functional Theory Reactivity Indices. *Chem. - Eur. J.* **2013**, *19*, 519–530.
- (38) Kozuch, S.; Martin, J. M. L. Halogen Bonds: Benchmarks and Theoretical Analysis. *J. Chem. Theory Comput.* **2013**, *9*, 1918–1931.
- (39) Forni, A.; Pieraccini, S.; Rendine, S.; Sironi, M. Halogen bonds with benzene: An assessment of DFT functionals. *J. Comput. Chem.* **2014**, *35*, 386–394.
- (40) Tognetti, V.; Joubert, L. Electron density Laplacian and halogen bonds. *Theor. Chem. Acc.* **2015**, *134*.10.1007/s00214-015-1685-8
- (41) Wang, C.; Danovich, D.; Mo, Y.; Shaik, S. On The Nature of the Halogen Bond. *J. Chem. Theory Comput.* **2014**, *10*, 3726–3737.
- (42) George, J.; Deringer, V. L.; Dronskowski, R. Cooperativity of Halogen, Chalcogen, and Pnictogen Bonds in Infinite Molecular Chains by Electronic Structure Theory. *J. Phys. Chem. A* **2014**, *118*, 3193–3200.
- (43) Parker, A. J.; Stewart, J.; Donald, K. J.; Parish, C. A. Halogen Bonding in DNA Base Pairs. *J. Am. Chem. Soc.* **2012**, *134*, 5165–5172.
- (44) Palusiak, M. On the nature of halogen bond - The Kohn-Sham molecular orbital approach. *J. Mol. Struct.: THEOCHEM* **2010**, *945*, 89–92.
- (45) Del Bene, J. E.; Alkorta, I.; Elguero, J. Influence of Substituent Effects on the Formation of P...Cl Pnictogen Bonds or Halogen Bonds. *J. Phys. Chem. A* **2014**, *118*, 2360–2366.
- (46) Tawfik, M.; Donald, K. J. Halogen Bonding: Unifying Perspectives on Organic and Inorganic Cases. *J. Phys. Chem. A* **2014**, *118*, 10090–10100.
- (47) Bartashevich, E. V.; Tsirelson, V. G. Interplay between non-covalent interactions in complexes and crystals with halogen bonds. *Russ. Chem. Rev.* **2014**, *83*, 1181.
- (48) Duarte, D. J. R.; Peruchena, N. M.; Alkorta, I. Double Hole-Lump Interaction between Halogen Atoms. *J. Phys. Chem. A* **2015**, *119*, 3746–3752.

- (49) Jahromi, H. J.; Eskandari, K.; Alizadeh, A. Comparison of halogen bonds in M-X...N contacts (M = C, Si, Ge and X = Cl, Br). *J. Mol. Model.* **2015**, *21*, 10.1007/s00894-015-2660-y
- (50) Lo, R.; Ganguly, B. Revealing halogen bonding interactions with anomeric systems: An ab initio quantum chemical studies. *J. Mol. Graphics Modell.* **2015**, *55*, 123–133.
- (51) Sladek, V.; Skorna, P.; Poliak, P.; Lukes, V. The ab initio study of halogen and hydrogen  $\sigma$ N-bonded para-substituted pyridine...(X<sub>2</sub>/XY/HX) complexes. *Chem. Phys. Lett.* **2015**, *619*, 7–13.
- (52) Nepal, B.; Scheiner, S. Long-range behavior of noncovalent bonds. Neutral and charged H-bonds, pnictogen, chalcogen, and halogen bonds. *Chem. Phys.* **2015**, *456*, 34–40.
- (53) Huber, S. M.; Jimenez-Izal, E.; Ugalde, J. M.; Infante, I. Unexpected trends in halogen-bond based noncovalent adducts. *Chem. Commun.* **2012**, *48*, 7708–7710.
- (54) Alkorta, I.; Blanco, F.; Solimannejad, M.; Elguero, J. Competition of Hydrogen Bonds and Halogen Bonds in Complexes of Hypohalous Acids with Nitrogenated Bases. *J. Phys. Chem. A* **2008**, *112*, 10856–10863.
- (55) Grant Hill, J. The halogen bond in thiirane...ClF: an example of a Mulliken inner complex. *Phys. Chem. Chem. Phys.* **2014**, *16*, 19137–19140.
- (56) Grant Hill, J.; Legon, A. C. On the directionality and non-linearity of halogen and hydrogen bonds. *Phys. Chem. Chem. Phys.* **2015**, *17*, 858–867.
- (57) Jeffrey, G. *An Introduction to Hydrogen Bonding*; Oxford University Press: New York, 1997.
- (58) Jeffrey, G.; Saenger, W. *Hydrogen Bonding in Biological Structures*; Springer-Verlag: Berlin, 1991.
- (59) Scheiner, S. *Hydrogen bonding: A theoretical perspective*; Oxford University Press: New York, 1997.
- (60) Pihko, P. E. *Hydrogen Bonding in Organic Synthesis*; Wiley: New York, 2009.
- (61) Grabowski, E. *Hydrogen Bonding—New Insights (Challenges and Advances in Computational Chemistry and Physics)*; Springer: New York, 2006.
- (62) Gilli, G.; Gilli, P. *The Nature of the Hydrogen Bond*; IUCr Monographs on Crystallography 23; Oxford University Press: New York, 2009.
- (63) Cavallo, G.; Metrangolo, P.; Pilati, T.; Resnati, G.; Sansotera, M.; Terraneo, G. Halogen bonding: a general route in anion recognition and coordination. *Chem. Soc. Rev.* **2010**, *39*, 3772–3783.
- (64) Metrangolo, P.; Meyer, F.; Pilati, T.; Resnati, G.; Terraneo, G. Halogen Bonding in Supramolecular Chemistry. *Angew. Chem., Int. Ed.* **2008**, *47*, 6114–6127.
- (65) Adhikari, U.; Scheiner, S. Substituent Effects on Cl...N, S...N, and P...N Noncovalent Bonds. *J. Phys. Chem. A* **2012**, *116*, 3487–3497.
- (66) Scheiner, S. Detailed comparison of the pnictogen bond with chalcogen, halogen, and hydrogen bonds. *Int. J. Quantum Chem.* **2013**, *113*, 1609–1620.
- (67) Riley, K. E.; Murray, J. S.; Fanfrlík, J.; Rezáč, J.; Solá, R. J.; Concha, M. C.; Ramos, F. M.; Politzer, P. Halogen bond tunability II: the varying roles of electrostatic and dispersion contributions to attraction in halogen bonds. *J. Mol. Model.* **2013**, *19*, 4651–4659.
- (68) Stone, A. J. Are Halogen Bonded Structures Electrostatically Driven? *J. Am. Chem. Soc.* **2013**, *135*, 7005–7009.
- (69) Sedlak, R.; Kolár, M. H.; Hobza, P. Polar Flattening and the Strength of Halogen Bonding. *J. Chem. Theory Comput.* **2015**, *11*, 4727–4732.
- (70) Zierkiewicz, W.; Bienko, D. C.; Michalska, D.; Zeegers-Huyskens, T. Theoretical investigation of the halogen bonded complexes between carbonyl bases and molecular chlorine. *J. Comput. Chem.* **2015**, *36*, 821–832.
- (71) Dyduch, K.; Mitoraj, M. P.; Michalak, A. ETS-NOCV description of  $\sigma$ -hole bonding. *J. Mol. Model.* **2013**, *19*, 2747–2758.
- (72) Mitoraj, M. P.; Michalak, A. Theoretical description of halogen bonding - an insight based on the natural orbitals for chemical valence combined with the extended-transition-state method (ETS-NOCV). *J. Mol. Model.* **2013**, *19*, 4681–4688.
- (73) Bartashevich, E. V.; Tsirelson, V. G. Atomic dipole polarization in charge-transfer complexes with halogen bonding. *Phys. Chem. Chem. Phys.* **2013**, *15*, 2530–2538.
- (74) Duarte, D.; Sosa, G.; Peruchena, N. Nature of halogen bonding. A study based on the topological analysis of the Laplacian of the electron charge density and an energy decomposition analysis. *J. Mol. Model.* **2013**, *19*, 2035–2041.
- (75) Angelina, E. L.; Duarte, D. R.; Peruchena, N. M. Is the decrease of the total electron energy density a covalence indicator in hydrogen and halogen bonds? *J. Mol. Model.* **2013**, *19*, 2097–2106.
- (76) Grabowski, S. J. Non-covalent interactions - QTAIM and NBO analysis. *J. Mol. Model.* **2013**, *19*, 4713–4721.
- (77) Duarte, D.; Angelina, E. L.; Peruchena, N. Physical meaning of the QTAIM topological parameters in hydrogen bonding. *J. Mol. Model.* **2014**, *20*, 10.1007/s00894-014-2510-3
- (78) Shahi, A.; Arunan, E. Hydrogen bonding, halogen bonding and lithium bonding: an atoms in molecules and natural bond orbital perspective towards conservation of total bond order, inter- and intramolecular bonding. *Phys. Chem. Chem. Phys.* **2014**, *16*, 22935–22952.
- (79) Kaur, D.; Kaur, R.; Shiekh, B. Effects of substituents and charge on the RCHO...X-Y X= Cl, Br, I; Y:  $\ddot{A}^+$ -CF<sub>3</sub>, -CF<sub>2</sub>H, -CFH<sub>2</sub>, -CN, -CCH, -CCCN; R:  $\ddot{t}$ -OH, -OCH<sub>3</sub>, -NH<sub>2</sub>, -O- halogen-bonded complexes. *Struct. Chem.* **2016**, *27*, 961.
- (80) Joy, J.; Jemmis, E. D.; Vidya, K. Negative hyperconjugation and red-, blue- or zero-shift in X-Z...Y complexes. *Faraday Discuss.* **2015**, *177*, 33–50.
- (81) Joy, J.; Jose, A.; Jemmis, E. D. Continuum in the X-Z-Y weak bonds: Z= main group elements. *J. Comput. Chem.* **2016**, *37*, 270–279.
- (82) Alkorta, I.; Elguero, J.; Del Bene, J. E. Characterizing Traditional and Chlorine-Shared Halogen Bonds in Complexes of Phosphine Derivatives with ClF and Cl<sub>2</sub>. *J. Phys. Chem. A* **2014**, *118*, 4222–4231.
- (83) Freindorf, M.; Kraka, E.; Cremer, D. A Comprehensive Analysis of Hydrogen Bond Interactions Based on Local Vibrational Modes. *Int. J. Quantum Chem.* **2012**, *112*, 3174–3187.
- (84) Kraka, E.; Setiawan, D.; Cremer, D. Reevaluation of the Bond Length - Bond Strength Rule: The Stronger Bond is not always the Shorter Bond. *J. Comput. Chem.* **2016**, *37*, 130–142.
- (85) Konkoli, Z.; Cremer, D. A New Way of Analyzing Vibrational Spectra I. Derivation of Adiabatic Internal Modes. *Int. J. Quantum Chem.* **1998**, *67*, 1–9.
- (86) Cremer, D.; Larsson, J. A.; Kraka, E. In *Theoretical and Computational Chemistry, Vol. 5, Theoretical Organic Chemistry*; Parkanyi, C., Ed.; Elsevier: Amsterdam, The Netherlands, 1998; pp 259–327.
- (87) Zou, W.; Kalescky, R.; Kraka, E.; Cremer, D. Relating Normal Vibrational Modes To Local Vibrational Modes With The Help of an Adiabatic Connection Scheme. *J. Chem. Phys.* **2012**, *137*, 084114.
- (88) Zou, W.; Cremer, D. Properties of Local Vibrational Modes: The Infrared Intensity. *Theor. Chem. Acc.* **2014**, *133*, 1451-1–1451-15.
- (89) Kalescky, R.; Zou, W.; Kraka, E.; Cremer, D. Local Vibrational Modes of the Water Dimer - Comparison of Theory and Experiment. *Chem. Phys. Lett.* **2012**, *554*, 243–247.
- (90) Kalescky, R.; Kraka, E.; Cremer, D. Local Vibrational Modes of the Formic Acid Dimer - The Strength of the Double Hydrogen Bond. *Mol. Phys.* **2013**, *111*, 1497–1510.
- (91) Kalescky, R.; Kraka, E.; Cremer, D. Identification of the Strongest Bonds in Chemistry. *J. Phys. Chem. A* **2013**, *117*, 8981–8995.
- (92) Kalescky, R.; Zou, W.; Kraka, E.; Cremer, D. Vibrational properties of the Isotopomers of the Water Dimer Derived from Experiment and Computations. *Aust. J. Chem.* **2014**, *67*, 426–434.
- (93) Kraka, E.; Freindorf, M.; Cremer, D. Chiral Discrimination by Vibrational Spectroscopy Utilizing Local Modes. *Chirality* **2013**, *25*, 185–196.
- (94) Zhang, X.; Dai, H.; Yan, H.; Zou, H. Y. W.; Cremer, D. B-H... $\pi$  Interaction: A New Type of Nonclassical Hydrogen Bonding. *J. Am. Chem. Soc.* **2016**, *138*, 4334–4337.

- (95) Zou, W.; Kalescky, R.; Kraka, E.; Cremer, D. Relating normal vibrational modes to local vibrational modes benzene and naphthalene. *J. Chem. Phys.* **2012**, *137*, 084114-1–084114-13.
- (96) Zou, W.; Cremer, D.  $C_2$  in a Box: Determining its Intrinsic Bond Strength for the  $X^1\Sigma_g^+$  Ground State. *Chem. - Eur. J.* **2016**, *22*, 4087–4089.
- (97) Setiawan, D.; Kraka, E.; Cremer, D. Strength of the Pnictogen Bond in Complexes Involving Group Va Elements N, P, and As. *J. Phys. Chem. A* **2015**, *119*, 1642–1656.
- (98) Setiawan, D.; Kraka, E.; Cremer, D. Description of pnictogen bonding with the help of vibrational spectroscopy - The missing link between theory and experiment. *Chem. Phys. Lett.* **2014**, *614*, 136–142.
- (99) Raghavachari, K.; Trucks, G. W.; Pople, J. A.; Head-Gordon, M. *Chem. Phys. Lett.* **1989**, *157*, 479–483.
- (100) Woon, D.; Dunning, T. J. Gaussian Basis Sets for Use in Correlated Molecular Calculations. IV. Calculation of Static Electrical Response Properties. *J. Chem. Phys.* **1994**, *100*, 2975–2988.
- (101) Dunning, T. Gaussian Basis Sets for Use in Correlated Molecular Calculations. I. The Atoms Boron Through Neon and Hydrogen. *J. Chem. Phys.* **1989**, *90*, 1007–1023.
- (102) Woon, D.; Dunning, T. Gaussian Basis Sets for Use in Correlated Molecular Calculations. III. The Atoms Aluminum Through Argon. *J. Chem. Phys.* **1993**, *98*, 1358–1371.
- (103) Peterson, K. A.; Figgen, D.; Goll, E.; Stoll, H.; Dolg, M. Systematically convergent basis sets with relativistic pseudopotentials. II. Small-core pseudopotentials and correlation consistent basis sets for the post-d group 16–18 elements. *J. Chem. Phys.* **2003**, *119*, 11113–11123.
- (104) Grafenstein, J.; Cremer, D. Efficient DFT Integrations by Locally Augmented Radial Grids. *J. Chem. Phys.* **2007**, *127*, 164113.
- (105) Chai, J. D.; Head-Gordon, M. Long-range Corrected Hybrid Density Functionals with Damped Atom-atom Dispersion Corrections. *Phys. Chem. Chem. Phys.* **2008**, *10*, 6615–6620.
- (106) Chai, J. D.; Head-Gordon, M. Systematic Optimization of Long-range Corrected Hybrid Density Functionals. *J. Chem. Phys.* **2008**, *128*, 084106.
- (107) Becke, A. D. Density-Functional Thermochemistry. III. The Role of Exact Exchange. *J. Chem. Phys.* **1993**, *98*, 5648–5652.
- (108) Stephens, P. J.; Devlin, F. J.; Chabalowski, C. F.; Frisch, M. J. Ab Initio Calculation of Vibrational Absorption and Circular Dichroism Spectra Using Density Functional Force Fields. *J. Phys. Chem.* **1994**, *98*, 11623–11627.
- (109) Perdew, J. P.; Burke, K.; Ernzerhof, M. Generalized Gradient Approximation Made Simple. *Phys. Rev. Lett.* **1996**, *77*, 3865–3869.
- (110) Adamo, C.; Barone, V. Toward reliable density functional methods without adjustable parameters: The PBE0 model. *J. Chem. Phys.* **1999**, *110*, 6158–6169.
- (111) Zhao, Y.; Truhlar, D. G. The M06 suite of density functionals for main group thermochemistry, thermochemical kinetics, non-covalent interactions, excited states, and transition elements: two new functionals and systematic testing of four M06-class functionals and 12 other functionals. *Theor. Chem. Acc.* **2008**, *120*, 215–241.
- (112) Wilson, E. B.; Decius, J. C.; Cross, P. C. *Molecular Vibrations. The Theory of Infrared and Raman Vibrational Spectra*; McGraw-Hill: New York, 1955.
- (113) Mayer, I. Charge, Bond Order and Valence in the Ab Initio Theory. *Chem. Phys. Lett.* **1983**, *97*, 270–274.
- (114) Mayer, I. Bond orders and valences from ab initio wave functions. *Int. J. Quantum Chem.* **1986**, *29*, 477–483.
- (115) Kraka, E.; Larsson, J. A.; Cremer, D. *Generalization of the Badger Rule Based on the Use of Adiabatic Vibrational Modes in Vibrational Modes in Computational IR Spectroscopy*; Wiley, New York, 2010; pp 105–149.
- (116) Boys, S.; Bernardi, F. The Calculation of Small Molecular Interactions by The Differences of Separate Total Energies. Some Procedures with Reduced Errors. *Mol. Phys.* **1970**, *19*, 553–566.
- (117) Riplinger, C.; Neese, F. An efficient and near linear scaling pair natural orbital based local coupled cluster method. *J. Chem. Phys.* **2013**, *138*, 034106-1–034106-18.
- (118) Riplinger, C.; Sandhoefer, B.; Hansen, A.; Neese, F. Natural triple excitations in local coupled cluster calculations with pair natural orbitals. *J. Chem. Phys.* **2013**, *139*, 134101-1–134101-13.
- (119) Weigend, F.; Ahlrichs, R. Balanced basis sets of split valence, triple zeta valence and quadruple zeta valence quality for H to Rn: Design and assessment of accuracy. *Phys. Chem. Chem. Phys.* **2005**, *7*, 3297–3305.
- (120) Peterson, K. A.; Figgen, D.; Goll, E.; Stoll, H.; Dolg, M. Systematically convergent basis sets with relativistic pseudopotentials. II. Small-core pseudopotentials and correlation consistent basis sets for the post-d group 16–18 elements. *J. Chem. Phys.* **2003**, *119*, 11113–11123.
- (121) Cremer, D.; Kraka, E. A Description of the Chemical Bond in Terms of Local Properties of Electron Density and Energy. *Croatia Chemica Acta* **1984**, *57*, 1259–1281.
- (122) Cremer, D.; Kraka, E. Chemical Bonds without Bonding Electron Density - Does the Difference Electron Density Analysis Suffice for a Description of the Chemical Bond? *Angew. Chem., Int. Ed. Engl.* **1984**, *23*, 627–628.
- (123) Kraka, E.; Cremer, D. In *Theoretical Models of Chemical Bonding. The Concept of the Chemical Bond*; Maksic, Z., Ed.; Springer Verlag: Heidelberg, Germany, 1990; Vol. 2; pp 453–542.
- (124) Weinhold, F.; Landis, C. R. *Valency and Bonding: A Natural Bond Orbital Donor–Acceptor Perspective*; University Press: Cambridge, U.K., 2003.
- (125) Politzer, P.; Murray, J. S.; Clark, T. In *Halogen Bonding I: Impact on Materials Chemistry and Life Sciences*; Metrangolo, P., Resnati, G., Eds.; Springer International Publishing: Berlin, 2015; pp 19–42.
- (126) Clark, T.; Hennemann, M.; Murray, J.; Politzer, P. Halogen bonding: the  $\sigma$ -hole. *J. Mol. Model.* **2007**, *13*, 291–296.
- (127) Politzer, P.; Murray, J.; Concha, M. Halogen bonding and the design of new materials: organic bromides, chlorides and perhaps even fluorides as donors. *J. Mol. Model.* **2007**, *13*, 643–650.
- (128) Politzer, P.; Murray, J. S.; Clark, T. Halogen bonding: an electrostatically-driven highly directional noncovalent interaction. *Phys. Chem. Chem. Phys.* **2010**, *12*, 7748–7757.
- (129) Kraka, E.; Zou, W.; Filatov, M.; Grafenstein, J.; Izotov, D.; Gauss, J.; He, Y.; Wu, A.; Konkoli, Z.; Polo, V.; et al. *COLOGNE2016*; 2014; see <http://www.smu.edu/catco>.
- (130) Stanton, J. F.; Gauss, J.; Harding, M. E.; Szalay, P. G.; et al. *CFOUR, A Quantum Chemical Program Package*; 2010; see <http://www.cfour.de>.
- (131) Neese, F. The ORCA program system. *WIREs: Comp. Mol. Sci.* **2012**, *2*, 73–78.
- (132) Keith, T. TK Gristmill Software: Overland Park, KS, 2011; [aim.tkgristmill.com](http://aim.tkgristmill.com).
- (133) Frisch, M. J.; Trucks, G. W.; Schlegel, H. B.; Scuseria, G. E.; Robb, M. A.; Cheeseman, J. R.; Scalmani, G.; Barone, V.; Mennucci, B.; Petersson, G. A.; et al. *Gaussian 09*, revision A.1; Gaussian Inc.: Wallingford, CT, 2010.
- (134) Riley, K.; Murray, J.; Fanfrlík, J.; Rezác, J.; Solá, R.; Concha, M.; Ramos, F.; Politzer, P. Halogen bond tunability I: the effects of aromatic fluorine substitution on the strengths of halogen-bonding interactions involving chlorine, bromine, and iodine. *J. Mol. Model.* **2011**, *17*, 3309–3318.
- (135) Politzer, P.; Murray, J. S. Halogen bonding and beyond: factors influencing the nature of CN-R and SiN-R complexes with F-Cl and Cl<sub>2</sub>. *Theor. Chem. Acc.* **2012**, *131*.10.1007/s00214-012-1114-1
- (136) Kolar, M.; Hostas, J.; Hobza, P. The strength and directionality of a halogen bond are co-determined by the magnitude and size of the  $\sigma$ -hole. *Phys. Chem. Chem. Phys.* **2014**, *16*, 9987–9996.
- (137) Wang, C.; Guan, L.; Danovich, D.; Shaik, S.; Mo, Y. The origins of the directionality of noncovalent intermolecular interactions. *J. Comput. Chem.* **2016**, *37*, 34–45.

- (138) Dyal, K. G., Fægri, K. *Introduction to Relativistic Quantum Chemistry*; Oxford University Press: Oxford, U.K., 2007.
- (139) Rundle, R. E. Electron Deficient Compounds. II. Relative Energies of "Half-Bonds. *J. Chem. Phys.* **1949**, *17*, 671–675.
- (140) Pimentel, G. C. The Bonding of Trihalide and Bifluoride Ions by the Molecular Orbital Method. *J. Chem. Phys.* **1951**, *19*, 446–448.
- (141) Porterfield, W. W. *Inorganic Chemistry, A Unified Approach*; Academic Press: San Diego, 1993.
- (142) Greenwood, N. N.; Earnshaw, A. *Chemistry of the Elements*; Butterworth-Heinemann: Oxford, U.K., 1997.
- (143) Riley, K. E.; Hobza, P. Investigations into the Nature of Halogen Bonding Including Symmetry Adapted Perturbation Theory Analyses. *J. Chem. Theory Comput.* **2008**, *4*, 232–242.
- (144) Filatov, M.; Zou, W.; Cremer, D. Spin-orbit coupling calculations with the two-component normalized elimination of the small component method. *J. Chem. Phys.* **2013**, *139*, 014106-1–014106-8.
- (145) Marian, C. M. Spin-orbit coupling and intersystem crossing in molecules. *WIREs Comput. Mol. Sci.* **2012**, *2*, 187–203.
- (146) Fedorov, D. G.; Koseki, S.; Schmidt, M. W.; Gordon, M. S. Spin-orbit coupling in molecules: Chemistry beyond the adiabatic approximation. *Int. Rev. Phys. Chem.* **2003**, *22*, 551–592.
- (147) Clark, T.; Politzer, P.; Murray, J. S. Correct electrostatic treatment of noncovalent interactions: the importance of polarization. *WIREs Comp. Mol. Sci.* **2015**, *5*, 169–177.
- (148) Politzer, P.; Murray, J. S.; Clark, T. Mathematical modeling and Physical Reality in Non-covalent Interactions. *J. Mol. Model.* **2015**, *21*, 52–61.
- (149) Politzer, P.; Murray, J. S.; Clark, T.  $\sigma$ -Hole Bonding: A Physical Interpretation. *Top. Curr. Chem.* **2014**, *358*, 19–42.
- (150) Dominikowska, J.; Jablonski, M.; Palusiak, M. Feynman force components: basis for a solution of the covalent vs. ionic dilemma. *Phys. Chem. Chem. Phys.* **2016**, *18*, 25022–25026.
- (151) Metrangolo, P.; Resnati, G. Halogen Bonding: A Paradigm in Supramolecular Chemistry. *Chem. - Eur. J.* **2001**, *7*, 2511–2519.
- (152) Cincic, D.; Friscic, T.; Jones, W. Isostructural Materials Achieved by Using Structurally Equivalent Donors and Acceptors in Halogen-Bonded Cocrystals. *Chem. - Eur. J.* **2008**, *14*, 747–753.
- (153) Metrangolo, P.; Resnati, G.; Pilati, T.; Biella, S. In *Halogen Bonding: Fundamentals and Applications*; Metrangolo, P., Resnati, G., Eds.; Springer: Berlin, 2008; pp 105–136.
- (154) Perkins, C.; Libri, S.; Adams, H.; Brammer, L. Diiodoacetylene: compact, strong ditopic halogen bond donor. *CrystEngComm* **2012**, *14*, 3033–3038.
- (155) Luo, L.; Wilhelm, C.; Sun, A.; Grey, C. P.; Lauher, J. W.; Goroff, N. S. Poly(diiodoacetylene): Preparation, Isolation, and Full Characterization of a Very Simple Poly(diacetylene). *J. Am. Chem. Soc.* **2008**, *130*, 7702–7709.
- (156) Goroff, N. S.; Curtis, S. M.; Webb, J. A.; Fowler, F. W.; Lauher, J. W. Designed Cocrystals Based on the Pyridine-Iodoalkyne Halogen Bond. *Org. Lett.* **2005**, *7*, 1891–1893.

Paper III. Transition from metal-ligand bonding to halogen bonding involving a metal as halogen acceptor a study of Cu, Ag, Au, Pt, and Hg complexes



## Research paper

## Transition from metal-ligand bonding to halogen bonding involving a metal as halogen acceptor a study of Cu, Ag, Au, Pt, and Hg complexes



Vytor Oliveira\*, Dieter Cremer

Computational and Theoretical Chemistry Group (CATCO), Department of Chemistry, Southern Methodist University, 3215 Daniel Ave, Dallas, TX 75275-0314, USA

## ARTICLE INFO

## Article history:

Received 8 January 2017

In final form 16 May 2017

Available online 20 May 2017

## ABSTRACT

Utilizing all-electron Dirac-exact relativistic calculations with the Normalized Elimination of the Small Component (NESC) method and the local vibrational mode approach, the transition from metal-halide to metal halogen bonding is determined for Au-complexes interacting with halogen-donors. The local stretching force constants of the metal-halogen interactions reveal a smooth transition from weak non-covalent halogen bonding to non-classical 3-center-4-electron bonding and finally covalent metal-halide bonding. The strongest halogen bonds are found for dialkylaurates interacting with Cl<sub>2</sub> or FCl. Differing trends in the intrinsic halogen-metal bond strength, the binding energy, and the electrostatic potential are explained.

© 2017 Elsevier B.V. All rights reserved.

## 1. Introduction

Halogen bonding (XB) involves the interaction between a halogen donor molecule (YX) and a halogen acceptor molecule AR<sub>n</sub>, where A is an electron rich atom [1]. As in the case of hydrogen bonding, XB is a result of stabilizing covalent, electrostatic, inductive, and dispersion interactions, which are reduced by destabilizing exchange repulsion [1–3]. XB is of chemical relevance in catalysis, for the design of supramolecular structures, ion transport, and sensing [1]. There are numerous experimental and computational studies of the interactions between YX bonds and organic Lewis bases. However, XB has also been observed for transition metal complexes where the halogen accepting A is a metal M [1,4,5].

Koten and co-workers reported an organometallic complex in which a I<sub>2</sub> was coordinated to a metal center in a linear fashion (I-I-M close to 180) [6]. They suggested that the d<sub>z<sup>2</sup></sub> lone pair orbital of the metal would donate charge to the empty σ\*(I-I) of I<sub>2</sub>, which is typical of XB [6–9]. Cotton and co-workers [10] reported a complex where I<sub>2</sub> formed a bent interaction with a metal center. They suggested that the I<sub>2</sub> donates charge to the metal center in this case. Rogachev and Hoffmann [11] confirmed the I<sub>2</sub>···M bond mechanism for planar Pt-complexes. These authors studied also metal-iodine complexes in which I<sub>2</sub> acts as an electron donor thus replacing XB by normal covalent metal-iodine bonding. They also investigated how the binding energy and bond distance between

I<sub>2</sub> and the organometallic molecule is affected by having different types of metals (Co, Rh, Ir, Ni, Pd, Pt) and different ligands coordinated to the metal. Replacing Pt by Pd and then Ni leads to a weakening of XB.

An unusual octahedral cationic platinum complex with a neutral I<sub>2</sub> ligand coordinated to the metal in an end-on fashion was reported by Nagasawa and co-workers [12]. Notable is the large I-I distance in several of these complexes [6–9,11,12], which may not be only due to the donation of the lone pair of the metal into the σ\*(I-I) of iodine but may already indicate an advanced stage in the oxidative addition of I<sub>2</sub> where the metal is bound to I<sub>2</sub> by 3c-4e (3-center-4-electron) bonding or even due to an ion-pair I<sup>-</sup>···I-M<sup>+</sup> formation. Recently, Kukushkin and co-workers detected and studied theoretically the formation of XB and bifurcated XB between halocarbons and organoplatinum complexes [13]. Zeng and co-workers [14] did second order perturbation theory (MP2) calculations and found that strong halogen bonds of covalent character are formed between interhalogens and Pt(II) in cis/trans-Pt(NH<sub>3</sub>)<sub>2</sub>X<sub>2</sub> (X = OH, F, Cl, Br). Li and co-workers [15] carried out an MP2 investigation to study the formation of XB involving gold. Zhao studied the interaction between F<sub>3</sub>CX (X = I, Br, Cl) and small gold clusters (Au<sub>n</sub>, n = 2, 3, 4) and found that X can act as an electron donor, forming a stronger interaction, or as an electron acceptor forming weak XBs [16]. Young and co-workers [17] reported the formation of F<sub>2</sub>···Hg when Hg is trapped in argon matrices doped with F<sub>2</sub> and suggested that the analogous interaction of heavier halogens could be important for understanding the environmental chemistry of Hg. Blakey and co-workers used different spectroscopic techniques (Synchrotron X-ray photoelectron

\* Corresponding author.

E-mail addresses: [voliveira@smu.edu](mailto:voliveira@smu.edu) (V. Oliveira), [dcremer@smu.edu](mailto:dcremer@smu.edu) (D. Cremer).

spectroscopy, UV–vis, surface enhanced Raman spectroscopy) and found evidence for the formation of XB involving iodoperfluorobenzenes and gold nanoparticles [18].

In the current work, the interactions between X–Y (dihalogens, interhalogens, and haloalkanes) with X being Cl, Br, or I) and neutral or anionic metal complexes  $MR_n$  (M: Cu, Ag, Au, Pt, Hg) are quantum chemically investigated using an all-electron Dirac-exact scalar relativistic (spin free) method in combination with a rung 3 exchange–correlation functional. The strength of the metal–halogen bonding (XB–M) interactions will be quantified with the corresponding local stretching force constant [19–23]. The objectives of this work are to answer the following questions. (i) How strong are the interactions between Cu, Ag, Au ions and  $I_2$  or  $CF_3I$ ? (ii) What role do scalar relativistic effects play in this connection? (iii) How strong are covalent and/or electrostatic interactions between the metal complex and the X–donor? (iv) Can one tune the bonding mechanism between metal and iodine by varying the metal atom, possible ligands, or the halogen donor?

The computational methods used to answer these questions are described in the following section. Results and discussions are found in the third section of this work whereas the conclusions are given in the final section.

## 2. Computational methods

Molecular geometries and complex binding energies were computed utilizing the all-electron Dirac-exact Normalized Elimination of the Small Component (NESC) method [24] as developed and implemented by Zou, Filatov, and Cremer [25], which provides a more reliable account of energies, geometries, vibrational frequencies [26], and other response properties than the effective core potentials normally used [25–27]. NESC was used in connection with the rung 3 (meta-GGA) exchange correlation functional TPSS [28] that provides reliable data for transition metal complexes as has been documented in the literature [29,30]. TPSS was combined with the empirical dispersion correction D3 [31] and the Becke–Johnson damping parameters (BJ) [32] to accurately model dispersion interactions. Calculated binding energies were corrected for basis set superposition errors (BSSE) employing the counterpoise correction [33].

As suitable relativistic basis sets, the segmented contracted Sapporo triple zeta basis sets Sapporo-DKH3-TZP-2012 [34] for Cu, Ag, Au, Hg, and I were chosen, whereas for all other atoms (Cl, C, H, F and N) the non-relativistic Sapporo-TZP-2012 basis sets [35,36] were used. Since 24 of the 29 complexes studied are anionic and highly polarizable, s-, p-, d-, f-, etc. sets of basis functions were augmented by one set of diffuse functions to better describe the electron density far from the nuclei. All DFT calculations were performed with tight convergence criteria (changes in the density matrix elements in the converged SCF (self-consistent field):  $<10^{-10}$ ; changes in the forces of the optimized geometry:  $<10^{-7}$  hartree/bohr) and an ultrafine grid [37].

For all molecules investigated, analytical vibrational frequencies in the harmonic approximation were calculated to (i) characterize each stationary point as minimum (or saddle point) and (ii) determine local vibrational modes and their properties according to the method developed by Konkoli and Cremer [19,38,20]. The Konkoli–Cremer modes are the local equivalent of the normal vibrational modes and their frequencies can be experimentally determined in special cases [38]. The local stretching force constants can be used to determine the intrinsic strength of a bond [22]. Furthermore, the description of the intrinsic bond strength via local stretching force constants can be simplified by using the latter to determine a bond strength order (BSO) [39].

According to the generalized Badger rule [40,39], BSO values  $n(XB)$  of the XB are related to the calculated  $k^a(XB)$  values via a power relationship [40,22]

$$n = a(k^a)^b \quad (1)$$

where constants  $a = 0.696$  and  $b = 0.660$  define for the I–I bond in  $I_2$  a BSO value  $n = 1.00$  and for the corresponding 3c–4e bond in  $[I \cdots I \cdots I]^-$   $n = 0.50$ . According to the Rundle–Pimentel model of bonding, the  $[I \cdots I \cdots I]^-$  anion has 2e in a bonding and 2e in a non-bonding orbital, which suggests a non-classical (NC) BSO (I–I) value being half of that of the di-iodine bond. Eq. (1) also implies that for  $k^a = 0$ , an  $n$  value of zero results.

Since NC 3c–4e bonding can play an important role in XB [2], its magnitude was assessed in percentage using the ratio  $n(X \cdots A/n(XY)) \times 100$ . If the ratio of bond strengths leads to unity, 3c–4e bonding is fulfilled by 100% as in the  $[I \cdots I \cdots I]^-$  anion. Values below 75% indicate that 3c–4e bonding plays a minor role. Values above 100% indicate the formation of inverted 3c–4e bonding (i-NC): The XA interactions are stronger than the XY interactions. Values above 100% are listed in the tables to quickly identify inverted 3c–4e bonding, but can be compared with other values via their reciprocal ( $n(Y \cdots X/n(XA)) \times 100$ ).

Local properties of the electron density distribution,  $\rho(\mathbf{r})$ , and energy density distribution,  $H(\mathbf{r})$ , were also computed at the NESC/TPSSD3 level of theory and used to determine the covalent character of the XY and XA interactions with the help of the Cremer–Kraka criteria for covalent bonding [41,42]. According to these criteria a negative and therefore stabilizing energy density at the bond critical point  $\mathbf{r}_b$  ( $H(\mathbf{r}_b) = H_b < 0$ ) indicates a dominating covalent character, whereas a positive (destabilizing) energy density ( $H_b > 0$ ) is associated with predominant electrostatic interactions.

Using the natural bond orbital (NBO) method of Weinhold and co-workers [43], NBO atomic charges were calculated and used to assess the charge transfer between the monomers of an XB–M complex.

The electrostatic character of the interactions was investigated by using the extremal value  $V_{ext}$  of the electrostatic potential  $V(\mathbf{r})$  on the van der Waals surface (modeled by the  $0.001 \text{ e/Bohr}^3$  electron density surface) of the halogen donor monomers (i.e.  $V_{ext}$  is a maximum). The halogen acceptor ability of a monomer  $AR_n$  was assessed by determining the minimum value  $V_{ext}$  in the lp(A) region.  $V(\mathbf{r})$  (measured in eV) is positive in the case of a  $\sigma$ -hole of a halogen and negative in the lp-region of a hetero atom.

The calculation of the NESC energies, geometries and frequencies as well as the local mode properties was performed with the program COLOGNE2016 [44]. For the NBO analysis, the program NBO6 [45] was used. The local properties of the electron density distribution,  $\rho(\mathbf{r})$ , and energy density distribution,  $H(\mathbf{r})$  at the bond critical point (see Supporting Information (SI)) and the electrostatic potential at the van der Waals surface ( $0.001 \text{ e/bohr}^3$ ; e: electron) were analyzed with the Multiwfn program [46]. DFT calculations were performed with the package Gaussian09 [47].

## 3. Results and discussion

Fig. 1 summarizes for complexes (1–29) selected bond distances and bond angles. NESC/TPSS–D3 binding energies  $\Delta E$  and charge transfer (CT) values are listed in Table 1 for 1–29 where also the XA and XY interaction distances  $r$ , local stretching force constants  $k^a$ , local stretching frequencies  $\omega^a$ , and BSO values  $n$  are compared. Also given is the percentage of 3c–4e character that is used to distinguish between NC and XB–M bonding (see Fig. 2). In Table 2, X-donor properties such as  $r$ ,  $k^a$ ,  $n$ , and  $\omega^a$  for the XY bond are listed for 30–42. Also given is the extremal value  $V_{ext}$  in the van der Waals

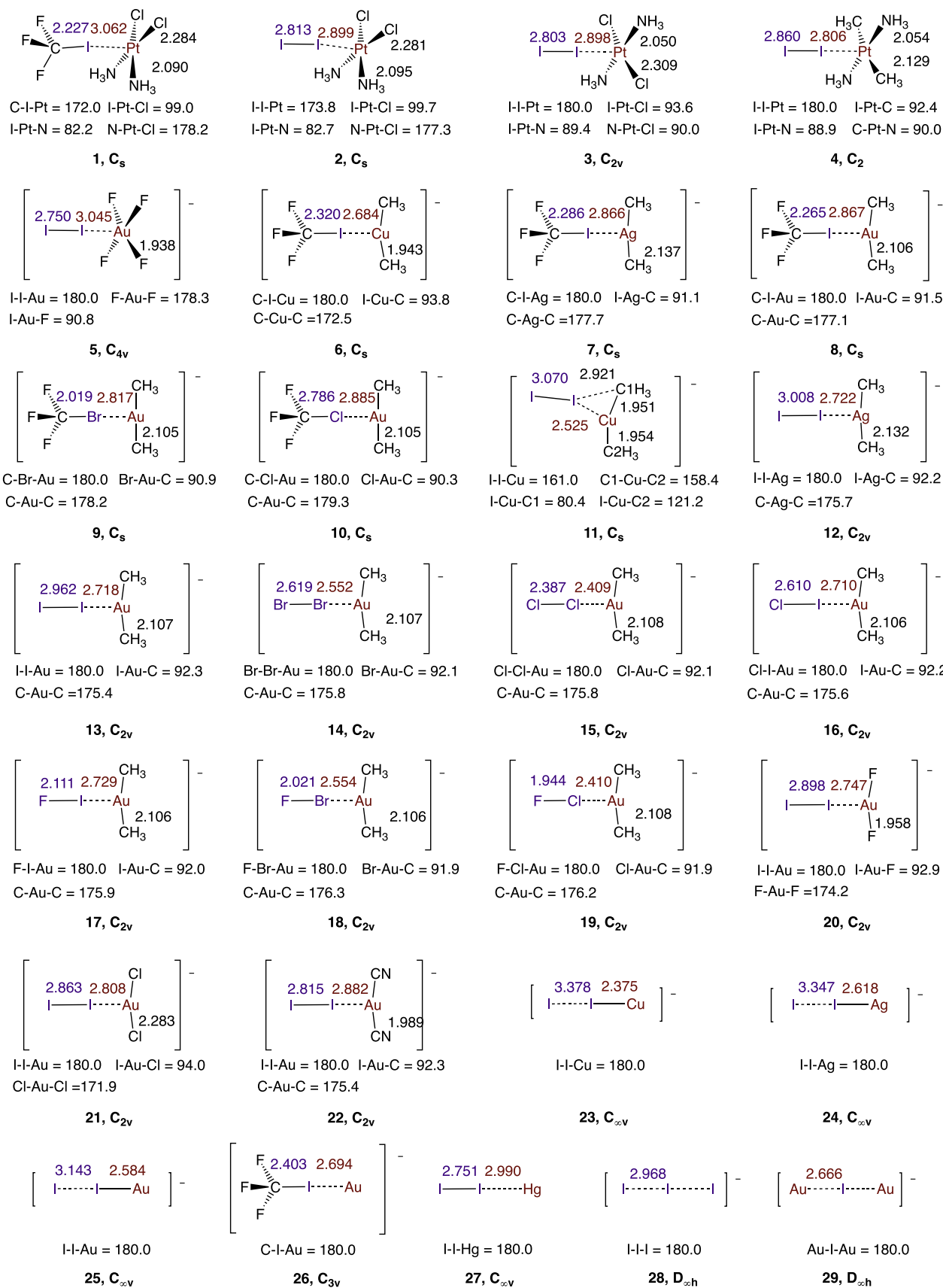


**Fig. 1.** Schematic presentation of the geometries of complexes 1–29. Selected XM distances are shown in red and XY distances in blue. Distances in Å and angles in degrees. NESC/TPSS calculations.

**Table 1**  
Summary of energy, geometry, and vibrational data of all complexes investigated.<sup>a</sup>

#	Complex (Symmetry)	$\Delta E$	CT	$r$ (XA)	$r$ (XY)	$k^a$ (XA)	$k^a$ (XY)	$\omega^a$ (XA)	$\omega^a$ (XY)	$n$ (XA)	$n$ (XY)	3c-4e %	Type
1	F <sub>3</sub> Cl...Pt(NH <sub>3</sub> ) <sub>2</sub> Cl <sub>2</sub> cis(C <sub>s</sub> )	12.0	0.152	3.062	2.227	0.134	1.289	54	447	0.185	0.823	22	XB-M
2	I <sub>2</sub> ...Pt(NH <sub>3</sub> ) <sub>2</sub> Cl <sub>2</sub> cis(C <sub>s</sub> )	17.9	0.288	2.899	2.813	0.496	1.016	105	165	0.438	0.703	62	XB-M
3	I <sub>2</sub> ...Pt(NH <sub>3</sub> ) <sub>2</sub> Cl <sub>2</sub> trans(C <sub>2v</sub> )	14.5	0.276	2.898	2.803	0.501	1.042	105	167	0.441	0.715	62	XB-M
4	I <sub>2</sub> ...Pt(NH <sub>3</sub> ) <sub>2</sub> (CH <sub>3</sub> ) <sub>2</sub> trans	27.7	0.357	2.806	2.860	0.699	0.906	124	156	0.549	0.652	84	NC
5	I <sub>2</sub> ...AuF <sub>4</sub> <sup>-</sup> (C <sub>4v</sub> )	9.9	0.175	3.045	2.750	0.255	1.207	75	180	0.282	0.788	36	XB-M
6	F <sub>3</sub> Cl...Cu(CH <sub>3</sub> ) <sub>2</sub> <sup>-</sup> (C <sub>s</sub> )	27.5	0.380	2.684	2.320	0.467	0.883	137	370	0.421	0.641	66	XB-M
7	F <sub>3</sub> Cl...Ag(CH <sub>3</sub> ) <sub>2</sub> <sup>-</sup> (C <sub>s</sub> )	23.2	0.328	2.866	2.286	0.432	0.992	112	392	0.400	0.692	58	XB-M
8	F <sub>3</sub> Cl...Au(CH <sub>3</sub> ) <sub>2</sub> <sup>-</sup> (C <sub>s</sub> )	23.9	0.297	2.867	2.265	0.472	1.116	102	416	0.424	0.748	57	XB-M
9	F <sub>3</sub> Br...Au(CH <sub>3</sub> ) <sub>2</sub> <sup>-</sup> (C <sub>s</sub> )	15.3	0.233	2.817	2.019	0.355	1.281	103	457	0.351	0.819	43	XB-M
10	F <sub>3</sub> Cl...Au(CH <sub>3</sub> ) <sub>2</sub> <sup>-</sup> (C <sub>s</sub> )	9.4	0.135	2.885	1.786	0.181	1.921	102	604	0.225	1.071	21	XB-M
11	I <sub>2</sub> ...Cu(CH <sub>3</sub> ) <sub>2</sub> <sup>-</sup> (C <sub>s</sub> )	46.8	0.659	2.525	3.070	0.715	0.421	170	106	0.558	0.393	142	i-XB-M
12	I <sub>2</sub> ...Ag(CH <sub>3</sub> ) <sub>2</sub> <sup>-</sup> (C <sub>2v</sub> )	40.3	0.613	2.722	3.008	0.733	0.533	146	119	0.567	0.459	124	i-NC
13	I <sub>2</sub> ...Au(CH <sub>3</sub> ) <sub>2</sub> <sup>-</sup> (C <sub>2v</sub> )	38.8	0.522	2.718	2.962	0.842	0.631	136	130	0.621	0.514	121	i-NC
14	Br <sub>2</sub> ...Au(CH <sub>3</sub> ) <sub>2</sub> <sup>-</sup>	38.3	0.585	2.552	2.619	0.908	0.690	165	172	0.653	0.545	120	i-NC
15	Cl <sub>2</sub> ...Au(CH <sub>3</sub> ) <sub>2</sub> <sup>-</sup> (C <sub>2v</sub> )	34.4	0.636	2.409	2.387	0.998	0.645	239	250	0.695	0.521	133	i-XB-M
16	ClI...Au(CH <sub>3</sub> ) <sub>2</sub> <sup>-</sup> (C <sub>2v</sub> )	41.9	0.507	2.710	2.610	0.885	0.816	139	225	0.642	0.608	106	i-NC
17	FI...Au(CH <sub>3</sub> ) <sub>2</sub> <sup>-</sup>	43.1	0.449	2.729	2.111	0.857	1.438	137	384	0.629	0.884	71	NC
18	FBr...Au(CH <sub>3</sub> ) <sub>2</sub> <sup>-</sup>	42.5	0.522	2.554	2.021	0.947	1.280	169	377	0.671	0.819	82	NC
19	FCl...Au(CH <sub>3</sub> ) <sub>2</sub> <sup>-</sup>	39.7	0.582	2.410	1.944	1.034	1.074	243	385	0.711	0.729	98	NC
20	I <sub>2</sub> ...AuF <sub>2</sub> <sup>-</sup> (C <sub>2v</sub> )	29.9	0.452	2.747	2.898	0.694	0.769	124	143	0.547	0.585	94	NC
21	I <sub>2</sub> ...AuCl <sub>2</sub> <sup>-</sup> (C <sub>2v</sub> )	23.7	0.383	2.808	2.863	0.552	0.825	110	149	0.470	0.613	77	NC
22	I <sub>2</sub> ...Au(CN) <sub>2</sub> <sup>-</sup>	17.3	0.282	2.882	2.815	0.454	0.970	100	161	0.413	0.682	61	XB-M
23	CuI...I <sup>-</sup> (C <sub>∞v</sub> )	9.5 (79.3) <sup>b</sup>	0.315	3.378	2.375	0.219	1.367	77	235	0.255	0.855	30	XB
24	AgI...I <sup>-</sup> (C <sub>∞v</sub> )	9.2 (69.7) <sup>b</sup>	0.341	3.347	2.618	0.228	0.972	78	169	0.262	0.683	38	XB
25	AuI...I <sup>-</sup> (C <sub>∞v</sub> )	23.1 (61.2) <sup>b</sup>	0.437	3.143	2.584	0.393	1.203	163	163	0.376	0.786	48	XB
26	F <sub>3</sub> Cl...Au <sup>-</sup> (C <sub>3v</sub> )	35.8	0.297	2.694	2.403	0.703	0.605	124	306	0.551	0.499	110	i-NC
27	I <sub>2</sub> ...Hg(C <sub>∞v</sub> )	6.4	0.207	2.990	2.751	0.248	1.168	73	177	0.277	0.771	36	XB-M
28	AuI...Au <sup>-</sup> (D <sub>∞h</sub> )	40.9	0.713	2.666	2.666	0.819	0.819	134	134	0.610	0.610	100	NC
29	I <sub>2</sub> ...I <sup>-</sup> (D <sub>∞h</sub> )	37.9	0.559	2.968	2.968	0.606	0.606	127	127	0.500	0.500	100	NC

<sup>a</sup> Computed at NESC/TPSS-D3(BJ)/sapporo-DKH3-TZP-2012 for I, Au, Ag, Cu and TZP-2012 for C, F and H. All atom basis sets are augmented by one set of diffuse functions per angular momentum. Binding energy  $\Delta E$  in kcal/mol, halogen-acceptor  $r(XA)$  and halogen-donor  $r(XY)$  distances in Å, local XA and XY stretching force constant in mdyn/Å, local stretching frequency  $\omega^a$  in cm<sup>-1</sup>, bond strength order  $n$ , and Y-X-A 3c-4e bond % character given by  $n(XA)/n(XY) \times 100$ . XB-M: halogen bonding involving metal M; NC: nonclassical 3c-4e bonding; i-XB-M: inverse XB-M, i.e.  $Y^- \cdots X - MR_2$ ; i-NC: inverse NC, i.e.  $BSO(X \cdots M) > BSO(X \cdots Y)$

<sup>b</sup> Numbers in parentheses refer to the  $M \cdots I$  bond dissociation energy.

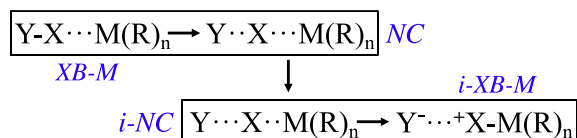


**Fig. 2.** Schematic presentation of the conversion of an XB-M interaction into a 3c-4e-bonding situation where either the XY interaction (NC: non-classical bonding) or the XM interaction (i-NC: inverted non-classical bonding) being somewhat stronger. The latter can convert into a covalent XM bond and interact with a negatively charged Y via i-XB-M (inverted XB-M).

surface of X. For X-acceptors **43–57**, just  $V_{ext}$  is given in Table 2. In Fig. 3, the BSO values of the various XB-M are compared. XB-M interactions can adopt BSO values from 0.2 to 0.8 where the lower values (<0.5) indicate weak and normal XB-M whereas values of 0.5 and larger give the transition from NC to i-NC and i-XB-M bonding. All XB-M turn out to have more or less covalent character ( $H_b < 0$ ; see SI).

In the following, we will discuss the interactions of X-donors with (i) planar transition metal complexes (TMC) leading to pyramidal interaction complexes, (ii) linear TMC leading to T-structures, and (iii) TM leading to linear structures.

**Halogen bonding involving square planar TMC.** TMC **1** is stabilized by a XB-M between F<sub>3</sub>Cl and cis-Pt(NH<sub>3</sub>)<sub>2</sub>Cl<sub>2</sub>. The binding energy  $\Delta E$  is only 12 kcal/mol and the BSO value 0.185. F<sub>3</sub>Cl is a too weak X-donor to establish a stronger XB-M. This is also reflected by comparing the  $\sigma$ -holes of the X-donors, which increase in the series F<sub>3</sub>C-Cl ( $V_{ext}$ : 0.86 eV) < F<sub>3</sub>C-Br (1.05) < Cl-Cl (1.11) < F<sub>3</sub>C-I (1.27) < Br-Br (1.28) < I-I (1.31) < Cl-I (1.83; Table 2).

A relatively strong XB-M is obtained by using I-I where  $n$  is 0.438 for cis-platin while a slightly larger value of 0.441 results for trans-platin. An identical amount of 3c-4e character is calculated for **2** and **3** (62%), i.e. the charge transferred from a d<sub>z<sup>2</sup></sub>(Pt) lone pair into the  $\sigma^*(I-I)$  orbital weakens (lengthens) the I-I bond and strengthens (shortens) the Pt...I interaction. The  $\Delta E$  value (cis: 17.9; trans: 14.5 kcal/mol) is influenced by both the XB-M and the mutual polarizability of the monomers, which is larger for cis-platin and can be enhanced by a slight tilting of the plane of cis-platin relative to the I-I bond axis (Fig. 1). In this way the positively charged H atoms of the NH<sub>3</sub> ligands can better interact with the  $\pi$ -density of the negatively charged I atom next to Pt.

The strength of the XB-M interactions can be increased by replacing the Cl ligands by electron donor ligands such as methyl (**4**):  $\Delta E$  raises to 27.7 kcal/mol. This is parallel to an increase of the calculated CT to 0.357 e (Table 1; TMC **1**: 0.152; **3**: 0.276; **2**: 0.288 e). The larger CT causes a stronger Pt...I interaction (BSO: 0.549) and a weakening of the I-I bond (0.652) so that a delocalized 3c-4e system with 84% 3c-4e character and NC bonding results. Electron-withdrawing ligands in the TMC have the opposite effect as is documented by the low  $\Delta E$  of I<sub>2</sub>...AuF<sub>4</sub><sup>-</sup> (**5**) (9.9 kcal/mol; CT: 0.175 e, BSO: 0.282).

**Halogen bonding leading to T-structures.** The anionic dimethylcuprate, dimethylargentate, and dimethylaurate (M: Cu, Ag, Au) are stronger electron donors and therefore their complexes with F<sub>3</sub>C-I, **6**, **7**, and **8**, have BSO values of 0.421, 0.400, and 0.424, respectively (Table 1). It is remarkable that a similar trend is obtained for the electrostatic potential  $V_{ext}$  in the d-electron region of monomers MMe<sub>2</sub><sup>-</sup> (Cu: -4.83, Ag: -4.65, Au: -4.88 eV, Fig. 4), which suggests that there is first a decrease in the polarization of

**Table 2**  
Geometry, vibrational data, and values of the electrostatic potential for halogen donors and acceptors.<sup>a</sup>

#	X-Donor	r	k <sup>a</sup>	n	ω <sup>a</sup>	V <sub>ext</sub> (X)	#	X-Acceptors	V <sub>ext</sub> (A)
30	I-I	2.679	1.732	1.000	215	1.31	43	Cu(CH <sub>3</sub> ) <sub>2</sub> <sup>-</sup>	-4.83
31	Br-Br	2.305	2.298	1.205	314	1.28	44	Ag(CH <sub>3</sub> ) <sub>2</sub> <sup>-</sup>	-4.65
32	Cl-Cl	2.009	2.981	1.431	538	1.11	45	Au(CH <sub>3</sub> ) <sub>2</sub> <sup>-</sup>	-4.88
33	Cl-I	2.336	2.310	1.209	378	1.83	46	AuF <sub>2</sub> <sup>-</sup>	-4.63
34	F-I	1.931	3.492	1.589	599	2.32	47	AuCl <sub>2</sub> <sup>-</sup>	-4.21
35	F-Br	1.786	3.754	1.666	645	2.14	48	AuF <sub>4</sub> <sup>-</sup>	-3.76
36	F-Cl	1.655	4.135	1.776	755	1.73	49	Au(CN) <sub>2</sub> <sup>-</sup>	-3.71
37	F <sub>3</sub> C-I	2.168	1.828	1.036	532	1.27	50	Hg	0.16
38	F <sub>3</sub> C-Br	1.949	2.190	1.167	597	1.05	51	I <sup>-</sup>	-5.28
39	F <sub>3</sub> C-Cl	1.773	2.665	1.329	712	0.86	52	Cu <sup>-</sup>	-5.06
40	Cu-I	2.326	1.791	1.022	269	-0.04	53	Ag <sup>-</sup>	-4.91
41	Ag-I	2.560	1.354	0.850	199	-0.25	54	Au <sup>-</sup>	-5.35
42	Au-I	2.488	1.966	1.087	208	0.53	55	Pt(NH <sub>3</sub> ) <sub>2</sub> Cl <sub>2</sub> <i>cis</i>	-0.65
							56	Pt(NH <sub>3</sub> ) <sub>2</sub> Cl <sub>2</sub> <i>trans</i>	-0.51
							57	Pt(NH <sub>3</sub> ) <sub>2</sub> (CH <sub>3</sub> ) <sub>2</sub> <i>trans</i>	-0.92

<sup>a</sup> Halogen-donor r(XY) distances in Å, XY stretching force constant in mdyn/Å, local stretching frequency ω<sup>a</sup> in cm<sup>-1</sup>. Since the I-I bond is chosen as a reference (n = 1.00), the BSO values n of other dihalogens are significantly stronger whereas M-I bonds are comparable in strength or weaker. Electrostatic potential at the σ-hole region of the X-donors V<sub>ext</sub>(X) and at the lp region of X-acceptors V<sub>ext</sub>(A) in eV. Computed at the 0.001 e/Bohr<sup>3</sup> electron density surface using NESC/TPSS-D3(BJ)/sapporo-DKH3-TZP-2012 method.

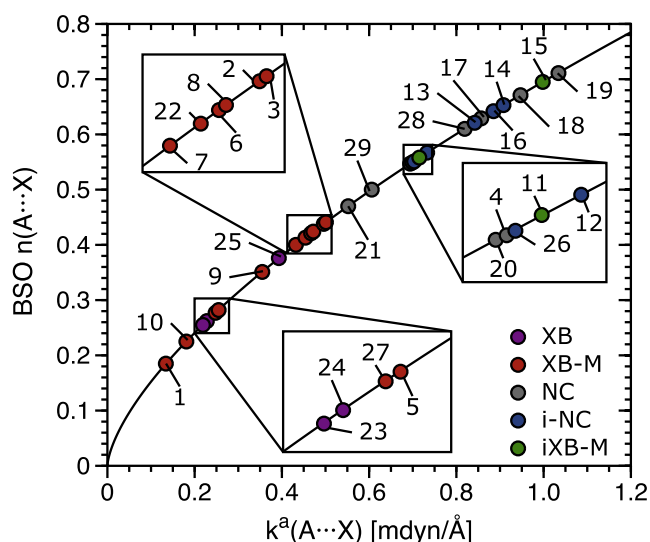


**Fig. 3.** Bond strength orders (BSO) *n* of the halogen bond XB-M given as a function of the local XB stretching force constant. For numbering of complexes, see Fig. 1. Green dots: XB-M; blue dots: NC and i-NC; red dots: i-XB bonding mechanisms. NESC/TPSS calculations. (For interpretation of the references to color in this figure legend, the reader is referred to the web version of this article.)

the electron density when moving from XB-M complex **6** to **7** and then an increase again for **8**. The decrease in the polarization results from the higher electronegativity of Ag compared to Cu (Pauling scale: χ(M) = 1.90 (Cu); 1.93 (Ag); 2.54 (Au) [48]), which is confirmed by the trend in the positive metal NBO charges of the anions (0.413, 0.336, 0.213 e). The increase of the BSO value for **8** is a result of scalar relativistic effects, which lead to a contraction of the 6s orbital, but to an expansion of the 5d-orbitals where the latter are important for XB-M (see SI). The 5d-expansion facilitates the polarization of the dimethylaurate anion density as caused by F<sub>3</sub>C-I thus leading to a BSO value of 0.424. The ΔE values decrease from 27.5 to 23.2 and 23.9 kcal/mol where the stability of **6** is a result of charge transfer/polarization (CT: 0.380, 0.328, 0.297 e; reduction in the length of the C-I bond: 2.320, 2.286, 2.265 relative to 2.168 Å), and the electrostatic attraction of positively charged methyl H atoms and the π(I) density (distance H...I: 3.471, 3.620, 3.611 Å; charge of closest H: 0.179, 0.174, 0.175 e). The polarizing power of F<sub>3</sub>C-Br or F<sub>3</sub>C-Cl is no longer sufficient

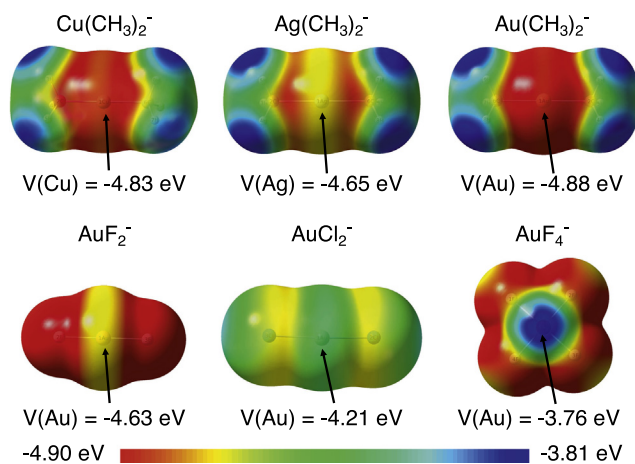


**Fig. 4.** Perspective drawings of the electrostatic potential *V* of some anionic halogen acceptors in eV, computed for the 0.001 e/Bohr<sup>3</sup> electron density surface. NESC/TPSS calculations.

(σ(Br))-hole in F<sub>3</sub>C-Br: V<sub>ext</sub> = 1.05; F<sub>3</sub>C-Cl: 0.86; F<sub>3</sub>C-I: 1.27 eV; Table 2) to form a strong complex: **9**: ΔE: 15.3 kcal/mol, BSO: 0.351; 9.4, 0.225; Table 1). In the series **8**, **9**, **10**, ΔE, CT, V<sub>ext</sub>, and BSO change in an adequate way indicating that XB-M dominates the complex stability.

The complexes so far discussed follow simple trends: The CT determines the strength of the XB-M (BSO value) and by this the ΔE value. This changes for the complexes formed between a di- or interhalogen and a dimethylmetal anionic X-acceptor M(CH<sub>3</sub>)<sub>2</sub><sup>-</sup> (M = Cu, Ag, Au). In the series **11**, **12**, **13**, the M...I<sub>2</sub> interactions increase from Cu to Au (BSO: 0.558, 0.567, 0.621; Table 1), which surprisingly is parallel to an increase in the strength of the I-I bond (n: 0.393, 0.459, 0.514) caused by a reduced charge transfer (0.659, 0.613, 0.522 e, see Table 1). The strength of XB-M changes opposite to the change in ΔE: 46.8, 40.3, 38.8 kcal/mol (Table 1), which indicates that other factors than XB-M dominate the complex stability. The reason for this becomes obvious when investigating the T-structure of the Cu complex **11**: This is unstable because of a pseudo-Jahn-Teller effect. The first excited state, <sup>1</sup>A' can interact with the <sup>1</sup>A<sub>1</sub> ground state via a a'-symmetrical vibration, which leads to distortion of the C<sub>2v</sub>-symmetrical structure (Fig. 1) and converts XB-M into a interaction of I with both Cu and one of the

methyl groups. For **12** and **13**, the symmetrical T-structure remains. The favorable electrostatic potentials for M and X (Ag:  $-4.65$ ; Au:  $-4.88$ ; I:  $1.31$  eV, Table 2) seem to strengthen XB-M whereas CT and the electrostatic interactions with the methyl groups dominate the overall stability. In this connection the 3c4e interactions (Cu: 142; Ag: 124; Au: 121%) also favor the interaction between I and Au or Ag.

In general, the electrostatic potential has to be used with care [49] when explaining different trends between  $\Delta E$  and BSO. Depending on the TMC geometry, it helps to understand the complex binding energy, but often  $V_{ext}$  fails to be useful for the analysis of the BSO values. This is quite obvious for the series of dihalogens  $I_2$ ,  $Br_2$ ,  $Cl_2$  or interhalogens FCl, FBr, FI interacting with dimethylaurate (**13–15** and **17–19**, respectively).  $\Delta E$  values decrease in line with  $V_{ext}$  of X whereas BSO and CT values increase (Table 1). Again, these are cases for which the intrinsic XB-M strength does not dominate the binding energy. The latter is strongly influenced by the strength of the XY bond, which, due to CT, weakens (e.g., for FCl, FBr, FI by 59, 51, 44% according to calculated BSO values; Table 1) and thereby reduces  $\Delta E$ . The CT is directly related to the electronegativity  $\chi$  of X: The larger  $\chi(X)$  is the lower is the  $\sigma^*(XY)$  orbital and the stronger the CT.

In the series **13–15** and **17–19**, the XB-M is dominated by the electrostatic attraction between atoms Au and X (see SI), which is largest for the more electronegative Cl. The potential  $V_{ext}$  reflects the overall electrostatic interactions and therefore can only be related in a qualitative way to the TMC stability rather than the intrinsic strength of XB-M. Only if the latter is BSO-dominated,  $V_{ext}$  might be used to rationalize trends in the BSO. Hence, by comparing changes in  $\Delta E$  and BSO values, different electronic effects determining the stability of the TMC can be distinguished (see SI).

If CT is the major reason for the XB-M strength, it gives insight into the covalent part of XB-M bonding, but there are also electrostatic, exchange repulsion, and dispersion interactions between X and M (see SI). None of the currently available methods including SAPT (Symmetry-Adapted Perturbation Theory [50]) can single out any of these interactions between the two atoms X and M, which is the reason why here only indirect information on these effects can be provided.

**Forming a metal lone pair orbital of high density.** In linear  $[MY_2]^-$  with Y being a halogen or another ligand with  $\pi$ -electrons, bonding and antibonding  $p\pi(Y) - d\pi(M) - p\pi(Y)$ -orbitals are doubly occupied. For the bonding orbital, the Y-coefficient is large if the electronegativity of Y is large. Then, the orthogonal antibonding orbital has a large M-coefficient, i.e. antibonding  $p\pi(Y) - d\pi(M) - p\pi(Y)$ -orbital gets some lone-pair character (see orbital pictures in SI). This effect is enhanced for a relativistic M because of the well-known scalar relativistic expansion of the d-orbitals (see SI).  $V_{ext}$  values of  $AuF_2^-$  ( $-4.63$ ),  $AuCl_2^-$  ( $-4.21$ ), and  $Au(CN)_2^-$  ( $-3.71$ ; Table 2) confirm this effect. Hence,  $AuF_2^-$  is better suited than  $AuCl_2^-$  or  $Au(CN)_2^-$  to bind  $I_2$ , which is in line with the  $\Delta E$  (29.9, 23.7, 17.3 kcal/mol), CT (0.452, 0.383, 0.282 e), BSO (0.547, 0.470, 0.413) and 3c-4e values (94, 77, 61%). In these cases, the binding energy is dominated by the  $M \cdots X$ -interaction and makes it possible to fine-tune XB-M via the M,X-electronegativity difference in an easy to predict way.

**Metal-halogen bonding leading to linear TMC.** Despite the fact that the Hg atom has a  $6s^2$ -electron configuration and a relatively small positive electrostatic potential ( $V_{ext}(Hg)$ : 0.16 eV), it can still be polarized by  $I_2$  ( $\Delta E = 6.4$  kcal/mol) resulting in a weak XB-M ( $n = 0.277$ ) for **27**. For  $Br_2$  and  $Cl_2$ , smaller  $\Delta E$  are obtained whereas FI leads to a  $\Delta E$  of 10.8 kcal/mol. Attempts to find stable  $HgF_2 \cdots X_2$  or XY complexes led to unstable structures. Bare metal anions such as  $Cu^-$ ,  $Ag^-$  and  $Au^-$  have a strongly negative electrostatic potential due to the extra electron ( $V_{ext}(Cu^-)$ :  $-5.06$  eV;

$V_{ext}(Ag^-)$ :  $-4.91$ ;  $V_{ext}(Au^-)$ :  $-5.35$  eV). There is a strong charge transfer from the metal to the  $\sigma^*(XY)$ -orbital so that a covalent M-I bond is formed, and the I-I bond dissolves: An  $MI \cdots I^-$  complex results, which is characterized as i-XB-M bonding.

To confirm that no local minimum structure with a normal XB-M bond exists, a relaxed scan for the  $I_2 \cdots Au^-$  distance was carried out in the range 2.584 to 4.784 Å using increments of 0.2 Å. A single-well potential was found, which confirmed that an XB-M structure of the type  $I-I \cdots Au$  does not exist. The strongest  $MI \cdots I^-$  interactions are found for M = Au (BSO: 0.376,  $\Delta E$ : 23.1 kcal/mol; Table 1, Cu: BSO: 0.255,  $\Delta E$ : 9.5; Ag: BSO: 0.262,  $\Delta E$ : 9.2). The stronger XB in  $AuI \cdots I^-$  is due to the larger electrophilic character of Au, (NBO values for Au, Cu, Ag:  $-0.166$ ,  $0.139$ ,  $0.126$  e) resulting in the formation of a positive electrostatic potential at the  $\sigma$ -hole of I ( $V_{ext}(I) = 0.53$  eV) whereas negative  $V_{ext}$  values at I are obtained for CuI and AgI ( $V_{ext}(I)$ :  $-0.04$  and  $-0.25$  eV; Table 2).

Replacing the terminal iodine atoms by Au leads to TMC **28**, which because of the relativistic  $d$ -expansion, has stronger 3c-4e bonds than  $I_3^-$  ( $n = 0.610$  for **28**) and a larger  $\Delta E$  (40.9 kcal/mol compared to 37.9 kcal/mol for **29**, Table 1).

#### 4. Conclusions

In this work, we have for the first time determined the intrinsic XB-M strength by singling it out from the manifold of monomer-monomer interactions with the help of local XB-M stretching force constants and associated BSO values where we used Dirac-exact NESC calculations to reliably determine scalar relativistic effects for second order response properties. We note that this approach is based on features of the potential energy surface and its results can be directly verified with the help of vibrational spectroscopy. Hence, it can obtain atom-atom interactions, which are not accessible by SAPT or any other energy decomposition methods. Using this advantage and those of NESC the following results were obtained:

- (1) XB-M bonding has chameleon-character as small electronic effects lead to a change in its nature, which varies from M, X-interactions typical of a heteroatom to non-classical 3c-4e bonding and, finally, the formation of an M-X ligand bond. The approach used in this work for the first time quantitatively reveals these changes via the BSO values, which are based on measurable quantities.
- (2) XB-M can be found for planar and linear TMC of Au and Pt. For negatively charged atoms, a strong interaction with dihalogens results.
- (3) XB-M involving derivatives of halotrifluoromethanes is weak or modestly strong. The BSO values are in line with the  $\Delta E$  values (XB-M-dominated TMCs) and can be related to CT and  $V_{ext}$  values.
- (4) In general,  $V_{ext}$  does not correlate with the BSO of XB-M. There is only a qualitative relationship with the binding energy. Similarly, the CT relates with  $\Delta E$ , but not always with the BSO values of XB-M.
- (5) Gold is a candidate for strong XB-M interactions due to its d-lone pair orbitals, which are easily accessible because of their scalar relativistic expansion and the negative charge of an aurate. If the latter has two strongly electronegative ligands with  $\pi$ -electron lone pairs (e.g., F), the availability of the Au lone pair is increased and XB-M strengthened as shown in this work.
- (6) Interactions of aurates with XX or XY (X,Y: halogen) are no longer XB-M-dominated as the mutual polarization of the monomers determines the relatively high TMC stability whereas XB-M is best described as 3c4e-nonclassical

bonding that can vary strongly: the strongest XB-M bond is found for FCl rather than FI. Similarly, Cl<sub>2</sub> establishes a stronger XB-M than I<sub>2</sub> where the reason is the larger electronegativity of Cl that makes it possible that covalent contributions are supported by electrostatic attraction between Au and Cl.

Future work will focus on the “lone pair activation effect” in planar TMCs by using beside methyl also F ligands where the relativistic metals Pt and Au are first candidates. The planar TMCs are interesting as by front- and backside XB-M interactions long strands of TMCs with X-donors as di-iodo-acetylene or 1,4-diiodobenzene can be formed.

## Acknowledgement

This work was financially supported by the National Science Foundation, Grant CHE 1464906. We thank SMU for providing computational resources. VO acknowledges financial support by CAPES (Brazil; fellowship grant BEX 9534-13-0).

## Appendix A. Supplementary material

Supplementary data associated with this article can be found, in the online version, at <http://dx.doi.org/10.1016/j.cplett.2017.05.045>.

## References

- G. Cavallo, P. Metrangolo, R. Milani, T. Pilati, A. Priimagi, G. Resnati, G. Terraneo, The halogen bond, *Chem. Rev.* 116 (4) (2016) 2478–2601.
- V. Oliveira, E. Kraka, D. Cremer, The intrinsic strength of the halogen bond: electrostatic and covalent contributions described by coupled cluster theory, *Phys. Chem. Chem. Phys.* 18 (2016) 33031–33046.
- V. Oliveira, E. Kraka, D. Cremer, Quantitative assessment of halogen bonding utilizing vibrational spectroscopy, *Inorg. Chem.* 56 (1) (2016) 488–502.
- L. Brammer, G. Minguez Espallargas, S. Libri, Combining metals with halogen bonds, *CrystEngComm.* 10 (2008) 1712–1727.
- R. Bertani, P. Sgarbossa, A. Venzo, F. Leij, M. Amati, G. Resnati, T. Pilati, P. Metrangolo, G. Terraneo, Halogen bonding in metal-organic-supramolecular networks, *Coord. Chem. Rev.* 254 (5–6) (2010) 677–695 (a Tribute to Fausto Calderazzo on the Occasion of his 80th Birthday).
- J.A.M. Van Beek, G. Van Koten, W.J.J. Smeets, A.L. Spek, Model for the initial stage in the oxidative addition of I<sub>2</sub> to organoplatinum(II) compounds. X-ray structure of square-pyramidal [Pt<sup>II</sup>IC<sub>6</sub>H<sub>3</sub>(CH<sub>2</sub>NMe<sub>2</sub>)<sub>2</sub>-o,o'(η<sup>1</sup>-I<sub>2</sub>)] containing a linear Pt-I-I arrangement, *J. Am. Chem. Soc.* 108 (16) (1986) 5010–5011.
- J.A. van Beek, G. van Koten, G.P. Dekker, E. Wissing, M.C. Zoutberg, C.H. Stam, Synthesis and reactivity towards diiodine of palladium(II) and platinum(II) complexes with non-cyclic and cyclic ligands (C<sub>6</sub>H<sub>3</sub>{CH<sub>2</sub>NR<sup>1</sup>R<sup>2</sup>})<sub>2</sub>-2,6). End-on diiodine-platinum(II) bonding in macrocyclic [PtI(C<sub>6</sub>H<sub>3</sub>CH<sub>2</sub>NMe(CH<sub>2</sub>)<sub>7</sub>MeNCH<sub>2</sub>-2,6)(η<sup>1</sup>-I<sub>2</sub>)], *J. Organomet. Chem.* 394 (1) (1990) 659–678.
- G. van Koten, Novel aspects of η<sup>1</sup>-diiodine coordination and diiodine oxidative addition to platinum(II) and halide transfer oxidation reactions of organoplatinum(II) with Cu<sup>II</sup>X<sub>2</sub>, *Pure Appl. Chem.* 62 (6) (1990) 1155–1159.
- R.A. Gossage, A.D. Ryabov, A.L. Spek, D.J. Stufkens, J.A.M. van Beek, R. van Eldik, G. van Koten, Models for the initial stages of oxidative addition. Synthesis, characterization, and mechanistic investigation of η<sup>1</sup>-I<sub>2</sub> organometallic pincer complexes of platinum. X-ray crystal structures of [PtI(C<sub>6</sub>H<sub>3</sub>(CH<sub>2</sub>NMe<sub>2</sub>)<sub>2</sub>-2,6)(η<sup>1</sup>-I<sub>2</sub>)] and exo-meso-[Pt(η<sup>1</sup>-I<sub>3</sub>)(η<sup>1</sup>-I<sub>2</sub>)(C<sub>6</sub>H<sub>3</sub>CH<sub>2</sub>N(t-Bu)Me<sub>2</sub>-2,6)], *J. Am. Chem. Soc.* 121 (11) (1999) 2488–2497.
- F.A. Cotton, E.V. Dikarev, M.A. Petrukhina, Coordinated and clathrated molecular diiodine in [Rh<sub>2</sub>(O<sub>2</sub>CCF<sub>3</sub>)<sub>4</sub>I<sub>2</sub>]·I<sub>2</sub>, *Angew. Chem. Int. Ed. Engl.* 39 (13) (2000) 2362–2364.
- A.Y. Rogachev, R. Hoffmann, Iodine (I<sub>2</sub>) as a janus-faced ligand in organometallics, *J. Am. Chem. Soc.* 135 (8) (2013) 3262–3275.
- R. Makiura, I. Nagasawa, N. Kimura, S. Ishimaru, H. Kitagawa, R. Ikeda, An unusual six-co-ordinate platinum(II) complex containing a neutral I<sub>2</sub> ligand, *Chem. Commun.* (2001) 1642–1643.
- D.M. Ivanov, A.S. Novikov, I.V. Ananyev, Y.V. Kirina, V.Y. Kukushkin, Halogen bonding between metal centers and halocarbons, *Chem. Commun.* 52 (2016) 5565–5568.
- B. Lu, X. Zhang, L.P. Meng, Y.L. Zeng, The Pt (II)···Cl interactions: nature and strength, *Chem. Select* 1 (18) (2016) 5698–5705.
- M. Gao, Q. Li, H.-B. Li, W. Li, J. Cheng, How do organic gold compounds and organic halogen molecules interact? Comparison with hydrogen bonds, *RSC Adv.* 5 (2015) 12488–12497.
- Q. Zhao, The X···Au interactions in the CF<sub>3</sub>X (X = Cl, Br)···Au<sub>n</sub> (n = 2, 3, and 4) complexes, *J. Mol. Model.* 20 (3) (2014) 2133.
- J.F. Rooms, A.V. Wilson, I. Harvey, A.J. Bridgeman, N.A. Young, Mercury-fluorine interactions: a matrix isolation investigation of Hg···F<sub>2</sub>, HgF<sub>2</sub> and HgF<sub>4</sub> in argon matrices, *Phys. Chem. Chem. Phys.* 10 (2008) 4594–4605.
- I. Blakey, Z. Merican, L. Rintoul, Y.-M. Chuang, K.S. Jack, A.S. Micallef, Interactions of iodoperfluorobenzene compounds with gold nanoparticles, *Phys. Chem. Chem. Phys.* 14 (2012) 3604–3611.
- Z. Konkoli, D. Cremer, A new way of analyzing vibrational spectra I. Derivation of adiabatic internal modes, *Int. J. Quant. Chem.* 67 (1998) 1–11.
- W. Zou, R. Kalescky, E. Kraka, D. Cremer, Relating normal vibrational modes to local vibrational modes with the help of an adiabatic connection scheme, *J. Chem. Phys.* 137 (2012) 084114.
- W. Zou, D. Cremer, Properties of local vibrational modes: the infrared intensity, *Theor. Chem. Acc.* 133 (2014) 1451.
- W. Zou, D. Cremer, C<sub>2</sub> in a box: determining its intrinsic bond strength for the X<sup>1</sup>Σ<sub>g</sub><sup>+</sup> ground state, *Chem. Eur. J.* 22 (2016) 4087–4089.
- M. Freindorf, E. Kraka, D. Cremer, A comprehensive analysis of hydrogen bond interactions based on local vibrational modes, *Int. J. Quantum Chem.* 112 (19) (2012) 3174–3187.
- K.G. Dyall, Interfacing relativistic and nonrelativistic methods. I. Normalized elimination of the small component in the modified Dirac equation, *J. Chem. Phys.* 106 (23) (1997) 9618–9626.
- W. Zou, M. Filatov, D. Cremer, An improved algorithm for the normalized elimination of the small-component method, *Theor. Chem. Acc.* 130 (2011) 633–644.
- W. Zou, M. Filatov, D. Cremer, Development, implementation, and application of an analytic second derivative formalism for the normalized elimination of the small component method, *J. Chem. Theory Comput.* 8 (8) (2012) 2617–2629.
- D. Cremer, W. Zou, M. Filatov, Dirac-exact relativistic methods: the normalized elimination of the small component method, *WIREs Comput. Mol. Sci.* 4 (2016) 436–467.
- J. Tao, J.P. Perdew, V.N. Staroverov, G.E. Scuseria, Climbing the density functional ladder: nonempirical meta-generalized gradient approximation designed for molecules and solids, *Phys. Rev. Lett.* 91 (2003) 146401.
- K.P. Kepp, Benchmarking density functionals for chemical bonds of gold, *J. Phys. Chem. A* 121 (9) (2017) 2022–2034.
- P. Nava, D. Hagebaum-Reignier, S. Humbel, Bonding of gold with unsaturated species, *ChemPhysChem* 13 (2012) 2090.
- S. Grimme, J. Antony, S. Ehrlich, H. Krieg, A consistent and accurate ab initio parametrization of density functional dispersion correction (DFT-D) for the 94 elements H-Pu, *J. Chem. Phys.* 132 (15) (2010) 154104.
- S. Grimme, S. Ehrlich, L. Goerigk, Effect of the damping function in dispersion corrected density functional theory, *J. Comput. Chem.* 32 (7) (2011) 1456–1465.
- S. Boys, F. Bernardi, The calculation of small molecular interactions by the differences of separate total energies. some procedures with reduced errors, *Mol. Phys.* 19 (4) (1970) 553–566.
- T. Noro, M. Sekiya, T. Koga, Sapporo-(DKH3)-nZP (n = D, T, Q) sets for the sixth period s-, d-, and p-block atoms, *Theor. Chem. Acc.* 132 (5) (2013) 1363.
- T. Noro, M. Sekiya, T. Koga, Segmented contracted basis sets for atoms H through Xe: sapporo-(DK)-nZP sets (n = D, T, Q), *Theor. Chem. Acc.* 131 (2) (2012) 1124.
- T. Noro, M. Sekiya, T. Koga, Correlating basis sets for the H atom and the alkali-metal atoms from Li to Rb, *Theor. Chem. Acc.* 109 (2) (2003) 85–90.
- D. Cremer, J. Grafenstein, T. Koga, Efficient dft integrations by locally augmented radial grids, *J. Chem. Phys.* 127 (2) (2007) 164113.
- D. Cremer, J.A. Larsson, E. Kraka, New developments in the analysis of vibrational spectra: on the use of adiabatic internal vibrational modes, in: C. Parkanyi (Ed.), *Theoretical and Computational Chemistry, Theoretical Organic Chemistry*, vol. 5, Elsevier, Amsterdam, 1998, pp. 259–327.
- R. Kalescky, E. Kraka, D. Cremer, Identification of the strongest bonds in chemistry, *J. Phys. Chem. A* 117 (2013) 8981–8995.
- E. Kraka, J.A. Larsson, D. Cremer, Generalization of the badger rule based on the use of adiabatic vibrational modes in vibrational modes in computational IR spectroscopy, in: J. Grunenberg (Ed.), *Computational Spectroscopy: Methods, Experiments and Applications*, Wiley, New York, 2010, pp. 105–149.
- D. Cremer, E. Kraka, A description of the chemical bond in terms of local properties of electron density and energy, *Croat. Chem. Acta* 57 (6) (1984) 1259–1281.
- D. Cremer, E. Kraka, Chemical bonds without bonding electron density – does the difference electron density analysis suffice for a description of the chemical bond?, *Agnew Chem. Int. Ed. Engl.* 23 (1984) 627–628.
- F. Weinhold, C.R. Landis, Valency and Bonding: A Natural Bond Orbital Donor-Acceptor Perspective, Cambridge University Press, Cambridge, UK, 2003.
- E. Kraka, W. Zou, M. Filatov, J. Grafenstein, D. Izotov, J. Gauss, Y. He, A. Wu, Z. Konkoli, V. Polo, L. Olsson, Z. He, D. Cremer, COLGNE2016, see <http://www.smu.edu/catco>, 2014.
- E.D. Glendening, C.R. Landis, F. Weinhold, NBO 6.0: natural bond orbital analysis program, *J. Comput. Chem.* 34 (16) (2013) 1429–1437, <http://dx.doi.org/10.1002/jcc.23266>.

- [46] T. Lu, F. Chen, Multiwfn: a multifunctional wavefunction analyzer, *J. Comput. Chem.* 33 (2012) 580–592.
- [47] M.J. Frisch, G.W. Trucks, H.B. Schlegel, G.E. Scuseria, M.A. Robb, J.R. Cheeseman, G. Scalmani, V. Barone, B. Mennucci, G.A. Petersson, et al., Gaussian 09 Revision A. 1, Gaussian Inc., Wallingford, CT, 2010.
- [48] W.W. Porterfield, *Inorganic Chemistry, A Unified Approach*, Academic Press, San Diego, 1993.
- [49] S.M. Huber, E. Jimenez-Izal, J.M. Ugalde, I. Infante, Unexpected trends in halogen-bond based noncovalent adducts, *Chem. Commun.* 48 (2012) 7708–7710.
- [50] K. Szalewicz, Symmetry-adapted perturbation theory of intermolecular forces, *WIREs Comput. Mol. Sci.* 2 (2) (2012) 254–272.

Paper IV. The many facets of chalcogen bonding: Described by vibrational spectroscopy

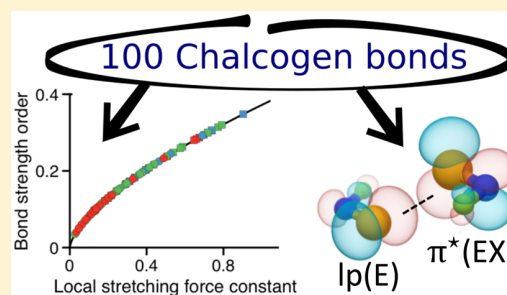
# The Many Facets of Chalcogen Bonding: Described by Vibrational Spectroscopy

Vytor Oliveira, Dieter Cremer,<sup>†</sup> and Elfi Kraka<sup>\*ID</sup>

Computational and Theoretical Chemistry Group (CATCO), Department of Chemistry, Southern Methodist University, 3215 Daniel Ave, Dallas, Texas 75275-0314, United States

## Supporting Information

**ABSTRACT:** A diverse set of 100 chalcogen-bonded complexes comprising neutral, cationic, anionic, divalent, and double bonded chalcogens has been investigated using  $\omega$ B97X-D/aug-cc-pVTZ to determine geometries, binding energies, electron and energy density distributions, difference density distributions, vibrational frequencies, local stretching force constants, and associated bond strength orders. The accuracy of  $\omega$ B97X-D was accessed by CCSD(T)/aug-cc-pVTZ calculations of a subset of 12 complexes and by the CCSD(T)/aug-cc-pVTZ //  $\omega$ B97X-D binding energies of 95 complexes. Most of the weak chalcogen bonds can be rationalized on the basis of electrostatic contributions, but as the bond becomes stronger, covalent contributions can assume a primary role in the strength and geometry of the complexes. Covalency in chalcogen bonds involves the charge transfer from a lone pair orbital of a Lewis base into the  $\sigma^*$  orbital of a divalent chalcogen or a  $\pi^*$  orbital of a double bonded chalcogen. We describe for the first time a symmetric chalcogen-bonded homodimer stabilized by a charge transfer from a lone pair orbital into a  $\pi^*$  orbital. New polymeric materials based on chalcogen bonds should take advantage of the extra stabilization granted by multiple chalcogen bonds, as is shown for 1,2,5-telluradiazole dimers.



## 1. INTRODUCTION

Chalcogen bonding (ChB, which in the following is also used for chalcogen bond and chalcogen-bonded) is the noncovalent interaction between an electrophilic region of a chalcogen atom (S, Se, and Te) with a Lewis base in the same molecular entity (intramolecular ChB) or with another molecule (intermolecular ChB). Similar to other interactions involving the main block elements, such as halogen bonding (XB) and pnictogen bonding (PnB), the ChB is a secondary bond interaction (SBI). The term SBI was coined by Alcock in 1972<sup>1</sup> based on crystallographic data and is used to designate interactions that are longer than covalent bonds but shorter than the sum of the van der Waals radii of the atoms involved. SBIs typically form a close to linear angle with the covalent bond formed by the central atom (e.g., a halogen, chalcogen, or pnictogen) and its most electronegative ligand.<sup>1–3</sup>

Although less explored than hydrogen bonding (HB) or XB, the ChB has a great potential, with applications in a myriad of different fields. In supramolecular chemistry, ChBs are used to synthesize columnar structures,<sup>4–6</sup> macrocycles,<sup>7</sup> rotaxanes,<sup>8</sup> and ribbon-like polymeric structures formed by chalcogenadiazoles derivatives.<sup>9–18</sup> In biochemistry, ChBs are found to control to some extent the tertiary structure of several proteins, suggesting that they could be used for protein engineering.<sup>19,20</sup> ChBs also play key roles in biological processes. For example, the mechanism of regioselective deiodination of thyroid hormones catalyzed by selenoenzymes involves a cooperative ChB and XB.<sup>21</sup> Besides that, ChB finds application in

catalysis<sup>22–24</sup> ion sensing and transport,<sup>8,25–27</sup> materials with nonlinear optic properties,<sup>14,17</sup> substrate recognition,<sup>28</sup> and drug design.<sup>29–32</sup>

Experimentally, the ChBs are accessed mostly via NMR chemical shifts and coupling constants,<sup>8,33–36</sup> the analysis of bond distances and angles in X-ray crystallographic structures,<sup>2,19,20,32,37</sup> and the analysis of UV–vis absorbance and emission spectra.<sup>16,25,26</sup>

Theoretical investigations on ChBs are mostly based on quantum mechanical calculations utilizing second order Møller-Plesset perturbation theory<sup>38–51</sup> or density functional theory (DFT),<sup>27,43,52–56</sup> where the accuracy of these methods are often validated by high accuracy CCSD(T) single point energy calculations of a subset of complexes.<sup>24,48–50,57–63</sup> These investigations were carried to better understand: (i) the ChB bonding mechanism, (ii) the dominant forces involved in the formation of the ChB, (iii) the high directionality of the ChBs,<sup>53,64–67</sup> (iv) the strength of the ChB and how it can be fine-tuned (v) to compare ChB with other SBIs (vi) and to support experimental analyses.

A comparison of ChB with XB, HB, PnB, or tetrel bonding was carried out by several authors.<sup>27,53,60,68–82</sup> The bonding mechanism of these SBIs have many common features, e.g., they all involve an electrostatic and a covalent part. The

Received: July 1, 2017

Revised: August 5, 2017

Published: August 7, 2017

electrostatic part is due to a Coulomb attraction between the negative electrostatic potential at the lone pairs  $\text{lp}(\text{A})$  or  $\pi$ -bond of a Lewis base and a region of positive electrostatic potential collinear to the covalent bond formed between a pnictogen (in PnB), chalcogen (in ChB) or halogen (in XB) and its most electronegative substituent (the so-called  $\sigma$ -hole region<sup>64,83,84</sup>). The covalent part is due to a charge transfer (CT) from the  $\text{lp}(\text{A})$  orbital of the Lewis base into the  $\sigma^*(\text{XE})$  orbital (E is a pnictogen (for PnB), chalcogen (for ChB) or halogen (for XB) and X is the most electronegative substituent), thus leading to a 2e-delocalization and stabilization of  $\text{lp}(\text{A})$  (as shown on Figure 1). The magnitude of the 2e-

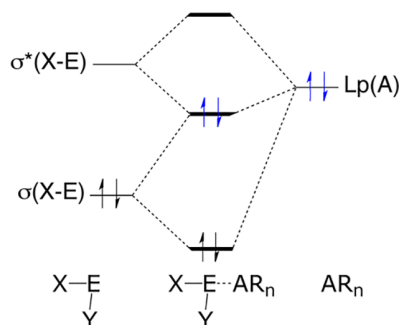


**Figure 1.** Perturbation molecular orbital showing the 2e-delocalization of an electron lone pair at the Ch acceptor (A) into the  $\sigma^*(\text{XE})$  orbital of the Ch donor.

delocalization is proportional to  $\text{lp}-\sigma^*$  orbital overlap and inversely proportional to the energy gap  $\Delta\epsilon(2e)$  between  $\text{lp}(\text{A})$  and the  $\sigma^*(\text{XE})$  orbital. A slightly different CT mechanism can take place in  $\text{sp}^2$  hybridized<sup>48–50,77–79,85–88</sup> and hypervalent chalcogens,<sup>40,42,43,45</sup> where charge is transferred from the  $\text{lp}(\text{A})$  into an empty  $\pi^*(\text{XE})$  orbital, which is higher in energy compared to the  $\sigma^*(\text{XE})$  orbital (thus has a smaller  $\Delta\epsilon(2e)$  energy gap).

XBs tend to form stronger interactions than PnB or ChB, when combined with an electronegative substituents such as F.<sup>75</sup> However, for less electronegative substituents, ChB, PnB, and XB are of comparable strength.<sup>43,72,74</sup> The ChB strength can be enhanced by an anionic chalcogen donor<sup>89</sup> or a cationic chalcogen.<sup>41,44,47</sup> These strong interactions, classified as charge assisted ChBs, can have binding energies ( $\Delta E$ ) as high as 54.7 kcal/mol.<sup>89</sup>

The energy decomposition analysis of various ChB complexes, based on symmetry adapted theory (SAPT)<sup>24,39,42,48,57,62,63,72,78</sup> or other energy decomposition schemes<sup>49–51,74,79,90</sup> clearly shows that the dominant contributions to ChB are system dependent. Very weak and weak ChBs depend on an interplay between dispersion and electrostatic contributions,<sup>38,39,48,62,78,91</sup> whereas induction plays an essential role in normal and strong ChBs.<sup>42,89</sup> Alternatively, the nature of the ChBs can be classified as covalent or electrostatic according to the electron density distribution, its Laplacian or the energy density distribution at the electron density critical bond point.<sup>35,44,45,56,81,92</sup>

Gleiter and co-workers<sup>38,39</sup> performed MP2 calculations and SAPT analyses of chalcogen bonds in  $\text{X}(\text{CH}_3)\text{E}\cdots\text{E}(\text{CH}_3)_2$  ( $\text{X} = \text{CH}_3$ , CCH or CN and  $\text{E} = \text{O}$ , S, Se, Te) complexes. From the  $\Delta E$  and the interatomic distances they concluded that the ChB becomes stronger with increasing polarizability of the chalcogen atom and polarizing power of the substituent

collinear to the ChB. SAPT based energy decomposition analyses showed that electrostatic contributions dominate only for complexes where one of the chalcogens is S or O.

The combination of experimental and theoretical studies led to important insights about ChB strength and nature. Tomoda and co-workers carried out a series of experimental and theoretical studies of intramolecular chalcogen bonds between Se and N, O, F, Cl, and Br heteroatoms in selenobenzyl derivatives.<sup>33–36</sup> The ChBs were accessed experimentally through the analysis of NMR chemical shifts and coupling constants. Binding energies were estimated by variable temperature NMR analysis. The natural bond orbital (NBO) analysis was used to describe CT. Solvents with different dielectric constants were used to evaluate the role of electrostatic contributions. They found that the strength of the ChB increases with the electron-donating ability of the heteroatoms<sup>35</sup>  $\text{F} < \text{O} < \text{N}$  and decreases for heavier heteroatoms<sup>36</sup>  $\text{F} > \text{Cl} > \text{Br}$ . Several of these ChB were considered to have a strong covalent character, with some electrostatic influence.<sup>36</sup> In another combined theoretical and experimental investigation Vargas-Baca and co-workers<sup>90,93,94</sup> performed theoretical and experimental studies on the ChBs between S, Se, Te, and N in 1,2,5-chalcogendiazole dimers. They concluded that  $\text{Te}\cdots\text{N}$  interactions were as strong as hydrogen bonds and suitable to guide supramolecular formation. Further studies from the same group led to the development of new optically active materials based on telluradiazole derivatives.<sup>17,95,96</sup>

Although  $\Delta E$  values and their (model dependent) decomposition into electrostatic, induction, dispersion and exchange components may provide useful information about the stabilizing forces involved in the formation of ChB complexes, they can give only a limited insight into the intrinsic strength of a bond.<sup>75,97,98</sup>  $\Delta E$  measures the stabilization brought by complexation in an unspecific way, where the interaction between all atoms are accounted for, including secondary contributions unrelated to the atom–atom interaction of interest.  $\Delta E$  is also flawed by energetic contributions from geometry and electronic relaxation processes that accompany bond dissociation. Although interatomic distances are free from these problems, they depend on the effective covalent radii of the atoms involved, which vary significantly for atoms of different periods of the periodic table (PT) and also depend on the nature of their substituents.<sup>99–101</sup>

A more suitable parameter capable to measure the intrinsic strength of a bond is the Konkoli–Cremer local stretching force constant,<sup>102–104</sup> derived from a mass-decoupled equivalent of Wilson's vibrational equation,<sup>105</sup> and therefore, free from mode–mode coupling. The local stretching force constant measures the curvature of the potential energy surface between the two atoms involved by applying an infinitesimally small perturbation to the bond length. Since the local stretching force constant is a second order response property, it is extremely sensitive to differences in the electronic structure (e.g., caused by changing a substituent), with the advantage that it captures only electronic effects associated with the intrinsic strength of the atom–atom interaction being analyzed.<sup>106</sup> The analysis of the local stretching modes and other local vibrational modes were successfully employed to investigate the strength of covalent bonds, weak interactions (such as HB, XB, PnB), and also to derive more reliable electronic parameters to describe 3c–4e bond character, aromaticity and transition metal–ligand

bonds. These and other applications are summarized on Table 1.

**Table 1. Previous Applications of the Local Mode Analysis**

topics	references
weak bonds:	
hydrogen bonding	142–147
halogen bonding	75, 97, 148
pnictogen bonding	129, 130, 149
new electronic parameters	
aromaticity index	98, 150, 151
generalized Tolman parameter	106, 152, 153
generalized badger rule	101
covalent bonds	
the strongest bond in chemistry	122
long carbon–carbon bonds	154
carbon–halogen bonds	155, 156
bond strength bond length relationship	99–101

In the present study we will provide for the first time a quantitative analysis of the intrinsic strength of 100 ChB, aiming at answering the following questions:

- (i) Can we describe the ChB mechanism and strength trends in simple but insightful terms?
- (ii) How strong and covalent are the ChBs in neutral and charged complexes? Do electrostatic and covalent contributions always support each other?
- (iii) How does the Lewis base influence the strength of the ChB?
- (iv) How do the substituents colinear and orthogonal to the ChB affect the strength of the interactions?
- (v) Can a sp<sup>2</sup>-hybridized chalcogen form a strong ChB?
- (vi) What type of molecules are more suitable for new materials based on ChB?

These questions will be addressed by the investigation of 100 neutral and charge assisted ChB complexes shown in Figure 2. In section 2, we describe all quantum-chemical tools employed in this work. The interplay between decisive electronic effects and ChB strength trends are clarified in section 3. In the last section we draw the conclusion and provide an outlook on important aspects of the ChB to be explored for the development of new materials.

The chemical structures of the ChB complexes in the present work will be denoted by X(Y)E...AR<sub>n</sub>, where X(Y)E is the chalcogen donor (Ch donor), composed of a chalcogen atom E, its X ligand collinear to the ChB, and the Y ligand orthogonal to the ChB, which will be given in parentheses. The ChB is denoted by three dots and the AR<sub>n</sub> is the chalcogen acceptor (Ch acceptor) formed by a heteroatom A and its ligands R.

## 2. COMPUTATIONAL METHODS

To define a reliable method of accessible computational costs to be employed for the investigation of all 100 ChB complexes (Figure 2), the accuracy of MP2<sup>107</sup> and three popular exchange-correlation functionals, B3LYP-D3<sup>108,109</sup> (including D3(BJ) dispersion correction<sup>110,111</sup>), M06-2X,<sup>112</sup>  $\omega$ B97X(-D)<sup>113,114</sup> (with and without empirical dispersion corrections D) was tested against CCSD(T) (coupled cluster theory including all singles, doubles and perturbative triple excitations)<sup>115</sup> calculated ChB distances  $r(\text{EA})$ ,  $\Delta E$  and ChB local stretching force

constants  $k^a(\text{EA})$  for a small set of 12 sulfur containing ChB complexes (Tables S1–S3 of the Supporting Information).

The geometry of these 12 complexes were optimized and the analytical frequencies were calculated utilizing CCSD(T) and Dunning's augmented triple- $\zeta$  basis set aug-cc-pVTZ,<sup>116–118</sup> which contain diffuse basis functions to describe the charge distribution of highly polarizable anions, heteroatoms, and the dispersion interactions in noncovalently bonded complexes. The  $\Delta E$  values, corrected for the basis set superposition error (BSSE) employing the counterpoise correction procedure,<sup>119</sup>  $r(\text{EA})$  and  $k^a(\text{EA})$  values obtained at CCSD(T)/aug-cc-pVTZ level were then compared with MP2, B3LYP-D3,  $\omega$ B97X, and  $\omega$ B97X-D values. All calculations were performed with tight convergence criteria (SCF (self-consistent field), 10<sup>-9</sup>; geometry iterations; forces, 10<sup>-6</sup> hartree/bohr), employing aug-cc-pVTZ basis set. The DFT calculations were done with a superfine integration grid.<sup>120</sup>

All methods were able to reproduce CCSD(T)  $\Delta E$ ,  $r(\text{EA})$  and  $k^a(\text{EA})$  values reasonably well (Tables S1–S3). MP2 provided more accurate  $\Delta E$ , whereas the long-range corrected hybrid density functional with dispersion correction  $\omega$ B97X-D<sup>113,114</sup> had lower deviations for the  $r(\text{EA})$  values and a smaller maximum deviation for the  $k^a(\text{EA})$  values. Inclusion of dispersion correction in  $\omega$ B97X-D improved  $r(\text{EA})$  and  $k^a(\text{EA})$  values but had a smaller impact on  $\Delta E$ . Because of its lower computational cost compared to MP2 and its accurate  $r(\text{EA})$  and  $k^a(\text{EA})$  values,  $\omega$ B97X-D was then picked as the method of choice to be applied for the study of the complete set of 100 ChB complexes (Figure 2).

The BSSE-corrected  $\Delta E$  values of complexes 1–100 were calculated at the  $\omega$ B97X-D/aug-cc-pVTZ(-PP) level, where relativistic effective core potentials (pseudo potentials PP) were used for Te, Se, and As.<sup>121</sup> For complexes 1–93, the BSSE-corrected CCSD(T)/aug-cc-pVTZ(-PP)// $\omega$ B97X  $\Delta E$  values were also calculated to provide an estimate of the reliability of the  $\omega$ B97X-D/aug-cc-pVTZ(-PP) calculations throughout the role set (Table 2). The analysis of the local stretching force constants  $k^a$  of the ChBs was simplified by converting to bond strength orders (BSO  $n$ ) using a power relationship:<sup>101,122</sup>

$$n = a(k^a)^b \quad (1)$$

Here the constants  $a = 0.372$  and  $b = 0.657$  were determined from the  $k^a$  values of two references of well-defined bond order (in the present work the NO single bond in H<sub>2</sub>NOH with  $k^a = 4.497$  mdyne/Å was considered to have a BSO  $n = 1$  and the NO double bond in HNO with  $k^a = 12.918$  mdyne/Å was considered to have a BSO  $n = 2$ ). It was further assumed that a  $k^a$  of zero results in a BSO  $n$  equals to zero.

The important role of 3c–4e and other multicenter bonding mechanisms in connection with ChB was emphasized by several authors.<sup>61,123–125</sup> However, no quantitative assessment of the 3c–4e character of ChB complexes was made so far. Previously, we defined a quantitative parameter based on the BSO to measure the 3c–4e character of XB complexes,<sup>75,97,98</sup> which can easily be extended to ChBs. Considering that a 3c–4e bond is formed when the X, E and A atoms in the ChB complex adopt a symmetrical arrangement (e.g., SF<sub>4</sub> or SF<sub>3</sub><sup>-</sup>). The three atomic orbitals involved lead to the formation of three molecular orbitals. Four electrons fill the bonding and nonbonding orbitals leaving the antibonding orbital unoccupied, resulting in XE and EA bonds of same strength and covalent character. A quantitative way to determine how close an asymmetric complex is to a symmetric 3c–4e bond situation

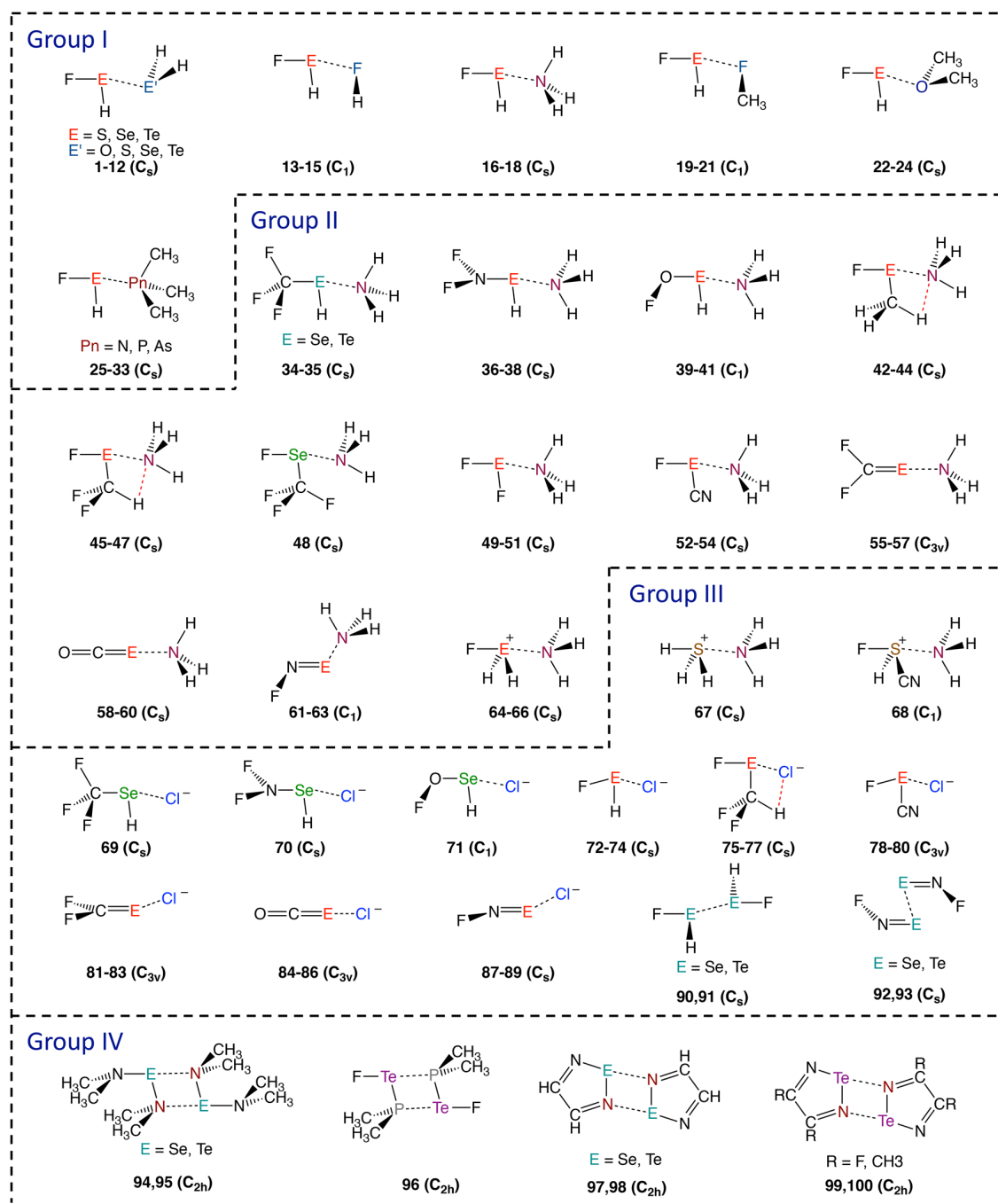


Figure 2. Schematic representation of complexes 1–100.

is given by the ratio  $n(XE)/n(EA) \times 100$ . If this ratio leads to unity, 3c–4e bonding is fulfilled by 100%. Values smaller than 100% indicate a partial 3c–4e character.

Local properties of the electron density distribution,  $\rho(\mathbf{r})$ , and the energy density distribution,  $H(\mathbf{r}) = G(\mathbf{r}) + V(\mathbf{r})$  ( $G(\mathbf{r})$ , kinetic energy density (positive, destabilizing);  $V(\mathbf{r})$ , potential energy density (negative, stabilizing)), were computed at the  $\omega$ B97X-D/aug-cc-pVTZ(-PP) level of theory. The Cremer–Kraka criteria for covalent bonding were applied.<sup>126–128</sup> These associate a negative and therefore stabilizing energy density at the bond critical point  $\mathbf{r}_b$  ( $H(\mathbf{r}_b) = H_b < 0$ ) with dominant covalent character, whereas a positive (destabilizing) energy

density ( $H_b > 0$ ) is associated with a predominant electrostatic interaction.

Similar to that for PnB and XB,<sup>75,97,129,130</sup> the covalent character of the ChB is determined by the CT from the lp(A) of the Ch acceptor to the antibonding  $\sigma^*(EX)$  orbital ( $\pi^*(EX)$  for an  $sp^2$  hybridized chalcogen) of the Ch donor, which can be assessed by calculating the NBO delocalization energy  $\Delta E[lp(A) \rightarrow \sigma^*(EX)$  (or  $\pi^*(EX)) = \Delta E(del)$ . The magnitude of  $\Delta E(del)$  was determined by second order perturbation theory.<sup>131</sup>

In all complexes, CT was found to involve frontier molecular orbitals (Figures S1 and S2), where the highest occupied

Table 2. Summary of Energetic, Geometric, and Vibrational Data for Complexes 1–100<sup>a</sup>

#	complexes (sym.)	r (XE)	r (EA)	ΔE DFT	ΔE CCSD(T)	ρ <sub>b</sub> (EA)	H <sub>b</sub> (EA)	ΔE(del) <sup>b</sup> lp-σ*	CT	k <sup>a</sup> (XE)	n (XE)	k <sup>a</sup> (EA)	n (EA)	3c-4e %	ω <sup>a</sup> (EA)	ω <sub>μ</sub> (% ω <sup>a</sup> )
<b>F(H)E...AR<sub>n</sub></b>																
1	F(H)S...OH <sub>2</sub> (C <sub>2</sub> )	1.641	2.646	5.2	5.1	0.144	0.012	9.4	0.035	4.122	0.944	0.185	0.123	13	172	136 (2;9.4), 163 (3;90.5)
2	F(H)Se...OH <sub>2</sub> (C <sub>2</sub> )	1.779	2.615	7.0	6.5	0.166	0.010	14.8	0.048	3.611	0.866	0.216	0.136	16	166	159 (3;99.7)
3	F(H)Te...OH <sub>2</sub> (C <sub>2</sub> )	1.947	2.695	8.3	7.7	0.173	0.004	16.5	0.045	3.376	0.828	0.252	0.151	18	173	165 (3;99.9)
4	F(H)S...SH <sub>2</sub> (C <sub>2</sub> )	1.642	3.074	4.1	4.0	0.120	0.003	11.4	0.054	3.964	0.920	0.125	0.095	10	106	104 (2;100.0)
5	F(H)Se...SH <sub>2</sub> (C <sub>2</sub> )	1.784	2.998	6.1	5.5	0.158	-0.005	21.8	0.085	3.383	0.829	0.155	0.109	13	107	104 (2;100.0)
6	F(H)Te...SH <sub>2</sub> (C <sub>2</sub> )	1.950	3.101	7.2	6.6	0.160	-0.009	24.0	0.091	3.212	0.802	0.161	0.112	14	103	98 (2;69.1), 105 (3;30.9)
7	F(H)S...SeH <sub>2</sub> (C <sub>2</sub> )	1.644	3.138	4.0	3.9	0.158	-0.005	12.6	0.060	3.852	0.903	0.107	0.086	9	89	77 (2;100.0)
8	F(H)Se...SeH <sub>2</sub> (C <sub>2</sub> )	1.787	3.087	6.2	5.7	0.155	-0.007	23.6	0.100	3.265	0.810	0.147	0.106	13	79	76 (2;100.0)
9	F(H)Te...SeH <sub>2</sub> (C <sub>2</sub> )	1.953	3.192	7.5	6.9	0.157	-0.011	26.0	0.108	3.152	0.792	0.184	0.123	15	79	77 (2;99.9)
10	F(H)S...TeH <sub>2</sub> (C <sub>2</sub> )	1.647	3.273	4.3	4.1	0.126	-0.002	15.1	0.078	3.648	0.872	0.093	0.078	9	79	67 (1;100.0)
11	F(H)Se...TeH <sub>2</sub> (C <sub>2</sub> )	1.793	3.200	6.6	6.0	0.163	-0.010	28.5	0.128	3.060	0.777	0.144	0.104	13	70	67 (1;100.0)
12	F(H)Te...TeH <sub>2</sub> (C <sub>2</sub> )	1.959	3.311	8.1	7.4	0.163	-0.013	32.1	0.141	2.980	0.763	0.169	0.116	15	66	64 (1;100.0)
13	F(H)S...FH (C <sub>1</sub> )	1.629	2.828	2.3	2.5	0.086	0.012	3.3	0.010	4.411	0.987	0.048	0.051	5	82	59 (1;72.5), 94 (2;27.2)
14	F(H)Se...FH (C <sub>1</sub> )	1.766	2.780	3.1	3.1	0.099	0.012	5.8	0.016	3.911	0.912	0.134	0.099	11	113	120 (3;98.9)
15	F(H)Te...FH (C <sub>1</sub> )	1.934	2.864	3.8	3.6	0.104	0.009	6.8	0.018	3.584	0.862	0.143	0.104	12	121	119 (3;99.5)
16	F(H)S...NH <sub>3</sub> (C <sub>2</sub> )	1.663	2.518	8.1	7.6	0.238	-0.014	23.9	0.092	3.315	0.818	0.183	0.122	15	177	159 (2;100.0)
17	F(H)Se...NH <sub>3</sub> (C <sub>2</sub> )	1.806	2.501	11.7	10.6	0.267	-0.027	34.6	0.114	2.999	0.766	0.287	0.164	21	202	186 (4;100.0)
18	F(H)Te...NH <sub>3</sub> (C <sub>2</sub> )	1.968	2.616	13.9	12.9	0.254	-0.029	33.7	0.111	2.960	0.760	0.382	0.198	26	226	207 (4;100.0)
<b>F(H)E...AR<sub>n</sub></b>																
19	F(H)S...FCH <sub>3</sub> (C <sub>1</sub> )	1.633	2.747	3.0	3.6	0.125	0.009	3.6	0.011	4.365	0.981	0.112	0.088	9	126	79 (3;1.5) 104 (4;3.4), 116 (5;94.3)
20	F(H)Se...FCH <sub>3</sub> (C <sub>1</sub> )	1.769	2.706	4.0	4.4	0.114	0.013	6.4	0.018	3.856	0.904	0.140	0.102	11	124	83 (3;6.0) 113 (5;88.9), 113 (6;4.1)
21	F(H)Te...FCH <sub>3</sub> (C <sub>1</sub> )	1.937	2.769	5.0	5.1	0.125	0.009	8.2	0.022	3.529	0.853	0.137	0.101	12	118	87 (3;39.7), 117 (5;56.4), 162 (6;3.6)
22	F(H)S...O(CH <sub>3</sub> ) <sub>2</sub> (C <sub>2</sub> )	1.646	2.540	6.6	7.2	0.185	0.007	9.3	0.040	3.937	0.916	0.202	0.130	14	179	68 (1;1.1), 136 (4;98.3)
23	F(H)Se...O(CH <sub>3</sub> ) <sub>2</sub> (C <sub>2</sub> )	1.785	2.527	8.8	9.0	0.207	0.002	15.2	0.052	3.463	0.842	0.263	0.155	18	183	129 (4;85.6), 147 (5;13.2)
24	F(H)Te...O(CH <sub>3</sub> ) <sub>2</sub> (C <sub>2</sub> )	1.951	2.620	10.4	10.5	0.204	-0.003	16.0	0.052	3.263	0.810	0.308	0.172	21	192	114 (4;2.6), 133 (5;97.0)
25	F(H)S...N(CH <sub>3</sub> ) <sub>3</sub> (C <sub>1</sub> )	1.691	2.306	12.3	13.2	0.397	-0.088	36.8	0.141	2.648	0.706	0.329	0.179	25	240	147 (4;98.3), 433 (10;1.6)
26	F(H)Se...N(CH <sub>3</sub> ) <sub>3</sub> (C <sub>1</sub> )	1.822	2.391	15.8	16.5	0.360	-0.074	40.1	0.133	2.701	0.715	0.442	0.218	30	251	142 (4;97.8), 445 (12;2.2)
27	F(H)Te...N(CH <sub>3</sub> ) <sub>3</sub> (C <sub>1</sub> )	1.976	2.545	17.9	18.9	0.313	-0.058	34.4	0.114	2.776	0.728	0.465	0.225	31	250	137 (3;97.9), 450 (12;2.1)
28	F(H)S...P(CH <sub>3</sub> ) <sub>3</sub> (C <sub>1</sub> )	1.792	2.316	13.4	11.3	0.633	-0.244	198.9	0.415	1.194	0.418	0.489	0.233	56	230	154 (4;92.9), 322 (11;6.6)
29	F(H)Se...P(CH <sub>3</sub> ) <sub>3</sub> (C <sub>1</sub> )	1.887	2.497	17.4	15.3	0.385	-0.113	115.5	0.329	1.711	0.530	0.502	0.237	45	195	126 (4;96.2), 311 (12;3.8)
30	F(H)Te...P(CH <sub>3</sub> ) <sub>3</sub> (C <sub>1</sub> )	2.016	2.714	19.4	17.8	0.385	-0.113	87.9	0.259	2.129	0.612	0.524	0.244	40	189	118 (4;96.5) 308 (12;3.4)
31	F(H)S...As(CH <sub>3</sub> ) <sub>3</sub> (C <sub>2</sub> )	1.696	2.686	7.9	7.5	0.319	-0.058	43.0	0.216	1.772	0.542	0.131	0.098	18	100	78 (4;99.9)
32	F(H)Se...As(CH <sub>3</sub> ) <sub>3</sub> (C <sub>2</sub> )	1.843	2.717	12.1	11.2	0.333	-0.068	59.9	0.249	2.059	0.599	0.290	0.165	28	113	204 (3;100.0)
33	F(H)Te...As(CH <sub>3</sub> ) <sub>3</sub> (C <sub>2</sub> )	1.994	2.882	14.2	13.6	0.288	-0.059	53.9	0.224	2.331	0.649	0.359	0.190	29	113	90 (4;99.5)
<b>X(H)E...NH<sub>3</sub></b>																
34	F <sub>3</sub> C(H)Se...NH <sub>3</sub> (C <sub>2</sub> )	1.964	3.029	4.3	4.1	0.097	0.010	6.8	0.025	2.573	0.693	0.119	0.092	13	130	118 (4;99.8)
35	F <sub>3</sub> C(H)Te...NH <sub>3</sub> (C <sub>2</sub> )	2.187	2.987	6.2	5.6	0.126	0.005	11.4	0.044	2.048	0.597	0.121	0.093	16	127	116 (4;100.0)
36	F <sub>2</sub> N(H)S...NH <sub>3</sub> (C <sub>2</sub> )	1.759	2.862	5.1	5.1	0.116	0.010	7.2	0.032	2.536	0.686	0.124	0.095	14	147	82 (3;10.0), 134 (4;90.0)
37	F <sub>2</sub> N(H)Se...NH <sub>3</sub> (C <sub>2</sub> )	1.931	2.763	7.2	6.4	0.163	0.004	16.3	0.061	2.064	0.600	0.166	0.115	19	154	140 (5;99.8)
38	F <sub>2</sub> N(H)Te...NH <sub>3</sub> (C <sub>1</sub> )	2.154	2.758	9.8	8.7	0.197	-0.010	23.3	0.088	1.723	0.532	0.218	0.137	26	171	145 (4;1.4), 157 (5;98.6)
39	FO(H)S...NH <sub>3</sub> (C <sub>1</sub> )	1.617	2.784	6.2	6.1	0.141	0.008	9.3	0.041	2.884	0.747	0.145	0.105	14	159	125 (3;47.9), 149 (4;52.0)

Table 2. continued

#	complexes (sym.)	$r$ (XE)	$r$ (EA)	$\Delta E$ DFT	$\Delta E$ CCSD(T)	$\rho_b$ (EA)	$H_b$ (EA)	$\Delta E(\text{del})^b$ $lp-\sigma^*$	CT	$k^a$ (XE)	$n$ (XE)	$k^a$ (EA)	$n$ (EA)	3c-4e %	$\omega^c$ (EA)	$\omega_\mu$ (% $\omega^c$ )
<b>X(H)E...NH<sub>3</sub></b>																
40	FO(H)Se...NH <sub>3</sub> (C <sub>1</sub> )	1.807	2.664	9.0	8.1	0.190	-0.001	20.0	0.074	2.478	0.676	0.212	0.134	20	174	159 (4;99.9)
41	FO(H)Te...NH <sub>3</sub> (C <sub>1</sub> )	2.013	2.695	11.7	10.6	0.218	-0.016	26.3	0.096	2.308	0.645	0.291	0.166	26	198	181 (4;100.0)
<b>F(Y)E...NH<sub>3</sub></b>																
42	F(CH <sub>3</sub> )S...NH <sub>3</sub> (C <sub>2</sub> )	1.648	2.917	4.3	4.4	0.101	0.011	5.6	0.022	3.780	0.892	0.062	0.060	7	104	90 (2;99.8)
43	F(CH <sub>3</sub> )Se...NH <sub>3</sub> <i>anti</i> (C <sub>1</sub> )	1.804	2.624	7.9	7.2	0.207	-0.006	23.4	0.079	2.989	0.765	0.184	0.123	16	162	128 (3;15.4), 154 (5;84.6)
	F(CH <sub>3</sub> )Se...NH <sub>3</sub> <i>syn</i> (C <sub>1</sub> )	1.810	2.568	9.1	8.5	0.232	-0.014	26.9	0.094	2.910	0.751	0.244	0.147	20	186	171 (5;100.0)
44	F(CH <sub>3</sub> )Te...NH <sub>3</sub> (C <sub>1</sub> )	1.843	2.717	12.1	11.2	0.333	-0.068	59.9	0.249	2.059	0.599	0.290	0.165	28	113	204 (3;100.0)
45	F(CF <sub>3</sub> )S...NH <sub>3</sub> (C <sub>2</sub> )	1.638	2.729	7.0	7.0	0.147	0.007	10.1	0.046	3.799	0.895	0.084	0.073	8	121	106 (3;100.0)
46	F(CF <sub>3</sub> )Se...NH <sub>3</sub> <i>anti</i> (C <sub>1</sub> )	1.788	2.578	10.9	10.3	0.233	-0.014	26.0	0.092	3.274	0.812	0.242	0.147	18	186	161 (5;77.8), 185 (6;22.2)
	F(CF <sub>3</sub> )Se...NH <sub>3</sub> <i>syn</i> (C <sub>2</sub> )	1.819	2.421	15.7	14.2	0.323	-0.052	40.7	0.142	2.784	0.730	0.414	0.209	29	243	212 (5;2.7), 225 (6;97.2)
47	F(CF <sub>3</sub> )Te...NH <sub>3</sub> (C <sub>1</sub> )	1.955	2.650	13.8	13.1	0.240	-0.024	28.2	0.100	3.161	0.793	0.333	0.181	23	211	196 (6;99.5)
48	F(CF <sub>3</sub> )Se...NH <sub>3</sub> <i>anti</i> (C <sub>1</sub> )	1.801	2.458	11.5	11.0	0.302	-0.041	37.0	0.132	3.038	0.773	0.333	0.181	23	218	159 (3;13.8), 182 (5;2.7), 211 (6;83.4)
	F(CF <sub>3</sub> )Se...NH <sub>3</sub> <i>syn</i> (C <sub>2</sub> )	1.795	2.454	14.6	14.2	0.303	-0.042	36.0	0.133	3.142	0.790	0.376	0.196	25	231	209 (5;87.8), 217 (6;12.1)
49	F <sub>2</sub> S...NH <sub>3</sub> (C <sub>2</sub> )	1.629	2.572	6.7	6.3	0.221	-0.008	15.8	0.072	3.795	0.895	0.156	0.110	12	165	129 (2;18.8), 152 (4;81.2)
50	F <sub>2</sub> Se...NH <sub>3</sub> (C <sub>2</sub> )	1.775	2.477	11.7	10.7	0.289	-0.036	28.2	0.109	3.343	0.823	0.297	0.168	20	206	190 (4;99.1)
51	F <sub>2</sub> Te...NH <sub>3</sub> (C <sub>2</sub> )	1.943	2.560	15.5	14.6	0.292	-0.046	27.5	0.118	3.251	0.808	0.376	0.196	24	225	207 (4;98.2)
52	F(CN)S...NH <sub>3</sub> (C <sub>1</sub> )	1.653	2.465	10.8	10.4	0.275	-0.026	26.3	0.127	3.372	0.828	0.220	0.138	17	196	175 (3;99.9)
53	F(CN)Se...NH <sub>3</sub> (C <sub>1</sub> )	1.792	2.465	15.1	14.1	0.298	-0.040	37.2	0.143	3.177	0.796	0.366	0.192	24	228	210 (5;100.0)
54	F(CN)Te...NH <sub>3</sub> (C <sub>1</sub> )	1.953	2.572	17.9	17.0	0.286	-0.044	36.9	0.137	3.178	0.796	0.400	0.204	26	232	213 (5;100.0)
<b>X=E...NH<sub>3</sub></b>																
55	F <sub>2</sub> CS...NH <sub>3</sub> (C <sub>1</sub> )	1.595	3.381	1.0	1.5	0.045	0.009	1.5	0.006	6.702	1.300	0.034	0.040	3	77	64 (4;100.0)
56	F <sub>2</sub> CSe...NH <sub>3</sub> (C <sub>1</sub> )	1.749	3.198	2.5	2.5	0.072	0.009	4.2	0.028	5.004	1.073	0.062	0.060	6	94	84 (4;100.0)
57	F <sub>2</sub> CTe...NH <sub>3</sub> (C <sub>1</sub> )	1.984	3.148	4.3	3.9	0.096	0.008	7.7	0.014	3.395	0.831	0.131	0.098	12	133	121 (4;100.0)
58	OCS...NH <sub>3</sub> (C <sub>3v</sub> )	1.566	3.273	1.7	2.0	0.054	0.010	2.1	0.008	7.248	1.368	0.047	0.050	4	90	77 (3;100.0)
59	OCSe...NH <sub>3</sub> (C <sub>3v</sub> )	1.721	3.091	3.5	3.3	0.085	0.010	5.9	0.019	5.037	1.077	0.105	0.085	8	122	111 (3;100.0)
60	OCTe...NH <sub>3</sub> (C <sub>3v</sub> )	1.967	3.033	5.7	5.0	0.116	0.007	11.1	0.040	2.836	0.739	0.131	0.098	13	133	122 (3;100.0)
61	FNS...NH <sub>3</sub> (C <sub>1</sub> )	1.534	2.659	5.5	4.4	0.192	0.000	11.3	0.084	7.073	1.346	0.137	0.101	7	155	69 (2;1.1) 143 (3;97.7), 185 (4;1.3)
62	FNSE...NH <sub>3</sub> (C <sub>1</sub> )	1.690	2.649	7.0	5.3	0.213	-0.005	26.1	0.099	5.656	1.163	0.169	0.116	10	155	145 (3;99.3)
63	FNTe...NH <sub>3</sub> (C <sub>1</sub> )	1.905	2.661	9.2	6.6	0.248	-0.026	37.7	0.124	4.326	0.975	0.219	0.137	14	172	160 (3;99.5)
<b>FH<sub>2</sub>E'...NH<sub>3</sub></b>																
64	F(H <sub>2</sub> )S'...NH <sub>3</sub> (C <sub>1</sub> )	1.614	2.188	38.7	36.9	0.528	-0.173	57.8	0.249	4.008	0.927	0.674	0.287	31	343	308 (4;99.9)
65	F(H <sub>2</sub> )Se'...NH <sub>3</sub> (C <sub>1</sub> )	1.748	2.308	39.2	37.5	0.439	-0.123	59.0	0.218	3.921	0.914	0.718	0.300	33	320	294 (4;100.0)
66	F(H <sub>2</sub> )Te'...NH <sub>3</sub> (C <sub>1</sub> )	1.906	2.451	38.9	37.6	0.382	-0.096	51.1	0.190	3.833	0.900	0.739	0.305	34	315	290 (4;100.0)
67	H <sub>3</sub> S'...NH <sub>3</sub> (C <sub>1</sub> )	1.362	2.730	19.1	18.4	0.171	0.002	9.9	0.053	3.803	0.896	0.291	0.166	18	225	208 (2;100.0)
68	FH(CN)S'...NH <sub>3</sub> (C <sub>1</sub> )	1.607	2.189	39.1	37.8	0.542	-0.178	57.8	0.279	4.035	0.931	0.658	0.283	30	339	300 (5;17.7), 305 (6;82.0)
<b>X(Y)E...Cl<sup>-</sup></b>																
69	F <sub>2</sub> C(H)Se...Cl <sup>-</sup> (C <sub>2</sub> )	1.986	2.892	17.0	17.4	0.183	-0.006	24.9	0.118	2.105	0.607	0.244	0.147	24	131	130 (3;99.0)
70	F <sub>2</sub> N(H)Se...Cl <sup>-</sup> (C <sub>2</sub> )	2.015	2.639	25.9	25.8	0.308	-0.050	59.6	0.247	1.253	0.432	0.412	0.208	48	170	170 (4;99.8)
71	FO(H)Se...Cl <sup>-</sup> (C <sub>1</sub> )	1.880	2.623	28.4	28.2	0.315	-0.054	58.5	0.250	1.206	0.421	0.437	0.216	51	175	175 (3;99.9)
72	F(H)S...Cl <sup>-</sup> (C <sub>2</sub> )	1.786	2.479	22.5	22.5	0.389	-0.086	74.6	0.308	1.432	0.472	0.397	0.203	43	201	195 (1;100.0)
73	F(H)Se...Cl <sup>-</sup> (C <sub>2</sub> )	1.920	2.538	30.2	29.4	0.371	-0.084	85.3	0.306	1.595	0.506	0.587	0.263	52	173	202 (3;100.0)

Table 2. continued

#	complexes (sym.)	$r$ (XE)	$r$ (EA)	$\Delta E$ DFT	$\Delta E$ CCSD(T)	$\rho_b$ (EA)	$H_b$ (EA)	$\Delta E(\text{del})^b$ $lp-\sigma^*$	CT	$k^a$ (XE)	$n$ (XE)	$k^c$ (EA)	$n$ (EA)	3c-4e %	$\omega^d$ (EA)	$\omega_\mu$ (% $\omega^d$ )
<b>X(Y)E...Cl<sup>-</sup></b>																
74	F(H)Te...Cl <sup>-</sup> (C <sub>2v</sub> )	2.068	2.656	36.6	36.1	0.349	-0.083	78.6	0.287	1.807	0.549	0.718	0.300	55	202	210 (3;100.0)
75	F(CF <sub>2</sub> H)S...Cl <sup>-</sup> (C <sub>2v</sub> )	1.741	2.546	27.3	29.0	0.346	-0.076	57.3	0.277	1.814	0.551	0.311	0.173	31	178	167 (2;99.1)
76	F(CF <sub>2</sub> H)Se...Cl <sup>- anti</sup> (C <sub>2v</sub> )	1.886	2.560	36.1	36.9	0.359	-0.076	72.6	0.294	1.881	0.564	0.538	0.248	44	194	196 (5;98.8)
	F(CF <sub>2</sub> H)Se...Cl <sup>- syn</sup> (C <sub>2v</sub> )	1.952	2.455	34.8	35.0	0.449	-0.129	108.1	0.372	1.373	0.459	0.772	0.314	69	232	232 (5;99.6)
77	F(CF <sub>2</sub> H)Te...Cl <sup>-</sup> (C <sub>2v</sub> )	2.043	2.661	43.5	44.2	0.348	-0.082	68.8	0.286	1.996	0.587	0.699	0.294	50	207	209 (5;99.9)
78	F(CN)S...Cl <sup>-</sup> (C <sub>2v</sub> )	1.785	2.393	33.1	33.6	0.485	-0.135	94.9	0.410	1.571	0.501	0.647	0.280	56	256	249 (4;99.6)
79	F(CN)Se...Cl <sup>-</sup> (C <sub>2v</sub> )	1.906	2.474	41.3	40.9	0.439	-0.121	102.5	0.376	1.779	0.544	0.792	0.320	59	235	235 (4;100.0)
80	F(CN)Te...Cl <sup>-</sup> (C <sub>2v</sub> )	2.047	2.597	47.7	47.5	0.399	-0.111	90.1	0.339	1.973	0.582	0.903	0.348	60	236	237 (4;100.0)
<b>X=E...Cl<sup>-</sup></b>																
81	F <sub>2</sub> CS...Cl <sup>-</sup> (C <sub>2v</sub> )	1.582	2.997	6.0	7.3	0.144	0.004	15.1	0.094	6.874	1.321	0.126	0.096	7	113	112 (3;99.1)
82	F <sub>2</sub> CSe...Cl <sup>-</sup> (C <sub>2v</sub> )	1.745	2.962	9.9	10.9	0.164	0.000	15.0	0.113	4.509	1.002	0.183	0.122	12	113	28 (1;3.9), 120 (3;96.2)
83	F <sub>2</sub> CTe...Cl <sup>-</sup> (C <sub>2v</sub> )	2.005	2.935	16.2	17.7	0.203	-0.015	19.2	0.152	2.503	0.681	0.215	0.136	20	115	19 (1;9.4), 131 (3;90.6)
84	OCSe...Cl <sup>-</sup> (C <sub>2v</sub> )	1.564	3.127	8.0	9.1	0.106	0.008	7.0	0.042	7.071	1.346	0.134	0.099	7	117	102 (3;100.0)
85	OCSe...Cl <sup>-</sup> (C <sub>2v</sub> )	1.730	2.987	13.2	13.3	0.150	0.002	16.5	0.083	4.409	0.987	0.200	0.129	13	118	115 (3;100.0)
86	OCTe...Cl <sup>-</sup> (C <sub>2v</sub> )	2.009	2.893	20.2	20.5	0.218	-0.021	35.1	0.159	1.955	0.579	0.338	0.183	32	144	144 (3;100.0)
87	FNS...Cl <sup>-</sup> (C <sub>2v</sub> )	1.535	2.431	26.7	25.8	0.452	-0.107	74.0	0.376	5.992	1.207	0.507	0.238	20	227	113 (1;8.1), 227 (2;88.8), 314 (3;3.1)
88	FNSe...Cl <sup>-</sup> (C <sub>2v</sub> )	1.702	2.509	30.0	28.2	0.410	-0.095	56.8	0.361	4.911	1.060	0.576	0.259	24	201	97 (1;1.7), 205 (2;98.0)
89	FNTe...Cl <sup>-</sup> (C <sub>2v</sub> )	1.923	2.595	36.8	33.9	0.401	-0.107	116.6	0.361	3.814	0.897	0.740	0.306	34	213	240 (3;94.9)
<b>homodimers</b>																
90	(F(H)Se) <sub>2</sub> (C <sub>2v</sub> )	1.786	2.665	7.7	6.4	0.301	-0.047	37.9	0.000	2.512	0.682	0.252	0.151	22	104	92 (2;99.9)
91	(F(H)Te) <sub>2</sub> (C <sub>2v</sub> )	1.956	2.943	11.0	10.1	0.318	-0.074	44.4	0.000	2.519	0.683	0.405	0.206	30	103	92 (2;99.4)
92	(FNSe) <sub>2</sub> (C <sub>2v</sub> )	1.691	3.686	2.7	2.9	0.060	0.002	1.2	0.000	5.674	1.165	0.027	0.035	3	34	28 (3;83.0), 41 (4;17.0)
93	(FNTe) <sub>2</sub> (C <sub>2v</sub> )	1.928	2.828	8.5	7.9	0.413	-0.123	67.9	0.000	3.631	0.869	0.391	0.201	23	101	54 (3;17.2), 113 (4;82.8)
94	(Me <sub>2</sub> N) <sub>2</sub> Se <sub>2</sub> (C <sub>2h</sub> )	1.832	3.216	4.7		0.073	0.007	2.6	0.000	2.846	0.740	0.075	0.068	9	104	37 (3;27.2), 49 (5;70.7)
95	(Me <sub>2</sub> N) <sub>2</sub> Te <sub>2</sub> (C <sub>2h</sub> )	2.011	3.005	9.8		0.130	0.002	8.1	0.000	2.662	0.709	0.081	0.071	10	104	44 (3;96.7), 52 (5;2.8)
96	(F(PMe <sub>2</sub> )Te) <sub>2</sub> (C <sub>2h</sub> )	2.061	2.670	28.0		0.429	-0.139	86.4	0.000	1.657	0.519	0.690	0.292	56	216	103 (4;57.1), 117 (5;34.3), 296 (19;2.5)
97	(H <sub>2</sub> C <sub>2</sub> N <sub>2</sub> Se) <sub>2</sub> (C <sub>2h</sub> )	1.787	2.994	6.0	6.3	0.095	0.011	3.6	0.000	3.331	0.821	0.121	0.093	11	131	58 (3;43.2), 73 (4;56.8)
98	(H <sub>2</sub> C <sub>2</sub> N <sub>2</sub> Te) <sub>2</sub> (C <sub>2h</sub> )	2.004	2.707	13.5	13.6	0.210	-0.013	11.8	0.000	2.471	0.675	0.180	0.121	18	155	69 (2;81.3), 80 (4;18.6)
99	(F <sub>2</sub> C <sub>2</sub> N <sub>2</sub> Te) <sub>2</sub> (C <sub>2h</sub> )	2.022	2.685	15.3		0.213	-0.013	13.4	0.000	2.378	0.658	0.241	0.146	22	180	58 (3;19.2), 69 (4;80.6)
100	(Me <sub>2</sub> C <sub>2</sub> N <sub>2</sub> Te) <sub>2</sub> (C <sub>2h</sub> )	2.015	2.695	13.8		0.216	-0.015	12.6	0.000	2.569	0.692	0.210	0.134	19	168	58 (3;13.6), 65 (4;86.3)

<sup>a</sup>Computed at  $\omega$ B97X-D/aug-cc-pVTZ(-PP for Se, As, and Te). Bond distances  $r(\text{XE})$  and  $r(\text{EA})$  in Å; binding energy  $\Delta E(\text{DFT})$  and  $\text{CCSD(T)}/\omega$ B97X-D  $\Delta E$  in kcal/mol, where the latter was used to estimate  $\omega$ B97X-D reliability. Density at EA critical point  $\rho_b$  in  $e/\text{Å}^3$ ; energy density at EA critical point  $H_b$  in Hartree/Å<sup>3</sup>;  $lp(\text{A}) \rightarrow \sigma^*(\text{XE})$  delocalization energy  $\Delta E(\text{del})$  in kcal/mol; NPA charge transfer in e, local XE and EA stretching force constants in mdyn/Å, EA local stretching frequency  $\omega^d$  in  $\text{cm}^{-1}$ , 3c-4e % character calculated from  $n(\text{EA})/n(\text{XE})$ , and normal-mode frequencies related to EA stretching  $\omega_\mu$  in  $\text{cm}^{-1}$ , their mode order no., and % local stretching character ( $\omega^d$  %). <sup>b</sup> $\Delta E(\text{del})$  values for  $lp \rightarrow \pi^*$  are given in bold.

molecular orbital (HOMO) of the Ch acceptors is the lp(A) orbital, and the lowest unoccupied molecular orbital (LUMO) of the Ch donors is the  $\sigma^*(EX)$  for divalent chalcogens and  $\pi^*(EX)$  for double bonded chalcogens. Orbital energies calculated at the HF/6-31g(d) level were used to measure the electron donor ability of the Ch acceptors (Figure S1) and electron acceptor ability of the Ch donors (Figure S2), where a HOMO of higher energy or a LUMO of lower energy results in a smaller HOMO–LUMO energy gap ( $\Delta\epsilon$ ) and therefore, in a stronger CT. Because of the basis set dependence of orbital energies, vertical ionization potentials calculated at CCSD(T)aug-cc-pVTZ(-PP)// $\omega$ B97X-D were used to compare the electron donor ability of Ch acceptors of different periods.

The electrostatic attractive capabilities of the monomers were accessed by investigating the electrostatic potential  $V(\mathbf{r})$  mapped on the 0.001 e/Bohr<sup>3</sup> electron density surface of the monomers (Figures S3 and S4). Where the maximum  $V(\mathbf{r})$  at the  $\sigma$ -hole region of Ch donors ( $V_{max}$ ) and the minimum  $V(\mathbf{r})$  at the lp(A) region of the Ch acceptors provide a measure for the electrostatic attraction (Table 3 and 4).

**Table 3. Summary of Chalcogen Acceptor Properties<sup>a</sup>**

acceptors	IP(CCSD(T))	NBO(A)	$V(\mathbf{r})_{min}$	$\alpha_{iso}$
HF	16.2	-0.554	-0.90	5.6
OH <sub>2</sub>	12.7	-0.929	-1.43	9.7
SH <sub>2</sub>	10.4	-0.281	-0.74	24.7
SeH <sub>2</sub>	9.8	-0.172	-0.67	31.7
TeH <sub>2</sub>	9.0	0.038	-0.57	44.2
NH <sub>3</sub>	10.9	-1.056	-1.63	14.3
PH <sub>3</sub>	10.5	0.025	-0.73	30.8
AsH <sub>3</sub>	10.5	0.114	-0.46	36.0
FMe	13.4	-0.380	-0.98	17.1
OMe <sub>2</sub>	10.2	-0.559	-1.34	33.6
NMe <sub>3</sub>	8.5	-0.512	-1.34	50.8
PMe <sub>3</sub>	8.6	0.761	-1.25	67.6
AsMe <sub>3</sub>	8.7	0.801	-0.95	73.2
H <sub>2</sub> C <sub>2</sub> N <sub>2</sub> Se	9.7	-0.618	-1.17	60.2
H <sub>2</sub> C <sub>2</sub> N <sub>2</sub> Te	10.2	-0.678	-1.24	73.6
F <sub>2</sub> C <sub>2</sub> N <sub>2</sub> Te	9.3	-0.710	-0.99	72.9
Me <sub>2</sub> C <sub>2</sub> N <sub>2</sub> Te	8.4	-0.698	-1.30	101.3
F <sup>-</sup>	3.3	-1.000	-7.31	9.0
Cl <sup>-</sup>	3.5	-1.000	-6.05	29.0

<sup>a</sup>Vertical ionization potential computed at  $\omega$ B97X-D/aug-cc-pVTZ (PP for Se As and Te) geometry and with CCSD(T) /aug-cc-pVTZ(-PP) energies (without including the zero point energy) in eV. NBO charges at the Ch acceptor heteroatom A, minimum electrostatic potential at the lone pair region of A ( $V_{min}$ ) in kcal/mol, isotropic polarizability in Bohr<sup>3</sup>, and total dipole moment in Debye.

It is well-known that other contributions such as dispersion and exchange-repulsion can also play an important role for the stability of ChB complexes.<sup>38,39,67</sup> These contributions will be explicitly discussed only when they are required to explain qualitative changes in the ChB strength order. A SAPTO energy decomposition was used<sup>132–134</sup> for this purpose.

The calculation of the local mode properties was performed with the program COLOGNE2016.<sup>135</sup> CCSD(T) energies were obtained with the package CFOUR.<sup>136</sup> For the NBO analysis, the program NBO 6<sup>131</sup> was used. The local properties of the electron density distribution  $\rho(\mathbf{r})$  and energy density distribution  $H(\mathbf{r})$  at the ChB critical point  $\mathbf{r}_b$  and the

electrostatic potentials were analyzed with the program Multiwfn.<sup>137</sup> The SAPTO energy decomposition<sup>132</sup> was carried out with Molpro<sup>138</sup> and DFT calculations were performed with Gaussian09.<sup>139</sup>

### 3. RESULTS AND DISCUSSION

Figure 2 contains a schematic representation of complexes 1–100. They are separated into four groups (I–IV). Group I (1–33) provides a systematic investigation of the effect of varying the Ch acceptor AR<sub>n</sub>. Group II is used to study the effect of different substituents at the chalcogen (34–63). Group III (64–89) contains charge assisted ChB complexes, whereas group IV (90–100) is used to investigate ChB in symmetric homodimer complexes.

The data for all ChB complexes are summarized in Table 2, which contains bond lengths  $r(XE)$  and  $r(EA)$  in Å, binding energies ( $\Delta E(\text{DFT})$  and  $\Delta E(\text{CCSD(T)})$ ) in kcal/mol, the electron density  $\rho_b(EA)$  in electron/Å<sup>3</sup>, and the energy density  $H_b(EA)$  in hartree/Å<sup>3</sup> at the ChB density critical point ( $\mathbf{r}$ ), NBO delocalization energies  $\Delta E(\text{del})$  in kcal/mol, intermonomer CT obtained from the natural population analysis (NPA) partial atomic charges<sup>140</sup> in electrons, local stretching force constants  $k^a(XE)$  and  $k^a(EA)$  in mdyn/Å, BSO values  $n(XE)$  and  $n(EA)$ , degree of 3c–4e bonding in %, and the frequency of that normal mode, which has dominant XB stretching character. The latter is given to provide vibrational spectroscopist information where the ChB stretching band should be found when recording either infrared or Raman spectra.

Tables 3 and 4 provide a summary of the Ch acceptors (Tables 3) and the Ch donors (Tables 4) properties. Including vertical ionization energies of Ch acceptors in eV, NPA partial atomic charges of A and E atoms, electrostatic potentials  $V_{min}$  and  $V_{max}$  in eV, isotropic polarizabilities  $\alpha_{iso}$  in Bohr<sup>3</sup>,  $r(XE)$  in Å,  $k^a(XE)$  in mdyn/Å, and  $n(XE)$ .

Figure 3 provides an ordering of all ChBs investigated according to their intrinsic bond strength given by the BSO values. ChBs vary from weak interactions ( $n(EA) < 0.1$ ) to normal ( $0.1 \leq n(EA) \leq 0.2$ ) and to strong interactions ( $n(EA) > 0.2$ ), where the latter are mostly charge assisted ChBs.

The relationship between the strength and the nature of the ChBs is shown on Figure 4. As the ChB varies from weak to strong bonds,  $H_b$  changes from slightly positive (electrostatic) to negative (covalent), indicating that an increase in the strength of the ChB tend to be accompanied by an increase in its covalent character, given by a more negative  $H_b$  according to Cremer–Kraka criteria.<sup>126</sup> A comparison of the  $n(EA)$  values of complexes where E = S, Se and Te (Table 2) confirms that the ChB becomes stronger with the increase in the polarizability of the chalcogen atom ( $S < Se < Te$ ) for the entire set (a similar trend is not always found for XB<sup>97,98</sup>).

In the following section, rather than discussing each complex individually, we describe the most important electronic effects present in each group (I–IV), which are responsible for the ChB strength trends shown in the  $k^a(EA)$  vs  $n(EA)$  power relationship diagrams. Some representative complexes, and complexes that deviate from the expected trends are discussed individually.

**ChB Strength Dependence on the Ch Acceptors.** The ChB strength ordering of the chalcogen-chalcogen interactions in F(H)E...E'H<sub>2</sub> (complexes 1–12), shown on Figure 5a can be rationalized by considering two major electronic effects with opposing impact on the ChB strength. (i) Descending within

Table 4. Summary of Chalcogen Donor Properties<sup>a</sup>

Ch donors	$r(\text{XE})$	$k^s(\text{XE})$	$n(\text{XE})$	NBO(E)	$V(r)_{\text{max}}$	$\alpha_{\text{iso}}$
F <sub>3</sub> C(H)Se	1.961	2.598	0.697	0.051	1.29	44.7
F <sub>3</sub> C(H)Te	2.176	2.144	0.615	0.235	1.50	57.3
F <sub>2</sub> N(H)S	1.754	2.635	0.704	0.183	1.56	36.6
F <sub>2</sub> N(H)Se	1.914	2.215	0.628	0.274	1.69	43.8
F <sub>2</sub> N(H)Te	2.124	1.839	0.556	0.456	1.90	56.5
FO(H)S	1.606	3.386	0.830	0.437	1.81	32.5
FO(H)Se	1.774	3.144	0.790	0.486	2.02	38.2
FO(H)Te	1.971	2.811	0.734	0.653	2.25	49.4
F(H)S	1.626	4.605	1.016	0.393	1.75	24.0
F(H)Se	1.759	3.993	0.925	0.503	2.14	30.2
F(H)Te	1.926	3.652	0.872	0.691	2.40	41.4
F(CH <sub>3</sub> )S	1.633	4.404	0.986	0.586	1.25	36.2
F(CH <sub>3</sub> )Se( <i>anti</i> )	1.766	3.795	0.895	0.687	1.74	42.7
F(CH <sub>3</sub> )Se( <i>syn</i> )	1.768	3.872	0.906	0.677	1.81	42.6
F(CH <sub>3</sub> )Te	1.935	3.544	0.855	0.854	2.13	54.3
F(CF <sub>2</sub> H)S	1.616	4.747	1.036	0.588	1.98	37.5
F(CF <sub>2</sub> H)Se( <i>anti</i> )	1.751	4.128	0.945	0.671	2.43	44.0
F(CF <sub>2</sub> H)Se( <i>syn</i> )	1.760	4.036	0.931	0.665	2.75	43.9
F(CF <sub>2</sub> H)Te	1.920	3.711	0.881	0.831	2.71	55.6
F(CF <sub>3</sub> )Se( <i>anti</i> )	1.750	4.221	0.959	0.673	1.94	44.2
F(CF <sub>3</sub> )Se( <i>syn</i> )	1.747	4.265	0.966	1.066	2.49	44.4
F <sub>2</sub> S	1.600	4.922	1.061	0.937	1.58	23.7
F <sub>2</sub> Se	1.734	4.378	0.983	1.053	2.11	29.2
F <sub>2</sub> Te	1.905	3.821	0.899	1.223	2.42	39.0
F(CN)S	1.614	4.636	1.020	0.735	1.95	37.8
F(CN)Se	1.746	4.141	0.947	0.849	2.44	43.4
F(CN)Te	1.912	3.767	0.890	1.036	2.72	53.8
F <sub>2</sub> CS	1.595	6.736	1.304	-0.028	0.51	35.5
F <sub>2</sub> CSe	1.743	5.316	1.116	0.017	0.87	43.3
F <sub>2</sub> CTe	1.967	3.837	0.901	0.098	1.15	58.1
OCS	1.564	7.514	1.401	0.003	0.82	34.1
OCSe	1.711	5.545	1.148	0.041	1.21	41.8
OCTe	1.938	3.973	0.922	0.103	1.48	56.4
FNS	1.540	7.168	1.358	0.406	1.23	31.2
FNSE	1.694	5.601	1.155	0.452	1.40	38.1
FNTe	1.909	4.472	0.996	0.551	1.50	51.1
H <sub>2</sub> C <sub>2</sub> N <sub>2</sub> Se	1.788	3.261	0.810	0.885	1.08	60.2
H <sub>2</sub> C <sub>2</sub> N <sub>2</sub> Te	1.993	2.631	0.703	1.004	1.30	73.6
F <sub>2</sub> C <sub>2</sub> N <sub>2</sub> Te	2.002	2.733	0.721	1.042	1.87	72.9
Me <sub>2</sub> C <sub>2</sub> N <sub>2</sub> Te	1.994	2.715	0.718	0.976	1.09	101.3
H <sub>3</sub> S <sup>+</sup>	1.356	3.973	0.922	0.292	7.29	17.7
FH <sub>2</sub> S <sup>+</sup>	1.553	5.819	1.184	1.021	8.66	18.5
FH <sub>2</sub> Se <sup>+</sup>	1.692	5.387	1.126	1.200	8.66	23.2
FH <sub>2</sub> Te <sup>+</sup>	1.861	4.806	1.045	1.538	8.53	31.0
FH(CN)S <sup>+</sup>	1.551	5.610	1.156	1.250	8.28	32.9

<sup>a</sup>Computed at  $\omega$ B97X-D/aug-cc-pVTZ (PP for Se As and Te). Bond distances  $r(\text{XE})$  in Å, local YX stretching force constant  $k^s(\text{XE})$  in mdyn/Å, and bond strength order  $n$ . NBO charges at E, maximum electrostatic potential at the  $\sigma$ -hole of E ( $V_{\text{max}}$ ) in kcal/mol, isotropic polarizability in Bohr<sup>3</sup>, and total dipole moment in Debye.

group XVI of the PT from A = O, S, Se, Te for AH<sub>2</sub> Ch acceptors, the lp(A) orbitals at AH<sub>2</sub> become increasingly diffuse, due to the higher number of occupied electron shells, leading to a decrease in the magnitude of the electrostatic potential ( $V_{\text{min}} = -1.43$  (OH<sub>2</sub>)  $\ll$   $-0.74$  (SH<sub>2</sub>)  $<$   $-0.67$  (SeH<sub>2</sub>)  $<$   $-0.57$  (TeH<sub>2</sub>) eV). (ii) Another consequence of the higher number of occupied electron shells is the decrease in the electronegativity of A atom (Pauling scale:  $\chi = 3.44$  (O); 2.58 (S); 2.55 (Se); 2.10 (Te)) resulting in lp(A) orbitals, which are higher in energy (lower IP, Table 3, thus decreased  $\Delta\epsilon(2e)$ ) allowing a stronger CT (e.g.,  $\Delta E(\text{del}) = 32.1$  (12) compared to

16.5 (3) kcal/mol). Complexes formed with OH<sub>2</sub> Ch acceptor (1–3) have the strongest ChBs among complexes 1–12 ( $n(\text{EA}) = 0.123$  (1), 0.136 (2), 0.151 (3) and  $\Delta E = 5.1$  (1), 6.5 (2), 7.7 (3) kcal/mol), indicating that the decrease in the magnitude of  $V_{\text{min}}$  descending within a period has a stronger effect on the bond strength over the increase of CT.

A decrease in the electronegativity of the Ch acceptor atom (A) does not necessarily weaken the electrostatic contributions. Figure 5a shows the strength ordering of ChB involving FHE (E = S, Se and Te) Ch donors and Ch acceptors across the second period of the PT (HF, OH<sub>2</sub>, NH<sub>3</sub>). There is an increase

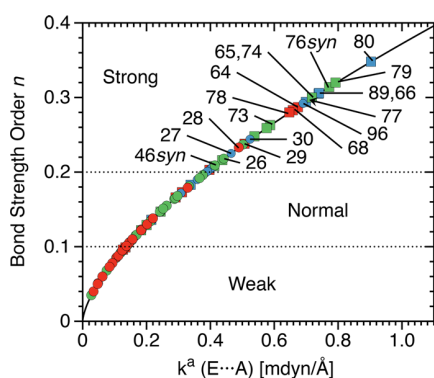


**Figure 3.** Power relationship between the relative bond strength order (BSO)  $n$  and the local stretching force constants  $k^a$  of complexes 1–100. S...A ChB are shown in red, Se...A in green, and Te...A in blue for neutral complexes (circles) and charged complexes (squares).

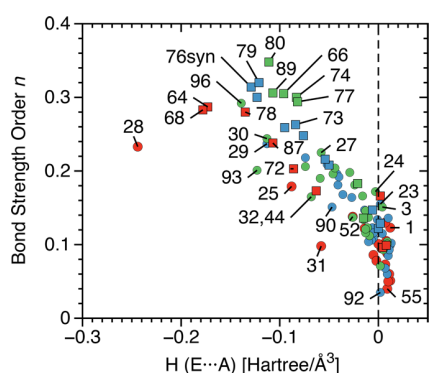


**Figure 4.** Comparison between the relative bond strength order (BSO)  $n$  and the energy density at the bond critical point  $H_b$  of the ChBs of complexes 1–100. S...A ChB are shown in red, Se...A in green, and Te...A in blue for neutral complexes (circles) and charged complexes (squares).

in the BSO from HF, to OH<sub>2</sub> and NH<sub>3</sub> (e.g., in this series the BSO for F(H)Te is  $n(EA) = 0.104$  (15), 0.151 (3), 0.198 (18)), which is supported by both an increase in CT (Table 2) and a lowering of  $V_{min}$  (−0.90 (HF); −1.43 (OH<sub>2</sub>); −1.63 (NH<sub>3</sub> eV). The decrease in the electronegativity of A (Pauling scale:  $\chi = 3.98$  (F); 3.44 (O); 3.04 (N)) leads to a less contracted but still localized lp(A), which has a lower  $V_{min}$  (Table 3) and a higher lp(A) energy (Figure S1).

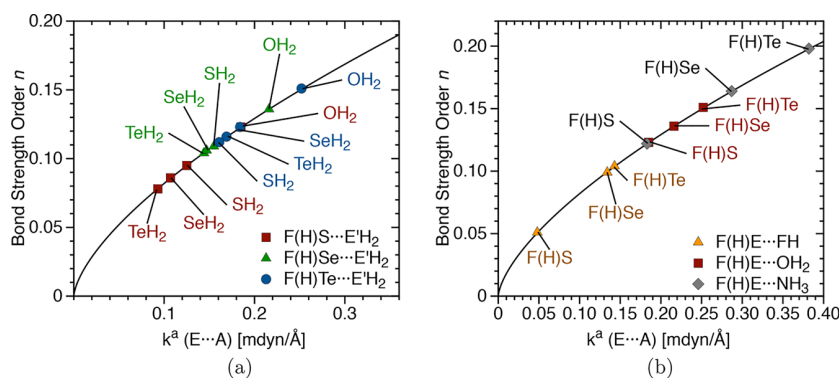
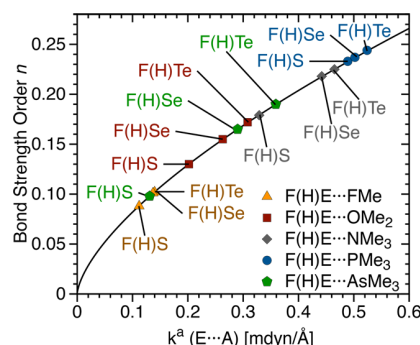


**Figure 5.** Power relationship between the relative bond strength order (BSO)  $n$  and the local stretching force constants  $k^a$  for (a) chalcogen–chalcogen interactions and (b) interactions between a chalcogen and a second period heteroatom.

Methyl substituents at the Ch acceptor strengthen the ChB by increasing the polarizability of the Ch acceptor and by decreasing the lp(A) energy (which result in a decrease of  $\Delta\epsilon(2e)$ ). In the case of the heteroatoms of third or higher periods, which are less electronegative than C (Pauling scale:  $\chi(A) = 2.55$  (C); 2.19 (P); 2.18 (As)), Me substituents withdraw charge from A (NPA partial atomic charge  $P = 0.761$  e in PMe<sub>3</sub> and As = 0.801 e in AsMe<sub>3</sub>), effectively contracting the density at lp(A). The more localized lp(A) forms a better overlap with  $\sigma^*(XE)$  and adopts a more negative electrostatic potential at lp(A) ( $V_{min} = -1.25$  (PMe<sub>3</sub>), −0.95 (AsMe<sub>3</sub>) compared to −0.73 (PH<sub>3</sub>), and −0.46 (AsH<sub>3</sub>) eV).

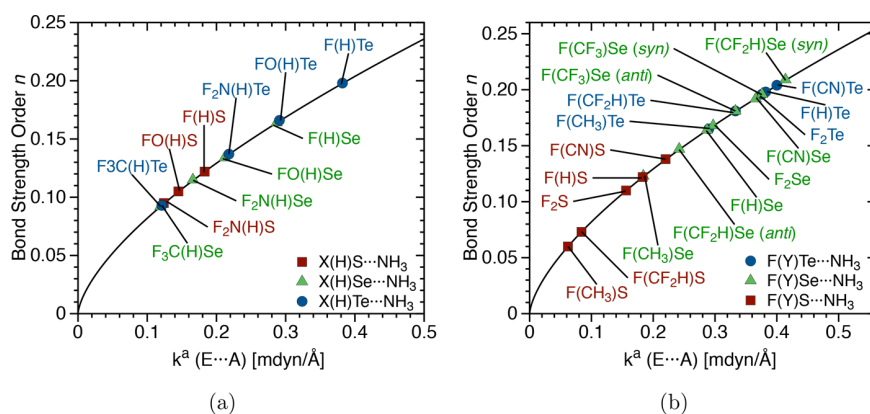
A similar effect is also found for XB complexes.<sup>75,97</sup> and is responsible for the formation of complete 3c–4e bonds, inverse 3c–4e bonds and ion-pairs between dihalogens, interhalogens and phosphines. However, comparable ChB complexes have lower CT and 3c–4e character (with a maximum 3c–4e character of 56% (28) for the neutral complexes). The reduced CT and 3c–4e character in ChB is due to the lower electronegativity of the chalcogens, resulting in higher  $\sigma^*$ -orbital energies thus larger  $\Delta\epsilon(2e)$  and also due to the less effective lp(A)– $\sigma^*$  overlap caused by the bent X–E–A geometry adopted by chalcogens to reduce the exchange-repulsion between lp(E) and lp(A) orbitals.

Figure 6 provides the ChB strength order for the complexes with methylated Ch acceptors (19–33). ChB complexes



**Figure 6.** Power relationship between the relative bond strength order (BSO)  $n$  and the local stretching force constants  $k^a$  for complexes involving a series of methylated Ch acceptors.

involving methylated Ch acceptors of the second period (19–27) form stronger bonds (compared to OH<sub>2</sub> (1–3), FH



**Figure 7.** Power relationship between the relative bond strength order (BSO)  $n$  and the local stretching force constants  $k^d$  for complexes involving  $\text{NH}_3$ : (a) with different substituents (X) colinear to the ChB and (b) with different substituents at Y position.

(16–18), and  $\text{NH}_3$  (16–18) Ch acceptors) but the strength order with regard to the A is not altered ( $\text{FMe} < \text{OMe}_2 < \text{NMe}_3$ ). The increase in strength occurs due to the increased CT in these complexes, which compensates the weaker electrostatic contribution ( $V_{\min} = -1.34 \text{ NMe}_3$ ,  $-1.34 \text{ OMe}_2$  compared to  $-1.63 \text{ NH}_3$ , and  $-1.43 \text{ OH}_2$ ). Descending within group XV of the PT (complexes 27–33), there is an increase in the ChB strength ( $\text{NMe}_3 < \text{PMe}_3$ ) followed by a decrease ( $\text{PMe}_3 > \text{AsMe}_3$ ). The decrease is a result of the contracted (less diffuse) lp(P), which is more available than lp(N) (Figures S1 and S3), leading to a stronger CT (CT = 0.415 (28), 0.329 (29), 0.259 (30) compared to 0.141 (25), 0.133 (26), and 0.114 e (27)) and which has only a slightly higher electrostatic potential ( $V_{\min} = -1.25 \text{ (PMe}_3)$ ;  $-1.34 \text{ (NMe}_3)$  eV), whereas the increase is a result of the increased diffuseness of lp(As) compared to lp(P), which decreases CT and increases  $V_{\min}$  ( $-1.25 \text{ (PMe}_3)$   $-0.95 \text{ (AsMe}_3)$  eV).

**ChB Dependence on Ch Donors.** Figure 7 shows the effect of different substituents at the X position (Figure 7a), and at the Y position, (Figure 7b), whereas Figure 8 shows the electron difference densities of selenium complexes for different Y substituents. The ChB bond becomes stronger when the most electronegative ligand (X) is arranged in a close to a collinear position to the ChB (in general  $\text{X-E-A} \approx 170^\circ$ ; Figures S9–S12). A more electronegative substituent ( $\text{X} = \text{F}_3\text{C} < \text{F}_2\text{N} < \text{FO} < \text{F}$ ) increases the CT by lowering the  $\sigma^*(\text{XE})$  orbital energies (Figure S2, decreasing  $\Delta\epsilon(2e)$ ), and by polarizing the chalcogen electron density leading to the formation of a more positive potential at the  $\sigma$ -hole region ( $V_{\max} = 1.29 \text{ (F}_3\text{C(H)Se)}$ ;  $1.56 \text{ (F}_2\text{N(H)Se)}$ ;  $1.56 \text{ (FO(H)Se)}$ ;  $2.14 \text{ (F(H)Se)}$  eV). The ligand Y, orthogonal to the ChB, plays a more subtle role, indirectly influencing the  $\sigma^*(\text{XE})$  orbital energy (Figure S2), the magnitude of the  $\sigma$ -hole electrostatic potential (Figure S4), and also via exchange repulsion with lp(A).

For the Y substituent, the ChB strength increases in the series  $\text{Y} = \text{CH}_3 < \text{CF}_2\text{H} < \text{F} \approx \text{H} < \text{CF}_3 < \text{CN}$ , where methyl substituents weaken the ChB by donating charge to the chalcogen (E), increasing the  $\sigma^*(\text{XE})$  orbital energy (Figure S2) and decreasing  $V_{\max}$  (Table 4). This can be reverted by substituting the hydrogens for fluorine atoms ( $\text{Y} = \text{CF}_2\text{H}$  and  $\text{CF}_3$ ). By this, the group electronegativity increases, and the  $\sigma^*(\text{XE})$  energy is lowered, enhancing charge transfer and strengthening the ChB. The CN group withdraws charge more effectively from the lone pairs of the chalcogen via  $\text{lp}(\text{E}) \rightarrow \pi^*$

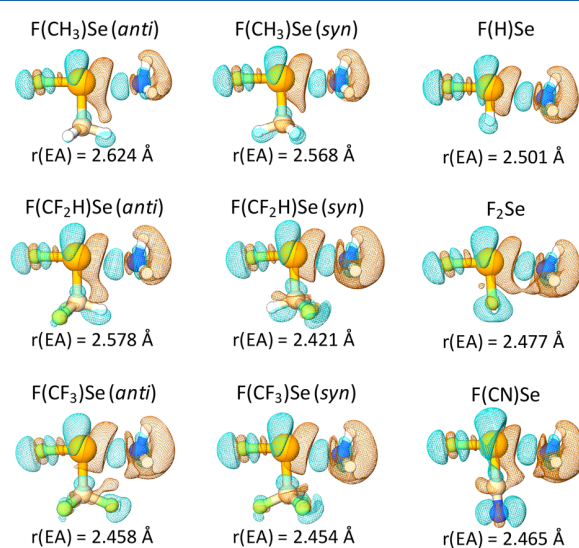


**Figure 8.** Electron difference density distributions  $\Delta\rho(r)$  given for  $\text{F(Y)Se}\cdots\text{NH}_3$  complexes.  $\Delta\rho(r)$  is plotted for an electron density surface of 0.001 au. Light blue regions indicate an increase in the electron density, and brown regions a density decrease relative to the superimposed density of the monomers. Calculated at  $\omega\text{B97X-D/aug-cc-pVTZ}$ .

charge transfer increasing  $V_{\max}$  ( $V_{\max} = 2.44 \text{ eV}$  in  $\text{F(CN)Se}$  compared to  $2.14 \text{ eV}$  in  $\text{F(H)Se}$ ) and lowering the  $\sigma^*(\text{XE})$  orbital energy (Figure S2). Although the  $\text{Y} = \text{F}$  substituent in  $\text{F}_2\text{E}$  withdraws charge from the chalcogen, it donates electron density back via  $\text{lp}(\text{F}) \rightarrow \sigma^*(\text{XE})$  ( $\Delta E(\text{del}) = 14.3 \text{ kcal/mol}$ ), lowering  $V_{\max}$  ( $V_{\max} = 2.11 \text{ eV}$  ( $\text{F}_2\text{Se}$ ) compared to  $2.14 \text{ eV}$  ( $\text{F(H)Se}$ )).

Exchange repulsion between lp(A) and Y weakens the ChB. This is evidenced in the electron difference densities of Figure 8 by a decrease of the electron density between Y and A (in brown) and by an electron density increase in the inferior extremity of Y (in light blue). If the Y group is rotated by  $180^\circ$  to the *syn* position, where the H (43, 46) or F (48) atom at the molecular plane is not facing toward the Ch acceptor atom (A), the extension of the brown region decreases and the ChB becomes shorter and stronger ( $n(\text{EA}) = 0.147$  (43 *syn*), 0.209 (46 *syn*), 0.196 (48 *syn*) compared to 0.123 (43 *anti*), 0.147 (46 *anti*), and 0.181 (48 *anti*)).

The SAPTO energy decomposition analysis (Table S4) confirms the important role of exchange repulsion for complex stabilization. By keeping the geometries of complexes **43**, **46**, and **48** frozen and rotating  $Y = \text{CH}_3$ ,  $\text{CF}_2\text{H}$ , and  $\text{CF}_3$  in  $\text{F}(Y)\text{Se}\cdots\text{NH}_3$  from the *anti* conformation to the *syn* position, the largest change in the interaction energy components occur for exchange repulsion, which decreases by 1.1 (**43**), 1.4 (**46**), and 2.4 (**48**) kcal/mol (see Supporting Information for other components).

**ChB in  $\text{sp}^2$  Hybridized Chalcogens.** ChB involving  $\text{sp}^2$ -hybridized chalcogens represents a special case, where electrostatic and charge transfer contributions are maximized for different geometries. Similar to the divalent ChB complexes, the electrostatic contribution in the  $\text{sp}^2$  chalcogens is maximized for the collinear geometry ( $X-E\cdots A = 180^\circ$ ), where  $V_{\text{min}}$  at  $\text{lp}(A)$  points toward  $V_{\text{max}}$  at the  $\sigma$ -hole region of E (Figure S4). However, due to the presence of an empty  $\pi^*(\text{EX})$  orbital (LUMO; Figure S4) lying lower in energy than the  $\sigma^*(\text{EX})$  (LUMO+1), a stronger  $\text{lp}(A)$  to  $\pi^*(\text{EX})$  CT can take place. This CT mechanism is maximized when  $\text{lp}(A)$  lays on top of the plane containing the Ch donor, close to a  $X-E\cdots A$  right-angle. The geometry of  $\text{F}_2\text{CE}\cdots\text{NH}_3$  (**55–57**) and  $\text{OCE}\cdots\text{NH}_3$  (**58–60**) are determined by the electrostatic contribution. These complexes are characterized by a linear  $X-E\cdots A$  geometry, weak ChBs ( $n(EA) < 0.1$ ), and small CT values ( $\text{CT} < 0.040$ ). On the other hand, the geometries of  $\text{FNE}\cdots\text{NH}_3$  (**61–63**) are determined by covalent contributions, characterized by stronger ChBs ( $n(EA) > 0.1$ ) bent geometry  $X-E-A < 120^\circ$  with larger CT values ( $\text{CT} > 0.080$ ) and  $H_b < 0$ . The stronger covalent character of **61–63** is due to the higher electronegativity of N compared to C, which lowers the  $\pi^*(\text{EX})$  orbital allowing a stronger  $\text{lp}(A) \rightarrow \sigma^*(\text{EX})$  CT to occur. Interesting to notice is that the  $\sigma$ -hole region in  $\text{FNE}$  is more strongly stretched in the  $\pi$  direction compared to  $\text{F}_2\text{CE}$  and  $\text{OCE}$  (Figure S2). Zhang, Ma, and Wang<sup>85</sup> found similar complexes, involving charge assisted XBs, where the geometries were not determined by the  $\sigma$ -hole position but by the charge transfer from  $\text{lp}(A) \rightarrow \pi^*(X-\text{Cl})$ . Here we show that this type of charge transfer mechanism can play a major role in the geometry of  $\text{sp}^2$ -hybridized ChB even for neutral complexes.

**Charge Assisted ChB.** The strongest ChBs found in the present study are realized for the charged complexes involving a cationic Ch donor ( $n(EA) = 0.305$  for **66** with  $\Delta E = 37.6$  kcal/mol) or an anionic Ch acceptor ( $n(EA) = 0.348$  for **80** with  $\Delta E = 47.5$  kcal/mol), with both, electrostatic and covalent contributions being magnified. For the cationic complexes, a more polarizable chalcogen ( $\text{S} < \text{Se} < \text{Te}$ ) does not lead to a significant change in the ChB strength ( $n(EA) = 0.287$  (**64**),  $0.300$  (**65**),  $0.305$  (**66**) or  $\Delta E = 36.9$  (**64**),  $37.5$  (**65**),  $37.6$  (**66**)), whereas an electronegative ligand F collinear to the ChB still play an important role ( $n(EA) = 0.287$  (**64**) compared to  $n(EA) = 0.166$  (**67**)). Different from the neutral complexes, the ChB strength in **68** is not enhanced by the addition of a CN substituent ( $n(EA) = 0.283$  (**68**)).

Figure 9 gives the relative ChBs strength of a series of charged complexes formed with chloride. These ChBs are stronger than the ones found for  $\text{NH}_3$ , but still have similar strength trends with regard to the chalcogen ( $\text{E} = \text{S} < \text{Se} < \text{Te}$ ), and the substituents ( $X = \text{F}_3\text{C} < \text{F}_2\text{N} < \text{FO} < \text{F}$  and  $Y = \text{CF}_2\text{H}$  *anti* <  $\text{CF}_2\text{H}$  *syn* <  $\text{CN}$ ).

Notable is that not only  $\text{FNE}\cdots\text{Cl}^-$  but also  $\text{F}_2\text{CE}\cdots\text{Cl}^-$  complexes adopt a geometry of minimum energy with the  $\text{C}-\text{E}-\text{Cl}$  angle bent in the direction orthogonal to the plane

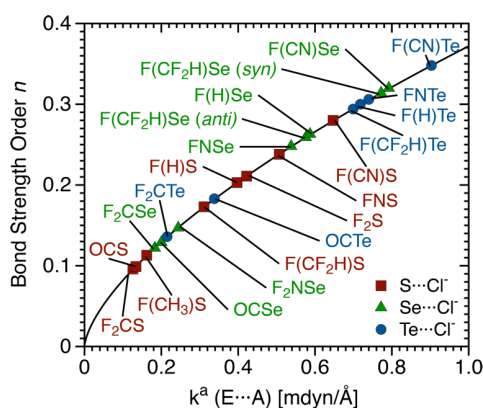


**Figure 9.** Power relationship between the relative bond strength order (BSO)  $n$  and the local stretching force constants  $k^a$  for complexes involving  $\text{Cl}^-$  and various Ch donors.

containing the Ch donor ( $\text{C}-\text{E}-\text{Cl}$  angle =  $125.3^\circ$  (**81**),  $142.4^\circ$  (**82**),  $158.1^\circ$  (**83**)), maximizing the  $\text{lp}(\text{Cl}) \rightarrow \pi^*(\text{CE})$  charge transfer in detriment of the electrostatic interaction with the  $\sigma$ -hole collinear to the  $\text{C}-\text{E}$  bond (Figure S2).

**ChB in Homodimers.** In the symmetric homodimer complexes (**90–100**) both monomers are Ch donors and Ch acceptors. However, in **90–93** the chalcogen atoms involved donates and accepts electron density simultaneously, whereas complexes **94–100** form multiple ChBs. In the first case (**90–93**), two different types of bonding mechanisms are possible (i) the charge transfer can occur from the  $\text{lp}(\text{E})$  orbital to the  $\sigma^*(\text{EF})$  antibonding orbital (**90**, **91**) or (ii) the charge transfer can occur from the  $\text{lp}(\text{E})$  to the  $\pi^*(\text{EN})$  antibonding orbital (**92**, **93**). In both cases a skewed conformation is adopted to minimize  $\text{lp}(\text{E})-\text{lp}(\text{E})$  repulsion between the monomers. Figure 10 shows the orbitals involved in the CT mechanism (Figure

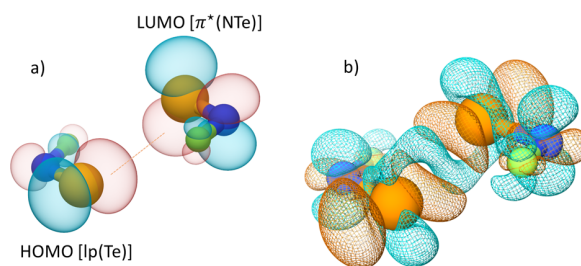


**Figure 10.** (a) Frontier molecular orbitals of  $\text{FNTe}_2$ , and (b) electron difference density distributions  $\Delta\rho(r)$  of  $\text{FNTe}_2$ .  $\Delta\rho(r)$  is plotted for an electron density surface of  $0.001$  au. Light blue regions indicate an increase in the electron density and brown regions a density decrease relative to the superimposed density of the monomers.

10a) and the electron difference density distribution (Figure 10b) for complex **93** ( $\text{FNTe}_2$ ). The CT from  $\text{lp}(\text{E})$  to  $\pi^*(\text{NTe})$  and the  $\text{lp}(\text{Te})-\text{lp}(\text{Te})$  repulsion result in a density increase in the intermonomer region (light blue region between Te atoms in Figure 10) and a density depletion close to the Te atoms (large brown region close to Te atoms in Figure 10). To the best of our knowledge this is the first ChB homodimer found, where both monomers donate and accept charge via a  $\text{lp}(\text{E}) \rightarrow \pi^*(\text{EF})$  CT mechanism. This unusual new type of interaction may lead to novel supramolecular materials with unique geometric and electronic features. The possibility of

similar interactions of this kind involving PnB is currently being investigated.

Figure 11 provides the ChB strength order for all symmetric homodimers 90–100. Although the selenium complex of type

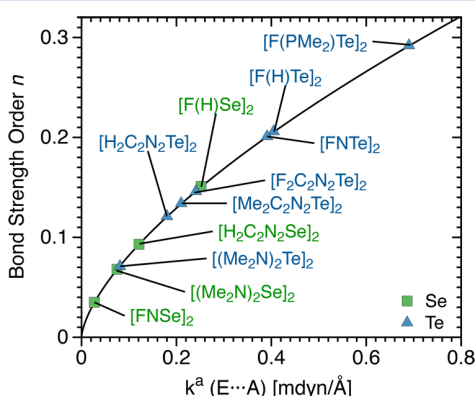


**Figure 11.** Power relationship between the relative bond strength order (BSO)  $n$  and the local stretching force constants  $k^a$  for the symmetric homodimers complexes.

ii (92) is much weaker than type i (90) ( $n(EA) = 0.151(90)$  and  $0.035(92)$ ), the tellurium complexes are of similar strength ( $n(EA) = 0.206(91)$ ;  $0.201(93)$ ). Experimental studies reveal that complex 94 is a liquid, whereas 95 forms a highly reactive polymeric solid.<sup>141</sup> Both complexes have weak ChBs ( $n(EA) = 0.068(94)$ ;  $0.071(95)$ ;  $\Delta E = 4.7(94)$   $9.8(95)$ ). The ChBs in 95 can be strengthened by substituting the NMe<sub>2</sub> groups collinear to the ChB by F atoms and the nitrogen Ch acceptor atoms with phosphorus, leading to (F(PMe<sub>2</sub>)Te)<sub>2</sub> (96). This complex has a strong ChB ( $n(EA) = 0.292$ ) and the highest binding energy among the neutral complexes ( $\Delta E = 28.0$  kcal/mol). However, 95 would form dimers, but not polymeric structures, due to the weak electron donor ability of the F atoms.

Better starting units forming relatively strong ChBs and polymeric structures are the seleno- and telluradiazoles (97–100), where 1,2,5-telluradiazole dimers have stronger ChBs ( $n(EA) = 0.121(98)$  compared to  $0.093(97)$ ). Although the difference between the BSO  $n(EA)$  values of these complexes are relatively small, the increase in  $\Delta E$  brought by the stronger ChBs in (98) is considerably large ( $\Delta E = 13.6(98)$ ;  $6.3(97)$  kcal/mol). Noteworthy is that both electron withdrawing (F) and electron donor (CH<sub>3</sub>) substituents slightly enhance the strength of the ChB in telluradiazoles ( $n(EA) = 0.146(99)$   $0.134(100)$  compared to  $0.121(98)$ ). The F substituents increase the electrostatic potential at the Te ( $V_{max} = 1.87$  for F<sub>2</sub>C<sub>2</sub>N<sub>2</sub>Te compared to  $1.30$  eV for H<sub>2</sub>C<sub>2</sub>N<sub>2</sub>Te) whereas the Me substituents strengthen the ChBs by increasing the polarizability of the monomers ( $\alpha_{iso} = 101.3$  for Me<sub>2</sub>C<sub>2</sub>N<sub>2</sub>Te compared to  $73.6$  Bohr<sup>3</sup> for H<sub>2</sub>C<sub>2</sub>N<sub>2</sub>Te). A possible strategy to form strong polymeric structures based on ChBs is to increase the number of ChB contacts between monomers by fusing suitable ring structures to the telluradiazole monomers (increasing also its polarizability).

#### 4. CONCLUSIONS AND OUTLOOK

In this work, we present for the first time a quantitative analysis of the intrinsic strength of 100 ChB based on the local stretching force constant and associated BSO, complemented

by the analysis of binding energies, SAPT energy contributions, NBO charges, electrostatic potentials, isotropic polarizabilities, electron and energy density distributions, and difference density distributions. The following conclusions were obtained:

- 1 The ChB mechanism is composed of both, a covalent and an electrostatic part. The electrostatic part can be rationalized on the basis of the electrostatic potential of the Ch donors and the Ch acceptors, whereas the covalent part is associated with two different CT mechanisms. In divalent chalcogens, the CT is associated with  $lp(A)$  to  $\sigma^*(XE)$  delocalization, whereas in double bonded chalcogens it is associated with  $lp(A)$  to  $\pi^*(XE)$  delocalization. The latter CT mechanism can lead to the formation of strongly bent ChB complexes, which cannot be predicted by the inspection of the electrostatic potential of the monomers.
- 2 Based on BSO  $n$  values, we can identify three different classes of ChBs: weak ChBs ( $n(EA) < 0.1$ ), normal ChBs ( $0.1 < n(EA) < 0.2$ ), and strong ChBs ( $n(EA) > 0.2$ ). The strongest neutral ChB found (96) has an  $n(EA)$  value of  $0.292$  ( $\Delta E = 28.0$  kcal/mol), whereas charge assisted ChBs reach values up to  $n(EA) = 0.348$  ( $\Delta E = 47.5$  kcal/mol) (80). The increase in the ChB strength is typically accompanied by a gradual increase in covalent character. Weak ChBs are dominated by electrostatic contributions and are characterized by  $H_b \geq 0$ , whereas all strong ChB are characterized by  $H_b < 0$ , which, according to the Cremer–Kraka criteria, indicates a dominant covalent character.
- 3 The ChB strength depends on the polarizability of the chalcogen atom ( $S < Se < Te$ ), the electronegativity of the Ch donor substituent collinear to the ChB ( $CF_3 < NF_2 < OF < F$ ), the electron withdrawing capability of the Ch donor substituent Y orthogonal to the ChB, and a small exchange–repulsion between  $lp(A)$  and the Y substituent (e.g., if Y = CF<sub>3</sub> is rotated to a *syn* conformation, where the F atom in the mirror plane of the complex is moved away from  $lp(A)$  there is an increase in the ChB strength).
- 4 The Ch acceptor also exerts a strong influence on the strength of the ChB. For a given period of the PT, the decrease in the electronegativity of the Ch acceptor atom A leads to an increase in the ChB strength due to the higher donor ability of  $lp(A)$  and decreased electrostatic potential. Descending within a group of the PT the ChB becomes weaker due to the increased diffuseness of  $lp(A)$ . Strong ChB involving heteroatoms of lower periods can be envisioned by adding substituents that effectively contract  $lp(A)$  (e.g., PMe<sub>3</sub>).
- 5 3c–4e character of chalcogen bonds can play an important role in strong ChB complexes, reaching up to 56% for the neutral complex 28 and 69% for the charged assisted complex 76 *syn*. However, these values are considerably lower than the ones found for halogen bonds.<sup>75,97,98</sup> CT and 3c–4e character in ChBs are reduced (in comparison with XB) due to the lower electronegativity of chalcogens compared to the halogens (resulting in  $\sigma^*(XE)$  orbitals of higher energy thus a larger  $\Delta\epsilon(2e)$  energy gap) and due to the bent conformation adopted by chalcogen complexes (resulting in a less effective overlap between  $lp(A)$  and  $\sigma^*(XE)$  orbitals).

- 6 Multiple ChBs in homodimers (94–100) can result in an extra stabilization. For example complex 96 has a  $\Delta E = 28.0$  kcal/mol, comparable to the strongest neutral XB complexes previously studied<sup>75,97,98</sup> and stronger than that of neutral hydrogen bonds<sup>142</sup> and pnictogen bonds in general.<sup>129</sup>
- 7 We describe for the first time a symmetric homodimer, where both monomers donate charge from lp(A) to  $\pi^*(XE)$  simultaneously. This new type of interaction may lead to the development of polymers with unique architecture and electronic properties.
- 8 New polymeric structures based on ChB should focus on molecules that can make multiple ChB contacts such as 1,2,5-Telluradiazole. The stability of these complexes can be improved by fusing rings to increase the polarizability and the number of possible ChB between the monomers.

By rationalizing the intrinsic strength of an extensive set of 100 ChBs on the basis of the analysis of the essential electronic effects and their interplay with the covalent and electrostatic contributions, we provide a concise description of the ChB, which is of general applicability and may serve as the basis for the design of larger and more complex ChB structures.

## ■ ASSOCIATED CONTENT

### ■ Supporting Information

This material is available free of charge via the Internet at The Supporting Information is available free of charge on the ACS Publications website at DOI: 10.1021/acs.jpca.7b06479.

Binding energies ( $\Delta E$ ), ChB distances  $r(EA)$ , and ChB force constants  $k^a(EA)$  for 12 complexes calculated using CCSD(T), MP2, and 3 DFTs (Tables S1–S3), SAPT0 energy component for complexes 43, 46, and 48 (Table S4), frontier molecular orbitals, orbital energies, and molecules electrostatic potential for all Ch donors and Ch acceptors (Figures S1–S4), a comparison of the ChB BSO values and  $\Delta E$  (Figure S5), interaction energies (Figure S6), density  $\rho_b(EA)$  (Figure S7) and  $\Delta E(\text{del})$  (Figure S8), schematic representation of complexes and monomers with geometric parameters (Figures S9–S13), and NPA partial atomic charges (Figures S14–S17). (PDF)

## ■ AUTHOR INFORMATION

### Corresponding Author

\*(E.K.) E-mail: ekraka@smu.edu.

### ORCID

Dieter Cremer: 0000-0002-6213-5555

Elfi Kraka: 0000-0002-9658-5626

### Notes

The authors declare no competing financial interest.

†In memoriam.

## ■ ACKNOWLEDGMENTS

This work was financially supported by the National Science Foundation, Grant CHE 1464906. We thank SMU for providing computational resources. The authors acknowledge financial support by CAPES (Brazil Fellowship Grant BEX 9534-13-0).

## ■ REFERENCES

- Alcock, N. W.; Emeleus, H. J.; Sharpe, A. G. Secondary Bonding to Nonmetallic Elements. *Adv. Inorg. Chem. Radiochem.* **1972**, *15*, 1–58.
- Cozzolino, A. F.; Elder, P. J.; Vargas-Baca, I. A survey of tellurium-centered secondary-bonding supramolecular synthons. *Coord. Chem. Rev.* **2011**, *255*, 1426–1438.
- Landrum, G. A.; Hoffmann, R. Secondary bonding between chalcogens or pnictogens and halogens. *Angew. Chem., Int. Ed.* **1998**, *37*, 1887–1890.
- Werz, D. B.; Gleiter, R.; Rominger, F. Nanotube formation favored by chalcogen-chalcogen interactions. *J. Am. Chem. Soc.* **2002**, *124*, 10638–10639.
- Gleiter, R.; Werz, D. B.; Rausch, B. J. A world beyond hydrogen bonds? Chalcogen-chalcogen interactions yielding tubular structures. *Chem. - Eur. J.* **2003**, *9*, 2676–2683.
- Gleiter, R.; Werz, D. B. Elastic cycles as flexible hosts: How tubes built by cyclic chalcogenaalkynes individually host their guests. *Chem. Lett.* **2005**, *34*, 126–131.
- Ho, P. C.; Szydowski, P.; Sinclair, J.; Elder, P. J. W.; Kübel, J.; Gendy, C.; Lee, L. M.; Jenkins, H.; Britten, J. F.; Morim, D. R.; et al. Supramolecular macrocycles reversibly assembled by Te(…)-O chalcogen bonding. *Nat. Commun.* **2016**, *7*, 11299.
- Lim, J. Y. C.; Marques, I.; Thompson, A. L.; Christensen, K. E.; Felix, V.; Beer, P. D. Chalcogen bonding macrocycles and [2]rotaxanes for anion recognition. *J. Am. Chem. Soc.* **2017**, *139*, 3122–3133.
- Allan, R. E.; Gornitzka, H.; Karcher, J.; Paver, M. A.; Rennie, M. A.; Russell, C. A.; Raithby, P. R.; Stalke, D.; Steiner, A.; Wright, D. S. Structure and reactivity of Te(NMe<sub>2</sub>)<sub>2</sub>∞; application to the preparation of metalloorganic tellurium(II) compounds. *J. Chem. Soc., Dalton Trans.* **1996**, 1727–1730.
- Eichstaedt, K.; Wasilewska, A.; Wicher, B.; Gdaniec, M.; Połński, T. Supramolecular synthesis based on a combination of Se…N secondary bonding interactions with hydrogen and halogen bonds. *Cryst. Growth Des.* **2016**, *16*, 1282–1293.
- Pavan, M. S.; Jana, A. K.; Natarajan, S.; Guru Row, T. N. Halogen bonding and chalcogen bonding in 4,7-dibromo-5,6-dinitro-2,1,3-benzothiadiazole. *J. Phys. Chem. B* **2015**, *119*, 11382–11390.
- Kremer, A.; Fermi, A.; Biot, N.; Wouters, J.; Bonifazi, D. Supramolecular wiring of benzo-1,3-chalcogenazoles through programmed chalcogen bonding interactions. *Chem. - Eur. J.* **2016**, *22*, 5665–5675.
- Tsuzuki, S.; Sato, N. Origin of attraction in chalcogen-nitrogen interaction of 1,2,5-chalcogenadiazole dimers. *J. Phys. Chem. B* **2013**, *117*, 6849–6855.
- Pati, P. B.; Zade, S. S. Benzosenadiazole containing donor-acceptor-donor small molecules: Nonbonding interactions, packing patterns, and optoelectronic properties. *Cryst. Growth Des.* **2014**, *14*, 1695–1700.
- Lonchakov, A. V.; Rakitin, O. A.; Gritsan, N. P.; Zibarev, A. V. Breathing some new life into an old topic: Chalcogen-nitrogen  $\pi$ -heterocycles as electron acceptors. *Molecules* **2013**, *18*, 9850–9900.
- Semenov, N. A.; Lonchakov, A. V.; Pushkarevsky, N. A.; Suturina, E. A.; Korolev, V. V.; Lork, E.; Vasiliev, V. G.; Konchenko, S. N.; Beckmann, J.; Gritsan, N. P.; et al. Coordination of halide and chalcogenolate anions to heavier 1,2,5-chalcogenadiazoles: Experiment and theory. *Organometallics* **2014**, *33*, 4302–4314.
- Cozzolino, A. F.; Yang, Q.; Vargas-Baca, I. Engineering second-order nonlinear optical activity by means of a noncentrosymmetric distortion of the [Te-N]<sub>2</sub> supramolecular synthon. *Cryst. Growth Des.* **2010**, *10*, 4959–4964.
- Lindner, B. D.; Coombs, B. A.; Schaffroth, M.; Engelhart, J. U.; Tverskoy, O.; Rominger, F.; Hamburger, M.; Bunz, U. H. F. From thia- to selenadiazoles: Changing interaction priority. *Org. Lett.* **2013**, *15*, 666–669.
- Iwaoka, M.; Takemoto, S.; Okada, M.; Tomoda, S. Weak nonbonded S…X (X = O, N, and S) interactions in proteins. Statistical and theoretical studies. *Bull. Chem. Soc. Jpn.* **2002**, *75*, 1611–1625.

- (20) Iwaoka, M.; Takemoto, S.; Tomoda, S. Statistical and theoretical investigations on the directionality of nonbonded S...O interactions. Implications for molecular design and protein engineering. *J. Am. Chem. Soc.* **2002**, *124*, 10613–10620.
- (21) Manna, D.; Mughesh, G. Regioselective deiodination of thyroxine by iodothyronine deiodinase mimics: An unusual mechanistic pathway involving cooperative chalcogen and halogen bonding. *J. Am. Chem. Soc.* **2012**, *134*, 4269–4279.
- (22) Benz, S.; López-Andarias, J.; Mareda, J.; Sakai, N.; Matile, S. Catalysis with chalcogen bonds. *Angew. Chem., Int. Ed.* **2017**, *56*, 812–815.
- (23) Mughesh, G.; Panda, A.; Kumar, S.; Apte, S. D.; Singh, H. B.; Butcher, R. J. Intramolecularly coordinated diorganyl ditellurides: Thiol peroxidase-like antioxidants. *Organometallics* **2002**, *21*, 884–892.
- (24) Nziko, V. d. P. N.; Scheiner, S. S... $\pi$  chalcogen bonds between SF<sub>2</sub> or SF<sub>4</sub> and C-C multiple bonds. *J. Phys. Chem. A* **2015**, *119*, 5889–5897.
- (25) Benz, S.; Macchione, M.; Verolet, Q.; Mareda, J.; Sakai, N.; Matile, S. Anion transport with chalcogen bonds. *J. Am. Chem. Soc.* **2016**, *138*, 9093–9096.
- (26) Garrett, G. E.; Carrera, E. I.; Seferos, D. S.; Taylor, M. S. Anion recognition by a bidentate chalcogen bond donor. *Chem. Commun.* **2016**, *52*, 9881–9884.
- (27) Scheiner, S. Highly selective halide receptors based on chalcogen, pnicoen, and tetrel Bonds. *Chem. - Eur. J.* **2016**, *22*, 18850–18858.
- (28) Fick, R. J.; Kroner, G. M.; Nepal, B.; Magnani, R.; Horowitz, S.; Houtz, R. L.; Scheiner, S.; Trievel, R. C. Sulfur-oxygen chalcogen bonding mediates AdoMet recognition in the lysine methyltransferase SET7/9. *ACS Chem. Biol.* **2016**, *11*, 748–754.
- (29) Thomas, S. P.; Jayatilaka, D.; Guru Row, T. N. S...O chalcogen bonding in sulfa drugs: Insights from multipole charge density and X-ray wavefunction of acetazolamide. *Phys. Chem. Chem. Phys.* **2015**, *17*, 25411–25420.
- (30) Thomas, S. P.; Satheshkumar, K.; Mughesh, G.; Guru Row, T. N. Unusually short chalcogen bonds involving organoselenium: Insights into the Se-N Bond cleavage mechanism of the antioxidant ebselen and analogues. *Chem. - Eur. J.* **2015**, *21*, 6793–6800.
- (31) Beno, B. R.; Yeung, K.-S.; Bartberger, M. D.; Pennington, L. D.; Meanwell, N. A. A Survey of the role of noncovalent sulfur interactions in drug design. *J. Med. Chem.* **2015**, *58*, 4383–4438.
- (32) Nagao, Y.; Hirata, T.; Goto, S.; Sano, S.; Kakehi, A.; Iizuka, K.; Shiro, M. Intramolecular nonbonded S...O interaction recognized in (acylimino)thiadiazoline derivatives as angiotensin II receptor antagonists and related compounds. *J. Am. Chem. Soc.* **1998**, *120*, 3104–3110.
- (33) Iwaoka, M.; Tomoda, S. Nature of the intramolecular Se...N nonbonded interaction of 2-selenobenzylamine derivatives. An experimental evaluation by <sup>1</sup>H, <sup>77</sup>Se, and <sup>15</sup>N NMR spectroscopy. *J. Am. Chem. Soc.* **1996**, *118*, 8077–8084.
- (34) Iwaoka, M.; Komatsu, H.; Katsuda, T.; Tomoda, S. Quantitative evaluation of weak nonbonded Se...F interactions and their remarkable nature as orbital interactions. *J. Am. Chem. Soc.* **2002**, *124*, 1902–1909.
- (35) Iwaoka, M.; Komatsu, H.; Katsuda, T.; Tomoda, S. Nature of nonbonded Se...O interactions characterized by <sup>17</sup>O NMR spectroscopy and NBO and AIM analyses. *J. Am. Chem. Soc.* **2004**, *126*, 5309–5317.
- (36) Iwaoka, M.; Katsuda, T.; Komatsu, H.; Tomoda, S. Experimental and theoretical studies on the nature of weak nonbonded interactions between divalent selenium and halogen atoms. *J. Org. Chem.* **2005**, *70*, 321–327.
- (37) Rosenfield, R. E.; Parthasarathy, R.; Dunitz, J. D. Directional preferences of nonbonded atomic contacts with divalent sulfur. I. Electrophiles and nucleophiles. *J. Am. Chem. Soc.* **1977**, *99*, 4860–4862.
- (38) Bleiholder, C.; Werz, D. B.; Köppel, H.; Gleiter, R. Theoretical investigations on chalcogen-chalcogen interactions: What makes these nonbonded interactions bonding? *J. Am. Chem. Soc.* **2006**, *128*, 2666–2674.
- (39) Bleiholder, C.; Gleiter, R.; Werz, D. B.; Köppel, H. Theoretical investigations on heteronuclear chalcogen-chalcogen interactions: On the nature of weak bonds between chalcogen centers. *Inorg. Chem.* **2007**, *46*, 2249–2260.
- (40) Azofra, L. M.; Alkorta, I.; Scheiner, S. Chalcogen bonds in complexes of SOXY (X, Y = F, Cl) with nitrogen bases. *J. Phys. Chem. A* **2015**, *119*, 535–541.
- (41) Scheiner, S. Comparison of CH...O, SH...O, chalcogen, and tetrel bonds formed by neutral and cationic sulfur-containing compounds. *J. Phys. Chem. A* **2015**, *119*, 9189–9199.
- (42) Nziko, V. d. P. N.; Scheiner, S. Chalcogen bonding between tetravalent SF<sub>4</sub> and amines. *J. Phys. Chem. A* **2014**, *118*, 10849–10856.
- (43) Esrafil, M. D.; Mohammadian-Sabet, F.  $\sigma$ -Hole bond tunability in YO<sub>2</sub>X<sub>2</sub>:NH<sub>3</sub> and YO<sub>2</sub>X<sub>2</sub>:H<sub>2</sub>O complexes (X = F, Cl, Br; Y = S, Se): Trends and theoretical aspects. *Struct. Chem.* **2016**, *27*, 617–625.
- (44) Esrafil, M. D.; Mohammadian-Sabet, F. An ab initio study on chalcogen-chalcogen bond interactions in cyclic (SHX)<sub>3</sub> complexes (X = F, Cl, CN, NC, CCH, OH, OCH<sub>3</sub>, NH<sub>2</sub>). *Chem. Phys. Lett.* **2015**, *628*, 71–75.
- (45) Esrafil, M. D.; Mohammadian-Sabet, F. Homonuclear chalcogen-chalcogen bond interactions in complexes pairing YO<sub>3</sub> and YHX molecules (Y = S, Se; X = H, Cl, Br, CCH, NC, OH, OCH<sub>3</sub>): Influence of substitution and cooperativity. *Int. J. Quantum Chem.* **2016**, *116*, 529–536.
- (46) Esrafil, M. D.; Nurazar, R. Chalcogen bonds formed through  $\pi$ -holes: SO<sub>3</sub> complexes with nitrogen and phosphorus bases. *Mol. Phys.* **2016**, *114*, 276–282.
- (47) Esrafil, M. D.; Mohammadian-Sabet, F. An ab initio study on cationic chalcogen bond interactions between F<sub>3-n</sub>H<sub>n</sub>S<sup>+</sup> (n = 0–2) and nitrogen bases. *Chem. Phys. Lett.* **2016**, *645*, 32–37.
- (48) Zierkiewicz, W.; Fanfrlik, J.; Hobza, P.; Michalska, D.; Zeegers-Huyskens, T. Ab initio and DFT studies of the interaction between carbonyl and thiocarbonyl groups. The role of S...O chalcogen bonds. *Theor. Chem. Acc.* **2016**, *135*, 217.
- (49) Zhao, Q.; Feng, D.; Sun, Y.; Hao, J.; Cai, Z. Theoretical investigations on the weak chalcogen-bonded complexes with nonbonded C = S...CH<sub>2</sub> interactions: Singlet carbene as an electron donor. *Int. J. Quantum Chem.* **2011**, *111*, 3881–3887.
- (50) Shukla, R.; Chopra, D. Crystallographic and theoretical investigation on the nature and characteristics of type I C-S...S-C interactions. *Cryst. Growth Des.* **2016**, *16*, 6734–6742.
- (51) Khan, I.; Panini, P.; Khan, S. U.-D.; Rana, U. A.; Andleeb, H.; Chopra, D.; Hameed, S.; Simpson, J. Exploiting the role of molecular electrostatic potential, deformation density, topology, and energetics in the characterization of S...N and Cl...N supramolecular motifs in crystalline triazolothiadiazoles. *Cryst. Growth Des.* **2016**, *16*, 1371–1386.
- (52) Nziko, V. d. P. N.; Scheiner, S. Intramolecular S...O chalcogen bond as stabilizing factor in geometry of substituted phenyl-SF<sub>3</sub> molecules. *J. Org. Chem.* **2015**, *80*, 2356–2363.
- (53) Wang, C.; Guan, L.; Danovich, D.; Shaik, S.; Mo, Y. The origins of the directionality of noncovalent intermolecular interactions. *J. Comput. Chem.* **2016**, *37*, 34–45.
- (54) Zhang, X.; Gong, Z.; Li, J.; Lu, T. Intermolecular sulfur...oxygen interactions: Theoretical and statistical investigations. *J. Chem. Inf. Model.* **2015**, *55*, 2138–2153.
- (55) Si, M. K.; Ganguly, B. Computational evidence that hyperconjugative orbital interactions are responsible for the stability of intramolecular Te...O/Te...S non-covalent interactions and comparable to hydrogen bonds in quasi-cyclic systems. *New J. Chem.* **2016**, *40*, 9132–9138.
- (56) Esrafil, M. D.; Mohammadian-Sabet, F. Bifurcated chalcogen bonds: A theoretical study on the structure, strength and bonding properties. *Chem. Phys. Lett.* **2015**, *634*, 210–215.
- (57) Adhikari, U.; Scheiner, S. Effects of charge and substituent on the S...N chalcogen bond. *J. Phys. Chem. A* **2014**, *118*, 3183–3192.
- (58) Esrafil, M. D.; Mohammadian-Sabet, F. Does single-electron chalcogen bond exist? Some theoretical insights. *J. Mol. Model.* **2015**, *21*, 65.

- (59) Esrafilı, M. D.; Mohammadian-Sabet, F. Prediction and characterisation of a chalcogen- $\pi$  interaction with acetylene as a potential electron donor in XHS $\cdots$ HCCH and XHSe $\cdots$ HCCH (X = F, Cl, Br, CN, OH, OCH<sub>3</sub>, NH<sub>2</sub>, CH<sub>3</sub>)  $\sigma$ -hole complexes. *Mol. Phys.* **2015**, *113*, 3559–3566.
- (60) Shukla, R.; Chopra, D. Pnicogen bonds or chalcogen bonds: Exploiting the effect of substitution on the formation of P $\cdots$ Se noncovalent bonds. *Phys. Chem. Chem. Phys.* **2016**, *18*, 13820–13829.
- (61) Haberhauer, G.; Gleiter, R. Double pancake versus long chalcogen-chalcogen bonds in six-membered C,N,S-heterocycles. *Chem. - Eur. J.* **2016**, *22*, 8646–8653.
- (62) Fanfrlik, J.; Prada, A.; Padelkova, Z.; Pecina, A.; Machacek, J.; Lepsik, M.; Holub, J.; Ruzicka, A.; Hnyk, D.; Hobza, P. The dominant role of chalcogen bonding in the crystal packing of 2D/3D aromatics. *Angew. Chem., Int. Ed.* **2014**, *53*, 10139–10142.
- (63) Antonijevic, I. S.; Janjic, G. V.; Milcic, M. K.; Zaric, S. D. Preferred geometries and energies of sulfur-sulfur interactions in crystal structures. *Cryst. Growth Des.* **2016**, *16*, 632–639.
- (64) Politzer, P.; Murray, J. S.; Clark, T. Halogen bonding: An electrostatically-driven highly directional noncovalent interaction. *Phys. Chem. Chem. Phys.* **2010**, *12*, 7748–7757.
- (65) Kolar, M.; Hostas, J.; Hobza, P. The strength and directionality of a halogen bond are co-determined by the magnitude and size of the  $\sigma$ -hole. *Phys. Chem. Chem. Phys.* **2014**, *16*, 9987–9996.
- (66) Grant Hill, J.; Legon, A. C. On the directionality and non-linearity of halogen and hydrogen bonds. *Phys. Chem. Chem. Phys.* **2015**, *17*, 858–867.
- (67) Stone, A. J. Are halogen bonded structures electrostatically driven? *J. Am. Chem. Soc.* **2013**, *135*, 7005–7009.
- (68) Pecina, A.; Lepsik, M.; Hnyk, D.; Hobza, P.; Fanfrlik, J. Chalcogen and pnicogen bonds in complexes of neutral icosahedral and bicapped square-antiprismatic heteroboranes. *J. Phys. Chem. A* **2015**, *119*, 1388–1395.
- (69) Joy, J.; Jose, A.; Jemmis, E. D. Continuum in the X-Z-Y weak bonds: Z = main group elements. *J. Comput. Chem.* **2016**, *37*, 270–279.
- (70) Nepal, B.; Scheiner, S. Long-range behavior of noncovalent bonds. Neutral and charged H-bonds, pnicogen, chalcogen, and halogen bonds. *Chem. Phys.* **2015**, *456*, 34–40.
- (71) Adhikari, U.; Scheiner, S. Substituent effects on Cl $\cdots$ N, S $\cdots$ N, and P $\cdots$ N noncovalent bonds. *J. Phys. Chem. A* **2012**, *116*, 3487–3497.
- (72) Scheiner, S. Detailed comparison of the pnicogen bond with chalcogen, halogen, and hydrogen bonds. *Int. J. Quantum Chem.* **2013**, *113*, 1609–1620.
- (73) Asiabar, B. M.; Esrafilı, M. D.; Mohammadian-Sabet, F.; Sobhi, H. R.; Javaheri, M. An ab initio study on the concerted interaction between chalcogen and pnicogen bonds. *J. Mol. Model.* **2014**, *20*, 2545.
- (74) Esrafilı, M. D.; Akhgarpour, H. An ab initio study on competition between pnicogen and chalcogen bond interactions in binary XHS:PH<sub>2</sub>X complexes (X = F, Cl, CCH, COH, CH<sub>3</sub>, OH, OCH<sub>3</sub>, and NH<sub>2</sub>). *Mol. Phys.* **2016**, *114*, 1847–1855.
- (75) Oliveira, V.; Kraka, E.; Cremer, D. The intrinsic strength of the halogen bond: Electrostatic and covalent contributions described by coupled cluster theory. *Phys. Chem. Chem. Phys.* **2016**, *18*, 33031–33046.
- (76) Fang, Y.; Li, A. Y.; Ma, F. Y. A comparative study of the chalcogen bond, halogen bond and hydrogen bond S $\cdots$ O/Cl/H formed between SHX and HOCl. *J. Mol. Model.* **2015**, *21*, 61.
- (77) Guo, X.; Liu, Y.-W.; Li, Q.-Z.; Li, W.-Z.; Cheng, J.-B. Competition and cooperativity between tetrel bond and chalcogen bond in complexes involving F<sub>2</sub>CX (X = Se and Te). *Chem. Phys. Lett.* **2015**, *620*, 7–12.
- (78) Guo, X.; An, X.; Li, Q. Se $\cdots$ N chalcogen bond and Se $\cdots$ X halogen bond involving F<sub>2</sub>CSe: Influence of hybridization, substitution, and cooperativity. *J. Phys. Chem. A* **2015**, *119*, 3518–3527.
- (79) Li, Q.-Z. Z.; Li, R.; Guo, P.; Li, H.; Li, W.-Z. Z.; Cheng, J.-B. B. Competition of chalcogen bond, halogen bond, and hydrogen bond in SCS-HOX and SeC-SeHOX (X = Cl and Br) complexes. *Comput. Theor. Chem.* **2012**, *980*, 56–61.
- (80) Bauza, A.; Quinonero, D.; Deya, P. M.; Frontera, A. Halogen bonding versus chalcogen and pnicogen bonding: A combined Cambridge structural database and theoretical study. *CrystEngComm* **2013**, *15*, 3137–3144.
- (81) Sanz, P.; Yáñez, M.; Mó, O. Competition between X $\cdots$ H $\cdots$ Y intramolecular hydrogen bonds and X $\cdots$ Y (X = O, S, and Y = Se, Te) chalcogen-chalcogen interactions. *J. Phys. Chem. A* **2002**, *106*, 4661–4668.
- (82) Sanz, P.; Yáñez, M.; Mó, O. The role of chalcogen-chalcogen interactions in the intrinsic basicity and acidity of  $\beta$ -chalcogenovinyl-(thio)aldehydes HC(=X)-CH = CH-CYH (X = O, S; Y = Se, Te). *Chem. - Eur. J.* **2002**, *8*, 3999–4007.
- (83) Clark, T.; Hennemann, M.; Murray, J.; Politzer, P. Halogen bonding: The  $\sigma$ -hole. *J. Mol. Model.* **2007**, *13*, 291–296.
- (84) Politzer, P.; Murray, J.; Concha, M. Halogen bonding and the design of new materials: Organic bromides, chlorides and perhaps even fluorides as donors. *J. Mol. Model.* **2007**, *13*, 643–650.
- (85) Zhang, Y.; Ma, N.; Wang, W. A new class of halogen bonds that avoids the  $\sigma$ -hole. *Chem. Phys. Lett.* **2012**, *532*, 27–30.
- (86) Ramasami, P.; Ford, T. A. Chalcogen-bonded complexes. Selenium-bound adducts of NH<sub>3</sub>, H<sub>2</sub>O, PH<sub>3</sub>, and H<sub>2</sub>S with OCS<sub>e</sub>, SCSe, and CSe<sub>2</sub>. *J. Mol. Model.* **2015**, *21*, 35.
- (87) Esrafilı, M. D.; Mohammadian-Sabet, F. Ab initio calculations of cooperativity effects on chalcogen bonding: Linear clusters of (OCS)<sub>2–8</sub> and (OCSe)<sub>2–8</sub>. *Struct. Chem.* **2015**, *26*, 199–206.
- (88) Wang, W.; Ji, B.; Zhang, Y. Chalcogen bond: A sister noncovalent bond to halogen bond. *J. Phys. Chem. A* **2009**, *113*, 8132–8135.
- (89) Alikhani, E.; Fuster, F.; Madebene, B.; Grabowski, S. J. Topological reaction sites - Very strong chalcogen bonds. *Phys. Chem. Chem. Phys.* **2014**, *16*, 2430–2442.
- (90) Cozzolino, A. F.; Vargas-Baca, I.; Mansour, S.; Mahmoudkhani, A. H. The nature of the supramolecular association of 1,2,5-chalcogenadiazoles. *J. Am. Chem. Soc.* **2005**, *127*, 3184–3190.
- (91) Esrafilı, M. D.; Vakili, M. Halogen bonds enhanced by  $\sigma$ -hole and  $\pi$ -hole interactions: A comparative study on cooperativity and competition effects between X $\cdots$ N and S $\cdots$ N interactions in H<sub>3</sub>N $\cdots$ XCN $\cdots$ SF<sub>2</sub> and H<sub>3</sub>N $\cdots$ XCN $\cdots$ SO<sub>2</sub> complexes (X = F, Cl, Br and I). *J. Mol. Model.* **2014**, *20*, 2291.
- (92) Esseffar, M.; Herrero, R.; Quintanilla, E.; Dávalos, J. Z.; Jiménez, P.; Abboud, J.-L. M.; Yáñez, M.; Mó, O. Activation of the disulfide bond and chalcogen-chalcogen interactions: An experimental (FTICR) and computational study. *Chem. - Eur. J.* **2007**, *13*, 1796–1803.
- (93) Cozzolino, A. F.; Vargas-Baca, I. The supramolecular chemistry of 1,2,5-chalcogenadiazoles. *J. Organomet. Chem.* **2007**, *692*, 2654–2657.
- (94) Cozzolino, A. F.; Elder, P. J. W.; Lee, L. M.; Vargas-Baca, I. The role of the Lewis acid-base properties in the supramolecular association of 1,2,5-chalcogenadiazoles. *Can. J. Chem.* **2013**, *91*, 338–347.
- (95) Cozzolino, A. F.; Britten, J. F.; Vargas-Baca, I. The effect of steric hindrance on the association of telluradiazoles through Te-N secondary bonding interactions. *Cryst. Growth Des.* **2006**, *6*, 181–186.
- (96) Cozzolino, A. F.; Whitfield, P. S.; Vargas-Baca, I. Supramolecular chromotropism of the crystalline phases of 4,5,6,7-tetrafluorobenzo-2,1,3-telluradiazole. *J. Am. Chem. Soc.* **2010**, *132*, 17265–17270.
- (97) Oliveira, V.; Kraka, E.; Cremer, D. Quantitative assessment of halogen bonding utilizing vibrational spectroscopy. *Inorg. Chem.* **2017**, *56*, 488–502.
- (98) Li, Y.; Oliveira, V.; Tang, C.; Cremer, D.; Liu, C.; Ma, J. The peculiar role of the Au<sub>3</sub> unit in Au<sub>m</sub> clusters:  $\sigma$ -aromaticity of the Au<sub>5</sub>Zn<sup>+</sup> Ion. *Inorg. Chem.* **2017**, *56*, 5793–5803.
- (99) Kraka, E.; Setiawan, D.; Cremer, D. Re-evaluation of the bond length - bond strength rule: The stronger bond is not always the shorter bond. *J. Comput. Chem.* **2016**, *37*, 130–142.
- (100) Setiawan, D.; Kraka, E.; Cremer, D. Hidden bond anomalies: The peculiar case of the fluorinated amine chalcogenides. *J. Phys. Chem. A* **2015**, *119*, 9541–9556.

- (101) Kraka, E.; Larsson, J. A.; Cremer, D. In *Computational spectroscopy: Methods, experiments and applications*; Grunenberg, J., Ed.; Wiley: New York, 2010; pp 105–149.
- (102) Konkoli, Z.; Cremer, D. A new way of analyzing vibrational spectra I. Derivation of adiabatic internal modes. *Int. J. Quantum Chem.* **1998**, *67*, 1–9.
- (103) Cremer, D.; Larsson, J. A.; Kraka, E.; et al. New developments in the analysis of vibrational spectra On the use of adiabatic internal vibrational modes. *Theor. Comput. Chem.* **1998**, *5*, 259–327.
- (104) Zou, W.; Kalescky, R.; Kraka, E.; Cremer, D. Relating normal vibrational modes to local vibrational modes with the help of an adiabatic connection scheme. *J. Chem. Phys.* **2012**, *137*, 084114.
- (105) Wilson, E. B.; Decius, J. C.; Cross, P. C. *Molecular vibrations. The theory of infrared and Raman vibrational spectra*; McGraw-Hill: New York, 1955.
- (106) Cremer, D.; Kraka, E. Generalization of the Tolman electronic parameter: The metal-ligand electronic parameter and the intrinsic strength of the metal-ligand bond. *Dalton Trans.* **2017**, *46*, 8323.
- (107) Möller, C.; Plesset, M. S. Note on an approximation treatment for many-electron systems. *Phys. Rev.* **1934**, *46*, 618–622.
- (108) Becke, A. D. Density-functional thermochemistry. III. The role of exact exchange. *J. Chem. Phys.* **1993**, *98*, 5648–5652.
- (109) Stephens, P. J.; Devlin, F. J.; Chabalowski, C. F.; Frisch, M. J. Ab initio calculation of vibrational absorption and circular dichroism spectra using density functional force fields. *J. Phys. Chem.* **1994**, *98*, 11623–11627.
- (110) Grimme, S.; Antony, J.; Ehrlich, S.; Krieg, H. A consistent and accurate ab initio parametrization of density functional dispersion correction (DFT-D) for the 94 elements H-Pu. *J. Chem. Phys.* **2010**, *132*, 154104.
- (111) Grimme, S.; Ehrlich, S.; Goerigk, L. Effect of the damping function in dispersion corrected density functional theory. *J. Comput. Chem.* **2011**, *32*, 1456–1465.
- (112) Zhao, Y.; Truhlar, D. G. The M06 suite of density functionals for main group thermochemistry, thermochemical kinetics, non-covalent interactions, excited states, and transition elements: Two new functionals and systematic testing of four M06-class functionals and 12 other functionals. *Theor. Chem. Acc.* **2008**, *120*, 215–241.
- (113) Chai, J. D.; Head-Gordon, M. Long-range corrected hybrid density functionals with damped atom-atom dispersion corrections. *Phys. Chem. Chem. Phys.* **2008**, *10*, 6615.
- (114) Chai, J. D.; Head-Gordon, M. Systematic optimization of long-range corrected hybrid density functionals. *J. Chem. Phys.* **2008**, *128*, 084106.
- (115) Raghavachari, K.; Trucks, G. W.; Pople, J. A.; Head-Gordon, M. A fifth-order perturbation comparison of electron correlation theories. *Chem. Phys. Lett.* **1989**, *157*, 479–483.
- (116) Woon, D.; Dunning, T. J. Gaussian basis sets for use in correlated molecular calculations. IV. Calculation of static electrical response properties. *J. Chem. Phys.* **1994**, *100*, 2975–2988.
- (117) Dunning, T. Gaussian basis sets for use in correlated molecular calculations. I. The atoms boron through neon and hydrogen. *J. Chem. Phys.* **1989**, *90*, 1007–1023.
- (118) Woon, D.; Dunning, T. Gaussian basis sets for use in correlated molecular calculations. III. The atoms aluminum through argon. *J. Chem. Phys.* **1993**, *98*, 1358–1371.
- (119) Boys, S.; Bernardi, F. The calculation of small molecular interactions by the differences of separate total energies. *Mol. Phys.* **1970**, *19*, 553–566.
- (120) Grafenstein, J.; Cremer, D. Efficient DFT integrations by locally augmented radial grids. *J. Chem. Phys.* **2007**, *127*, 164113.
- (121) Peterson, K. A.; Figgen, D.; Goll, E.; Stoll, H.; Dolg, M. Systematically convergent basis sets with relativistic pseudopotentials. II. Small-core pseudopotentials and correlation consistent basis sets for the post-d group 16–18 elements. *J. Chem. Phys.* **2003**, *119*, 11113–11123.
- (122) Kalescky, R.; Kraka, E.; Cremer, D. Identification of the strongest bonds in chemistry. *J. Phys. Chem. A* **2013**, *117*, 8981–8995.
- (123) Chivers, T.; Laitinen, R. S. Tellurium: A maverick among the chalcogens. *Chem. Soc. Rev.* **2015**, *44*, 1725–1739.
- (124) Nakanishi, W.; Hayashi, S.; Pitak, M. B.; Hursthouse, M. B.; Coles, S. J. Dynamic and static behaviors of N-Z-N  $\sigma(3c-4e)$  (Z = S, Se, and Te) interactions: Atoms-in-molecules dual functional analysis with high-resolution X-ray diffraction determination of electron densities for 2-(2-pyridylimino)-2H-1,2,4-thiadiazolo[2,3-a]pyrid. *J. Phys. Chem. A* **2011**, *115*, 11775–11787.
- (125) Gleiter, R.; Haberhauer, G. Long chalcogen-chalcogen bonds in electron-rich two and four center bonds: Combination of  $\pi$ - and  $\sigma$ -aromaticity to a three-dimensional  $\sigma/\pi$ -aromaticity. *J. Org. Chem.* **2014**, *79*, 7543–7552.
- (126) Cremer, D.; Kraka, E. A description of the chemical bond in terms of local properties of electron density and energy. *Croat. Chem. Acta* **1984**, *57*, 1259–1281.
- (127) Cremer, D.; Kraka, E. Chemical bonds without bonding electron density - Does the difference electron density analysis suffice for a description of the chemical bond? *Angew. Chem., Int. Ed. Engl.* **1984**, *23*, 627–628.
- (128) Kraka, E.; Cremer, D.; Maksic, Z. Chemical Implication of Local Features of the Electron Density Distribution. *Theoretical models of chemical bonding. The concept of the chemical bond* **1990**, *2*, 453–542.
- (129) Setiawan, D.; Kraka, E.; Cremer, D. Strength of the pnictogen bond in complexes involving group Va elements N, P, and As. *J. Phys. Chem. A* **2015**, *119*, 1642–1656.
- (130) Setiawan, D.; Kraka, E.; Cremer, D. Description of pnictogen bonding with the help of vibrational spectroscopy - The missing link between theory and experiment. *Chem. Phys. Lett.* **2014**, *614*, 136–142.
- (131) Weinhold, F.; Landis, C. R. *Valency and bonding: A natural bond orbital donor-acceptor perspective*; Cambridge University Press: Cambridge, U.K., 2003.
- (132) Szalewicz, K. Symmetry-adapted perturbation theory of intermolecular forces. *WIREs Comput. Mol. Sci.* **2012**, *2*, 254–272.
- (133) Hohenstein, E. G.; Parrish, R. M.; Sherrill, C. D.; Turney, J. M.; Schaefer, H. F., III Large-scale symmetry-adapted perturbation theory computations via density fitting and Laplace transformation techniques: Investigating the fundamental forces of DNA-intercalator interactions. *J. Chem. Phys.* **2011**, *135*, 174107.
- (134) Parrish, R. M.; Sherrill, C. D. Spatial assignment of symmetry adapted perturbation theory interaction energy components: The atomic SAPT partition. *J. Chem. Phys.* **2014**, *141*, 044115.
- (135) Kraka, E.; Zou, W.; Filatov, M.; Grafenstein, J.; Izotov, D.; Gauss, J.; He, Y.; Wu, A.; Konkoli, Z.; Polo, V. et al. COLOGNE2016. 2016; see <http://www.smu.edu/catco> (accessed Jul 31, 2017).
- (136) Stanton, J. F.; Gauss, J.; Harding, M. E.; Szalay, P. G. CFOUR, A quantum chemical program package 2010; see <http://www.cfour.de> (accessed Jul 31, 2017).
- (137) Lu, T.; Chen, F. Multiwfn: A multifunctional wavefunction analyzer. *J. Comput. Chem.* **2012**, *33*, 580–592.
- (138) Werner, H. J.; Knowles, P. J.; Knizia, G.; Manby, F. R.; Schütz, M.; Celani, P.; Korona, T.; Lindh, R.; Mitrushenkov, A.; Rauhut, G. et al. MOLPRO, Version 2010. 1. A package of ab initio programs 2010; see <http://www.molpro.net> (accessed Jul 31, 2017).
- (139) Frisch, M. J.; Trucks, G. W.; Schlegel, H. B.; Scuseria, G. E.; Robb, M. A.; Cheeseman, J. R.; Scalmani, G.; Barone, V.; Mennucci, B.; Petersson, G. A. et al. *Gaussian 09*, revision C. 1; 2010; Gaussian Inc.: Wallingford, CT.
- (140) Reed, A. E.; Weinstock, R. B.; Weinhold, F. Natural population analysis. *J. Chem. Phys.* **1985**, *83*, 735–746.
- (141) Bertini, V.; Dapporto, P.; Lucchesini, F.; Sega, A.; De Munno, A. 1,2,5-Telluradiazole, C<sub>2</sub>H<sub>2</sub>N<sub>2</sub>Te. *Acta Crystallogr., Sect. C: Cryst. Struct. Commun.* **1984**, *C40*, 653–655.
- (142) Freindorf, M.; Kraka, E.; Cremer, D. A comprehensive analysis of hydrogen bond interactions based on local vibrational modes. *Int. J. Quantum Chem.* **2012**, *112*, 3174–3187.
- (143) Tao, Y.; Zou, W.; Jia, J.; Li, W.; Cremer, D. Different ways of hydrogen bonding in water - Why does warm water freeze faster than cold water? *J. Chem. Theory Comput.* **2017**, *13*, 55–76.

(144) Kalescky, R.; Zou, W.; Kraka, E.; Cremer, D. Local vibrational modes of the water dimer - Comparison of theory and experiment. *Chem. Phys. Lett.* **2012**, *554*, 243–247.

(145) Kalescky, R.; Kraka, E.; Cremer, D. Local vibrational modes of the formic acid dimer - The strength of the double hydrogen bond. *Mol. Phys.* **2013**, *111*, 1497–1510.

(146) Zhang, X.; Dai, H.; Yan, H.; Zou, W.; Cremer, D. B-H... $\pi$  interaction: A new type of nonclassical hydrogen bonding. *J. Am. Chem. Soc.* **2016**, *138*, 4334–4337.

(147) Kraka, E.; Freindorf, M.; Cremer, D. Chiral discrimination by vibrational spectroscopy utilizing local modes. *Chirality* **2013**, *25*, 185–196.

(148) Oliveira, V.; Cremer, D. Transition from metal-ligand bonding to halogen bonding involving a metal as halogen acceptor a study of Cu, Ag, Au, Pt, and Hg complexes. *Chem. Phys. Lett.* **2017**, *681*, 56–63.

(149) Setiawan, D.; Cremer, D. Super-pnicogen bonding in the radical anion of the fluorophosphine dimer. *Chem. Phys. Lett.* **2016**, *662*, 182–187.

(150) Kalescky, R.; Kraka, E.; Cremer, D. Description of aromaticity with the help of vibrational spectroscopy: Anthracene and phenanthrene. *J. Phys. Chem. A* **2014**, *118*, 223–237.

(151) Setiawan, D.; Kraka, E.; Cremer, D. Quantitative assessment of aromaticity and antiaromaticity utilizing vibrational spectroscopy. *J. Org. Chem.* **2016**, *81*, 9669–9686.

(152) Kalescky, R.; Kraka, E.; Cremer, D. New approach to Tolman's electronic parameter based on local vibrational modes. *Inorg. Chem.* **2014**, *53*, 478–495.

(153) Setiawan, D.; Kalescky, R.; Kraka, E.; Cremer, D. Direct measure of metal-ligand bonding replacing the Tolman electronic parameter. *Inorg. Chem.* **2016**, *55*, 2332–2344.

(154) Humason, A.; Zou, W.; Cremer, D. 11,11-Dimethyl-1,6-methano[10]annulene - An annulene with an ultralong CC bond or a fluxional molecule? *J. Phys. Chem. A* **2015**, *119*, 1666–1682.

(155) Kalescky, R.; Zou, W.; Kraka, E.; Cremer, D. Quantitative assessment of the multiplicity of carbon-halogen bonds: Carbenium and halonium ions with F, Cl, Br, I. *J. Phys. Chem. A* **2014**, *118*, 1948–1963.

(156) Kraka, E.; Cremer, D. Characterization of CF bonds with multiple-bond character: Bond lengths, stretching force constants, and bond dissociation energies. *ChemPhysChem* **2009**, *10*, 686–698.

Paper V. A systematic coupled cluster study of noncovalent interactions involving halogens, chalcogens and pnictogens

# Systematic Coupled Cluster Study of Noncovalent Interactions Involving Halogens, Chalcogens, and Pnicogens

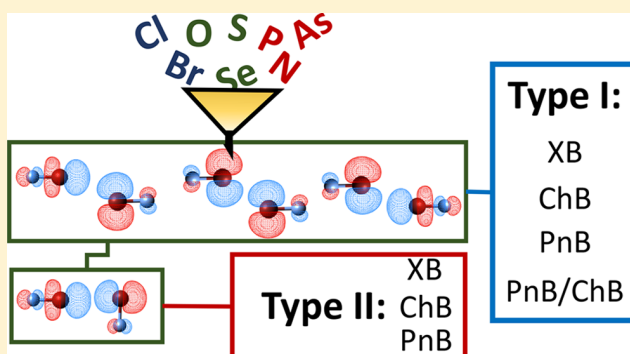
Published as part of *The Journal of Physical Chemistry virtual special issue "Manuel Yáñez and Otilia Mó Festschrift"*.

Vytor Oliveira and Elfi Kraka\*<sup>1b</sup>

Computational and Theoretical Chemistry Group (CATCO), Department of Chemistry, Southern Methodist University, 3215 Daniel Ave, Dallas, Texas 75275-0314, United States

## Supporting Information

**ABSTRACT:** The noncovalent interactions of 32 complexes involving pnicogens, chalcogens, and halogens atoms were investigated at the CCSD(T)/aug-cc-pVTZ level of theory. Two different types of complexes could be distinguished on the basis of geometric parameters, electron difference densities, and the charge transfer mechanisms associated with each type. In the type I conformation, the monomers adopt a skewed orientation allowing charge to be transfer between both monomers, whereas in the type II conformation the monomers adopt a linear arrangement, maximizing charge transfer in only one direction. Type I complexes involving the interaction between pnicogens and chalcogens cannot be unambiguously defined as chalcogen or pnicogen bonds, they are an admixture of both. The charge transfer dependence on the conformation adopted by the complexes described in this work can serve as a novel conformationally driven design concept for materials.



## 1. INTRODUCTION

The study of intermolecular interactions is an important topic in chemistry due to the key roles these interactions play in diverse fields. In supramolecular chemistry they can guide self-assembly<sup>1</sup> and stabilize the tertiary structures of macromolecules such as proteins, DNA, and RNA;<sup>2,3</sup> In drug design they can lead to drug-receptor recognition.<sup>4,5</sup> In catalysis they can help to stabilize the transition state of chemical reactions and guide stereoselectivity<sup>6,7</sup> to name just a few examples. Although hydrogen bonding (HB) continues to be the most studied noncovalent interaction, there has been a continuous discovery of other kinds of weak interactions,<sup>1,8–13</sup> which share many similarities with HB, such as high directionality<sup>14–16</sup> and tunable interaction strength.<sup>17–24</sup> Different types of interactions can possess unique electronic features relevant for the development of novel materials with special electrical,<sup>25</sup> magnetic,<sup>26,27</sup> and optical properties.<sup>28–30</sup> Among these new types of interactions, the ones involving pnicogen, chalcogen, and halogen atoms are already being exploited for the design and synthesis of liquid crystals, gels, molecular compartments,<sup>31,32</sup> molecular linkers,<sup>33</sup> ion transport, sensors, optically responsive materials,<sup>34</sup> and novel drugs.<sup>35,36</sup> These and other applications were the topic of recent reviews.<sup>1,37–42</sup>

A well established example of such a noncovalent interaction that is known to play a determining role in the supramolecular structures and properties of crystals is the interaction between

two halogens (halogen...halogen).<sup>43–46</sup> X-ray diffraction studies<sup>47</sup> supported by statistical analysis of crystal structures deposited on the Cambridge Database<sup>45,48</sup> revealed that two preferred conformers are associated with halogen...halogen interactions. These are shown in Figure 1. In the type I

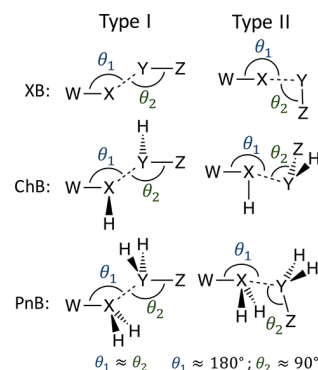


**Figure 1.** Representation of the two possible conformers involving halogen (XB), chalcogen (ChB), and pnicogen bonding (PnB) considered in this work.

**Received:** October 14, 2017

**Revised:** November 18, 2017

**Published:** November 20, 2017

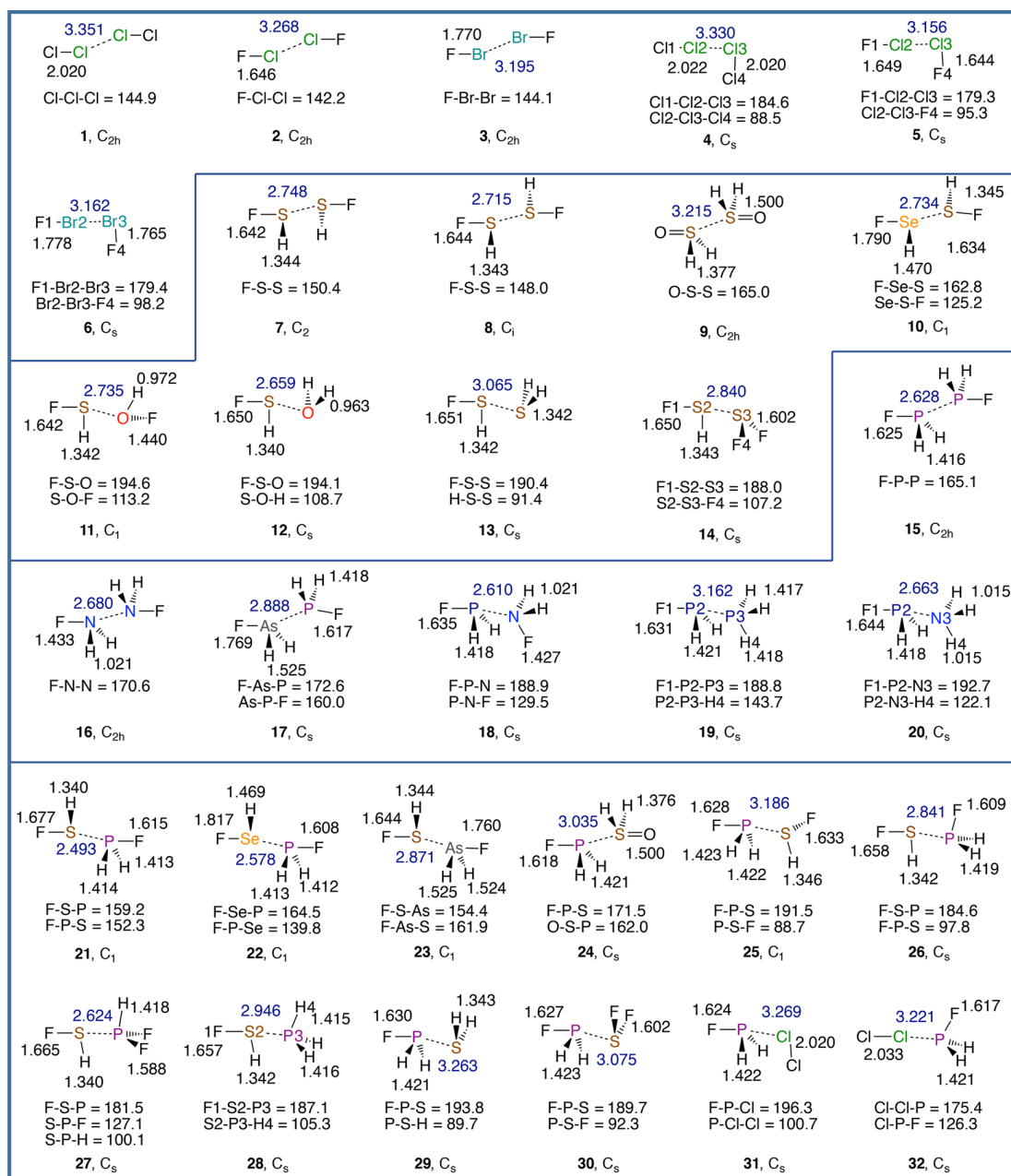


**Figure 2.** Schematic representation of the geometry of complexes 1–32. Bond distances in Å (intermolecular distances in blue) and selected angles in degrees.

conformation the two angles formed by the halogens X and Y and their substituents W and Z ( $\theta_1 = W-X-Y$  and  $\theta_2 = X-Y-Z$ ) have approximately the same value ( $\theta_1 \approx \theta_2$ ), whereas type II contacts are characterized by a linear angle  $\theta_1 \approx 180^\circ$  and a close to right angle  $\theta_2 \approx 90^\circ$ . Experimental and theoretical evidence suggests that type I halogen...halogen interactions are predominantly stabilized by dispersive forces.<sup>46,49,50</sup> However, covalent contributions in the form of electron delocalization (i.e., charge transfer) from the lone pair X (lp(X)) orbital into the empty  $\sigma^*(YZ)$  orbital and from lp(Y) into the  $\sigma^*(WX)$  orbital<sup>49</sup> and electrostatic attraction, originating from the anisotropic distribution of the X and Y electron density,<sup>51</sup> can also play a significant role for the stabilization of type I conformation. On the other hand, type II halogen...halogen interactions are considered to form true halogen bonds XB<sup>52</sup>

(in the following XB is used for both type I and II halogen...halogen interactions for the sake of simplicity), as a result of the attractive interaction between the nucleophilic region of the halogen (Y) and the electrophilic region of the halogen (X) (Figure 1). Although type II XBs (XB-II) are generally stronger than the type I (XB-I), the latter are commonly observed due to crystal packing effects.<sup>46,53</sup>

A different picture emerges for the closely related chalcogen...chalcogen and pnictogen...pnictogen interactions. Well-defined pnictogen bonds (PnBs) and chalcogen bonds (ChBs) are found for both type I<sup>12,23,54–61</sup> and type II<sup>23,54,60,62,63</sup> conformations (Figure 1). These are stabilized mostly by charge transfer and electrostatic contributions rather than by dispersion. Despite the many investigations on PnB and ChB exploring both type I and type II conformations, a

systematic comparison of XB, PnB, and ChB type I and type II conformations is still missing. Another topic of interest is the noncovalent interaction formed by atoms of different groups such as pnictogen...halogen or pnictogen...chalcogen, where multiple local minima involving different types of noncovalent interactions can be found. An example is the  $\text{Cl}_2\cdots\text{PFH}_2$  complexes studied by Del Bene, Alkorta, and Elguero,<sup>64,65</sup> involving three different types of  $\text{Cl}\cdots\text{P}$  interactions, referring to a classical XB, a chlorine shared XB, and a PnB. Another interesting case is the complex  $\text{FHSe}\cdots\text{PH}_2\text{F}$  studied by Shukla and Chopra,<sup>66</sup> which involves not only charge transfer (CT) from the phosphorus lone pair orbital ( $\text{lp}(\text{P})$ ) into the  $\sigma^*(\text{SeF})$  orbital of  $\text{FHSe}$ , characteristic of a ChB, but also the CT from  $\text{lp}(\text{Se})$  to  $\sigma^*(\text{PF})$ , characteristic of a PnB, making it difficult to unambiguously classify the interactions as PnB or ChB.

A reliable comparison of the different kinds of interactions involving halogens, chalcogens, and pnictogens considering both type I and type II conformations, requires a method of high accuracy being capable to describe dispersive, electrostatic and covalent contributions in a well-balanced and accurate way. Although density functional theory with empirical dispersion corrections (DFT-D) and  $\text{MP2}$ <sup>67</sup> have been employed in various studies of noncovalent interactions, leading in general to a reasonably accurate description of HB, ChB, PnB, and XB, the reliability of these methods is challenged, when very weak noncovalent interactions have to be described.<sup>68–70</sup> A more reliable choice in this case, especially when second or higher order properties are required, is the coupled cluster method with singles, doubles, and perturbative triples excitations ( $\text{CCSD}(\text{T})$ ).<sup>71</sup> Considered as the current gold standard,<sup>72</sup>  $\text{CCSD}(\text{T})$  is usually the method of choice to evaluate the reliability of less computationally demanding approaches,<sup>73,74</sup> and it is a particularly invaluable method in high-accuracy studies of small complexes.<sup>75,76</sup>

In previous work<sup>76</sup> we presented for the first time a quantitative description of the intrinsic strength of 36 XB complexes in comparison with 8 HB, ChB, and PnB systems (all of type II conformation) by combining vibrational spectroscopy and high-accuracy  $\text{CCSD}(\text{T})$  calculations. In the present study we will use a diverse set of 32 complexes consisting of XB, ChB, and PnB of both type I and type II conformations (shown in Figure 2) to explore the similarities and differences between the bonding mechanisms, the nature of the interactions, the intrinsic bond strength, and the influence of the atoms involved in the noncovalent interactions. For this purpose, we have addressed the following questions: (i) Is there a general mechanism to describe the noncovalent interactions formed by pnictogens, chalcogens, and halogens? (ii) Can we use other parameters besides the geometry to characterize the complex as been of type I or type II? (iii) How do the nature and the strength of the interaction depend on the atoms involved and on the conformation adopted? (iv) Is there any complex where type I and type II conformations are both minimum-energy points in the potential energy surface?

The paper is arranged as follows. In section 2 we provide details about the computational methods employed. In section 3 we describe the bonding mechanisms observed for type I and II conformations and discuss the most important factor involved in the stabilization of the complexes and in the intrinsic strength of the noncovalent interactions. In the last section we summarize the most important result and draw conclusion.

## 2. COMPUTATIONAL METHODS

The geometry of all complexes (1–32) and monomers (33–48) was fully optimized at coupled cluster level using  $\text{CCSD}(\text{T})$ <sup>71</sup> combined with Dunning's augmented triple- $\zeta$  basis sets aug-cc-pVTZ,<sup>77–79</sup> which contains diffuse basis functions for a proper description of the density far from the nuclei. For the geometry optimizations the convergence criteria was set to  $10^{-6}$  hartree bohr<sup>-1</sup> and a threshold of  $10^{-9}$  was used for the self-consistent field and coupled cluster amplitude equations. Analytical vibrational frequencies computed at the same level were used to verify that each stationary point obtained from the geometry optimization is a minimum (or a first-order saddle point as in the case of complexes 1, 2, 3).

The Konkoli–Cremer method<sup>80–83</sup> was used to convert the normal vibrational modes into local modes. This method makes use of a mass-decoupled analogue of Wilson equation of vibrational spectroscopy<sup>81,84</sup> to solve the electronic and mass coupling between normal vibrational modes, leading to local modes that are free from any mode–mode coupling. A unique set of  $3N - L$  ( $N$  = number of atoms;  $L$  = number of translations and rotations) local modes was determined for each complex, which could be connected to the normal modes in a one-to-one fashion via an adiabatic connection scheme.<sup>82</sup>

The local stretching force constant ( $k^a$ ) obtained from the corresponding local mode provides a direct measure of the intrinsic strength of a bond.<sup>85</sup> As pursued in our previous investigation on the halogen bonds strength,<sup>76</sup> the analysis of  $k^a$  was simplified by converting local stretching force constants into bond strength orders (BSOs)  $n$ . According to the generalized Badger rule,<sup>86</sup> BSO values are related to  $k^a$  via a power relationship (eq 1):

$$\text{BSO}n = a(k^a)^b \quad (1)$$

Constants  $a = 0.418$  and  $b = 0.564$  were determined by assuming an  $n$  value of 1 for the FF bond in  $\text{F}_2$ ,  $n = 0.5$  for the  $3c-4e$  FF bond in  $[\text{F}\cdots\text{F}\cdots\text{F}]^-$ , and assuming an  $n$  value of zero for  $k^a = 0$ .

Binding energies were calculated with and without counterpoise (CP) correction<sup>87</sup> for the analysis of the basis set superposition error (BSSE). It is often observed that the CP correction does not necessarily lead to results closer to the complete basis set limit.<sup>88</sup> This is due to a fortuitous error cancelation present in uncorrected values.<sup>89</sup> Therefore, we decided to test whether CP-corrected or uncorrected interaction energies were closer to the values obtained with a larger basis set. For this purpose, the CP-corrected and uncorrected interaction energies of 12 complexes were calculated with domain-based local pair natural orbital DLPNO- $\text{CCSD}(\text{T})$  approximation<sup>90,91</sup> utilizing both the aug-cc-pVTZ basis set and the more saturated aug-cc-pV5Z<sup>79,92</sup> basis set. It turned out that the CP-uncorrected DLPNO- $\text{CCSD}(\text{T})/\text{aug-cc-pVTZ}$  values are on the average closer to CP-corrected and uncorrected DLPNO- $\text{CCSD}(\text{T})/\text{aug-cc-pV5Z}$  values (Supporting Information). Because of this, no attempt was made to include CP corrections to gradient or Hessian calculations.

Local properties of the electron density  $\rho(\mathbf{r})$  and energy density distribution  $H(\mathbf{r})$  obtained from  $\text{CCSD}(\text{T})$  response densities were used to characterize the nature of the interactions. According to the Cremer–Kraka criteria for covalent bonding, a negative (stabilizing) energy density  $H_b$  at the bond critical point  $\mathbf{r}_b$  indicates predominant covalent

Table 1. Summary of Energetic, Geometric, and Vibrational Data for Complexes 1–32<sup>a</sup>

complexes (sym)	$r(XY)$	$\Delta E$	$\Delta E$	CP	$\rho_b(YX)$	$H_b(XY)$	CT	$\Delta E(\text{del})1$ WX ← Y	$\Delta E(\text{del})2$ X → YZ	$\Delta n(WX)$ %	$\Delta n(YZ)$ %	$k^a(XY)$	$n(XY)$	type
1	(Cl <sub>2</sub> ) <sub>2</sub> (C <sub>2h</sub> )	3.351	1.17	0.86	0.051	0.011	0.000	0.7	0.7	0	0	0.032	0.060	XB-I
2	(FCl) <sub>2</sub> (C <sub>2h</sub> )	3.268	1.02	0.72	0.061	0.011	0.000	1.3	1.3	0	0	0.027	0.054	XB-I
3	(FBr <sub>2</sub> ) <sub>2</sub> (C <sub>2h</sub> )	3.195	1.65	1.26	0.110	0.002	0.000	5.0	5.0	-1	-1	0.046	0.073	XB-I
4	(Cl <sub>2</sub> ) <sub>2</sub> (C <sub>2</sub> )	3.330	1.56	1.20	0.054	0.012	-0.009	2.0	0.0	-1	0	0.043	0.071	XB-II
5	(FCl) <sub>2</sub> (C <sub>2</sub> )	3.156	1.50	1.15	0.075	0.013	-0.017	4.5	0.2	-1	0	0.054	0.080	XB-II
6	(FBr <sub>2</sub> ) <sub>2</sub> (C <sub>2</sub> )	3.162	2.47	2.07	0.118	0.002	-0.046	12.5	0.7	-4	0	0.085	0.104	XB-II
7	(FSH) <sub>2</sub> (C <sub>2</sub> )	2.748	4.44	3.61	0.229	-0.029	0.000	14.0	14.0	-12	-12	0.097	0.112	ChB-I
8	(FSH) <sub>2</sub> (C <sub>1</sub> )	2.715	4.67	3.81	0.246	-0.035	0.000	15.8	15.8	-14	-14	0.095	0.111	ChB-I
9	(OH <sub>2</sub> S) <sub>2</sub> (C <sub>2h</sub> )	3.215	2.31	1.62	0.096	0.003	0.000	2.0	2.0	1	1	0.084	0.103	ChB-I
10	FHSe...SHF (C <sub>1</sub> )	2.734	6.12	5.22	0.272	-0.049	-0.087	37.8	9.2	-14	-15	0.087	0.105	ChB-I
11	FHS...OFH (C <sub>1</sub> )	2.735	3.62	3.00	0.116	0.013	-0.016	6.4	0.8	-5	-1	0.104	0.116	ChB-II
12	FHS...OH <sub>2</sub> (C <sub>1</sub> )	2.659	5.69	6.24	0.138	0.010	-0.028	9.4	0.1	-7	0	0.152	0.144	ChB-II
13	FHS...SH <sub>2</sub> (C <sub>1</sub> )	3.065	4.53	4.00	0.123	0.000	-0.049	12.0	0.1	-9	0	0.107	0.118	ChB-II
14	FHS...SF <sub>2</sub> (C <sub>1</sub> )	2.840	4.18	3.30	0.202	-0.019	-0.089	22.3	1.0	-12	0	0.077	0.098	ChB-II
15	(FH <sub>2</sub> P) <sub>2</sub> (C <sub>2h</sub> )	2.628	6.41	4.94	0.325	-0.087	0.000	28.2	28.2	-17	-17	0.143	0.139	PnB-I
16	(FH <sub>2</sub> N) <sub>2</sub> (C <sub>2h</sub> )	2.680	4.17	3.73	0.093	0.015	0.000	2.2	2.2	-1	-1	0.126	0.130	PnB-I
17	FH <sub>2</sub> As...PH <sub>2</sub> F (C <sub>1</sub> )	2.888	5.01	3.93	0.214	-0.037	-0.029	20.8	10.6	-14	-6	0.122	0.127	PnB-I
18	FH <sub>2</sub> P...NH <sub>2</sub> F (C <sub>1</sub> )	2.610	5.92	4.95	0.189	-0.017	-0.047	15.2	2.7	-19	0	0.120	0.126	PnB-II
19	FH <sub>2</sub> P...PH <sub>3</sub> (C <sub>1</sub> )	3.162	4.01	3.32	0.116	-0.005	-0.033	9.7	2.5	-17	1	0.079	0.100	PnB-II
20	FH <sub>2</sub> P...NH <sub>3</sub> (C <sub>1</sub> )	2.663	6.81	6.10	0.171	-0.012	-0.057	15.2	0.9	-21	0	0.144	0.140	PnB-II
21	FHS...PH <sub>2</sub> F (C <sub>1</sub> )	2.493	6.10	4.84	0.408	-0.118	-0.103	47.3	24.2	-37	-17	0.103	0.116	PnB/ChB-I
22	FHSe...PH <sub>2</sub> F (C <sub>1</sub> )	2.578	8.21	7.03	0.392	-0.113	-0.150	63.7	17.6	-26	-13	0.217	0.176	PnB/ChB-I
23	FHS...AsH <sub>2</sub> F (C <sub>1</sub> )	2.871	4.20	3.35	0.205	-0.027	-0.016	14.7	13.4	-10	-7	0.104	0.116	PnB/ChB-I
24	FH <sub>2</sub> P...SH <sub>2</sub> O (C <sub>1</sub> )	3.035	3.70	2.74	0.140	-0.010	-0.017	6.9	4.5	-13	1	0.087	0.105	PnB/ChB-I
25	FH <sub>2</sub> P...SHF (C <sub>1</sub> )	3.186	3.30	2.56	0.102	-0.001	-0.039	9.0	0.2	-16	-3	0.075	0.097	PnB-II
26	FHS...PH <sub>2</sub> F (C <sub>1</sub> )	2.841	4.66	3.89	0.211	-0.025	-0.088	22.3	0.5	-17	-11	0.080	0.100	ChB-II
27	FHS...PF <sub>2</sub> H (C <sub>1</sub> )	2.624	4.92	3.79	0.318	-0.066	-0.135	40.9	2.9	-35	2	0.043	0.071	ChB-II
28	FHS...PH <sub>3</sub> (C <sub>1</sub> )	2.946	4.87	4.29	0.168	-0.013	-0.062	16.6	0.1	-14	1	0.094	0.110	ChB-II
29	FH <sub>2</sub> P...SH <sub>2</sub> (C <sub>1</sub> )	2.104	3.68	3.08	0.088	0.001	-0.034	7.4	0.1	-16	0	0.087	0.105	PnB-II
30	FH <sub>2</sub> P...SE <sub>2</sub> (C <sub>1</sub> )	3.075	3.30	2.33	0.134	-0.008	-0.090	13.3	0.3	-16	0	0.082	0.102	PnB-II
31	FPH <sub>2</sub> ...Cl <sub>2</sub> (C <sub>1</sub> )	3.269	2.53	1.87	0.068	0.007	-0.035	4.2	0.1	-14	0	0.058	0.084	PnB-II
32	Cl <sub>2</sub> ...PH <sub>2</sub> F (C <sub>1</sub> )	3.221	2.38	1.93	0.098	0.007	-0.017	5.3	0.4	-12	-7	0.053	0.080	XB-II

<sup>a</sup>Computed at CCSD(T)/aug-cc-pVTZ. Bond distance  $r(YX)$  in Å, binding energy  $\Delta E$  and counterpoise (CP) corrected  $\Delta E$  in kcal/mol. Density at XY critical point  $\rho_b$  in e/Å<sup>3</sup>, energy density at XY critical point  $H_b$  in hartree/Å<sup>3</sup>. NPA charge transfer in e, NBO delocalization energies computed with  $\omega$ B97XD/aug-cc-pVTZ referent to lp(Y) →  $\sigma^*(WX)$  ( $\Delta E(\text{del})1$ ) and lp(X) →  $\sigma^*(YZ)$  ( $\Delta E(\text{del})2$ ) in kcal/mol, percent shifts in the BSO  $n$  values of WX and YZ ( $\Delta n$  (%)),  $YX$   $k^a$  in mdyn/Å and BSO  $n$  values, noncovalent interaction type (see text).

character, whereas a positive (destabilizing) energy density indicates the formation of an electrostatic or dispersive interaction.<sup>93–95</sup>

The possibility of electrostatic attraction between the unperturbed monomers was accessed by investigating the location and magnitude of the extreme values of the electrostatic potential  $V(\mathbf{r})$  mapped onto the 0.001 e/bohr<sup>3</sup> electron density surface of the monomers. The maximum  $V(\mathbf{r})$  associated with the  $\sigma$ -hole region ( $V_{\max}$ ) and the minimum ( $V_{\min}$ ) associated with the lp(A) region provide an approximated measure for electrostatic attraction.<sup>96,97</sup>

Covalent contributions to the intermolecular interactions were assessed via the analysis of the natural bond orbital (NBO) delocalization energies ( $\Delta E(\text{del})$ ) associated with both lp(Y)  $\rightarrow$   $\sigma^*(\text{WX})$  and lp(X)  $\rightarrow$   $\sigma^*(\text{YZ})$  charge transfer mechanisms. The magnitude of  $\Delta E(\text{del})$  was determined by second-order perturbation theory.<sup>98</sup> Due to the nonexistence of CCSD(T) orbitals,  $\Delta E(\text{del})$  was calculated with  $\omega\text{B97XD}/\text{aug-cc-pVTZ}$ .<sup>99,100</sup> Recently, Stone<sup>101</sup> asserted that the NBO analysis overestimates charge transfer contribution to intermolecular interaction energies due to an inherent BSSE contamination, originated from the orthogonalization procedure adopted by the NBO analysis. Therefore, in this work,  $\Delta E(\text{del})$  was only used for a qualitative analysis of lp(Y)  $\rightarrow$   $\sigma^*(\text{WX})$  and lp(X)  $\rightarrow$   $\sigma^*(\text{YZ})$  charge transfer mechanisms. No quantitative comparison between  $\Delta E(\text{del})$  and  $\Delta E$  or any other property was made. The  $\Delta E(\text{del})$  analysis was complemented by the evaluation of the weakening of the WX and YZ bonds due to the partial occupation of  $\sigma^*(\text{WX})$  and  $\sigma^*(\text{YZ})$ . This can be associated with the shift in the BSO values of the WX and YZ bonds, calculated according to eq 2:

$$\Delta n(\text{WX}) (\%) = \frac{n(\text{WX})_{\text{monomer}} - n(\text{WX})_{\text{dimer}}}{n(\text{WX})_{\text{monomer}} \times 100} \quad (2)$$

Deviations between trends in  $\Delta E(\text{del})$  and  $\Delta n(\text{WX})$  (%) indicate that contributions from other CT mechanisms or lone pair repulsion also influence the shifts in the strength of the WX and YZ bonds upon complex formation. The inspection of the CCSD(T) electron difference density distribution  $\Delta\rho(\mathbf{r}) = \rho(\text{complex},\mathbf{r}) - \rho(\text{monomer1},\mathbf{r}) - \rho(\text{monomer2},\mathbf{r})$ , determined for an electron density distribution of 0.001 e/bohr<sup>3</sup> was also used to distinguish between electrostatic and covalent interactions. An accumulation of electron density in the XY bonding region indicates covalent character.

All local mode calculations were performed with COLOGNE2016.<sup>102</sup> The CCSD(T) energy, energy gradient, and Hessian were calculated with CFOUR.<sup>103</sup> For the NBO analysis, NBO 6<sup>98</sup> was used, whereas the electron (energy) density distribution was investigated with the program AIMAll.<sup>104</sup> Correlated electron and energy density distributions were analyzed with the programs Molden2AIM, and MOLBO of Zou and co-workers.<sup>105</sup> The CCSD(T) electrostatic potential  $V(\mathbf{r})$  were calculated with Multiwfn.<sup>106</sup>

### 3. RESULTS AND DISCUSSION

Table 1 lists the noncovalent bond distances  $r(\text{XY})$ , the counterpoise corrected binding energies  $\Delta E$ , the electron density  $\rho_b$  and the energy density  $H_b$  at the density critical point associated with the corresponding intermolecular interaction. The CT derived from the natural population analysis (NPA) atomic charges, the delocalization energy associated with the lp(Y)  $\rightarrow$   $\sigma^*(\text{WX})$  ( $\Delta E(\text{del})1$ ) and lp(X)

$\rightarrow$   $\sigma^*(\text{YZ})$  ( $\Delta E(\text{del})2$ ) CT mechanisms, the percentage shift in the BSO  $n$  values ( $\Delta n$  (%)) of W–X and Y–Z bonds upon the complex formation (eq 2), the local stretching force constant  $k^a(\text{XY})$  and the BSO  $n(\text{XY})$  associate with the noncovalent bond are also reported. The last column of Table 1 shows the type of the noncovalent interaction of each complex, classified according to the complex conformation as type I or II, and as XB, ChB, or PnB according to the stronger electron acceptor. In other words, if the largest  $\Delta E(\text{del})$  value involves a  $\sigma^*(\text{WX})$  where X is a halogen, the interaction is classified as a XB; likewise, if X is a chalcogen or a pnictogen the interaction is termed ChB or PnB.

Monomer properties are listed in Table 2, which includes the  $r(\text{WX})$ ,  $k^a(\text{WX})$ , and  $n(\text{WX})$  values, the vertical ionization

**Table 2. Geometry, Vibrational Data, And Values of the Electrostatic Potential for the Monomers<sup>a</sup>**

	monomer	$r(\text{WX})$	$k^a(\text{WX})$	$n(\text{WX})$	IP	$V_{\max}(\text{X})$	$V_{\min}(\text{X})$
33	Cl <sub>2</sub>	2.019	3.025	0.780	11.5	1.10	−0.13
34	FCl	1.646	4.326	0.954	12.7	1.75	−0.01
35	FBr	1.770	4.019	0.915	11.9	2.12	0.01
36	FHS	1.626	4.569	0.984	10.4	1.75	−0.43
37	FHSe	1.765	3.998	0.913	9.9	2.02	−0.37
38	OH <sub>2</sub> S	1.504	7.163	1.268	10.2	1.77	0.02
39	H <sub>2</sub> S	1.342	4.249	0.945	10.4		−0.71
40	F <sub>2</sub> S	1.607	4.729	1.003	10.3	1.61	−0.20
41	H <sub>2</sub> O	0.962	8.260	1.375	12.7		−1.40
42	OHF	1.442	4.280	0.949	12.9		−0.72
43	AsH <sub>2</sub> F	1.761	3.991	0.912	8.7	1.83	−0.19
44	PH <sub>2</sub> F	1.577	5.791	1.125	10.1	1.59	−0.48
45	NH <sub>2</sub> F	1.433	4.138	0.931	11.6	1.40	−1.21
46	PF <sub>2</sub> H	1.427	3.150	0.798	11.0	0.88	−0.26
47	PH <sub>3</sub>	1.420	3.331	0.823	10.5	0.53	−0.68
48	NH <sub>3</sub>	1.015	6.798	1.232	10.9		−1.62

<sup>a</sup>Distances  $r(\text{WX})$  in Å, WX local stretching force constants in mdyn/Å, and bond strength order  $n(\text{WX})$ . Vertical ionization potential, maximum electrostatic potential at the  $\sigma$ -hole of X, and minimum electrostatic potential at the lp(X) in eV. All values were calculated with CCSD(T)/aug-cc-pVTZ.

potential (IP) and the extreme values of the electrostatic potential in the lone pair region ( $V_{\min}$ ) and in  $\sigma$ -hole region ( $V_{\max}$ ) of the atom X. Figure 3 shows the bond strength ordering of all noncovalent interactions investigated in this

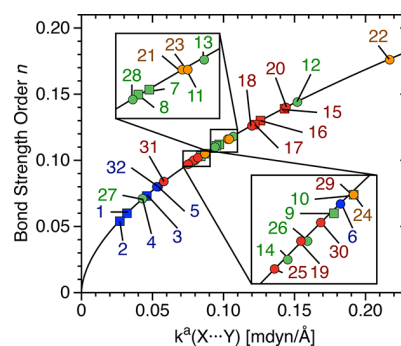


**Figure 3.** Power relationship between the relative bond strength order (BSO)  $n$  and the local stretching force constants  $k^a$  of complexes 1–32. XB in blue, ChB in green, PnB in red, and the mixed ChB/PnB in orange. Type I complexes are denoted by circles, and type II, by squares. Calculate at CCSD(T)/aug-cc-pVTZ level.

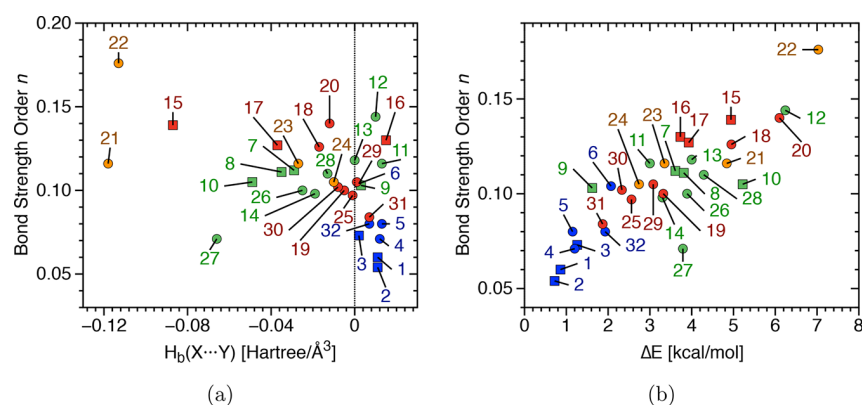


**Figure 4.** Comparison of the relative bond strength order (BSO)  $n$  with (a) the energy density at the bond critical point  $H_b$  of the ChBs of complexes 1–32 and with (b) binding energies ( $\Delta E$ ) for complexes 1–32. XB are shown in blue, ChB in green, PnB in red and the ChB/PnB in orange. Type I complexes are denoted by circles and type II by squares. Calculate at CCSD(T)/aug-cc-pVTZ level.

work, ranging from BSO  $n = 0.054$  (complex 2) to 0.176 (complex 22). Compared to the BSO values obtained in our previous studies on XB,<sup>22,24,76</sup> ChB,<sup>23</sup> and PnB,<sup>54,55</sup> the interactions considered in the present study can be classified as weak (BSO < 0.2 and  $\Delta E$  < 10 kcal/mol). According to the Cremer–Kraka criteria, about half of these complexes have a dominant electrostatic character with  $H_b \gtrsim 0.0$  and the others have partial covalent contributions  $H_b < 0$ .

**Comparison of BSO  $n$  Values and Other Properties.** A comparison of the BSO  $n$  values and  $H_b$  is given in Figure 4a. It is commonly found that as noncovalent interactions become stronger, they tend to have a higher covalent character.<sup>22,23,76</sup> However, for the relatively weak complexes considered in the present study, electrostatic interactions are able to surpass interactions with covalent character. This is in particular observed for interactions involving O and N atoms, which are not as polarizable as P, S, As, or Se but have a more negative electrostatic potential in the lp(X) region.

There is a scattered correlation between BSO  $n$  values and  $\Delta E$  (Figure 4b). The latter is a cumulative quantity that measures the energy required for the dissociation of the complexes into monomers, which includes besides the atom-to-atom bond strength, the energy required for the reorganization of the electron density and geometry of the monomers, and the fraction of any secondary intermonomers interactions that does not contribute to the atom-to-atom bond strength. Because of these reasons  $\Delta E$  does not reflect the intrinsic strength of the noncovalent interactions.<sup>76,107,108</sup>

**Bonding Mechanism of Type I and II Complexes.** In the present work we used the following protocol to analyze the strength and nature of the noncovalent interactions. First, the energy density is used to distinguish between interactions of dominant electrostatic and covalent character. Second, the strength of electrostatic interactions is rationalized on the basis of the analysis of the electrostatic potentials of the unperturbed monomers. Third, electrostatic interactions involving a weak electrostatic potential are considered to be dispersive and their strength is rationalized on the basis of polarizabilities. The fourth and last step is the analysis of covalent contributions on the basis of charge transfer involving specific orbitals.

On the basis of the protocol adopted, we can distinguish noncovalent interactions stabilized by electrostatic, covalent, and dispersive contributions in the following way: The electrostatic part refers to the attraction between the negative electrostatic potential in the lone pair region of atom Y and the

positive electrostatic potential formed at the  $\sigma$ -hole (region of depleted electron density formed collinear to a  $\sigma$ -bond) at the atom X (of the unperturbed monomers). Type II complexes tend to form stronger electrostatic attractions due to the collinear orientation between the negative electrostatic potential at the lp(Y) and the positive potential at the  $\sigma$ -hole of the WX bond, whereas the skewed orientation of type I complexes leads to a less effective alignment between the lp and the  $\sigma$ -hole electrostatic potential of the monomers. Electro-negative substituents withdraw charge from X and Y strengthening the positive potential at the  $\sigma$ -hole, but weakening the negative potential at the lone pair region.

Covalent contributions are rationalized in terms of the CT mechanism described in the orbital interaction diagram depicted in Figure 5. In type II complexes the covalent

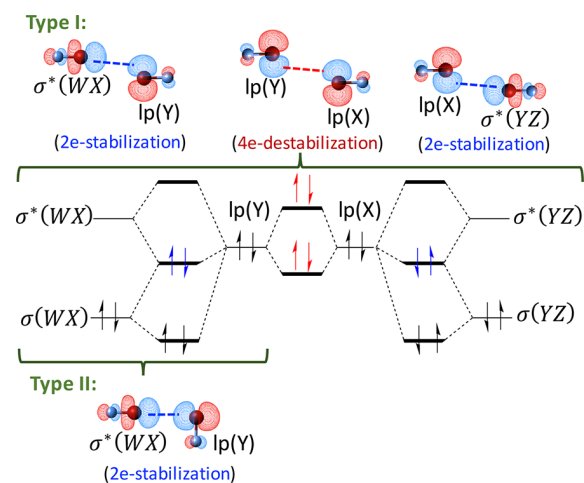


**Figure 5.** Orbital interaction diagram for type I and type II complexes, showing lp  $\rightarrow$   $\sigma^*$  (2e stabilization) and lp–lp (4e destabilization) charge transfer mechanisms for complexes 2 and 5.

contribution involves the charge transfer from the lp(Y) to the  $\sigma^*(WX)$  orbital, leading to 2e-delocalization and 2e-stabilization. A similar situation is also observed for type I complexes. However, the monomers in type I complexes adopt a skewed conformation allowing in addition the CT from the lp(X) to the  $\sigma^*(YZ)$  orbital, leading not only to an extra 2e-stabilization but also to a 4e-destabilization due to lp(X)–lp(Y) repulsion. The 2e-stabilization and 4e-destabilization are proportional to

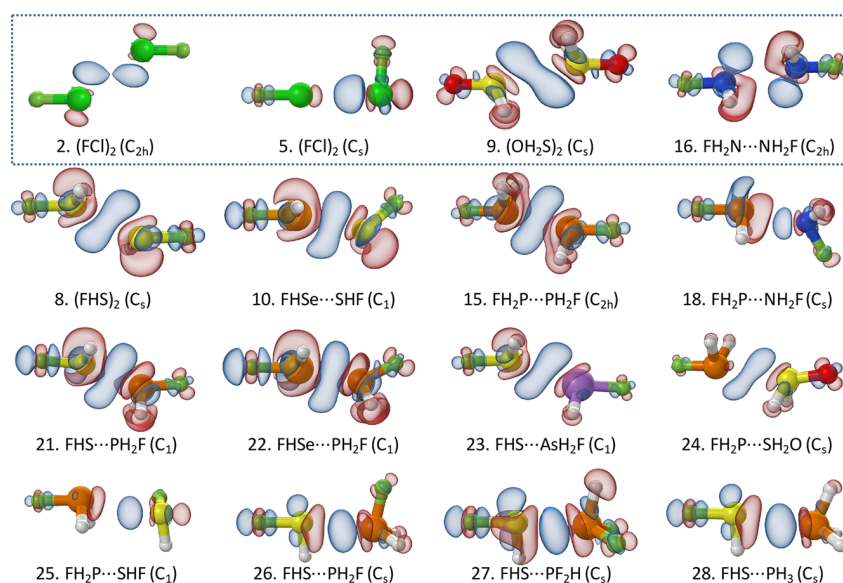


**Figure 6.** Electron difference density distributions  $\Delta\rho(r)$  given for selected complexes.  $\Delta\rho(r)$  is plotted for an electron density surface of 0.0004 au for the complexes in the rectangle (first row) and 0.001 au for the others. Blue regions indicate an increase in the electron density; red regions, a density decrease relative to the superimposed density of the monomers. Calculate at CCSD(T)/aug-cc-pVTZ level.

the magnitude of the orbital overlap and inversely proportional to the orbital energy gap ( $\Delta\epsilon$ ) between the molecular orbitals involved. Although only one CT mechanism is present in type II complexes, the  $\text{lp}(Y)-\sigma^*(WX)$  head-on overlap is more effective compared to the skewed overlap in type I complexes, and more importantly, the  $\text{lp}(X)-\text{lp}(Y)$  repulsion in type II complexes is minimized due to the smaller overlap.

The CT can be magnified by decreasing the  $\sigma^*(WX)$  and the  $\sigma^*(YZ)$  orbital energies or by increasing the  $\text{lp}(X)$  and  $\text{lp}(Y)$  orbital energies. A more electronegative W substituent lowers the energy of the  $\sigma(WX)$  and  $\sigma^*(WX)$  orbitals, thus decreasing the energy gap between  $\text{lp}(Y)$  and  $\sigma^*(WX)$ . The  $\text{lp}(Y)-\sigma(WX)$  orbital overlap is also improved by an electronegative W substituent, which reduces the X coefficient of the  $\sigma(WX)$  orbital. Due to orbital orthogonality, this in turn leads to a larger coefficient of  $\sigma^*(WX)$  orbital, thus increasing the  $\text{lp}(Y)-\sigma^*(WX)$  orbital overlap. An electronegative W atom also contracts the density at the X atom affecting the  $\text{lp}(X)$  orbital in two different ways (i) for atoms of the second period of the PT, the  $\text{lp}(X)$  orbitals becomes too compact decreasing  $\text{lp}(X)-\sigma^*(YZ)$  orbital overlap (ii) for atoms of the third or higher periods of the PT, the  $\text{lp}(X)$  becomes less diffuse, leading to improved  $\text{lp}(X)-\sigma^*(YZ)$  orbital overlap.<sup>23</sup>

Dispersive contributions play a dominant role only for complexes with minimal electrostatic and covalent contributions. In these cases the strength of the interaction can be rationalized on the basis of the polarizability of the monomers involved.

The different bonding mechanisms of type I and type II complexes are expected to result in different electronic structure changes upon complexation. This is demonstrated by the  $\Delta\rho(r)$  plots shown in Figure 6. Type II complexes (e.g., complexes 5, 18, 25, 26, 27, and 28 in Figure 6) are easily identify by a round shaped increase in the electron density in the intermonomer region (in blue), whereas type I complexes have a more stretched region of increased electron density (e.g., complexes 2, 8, 9, 10, 15, 21, 22, 23, and 24 in Figure 6). Therefore, rather than relying solely on geometric parameters we will make use of  $\Delta\rho(r)$  and the properties described in

Table 2 to distinguish between type I or type II complexes in the next sections.

#### Halogen...Halogen Interactions (Complexes 1–6).

Complexes 1–6 are only of electrostatic or dispersive nature. The high electronegativity of the halogen atoms results in X and Y lone pairs, which are too low in energy compared to the  $\sigma^*(WX)$  and  $\sigma^*(YZ)$  orbitals to lead to an effective CT (there is a large  $\Delta\epsilon(2e)$  energy gap). Therefore, small  $\Delta E(\text{del})$  and  $\Delta n$  (%) values are observed. The electrostatic potential at the lone pair ( $\pi$ ) region of the halogen Y is close to zero ( $V_{\text{min}} = -0.13$  eV for  $\text{Cl}_2$ ,  $-0.01$  eV for FCl, and  $0.01$  eV for FBr), resulting in weak electrostatic attraction with the  $V_{\text{max}}$  at the  $\sigma$ -hole of X atoms. The skewed conformation of XB-I complexes 1–3 leads to an even poorer electrostatic attraction between the extreme electrostatic potentials in the lp and in the  $\sigma$ -hole regions.

The strength of complexes 1–3 can only be rationalized on the basis of the polarizability of the monomers, in particular of the X and Y atoms. For these complexes the BSO  $n$  increases in the series  $(\text{FCl})_2$  (2) <  $(\text{Cl}_2)_2$  (1) <  $(\text{FBr})_2$  (3). The high polarizing power of the F substituents in 2 withdraws charge from Cl, decreasing its effective radius and, as a result, 2 has a  $\text{Cl}\cdots\text{Cl}$  distance  $0.083$  Å shorter than that found in 1. However, due to the lower polarizability of FCl compared to  $\text{Cl}_2$ , complex 2 forms a weaker interaction (BSO  $n$ :  $0.060$  (1),  $0.054$  (2)). In the case of  $(\text{FBr})_2$  the higher polarizability of Br compared to that of Cl, leads to a stronger bond (BSO  $n$ :  $0.073$  (3)).

By adopting a conformation in which the positive potential at the  $\sigma$ -hole is collinear with the negative potential of the lone pairs, XB-II complexes (4–6) are able to form true XBs. The strength of the XB in these complexes increases in the order  $(\text{Cl}_2)_2$  (4) <  $(\text{FCl})_2$  (5) <  $(\text{FBr})_2$  (6) and is determined by the magnitude of  $V_{\text{max}}$  at the  $\sigma$ -hole of X (Table 2). Although FBr has a slightly positive potential at the  $\pi$  region of Br suggesting a  $\text{lp}(\text{Br})\cdots\sigma\text{-hole}(\text{Br})$  repulsive interaction, one has to consider that the strong  $V_{\text{max}}$  at the Br  $\sigma$ -hole polarizes the  $\pi$  density of the second Br. An inverse relationship between  $\Delta E$  and the BSO  $n$  is found for complexes 4 and 5, indicating that secondary effects besides the  $\text{Cl}\cdots\text{Cl}$  XB help to stabilize

complex 4. This is evidenced by the inward tilted  $\theta_2 = 88.5^\circ$  angle adopted by 4 compared to the outward angle  $\theta_2 = 95.3^\circ$  of 5.

**Chalcogen...Chalcogen Interactions (Complexes 7–14).** There are two minima of ChB-I type for (FHS)<sub>2</sub> complexes (7, 8). One with C<sub>2</sub> symmetry where the H atoms are in a syn position (7), and the other with C<sub>i</sub> symmetry, where the H atoms are anti to each other (8). Both complexes are twice as strong as the isoelectronic XB-I complex 2, with YX distances of 2.748 Å for 7 and 2.715 Å for 8 compared to 3.268 for 2. The shorter and stronger interaction of these complexes is due to the more effective charge transfer ( $\Delta E(\text{del}) = 14.0$  (7), 15.8 (8), 1.3 (2) kcal/mol). Compared to Cl lone pairs, the lone pairs of S are higher in energy (IP: 12.7 kcal/mol for FCl and 10.4 kcal/mol for FHS), resulting in a smaller  $\Delta\epsilon(2e)$  energy gap. The lp– $\sigma^*$  overlap is also improved due the lower electronegativity of S compared to Cl (leading to a larger X coefficient in the  $\sigma^*(\text{WX})$  orbital). Due to the large lp(S)– $\sigma^*(\text{SO})$  energy gap and the weak electrostatic attraction, (OH<sub>2</sub>)<sub>2</sub> (9) forms a weak ChB-I.

If one S atom in 8 is substituted by the more polarizable Se, the heterodimer 10 (FHSe...SHF) is formed. This complex has a distorted geometry ( $\theta_1 = 162.8^\circ$  and  $\theta_2 = 125.2^\circ$ ), favoring a stronger electrostatic attraction between the Se  $\sigma$ -hole and the lp(S) and the CT from lp(S)  $\rightarrow \sigma^*(\text{SeF})$ . However, partial ChB-I character is still maintained. This is evidenced from the  $\Delta\rho(r)$  shown in Figure 6 by the stretched area of electron density increase (in blue), characteristic of type I complexes, and is confirmed by the sizable lp(Se)  $\rightarrow \sigma^*(\text{SF})$  2e-stabilization ( $\Delta(\text{del})_2 = 9.2$  kcal/mol) and by the weakening of both SF and SeF bonds by 14% and 15%, respectively (Table 1). It is noteworthy that the  $\Delta E$  of 10 is 1.4 kcal/mol larger than that of complex 8, but the BSO *n* of 10 is 0.105 compared to 0.111 in 8, suggesting that the geometry of this complex is distorted, not only to maximize the Se...S interaction but also due to the electrostatic attraction between the positively charged Se and the negative charge at the F. This is also reflected by the opposite trends between  $\Delta E(\text{del})$  and  $\Delta n$  (%) values (Table 1). Although  $\Delta E(\text{del})_1$  (referent to lp(S)  $\rightarrow \sigma^*(\text{SeF})$  CT) is much larger than  $\Delta E(\text{del})_2$  (referent to lp(S)  $\rightarrow \sigma^*(\text{SeF})$  CT), both SF and SeF bonds are weakened by about 15%.

In contrast, if S is substituted with the less polarizable O, only a ChB-II is formed (11). The OHF monomer has a lp(O) that is too low in energy (IP = 12.9 eV (OHF), 12.7 eV (OH<sub>2</sub>) compared to 10.4 eV (FHS)), leading to a large  $\Delta\epsilon(2e)$ , and thereby to a small CT. The large negative potential at the lp(O) ( $V_{\text{min}}$ : –1.40 eV (OH<sub>2</sub>) compared to –0.43 eV (FHS)) allows 12 to form an electrostatic interaction that is stronger than interactions with partial covalent character, such as the ones in complexes 8 and 10.

When an F atom is substituted with a H in complex 8, a stronger ChB (BSO *n*: 0.118 (13), 0.111 (8)) with lower covalent character, but improved electrostatic contribution, is formed (13). However, if a H atom is substituted by an F atom in 8, a weaker interaction (BSO *n*: 0.098 (14), but with a higher covalent character than 13, is formed. The extra F atom in 14 has a small impact on the lp(S) energy (IP: 10.3 eV for SF<sub>2</sub>, 10.4 eV for SFH); however, due to the high electronegativity of F, the electron density at the S atom is contracted leading to a shorter interaction distance ( $r(\text{SS}) = 2.840$  Å (14) compared to 3.065 Å (13)) and to a more effective lp(S)– $\sigma^*(\text{SF})$  overlap.

Similar effects are also present in XB and other ChB complexes.<sup>23,76</sup>

**Pnicogen...Pnicogen Interactions (Complexes 15–20).** Complex 15 ((FH<sub>2</sub>P)<sub>2</sub>) forms a shorter, stronger, and more covalent interaction than the isoelectronic XB-I (2) and ChB-I (8) complexes. P is less electronegative than S or Cl, thereby the lp(P) orbital is higher in energy, resulting in a smaller  $\Delta\epsilon(2e)$  energy gap and a stronger CT. Surprisingly, the complex formed by substituting both P atoms by the N (16) is also stronger than complexes 2 and 8. Different from 15, complex 16 has a high  $\Delta\epsilon(2e)$  energy gap and no significant covalent contribution; however, the lp(N) can form an electrostatic attraction with the positively charged H atoms at the opposite NH<sub>2</sub>F monomers. This electrostatic attraction is favored by the lp(N)–lp(N) repulsion, which pushes the electron density from the inter nitrogens region into the direction of the hydrogens (Figure 6).

Similar to the case for the chalcogens, substituting a P atom in 15 with the larger and more polarizable As yields a PnB-I complex (17) weaker than 15 (BSO *n*: 0.127 (17), 0.139 (15)). If a P atom is replaced with a N atom the PnB-II complex 18 is formed. This complex is weaker than both 15 and 16 (BSO *n* = 0.126 (18), 0.130 (16), 0.139 (15)).

A PnB-II complex with a BSO *n* comparable to that of the strongest PnB-I (complex 15) is realized for FH<sub>2</sub>P...NH<sub>3</sub> (20). The CT in 20 is similar to that in 18 (Table 1); however, due to the absence of an F substituent NH<sub>3</sub> has a lower electrostatic potential at the N than NH<sub>2</sub>F ( $V_{\text{min}} = -1.21$  eV (NH<sub>2</sub>F), –1.61 eV (NH<sub>3</sub>)). This results in a stronger electrostatic attraction with the  $\sigma$ -hole of FH<sub>2</sub>P. Noteworthy is that although 20 and 15 have BSO *n* values of 0.14, complex 20 has a  $\Delta E$  1.16 kcal/mol larger than that of 15. The extra stabilization in 20 is easily understood by considering the orientation of the dipoles moment of the monomers, which have opposite directions in 15 but the same direction in 20.

**Interactions Involving Atoms of Different Groups (Complexes 21–32).** From the investigation of XB-I, ChB-I, and PnB-I complexes it becomes evident that an interaction involving atoms of different groups of the periodic table (PT), which is capable of retaining a type I character is more likely a chalcogen–pnictogen combination. This is confirmed for complexes 21–24, where two CT mechanisms, one characteristic of a ChB and one characteristic of a PnB, are present. Therefore, these complexes were classified as a PnB/ChB-I type in this work. These complexes also have a  $\Delta\rho(r)$  that resembles those of the other type I complexes (Figure 6).

The combination of the monomers involved in the strongest ChB-I (7) and PnB-I (15) complexes leads to FHS...PH<sub>2</sub>F. This complex has three different minimum-energy conformations: one forming a PnB/ChB-I complex (21), one forming a PnB-II complex 25, and the other forming a ChB-II complex (26). The presence of both a charge transfer from lp(S) to  $\sigma^*(\text{PF})$  and also from lp(P) to  $\sigma^*(\text{SF})$  in 21 leads to an extra stabilization and to a stronger interaction compared to 25 and 26 (BSO *n* = 0.116 (21), 0.097 (25), 0.100 (26)), but weaker compared to the PnB-I homodimer 15 (BSO *n* = 0.139).

A complex with partial PnB/ChB-I character and a stronger noncovalent interaction than 15 is obtained by substituting S by Se in 21 (complex 22). Similar to 10, complex 22 has a distorted geometry favoring lp(P)  $\rightarrow \sigma^*(\text{SeF})$  CT and lp(Se)– $\sigma$ -hole electrostatic attraction ( $\Delta(\text{del})_1 = 63.7$  kcal/mol (22) compared to 47.3 kcal/mol (21)) in detriment of lp(Se)  $\rightarrow \sigma^*(\text{PFH}_2)$  CT ( $\Delta(\text{del})_2 = 17.6$  kcal/mol (22)

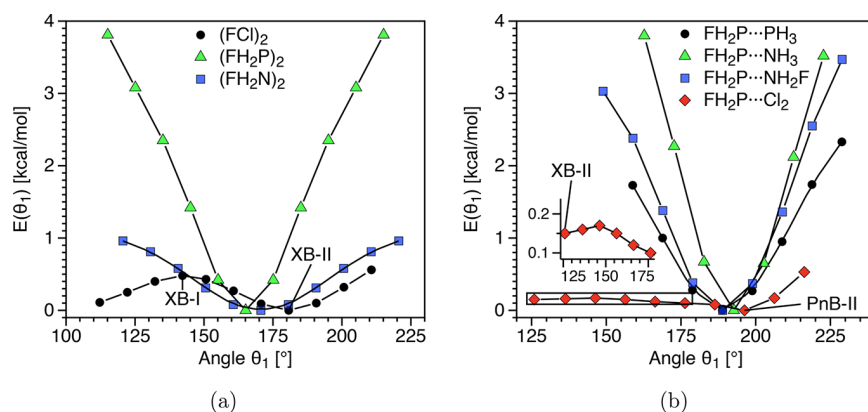


**Figure 7.** Relationship between the potential energy relative to the minimum energy point and  $\theta_1$  for (a) homodimers (b) PnB heterodimers. Black lines are used just to connect points.

compared to 24.2 kcal/mol (**21**)). Because of the substantial stabilization from both CT mechanisms and due to the characteristic  $\Delta\rho(r)$  of type I complexes (Figure 6), complex **22** is still of type I. If the P atom in **21** is replaced by a As, a complex of similar strength to **21** and with an equivalent admixture of PnB and ChB character is formed ( $\Delta E(\text{del})1 \approx \Delta E(\text{del})2$ ) (**23**). The higher polarizability of As in **23** results in a more diffuse lp(As), leading to a longer interaction distance with a less effective lp(As)– $\sigma^*(\text{SF})$  overlap, thus to a smaller CT. This is counterbalanced by the higher electrostatic potential at the As  $\sigma$ -hole, increasing the electrostatic contribution.

The combination of FPH<sub>2</sub> and SH<sub>2</sub>O also leads to a type I complex (**23**). This complex has an intermediate strength between the homodimers (OH<sub>2</sub>S)<sub>2</sub> (**9**) and (FH<sub>2</sub>P)<sub>2</sub> (**15**). Similar to what was observed for chalcogen...chalcogen and pnictogen...pnictogen complexes, substituting a F atom with a H or vice versa only type-II complexes are formed (**27–30**).

**Sensitivity to Angular Distortion.** To measure the angular distortion sensitivity for a set of seven complexes, the  $\theta_1$  angle was distorted from its fully optimized geometry in increments of 10°. At each step all geometric parameters but  $\theta_1$  were reoptimized. Figure 7 shows how the energy relative to the undistorted geometry varies as a function of  $\theta_1$  for three homodimers (Figure 7a) and four heterodimers (Figure 7b).

Type XB-I complexes (**1–3**) are first-order transition states. The imaginary frequencies of these complexes are of 12 (**1**), 25 (**2**), and 30 (**3**) cm<sup>-1</sup> and can be associated with the W–X–Y bending mode that leads to the type XB-II complexes **4**, **5**, and **6**, respectively. The bending potential of (FCl)<sub>2</sub> (complex **2**) shown in Figure 7 reveals that there is a small difference between the high-energy XB-I and the minimum-energy XB-II conformations (0.48 kcal/mol for (FCl)<sub>2</sub>, 0.39 kcal/mol for (Cl<sub>2</sub>)<sub>2</sub>, and 0.83 kcal/mol for (FBr)<sub>2</sub>), which could easily be overcome by crystal packing forces. This observation is inline with experimental studies on the halogen...halogen interactions in hexahalogenated benzenes, suggesting that Cl...Cl and Br...Br interactions are weak and nondirectional and can be easily deformed leading to a conformation that does not correspond strictly to type I or type II conformation.<sup>53</sup>

Other type I homodimers held together by stronger interactions such as (FNH<sub>2</sub>)<sub>2</sub> and (FPH<sub>2</sub>)<sub>2</sub> are minima in the potential energy surface. In these cases, the angular sensitivity increases with the increased strength and covalent character of the interaction. No type II minimum was found for these

complexes. The angular sensitivity in type II heterodimers also increases with the strength of the interaction following the order FH<sub>2</sub>P...Cl<sub>2</sub> < FH<sub>2</sub>P...PH<sub>3</sub> < FH<sub>2</sub>P...NH<sub>2</sub>F < FH<sub>2</sub>P...NH<sub>3</sub> (Figure 7b).

Although only a XB-II and a PnB-II minimum and no XB/PnB type I minimum-energy point were identified by bending Cl<sub>2</sub>...PFH<sub>2</sub>, the barrier separating the PnB-II complex **31** from the XB-II complex **32** is just 0.15 kcal/mol, suggesting that a dispersive force (similar to the ones found for complexes **1–3**) lowers the barrier separating these two types of interactions.

#### 4. CONCLUSIONS AND OUTLOOK

In the present work, we compared the nature, the intrinsic strength, and the binding energies of a series of weak noncovalent interactions involving pnictogen, chalcogens, and halogens atoms using highly accurate CCSD(T)/aug-cc-pVTZ geometries, vibrational frequencies, NPA atomic charges, energy and electron densities, and electrostatic potentials. By generalizing the description of type I and II interactions commonly employed for halogen...halogen complexes and including suitable molecular orbital diagrams, we obtained the following conclusions:

1. Noncovalent interactions involving chalcogens, pnictogens, and halogens can be described by a similar bonding mechanism, which only depends on the conformation adopted by the complex. Type I complexes adopt a skewed conformation allowing two different CT mechanisms (from the lp(Y) to the  $\sigma^*(\text{WX})$  orbital and from the lp(X) to the  $\sigma^*(\text{YZ})$  orbital), whereas type II complexes adopt a conformation where lp(Y) is collinear to  $\sigma^*(\text{WX})$ , maximizing the charge transfer from the lp(Y) to the  $\sigma^*(\text{WX})$  orbital.
2. Instead of relying solely on geometric parameters, we used for the first time in addition, electron difference densities, delocalization energies, and the shift in the bond strength order of the WX and YZ bonds to distinguish between type I and type II complexes. In this connection, type I complexes are easily distinguished by the stretched area of electron density increase in the intermonomer region, when compared to type II complexes.
3. Pnictogens can form stronger type I homodimers than chalcogens or halogens. The lower electronegativity of P compared to that of S or Cl leads to a smaller  $\Delta\epsilon(2e)$  energy gap, granting partial covalent character to the P...

P interactions. The higher electronegativity of halogens results in XB-I complexes of dispersive nature, which are first-order transition states.

- Heterodimers can also form type I complexes as long as the  $\text{lp}(Y)-\sigma^*(WX)$  and the  $\text{lp}(X)-\sigma^*(YZ)$  orbital overlaps and the orbital energy gaps are small. FHS...PH<sub>2</sub>F is an example of a stable type I complex involving two CT mechanisms, one characteristic of a PnB and the other of a ChB. This PnB/ChB-I complex is stronger than the ChB-II or PnB-II complexes formed by the same monomers.
- There is a scattered correlation between the binding energies and the intrinsic bond strength given by the  $k^2$  or BSO  $n$  values for all complexes investigated in this work. This scattering occurs when secondary contributions, not accounted for by the atom–atom interaction, are involved in the stabilization of the complex. The comparison of BSO and  $\Delta E$  trends are useful to identify the significance of such contributions.

Clark, Politzer, and Murray<sup>96,97,109</sup> recently suggested the analysis of the unperturbed electrostatic potentials of the monomers mapped onto a van der Waals surface as a practical approximation to predict the geometry and even the strength of noncovalent interactions that are not affected by polarization. However, a caveat is appropriate. Polarization can play a decisive role even for weak interactions (e.g.,  $\Delta E < 10$  kcal/mol). In these cases, orbital interaction diagrams (although based on model quantities rather than physical observables) provide the most insightful and intuitive way to describe the mechanism of these noncovalent interactions. When a specific charge transfer mechanism is singled out, a simple orbital interaction diagram can be used to rationalize the covalent contributions of the interactions involving halogens, chalcogens, and pnictogens of both type I and II conformations.

## ■ ASSOCIATED CONTENT

### Supporting Information

The Supporting Information is available free of charge on the ACS Publications website at DOI: [10.1021/acs.jpca.7b10196](https://doi.org/10.1021/acs.jpca.7b10196).

CP-corrected and uncorrected interaction energies of 12 complexes calculated with DLPNO-CCSD(T)/aug-cc-pVTZ, and DLPNO-CCSD(T)/aug-cc-pV5Z, molecular electrostatic potential of all monomers, selected molecular orbitals of the monomers, and complex geometries (PDF)

## ■ AUTHOR INFORMATION

### Corresponding Author

\*E. Kraka. E-mail: [ekraka@smu.edu](mailto:ekraka@smu.edu).

### ORCID

Elfi Kraka: [0000-0002-9658-5626](https://orcid.org/0000-0002-9658-5626)

### Notes

The authors declare no competing financial interest.

## ■ ACKNOWLEDGMENTS

This work was financially supported by the National Science Foundation grants CHE 1152357 and CHE 1464906. We thank SMU for providing computational resources. The authors acknowledge financial support by CAPES (Brazil; fellowship grant BEX 9534-13-0).

## ■ DEDICATION

Dedicated to the memory of Professor Dieter Cremer, whose pioneering work and insightful discussions on noncovalent interactions and vibrational spectroscopy were fundamental to this study.

## ■ REFERENCES

- Cavallo, G.; Metrangolo, P.; Milani, R.; Pilati, T.; Priimagi, A.; Resnati, G.; Terraneo, G. The halogen bond. *Chem. Rev.* **2016**, *116*, 2478–2601.
- Matta, C. F.; Castillo, N.; Boyd, R. J. Extended weak bonding interactions in DNA:  $\pi$ -stacking (base-base), base-backbone, and backbone-backbone interactions. *J. Phys. Chem. B* **2006**, *110*, 563–578.
- Sponer, J.; Riley, K. E.; Hobza, P. Nature and magnitude of aromatic stacking of nucleic acid bases. *Phys. Chem. Chem. Phys.* **2008**, *10*, 2595–2610.
- Bissantz, C.; Kuhn, B.; Stahl, M. A medicinal chemist's guide to molecular interactions. *J. Med. Chem.* **2010**, *53*, 5061–5084.
- Wilcken, R.; Zimmermann, M. O.; Lange, A.; Joerger, A. C.; Boeckler, F. M. Principles and applications of halogen bonding in medicinal chemistry and chemical biology. *J. Med. Chem.* **2013**, *56*, 1363–1388.
- Wheeler, S. E.; Seguin, T. J.; Guan, Y.; Doney, A. C. Noncovalent interactions in organocatalysis and the prospect of computational catalyst design. *Acc. Chem. Res.* **2016**, *49*, 1061–1069.
- Uyeda, C.; Jacobsen, E. N. Transition-state charge stabilization through multiple non-covalent interactions in the guanidinium-catalyzed enantioselective claisen rearrangement. *J. Am. Chem. Soc.* **2011**, *133*, 5062–5075.
- Yáñez, M.; Sanz, P.; Mó, O.; Alkorta, I.; Elguero, J. Beryllium bonds, do they exist? *J. Chem. Theory Comput.* **2009**, *5*, 2763–2771.
- Tama, R.; Mó, O.; Yáñez, M.; Montero-Campillo, M. M. Characterizing magnesium bonds: main features of a non-covalent interaction. *Theor. Chem. Acc.* **2017**, *136*, 36.
- Bauzá, A.; Frontera, A. Aerogen bonding interaction: A new supramolecular force? *Angew. Chem., Int. Ed.* **2015**, *54*, 7340–7343.
- Bauzá, A.; Mooibroek, T. J.; Frontera, A. Tetrel-bonding interaction: Rediscovered supramolecular force? *Angew. Chem., Int. Ed.* **2013**, *52*, 12317–12321.
- Del Bene, J. E.; Alkorta, I.; Elguero, J. In *Noncovalent forces*; Scheiner, S., Ed.; Springer International Publishing: Berlin, 2015; pp 191–263.
- Zhang, X.; Dai, H.; Zou, H. Y. W.; Cremer, D. B-H... $\pi$  interaction: A new type of nonclassical hydrogen bonding. *J. Am. Chem. Soc.* **2016**, *138*, 4334–4337.
- Stone, A. J. Are halogen bonded structures electrostatically driven? *J. Am. Chem. Soc.* **2013**, *135*, 7005–7009.
- Wang, C.; Guan, L.; Danovich, D.; Shaik, S.; Mo, Y. The origins of the directionality of noncovalent intermolecular interactions. *J. Comput. Chem.* **2016**, *37*, 34–45.
- Politzer, P.; Murray, J. S.; Clark, T. Halogen bonding: An electrostatically-driven highly directional noncovalent interaction. *Phys. Chem. Chem. Phys.* **2010**, *12*, 7748–7757.
- Esrafil, M. D.; Mohammadirad, N. An ab initio study on tunability of  $\sigma$ -hole interactions in XHS:PH<sub>2</sub>Y and XH<sub>2</sub>P:SHY complexes (X = F, Cl, Br; Y = H, OH, OCH<sub>3</sub>, CH<sub>3</sub>, C<sub>2</sub>H<sub>5</sub>, and NH<sub>2</sub>). *J. Mol. Model.* **2015**, *21*, 176.
- Albrecht, L.; Boyd, R. J.; Mó, O.; Yáñez, M. Changing weak halogen bonds into strong ones through cooperativity with beryllium bonds. *J. Phys. Chem. A* **2014**, *118*, 4205–4213.
- Alkorta, I.; Elguero, J.; Mó, O.; Yáñez, M.; Del Bene, J. E. Using beryllium bonds to change halogen bonds from traditional to chlorine-shared to ion-pair bonds. *Phys. Chem. Chem. Phys.* **2015**, *17*, 2259–2267.
- Brea, O.; Mó, O.; Yáñez, M.; Alkorta, I.; Elguero, J. Creating  $\sigma$ -holes through the formation of beryllium bonds. *Chem. - Eur. J.* **2015**, *21*, 12676–12682.

- (21) M6, O.; Yáñez, M.; Alkorta, I.; Elguero, J. Modulating the strength of hydrogen bonds through beryllium bonds. *J. Chem. Theory Comput.* **2012**, *8*, 2293–2300.
- (22) Oliveira, V.; Kraka, E.; Cremer, D. Quantitative assessment of halogen bonding utilizing vibrational spectroscopy. *Inorg. Chem.* **2017**, *56*, 488–502.
- (23) Oliveira, V.; Cremer, D.; Kraka, E. The many facets of chalcogen bonding: Described by vibrational spectroscopy. *J. Phys. Chem. A* **2017**, *121*, 6845–6862.
- (24) Oliveira, V.; Cremer, D. Transition from metal-ligand bonding to halogen bonding involving a metal as halogen acceptor a study of Cu, Ag, Au, Pt, and Hg complexes. *Chem. Phys. Lett.* **2017**, *681*, 56–63.
- (25) Bai, M.; Thomas, S. P.; Kottokkaran, R.; Nayak, S. K.; Ramamurthy, P. C.; Guru Row, T. N. A donor-acceptor-donor structured organic conductor with S··S chalcogen bonding. *Cryst. Growth Des.* **2014**, *14*, 459–466.
- (26) Atzori, M.; Artizzu, F.; Sessini, E.; Marchio, L.; Loche, D.; Serpe, A.; Deplano, P.; Concas, G.; Pop, F.; Avarvari, N.; et al. Halogen-bonding in a new family of tris(haloanilato)metallate(III) magnetic molecular building blocks. *Dalton Trans.* **2014**, *43*, 7006–7019.
- (27) Yamamoto, H. M.; Yamaura, J.-I.; Kato, R. Multicomponent molecular conductors with supramolecular assembly: Iodine-containing neutral molecules as building blocks. *J. Am. Chem. Soc.* **1998**, *120*, 5905–5913.
- (28) Virkki, M.; Tuominen, O.; Forni, A.; Saccone, M.; Metrangolo, P.; Resnati, G.; Kauranen, M.; Priimagi, A. Halogen bonding enhances nonlinear optical response in poled supramolecular polymers. *J. Mater. Chem. C* **2015**, *3*, 3003–3006.
- (29) Zhu, W.; Zheng, R.; Zhen, Y.; Yu, Z.; Dong, H.; Fu, H.; Shi, Q.; Hu, W. Rational design of charge-transfer interactions in halogen-bonded co-crystals toward versatile solid-state optoelectronics. *J. Am. Chem. Soc.* **2015**, *137*, 11038–11046.
- (30) Priimagi, A.; Cavallo, G.; Forni, A.; Gorynsztejn-Leben, M.; Kaivola, M.; Metrangolo, P.; Milani, R.; Shishido, A.; Pilati, T.; Resnati, G.; et al. Halogen bonding versus hydrogen bonding in driving self-assembly and performance of light-responsive supramolecular polymers. *Adv. Funct. Mater.* **2012**, *22*, 2572–2579.
- (31) Ho, P. C.; Szydlowski, P.; Sinclair, J.; Elder, P. J. W.; Kübel, J.; Gendy, C.; Lee, L. M.; Jenkins, H.; Britten, J. F.; Morim, D. R.; et al. Supramolecular macrocycles reversibly assembled by Te(···)O chalcogen bonding. *Nat. Commun.* **2016**, *7*, 11299.
- (32) Werz, D. B.; Gleiter, R.; Rominger, F. Nanotube formation favored by chalcogen-chalcogen interactions. *J. Am. Chem. Soc.* **2002**, *124*, 10638–10639.
- (33) Zahn, S.; Frank, R.; Hey-Hawkins, E.; Kirchner, B. Pnictogen bonds: A new molecular linker? *Chem. - Eur. J.* **2011**, *17*, 6034–6038.
- (34) Cozzolino, A. F.; Yang, Q.; Vargas-Baca, I. Engineering second-order nonlinear optical activity by means of a noncentrosymmetric distortion of the [Te-N]<sub>2</sub> supramolecular synthon. *Cryst. Growth Des.* **2010**, *10*, 4959–4964.
- (35) Beno, B. R.; Yeung, K.-S.; Bartberger, M. D.; Pennington, L. D.; Meanwell, N. A. A. Survey of the role of noncovalent sulfur interactions in drug design. *J. Med. Chem.* **2015**, *58*, 4383–4438.
- (36) Nagao, Y.; Hirata, T.; Goto, S.; Sano, S.; Kakehi, A.; Iizuka, K.; Shiro, M. Intramolecular nonbonded S··O interaction recognized in (acylimino)thiadiazoline derivatives as angiotensin II receptor antagonists and related compounds. *J. Am. Chem. Soc.* **1998**, *120*, 3104–3110.
- (37) Cavallo, G.; Metrangolo, P.; Pilati, T.; Resnati, G.; Sansotera, M.; Terraneo, G. Halogen bonding: A general route in anion recognition and coordination. *Chem. Soc. Rev.* **2010**, *39*, 3772–3783.
- (38) Mahmudov, K. T.; Kopylovich, M. N.; Guedes da Silva, M. F. C.; Pombeiro, A. J. L. Chalcogen bonding in synthesis, catalysis and design of materials. *Dalton Trans.* **2017**, *46*, 10121–10138.
- (39) Gilday, L. C.; Robinson, S. W.; Barendt, T. A.; Langton, M. J.; Mullaney, B. R.; Beer, P. D. Halogen Bonding in Supramolecular Chemistry. *Chem. Rev.* **2015**, *115*, 7118–7195.
- (40) Ho, P. In *Halogen bonding I*; Metrangolo, P., Resnati, G., Eds.; Topics in current chemistry; Springer International Publishing: Berlin, 2015; Vol. 358, pp 241–276.
- (41) Xu, Z.; Yang, Z.; Liu, Y.; Lu, Y.; Chen, K.; Zhu, W. Halogen bond: Its role beyond drug-target binding affinity for drug discovery and development. *J. Chem. Inf. Model.* **2014**, *54*, 69–78.
- (42) Jentzsch, A. V.; Matile, S. In *Halogen bonding I*; Metrangolo, P., Resnati, G., Eds.; Topics in current chemistry; Springer International Publishing: Berlin, 2015; Vol. 358, pp 205–239.
- (43) Zordan, F.; Brammer, L.; Sherwood, P. Supramolecular chemistry of halogens: Complementary features of inorganic (M-X) and organic (C-X) halogens applied to M-X···X-C halogen bond formation. *J. Am. Chem. Soc.* **2005**, *127*, 5979–5989.
- (44) Podsiadlo, M.; Olejniczak, A.; Katrusiak, A. Halogen···halogen contra C-H···halogen interactions. *CrystEngComm* **2014**, *16*, 8279–8285.
- (45) Tothadi, S.; Joseph, S.; Desiraju, G. R. Synthron modularity in cocrystals of 4-bromobenzamide with n-alkanedicarboxylic acids: Type I and type II halogen···halogen interactions. *Cryst. Growth Des.* **2013**, *13*, 3242–3254.
- (46) Mukherjee, A.; Desiraju, G. R. Halogen bonds in some dihalogenated phenols: Applications to crystal engineering. *IUCrJ* **2014**, *1*, 49–60.
- (47) Sakurai, T.; Sundaralingam, M.; Jeffrey, G. A. A nuclear quadrupole resonance and X-ray study of the crystal structure of 2,5-dichloroaniline. *Acta Crystallogr.* **1963**, *16*, 354–363.
- (48) Desiraju, G. R.; Parthasarathy, R. The nature of  $\sigma^*$  halogen···halogen interactions: Are short halogen contacts due to specific attractive forces or due to close packing of nonspherical atoms? *J. Am. Chem. Soc.* **1989**, *111*, 8725–8726.
- (49) Duarte, D. J. R.; Peruchena, N. M.; Alkorta, I. Double hole-lump interaction between halogen atoms. *J. Phys. Chem. A* **2015**, *119*, 3746–3752.
- (50) Capdevila-Cortada, M.; Castello, J.; Novoa, J. J. The nature of the C-Cl···Cl-C intermolecular interactions found in molecular crystals: A general theoretical-database study covering the 2.75–4.0 Å range. *CrystEngComm* **2014**, *16*, 8232–8242.
- (51) Awwadi, F. F.; Willett, R. D.; Peterson, K. A.; Twamley, B. The nature of halogen···halogen synthons: Crystallographic and theoretical studies. *Chem. - Eur. J.* **2006**, *12*, 8952–8960.
- (52) Metrangolo, P.; Resnati, G. Type II halogen···halogen contacts are halogen bonds. *IUCrJ* **2014**, *1*, 5–7.
- (53) Reddy, C. M.; Kirchner, M. T.; Gundakaram, R. C.; Padmanabhan, K. A.; Desiraju, G. R. Isostructurality, polymorphism and mechanical properties of some hexahalogenated benzenes: The nature of halogen···halogen interactions. *Chem. - Eur. J.* **2006**, *12*, 2222–2234.
- (54) Setiawan, D.; Kraka, E.; Cremer, D. Strength of the pnictogen bond in complexes involving group Va elements N, P, and As. *J. Phys. Chem. A* **2015**, *119*, 1642–1656.
- (55) Setiawan, D.; Cremer, D. Super-pnictogen bonding in the radical anion of the fluorophosphine dimer. *Chem. Phys. Lett.* **2016**, *662*, 182–187.
- (56) Antonijevic, I. S.; Janjic, G. V.; Milcic, M. K.; Zanic, S. D. Preferred geometries and energies of sulfur-sulfur interactions in crystal structures. *Cryst. Growth Des.* **2016**, *16*, 632–639.
- (57) Shukla, R.; Chopra, D. Crystallographic and theoretical investigation on the nature and characteristics of type I C-S···S-C interactions. *Cryst. Growth Des.* **2016**, *16*, 6734–6742.
- (58) Del Bene, J. E.; Sanchez-Sanz, G.; Alkorta, I.; Elguero, J. Homo- and heterochiral dimers (PHFX)<sub>2</sub>, X = Cl, CN, CH<sub>3</sub>, NC: To what extent do they differ? *Chem. Phys. Lett.* **2012**, *538*, 14–18.
- (59) Del Bene, J. E.; Alkorta, I.; Elguero, J. Substituent effects on the properties of pnictogen-bonded complexes H<sub>2</sub>XP:PYH<sub>2</sub>, for X, Y = F, Cl, OH, NC, CCH, CH<sub>3</sub>, CN, and H. *J. Phys. Chem. A* **2015**, *119*, 224–233.
- (60) Trujillo, C.; Sánchez-Sanz, G.; Alkorta, I.; Elguero, J. Halogen, chalcogen and pnictogen interactions in (XNO<sub>2</sub>)<sub>2</sub> homodimers (X = F, Cl, Br, I). *New J. Chem.* **2015**, *39*, 6791–6802.

- (61) Bleiholder, C.; Werz, D. B.; Köppel, H.; Gleiter, R. Theoretical investigations on chalcogen-chalcogen interactions: What makes these nonbonded interactions bonding? *J. Am. Chem. Soc.* **2006**, *128*, 2666–2674.
- (62) Bleiholder, C.; Gleiter, R.; Werz, D. B.; Köppel, H. Theoretical investigations on heteronuclear chalcogen-chalcogen interactions: On the nature of weak bonds between chalcogen centers. *Inorg. Chem.* **2007**, *46*, 2249–2260.
- (63) Azofra, L. M.; Alkorta, I.; Scheiner, S. Chalcogen bonds in complexes of SOXY (X, Y = F, Cl) with nitrogen bases. *J. Phys. Chem. A* **2015**, *119*, 535–541.
- (64) Alkorta, I.; Elguero, J.; Del Bene, J. E. Characterizing traditional and chlorine-shared halogen bonds in complexes of phosphine derivatives with ClF and Cl<sub>2</sub>. *J. Phys. Chem. A* **2014**, *118*, 4222–4231.
- (65) Del Bene, J. E.; Alkorta, I.; Elguero, J. Influence of substituent effects on the formation of P...Cl pnictogen bonds or halogen bonds. *J. Phys. Chem. A* **2014**, *118*, 2360–2366.
- (66) Shukla, R.; Chopra, D. Pnictogen bonds or chalcogen bonds: Exploiting the effect of substitution on the formation of P...Se noncovalent bonds. *Phys. Chem. Chem. Phys.* **2016**, *18*, 13820–13829.
- (67) Möller, C.; Plesset, M. S. Note on an approximation treatment for many-electron systems. *Phys. Rev.* **1934**, *46*, 618–622.
- (68) Steinmann, S. N.; Piemontesi, C.; Delachat, A.; Corminboeuf, C. Why are the interaction energies of charge-transfer complexes challenging for DFT? *J. Chem. Theory Comput.* **2012**, *8*, 1629–1640.
- (69) Bauzá, A.; Alkorta, I.; Frontera, A.; Elguero, J. On the reliability of pure and hybrid DFT methods for the evaluation of halogen, chalcogen, and pnictogen bonds involving anionic and neutral electron donors. *J. Chem. Theory Comput.* **2013**, *9*, S201–S210.
- (70) Kozuch, S.; Martin, J. M. L. Halogen bonds: Benchmarks and theoretical analysis. *J. Chem. Theory Comput.* **2013**, *9*, 1918–1931.
- (71) Raghavachari, K.; Trucks, G. W.; Pople, J. A.; Head-Gordon, M. A fifth-order perturbation comparison of electron correlation theories. *Chem. Phys. Lett.* **1989**, *157*, 479–483.
- (72) Rezac, J.; Hobza, P. Describing noncovalent interactions beyond the common approximations: How accurate is the "Gold Standard," CCSD(T) at the complete basis set limit? *J. Chem. Theory Comput.* **2013**, *9*, 2151–2155.
- (73) Brauer, B.; Kesharwani, M. K.; Kozuch, S.; Martin, J. M. L. The S66 × 8 benchmark for noncovalent interactions revisited: Explicitly correlated ab initio methods and density functional theory. *Phys. Chem. Chem. Phys.* **2016**, *18*, 20905–20925.
- (74) Rezac, J.; Hobza, P. Benchmark calculations of interaction energies in noncovalent complexes and their applications. *Chem. Rev.* **2016**, *116*, 5038–5071.
- (75) Hill, J. G.; Hu, X. Theoretical insights into the nature of halogen bonding in prereactive complexes. *Chem. - Eur. J.* **2013**, *19*, 3620–3628.
- (76) Oliveira, V.; Kraka, E.; Cremer, D. The intrinsic strength of the halogen bond: Electrostatic and covalent contributions described by coupled cluster theory. *Phys. Chem. Chem. Phys.* **2016**, *18*, 33031–33046.
- (77) Woon, D.; Dunning, T. J. Gaussian basis sets for use in correlated molecular calculations. IV. Calculation of static electrical response properties. *J. Chem. Phys.* **1994**, *100*, 2975–2988.
- (78) Dunning, T. Gaussian basis sets for use in correlated molecular calculations. I. The atoms boron through neon and hydrogen. *J. Chem. Phys.* **1989**, *90*, 1007–1023.
- (79) Woon, D.; Dunning, T. Gaussian basis sets for use in correlated molecular calculations. III. The atoms aluminum through argon. *J. Chem. Phys.* **1993**, *98*, 1358–1371.
- (80) Konkoli, Z.; Cremer, D. A new way of analyzing vibrational spectra I. Derivation of adiabatic internal modes. *Int. J. Quantum Chem.* **1998**, *67*, 1–11.
- (81) Cremer, D.; Larsson, J. A.; Kraka, E. In *Theoretical and Computational Chemistry, Vol. 5, Theoretical Organic Chemistry*; Parkanyi, C., Ed.; Elsevier: Amsterdam, 1998; pp 259–327.
- (82) Zou, W.; Kalescky, R.; Kraka, E.; Cremer, D. Relating normal vibrational modes to local vibrational modes with the help of an adiabatic connection scheme. *J. Chem. Phys.* **2012**, *137*, 084114.
- (83) Zou, W.; Cremer, D. Properties of local vibrational modes: The infrared intensity. *Theor. Chem. Acc.* **2014**, *133*, 1451.
- (84) Wilson, E. B.; Decius, J. C.; Cross, P. C. *Molecular vibrations. The theory of infrared and Raman vibrational spectra*; McGraw-Hill: New York, 1955.
- (85) Zou, W.; Cremer, D. C<sub>2</sub> in a box: Determining its intrinsic bond strength for the X<sup>1</sup>Σ<sub>g</sub><sup>+</sup> ground state. *Chem. - Eur. J.* **2016**, *22*, 4087–4089.
- (86) Kraka, E.; Larsson, J. A.; Cremer, D. In *Computational spectroscopy: Methods, experiments and applications*; Grunenberg, J., Ed.; Wiley: New York, 2010; pp 105–149.
- (87) Boys, S.; Bernardi, F. The calculation of small molecular interactions by the differences of separate total energies. Some procedures with reduced errors. *Mol. Phys.* **1970**, *19*, 553–566.
- (88) Mentel, L. M.; Baerends, E. J. Can the counterpoise correction for basis set superposition effect be justified? *J. Chem. Theory Comput.* **2014**, *10*, 252–267.
- (89) van Duijneveldt, F. B.; van Duijneveldt-van de Rijdt, J. G. C. M.; van Lenthe, J. H. State of the art in counterpoise theory. *Chem. Rev.* **1994**, *94*, 1873–1885.
- (90) Riplinger, C.; Neese, F. An efficient and near linear scaling pair natural orbital based local coupled cluster method. *J. Chem. Phys.* **2013**, *138*, 034106.
- (91) Riplinger, C.; Sandhoefer, B.; Hansen, A.; Neese, F. Natural triple excitations in local coupled cluster calculations with pair natural orbitals. *J. Chem. Phys.* **2013**, *139*, 134101.
- (92) Dunning, T. J. Gaussian basis sets for use in correlated molecular calculations I. The atoms boron through neon and hydrogen. *J. Chem. Phys.* **1989**, *90*, 1007–1023.
- (93) Cremer, D.; Kraka, E. A description of the chemical bond in terms of local properties of electron density and energy. *Croat. Chem. Acta* **1984**, *57*, 1259–1281.
- (94) Cremer, D.; Kraka, E. Chemical bonds without bonding electron density - Does the difference electron density analysis suffice for a description of the chemical bond? *Angew. Chem., Int. Ed. Engl.* **1984**, *23*, 627–628.
- (95) Kraka, E.; Cremer, D. In *Theoretical models of chemical bonding. The concept of the chemical bond*, Vol. 2; Maksic, Z., Ed.; Springer Verlag: Heidelberg, Germany, 1990; pp 453–542.
- (96) Clark, T. Halogen bonds and σ-holes. *Faraday Discuss.* **2017**, *203*, 9–27.
- (97) Murray, J. S.; Politzer, P. Molecular electrostatic potentials and noncovalent interactions. *WIREs Comput. Mol. Sci.* **2017**, *7*, e1326.
- (98) Weinhold, F.; Landis, C. R. *Valency and bonding: A natural bond orbital donor-acceptor perspective*; Cambridge University Press: Cambridge, U.K., 2003.
- (99) Chai, J. D.; Head-Gordon, M. Long-range corrected hybrid density functionals with damped atom-atom dispersion corrections. *Phys. Chem. Chem. Phys.* **2008**, *10*, 6615.
- (100) Chai, J. D.; Head-Gordon, M. Systematic optimization of long-range corrected hybrid density functionals. *J. Chem. Phys.* **2008**, *128*, 084106.
- (101) Stone, A. J. Natural bond orbitals and the nature of the hydrogen bond. *J. Phys. Chem. A* **2017**, *121*, 1531–1534.
- (102) Kraka, E.; Zou, W.; Filatov, M.; Grafenstein, J.; Izotov, D.; Gauss, J.; He, Y.; Wu, A.; Konkoli, Z.; Polo, V.; et al. *COLOGNE2016*; 2016; see <http://www.smu.edu/catco> (accessed Nov 10, 2017).
- (103) Stanton, J. F.; Gauss, J.; Harding, M. E.; Szalay, P. G. *CFour, A quantum chemical program package*, 2010; see <http://www.cfour.de> (accessed Nov 10, 2017).
- (104) Keith, T. *TK Gristmill Software (aim.tkgristmill.com)*, 2011; Overland Park, KS, USA.
- (105) Zou, W.; Nori-Shargh, D.; Boggs, J. E. On the covalent character of rare gas bonding interactions: A new kind of weak interaction. *J. Phys. Chem. A* **2013**, *117*, 207–212.

- (106) Lu, T.; Chen, F. Multiwfn: A multifunctional wavefunction analyzer. *J. Comput. Chem.* **2012**, *33*, 580–592.
- (107) Setiawan, D.; Kalescky, R.; Kraka, E.; Cremer, D. Direct measure of metal-ligand bonding replacing the Tolman electronic parameter. *Inorg. Chem.* **2016**, *55*, 2332–2344.
- (108) Kraka, E.; Setiawan, D.; Cremer, D. Re-evaluation of the bond length-bond strength rule: The stronger bond is not always the shorter bond. *J. Comput. Chem.* **2016**, *37*, 130–142.
- (109) Clark, T. Polarization, donor-acceptor interactions, and covalent contributions in weak interactions: A clarification. *J. Mol. Model.* **2017**, *23*, 297.

Paper VI.      The peculiar role of the  $\text{Au}_3$  unit in  $\text{Au}_m$  clusters:  $\sigma$ -aromaticity  
of the  $\text{Au}_5\text{Zn}^+$  ion

# The Peculiar Role of the Au<sub>3</sub> Unit in Au<sub>m</sub> Clusters: $\sigma$ -Aromaticity of the Au<sub>5</sub>Zn<sup>+</sup> Ion

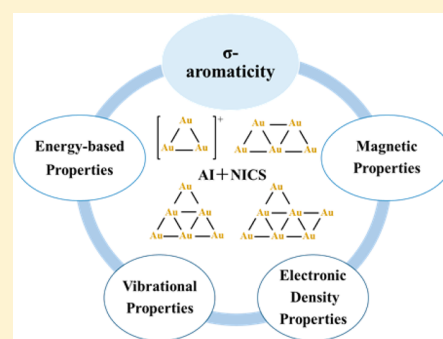
Yanle Li,<sup>†,§</sup> Vytor Oliveira,<sup>‡,§</sup> Chunmei Tang,<sup>†</sup> Dieter Cremer,<sup>\*,‡,§</sup> Chunyan Liu,<sup>†</sup> and Jing Ma<sup>\*,†,§</sup>

<sup>†</sup>Key Laboratory of Mesoscopic Chemistry of MOE, School of Chemistry and Chemical Engineering, Nanjing University, 22 Hankou Road, Nanjing, Jiangsu Province 210093, People's Republic of China

<sup>‡</sup>Computational and Theoretical Chemistry Group, Department of Chemistry, Southern Methodist University, 3215 Daniel Avenue, Dallas, Texas 75275-0314, United States

## Supporting Information

**ABSTRACT:** The stability of small Au<sub>m</sub> ( $m = 4-7$ ) clusters is investigated by analyzing their energetic, geometric, vibrational, magnetic, and electron density properties. Gold clusters can be constructed from stable cyclic 3-center-2-electron (3c-2e) Au<sub>3</sub><sup>+</sup> units (3-rings) with  $\sigma$ -aromaticity. The stabilization requires a flow of negative charge from internal 3-rings with electron-deficient bonding to peripheral 3-ring units with stronger Au–Au bonds. The valence-isoelectronic clusters Au<sub>6</sub> and Au<sub>5</sub>Zn<sup>+</sup> have similar electronic properties: Au<sub>5</sub>Zn<sup>+</sup> is a strongly  $\sigma$ -aromatic molecule. An understanding of the structure of Au<sub>m</sub> clusters is obtained by deriving a *Clar's Rule equivalent for polycyclic gold clusters*: The structure with the larger number of rings with dominant 3c-2e character and a smaller degree of 3c-3e character occupies the global minimum of the Au<sub>m</sub> potential energy surface.



## 1. INTRODUCTION

Gold clusters have received enhanced interest in nanoscience because of their unique catalytic, electronic, and optical properties.<sup>1–6</sup> The pronounced scalar relativistic effects of gold lead to the fact that Au<sub>m</sub> clusters exhibit unique structural and bonding properties that distinguish them from other metal clusters.<sup>7–12</sup> During the past three decades, pure gold clusters Au<sub>m</sub> in the small-to-medium size range have been described in experimental and theoretical studies.

In 2008, Gruene and co-workers determined the structure of neutral Au<sub>7</sub>, Au<sub>19</sub>, and Au<sub>20</sub> by comparing their experimental spectra obtained by far-IR multiple-photon dissociation (FIR-MPD) spectroscopy in the gas phase with the calculated vibrational spectra for multiple isomers.<sup>7</sup> De and co-workers investigated the finite temperature behavior of neutral Au<sub>m</sub> ( $m = 3-10$ ) clusters in the gas phase using molecular dynamical simulations based on relativistic density functional theory (DFT).<sup>8</sup> Zanti and Peeters studied Au<sub>m</sub> ( $m \leq 16$ ) clusters with B3LYP and explained their stability in terms of a donor–acceptor model, which suggested a cyclic flow of electrons within a cluster.<sup>9</sup> Sergeeva and Boldyrev demonstrated that small three-dimensional Au clusters could be built from the Au<sub>4</sub> tetrahedron characterized by 4c-2e bonding.<sup>10</sup> All these investigations established a deeper insight into the structure and thermodynamic stability of gold clusters. Recently, Xu and co-workers used the triangular, two-electron (2e) Au<sub>3</sub> (in short: Au<sub>3</sub>(2e)) and rhombic Au<sub>4</sub>(2e) rings as elementary units to investigate the stabilities of 71 reported thiolate-protected Au nanoclusters developing and applying the Grand Unified Model (GUM).<sup>11</sup> On the basis of GUM, the authors not only

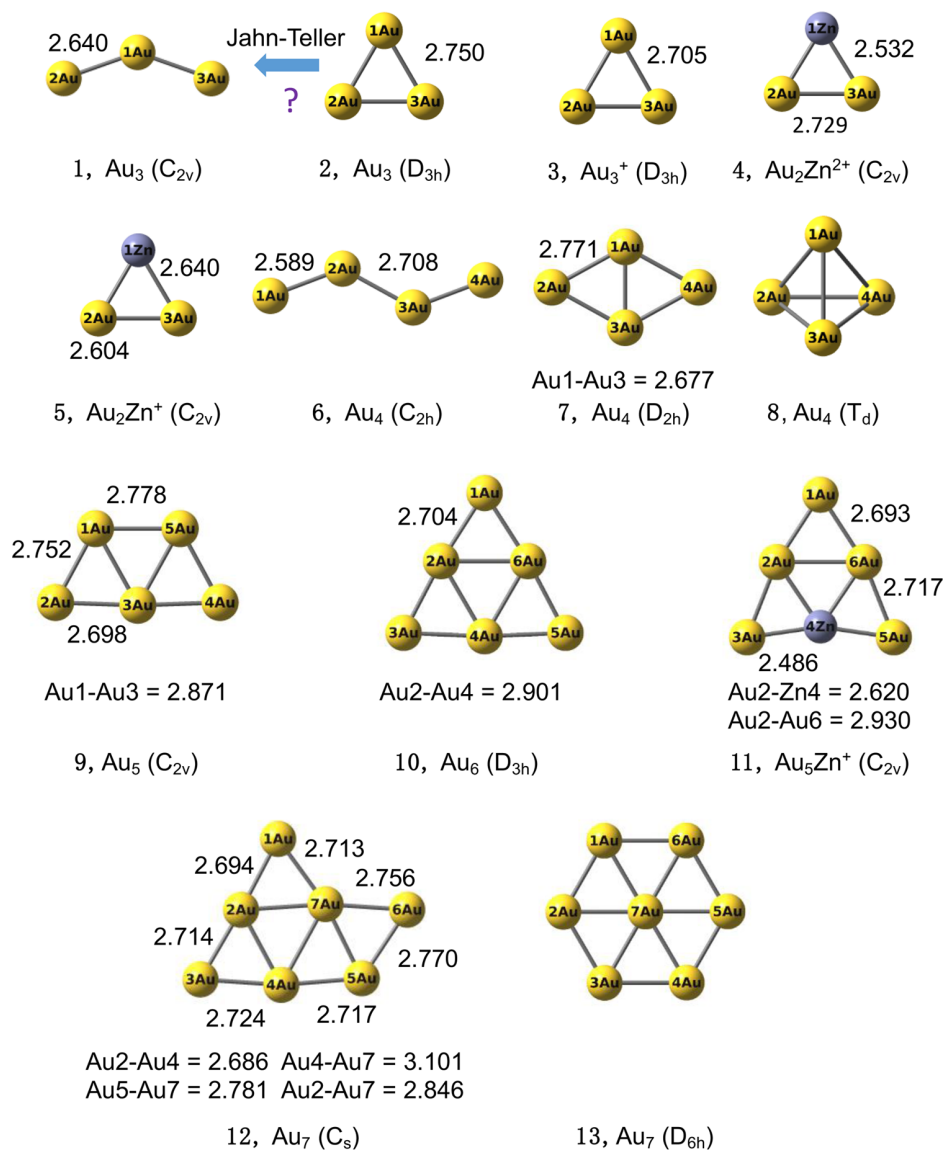
rationalized the stabilities of known thiolate-protected gold nanoclusters but also predicted new ligand-protected gold nanoclusters of distinct stability. Gilb and co-workers studied small Au cluster cations (Au<sub>m</sub><sup>+</sup>,  $m < 14$ ) utilizing ion mobility measurements and computational methods and found that gold cluster cations had planar structures for  $m = 3-7$  at room temperature.<sup>12</sup>

The concept of  $\sigma$ -aromaticity (stabilization by  $4p + 2$   $\sigma$ -electrons in radial or  $4p$   $\sigma$ -electrons in tangential occupied orbitals,  $p = 0, 1, 2, \dots$ , thus leading to aromatic Hückel and/or aromatic Möbius systems) can be traced to two different delocalization modes:<sup>13,14</sup> (i) *Peripheral (one-dimensional) delocalization along the  $\sigma$ -bonds*: In 1979, Dewar<sup>15</sup> discussed the small ring strain of cyclopropane and related this to the peripheral delocalization of  $\sigma$ -electrons. (ii) *Surface (two-dimensional) delocalization in the ring plane*: Cremer and Kraka<sup>13,14</sup> showed that  $\sigma$ -delocalization could lead to delocalization in the ring plane of cyclopropane, which in substituted cyclopropanes determined both geometry and stability. Later, Cremer and Gauss<sup>16</sup> provided further evidence for the phenomenon of surface delocalization. The potential  $\sigma$ -aromaticity of various small rings has caught the interest of many researchers.<sup>17–19</sup> The physical and chemical properties of hydrogen clusters,<sup>20</sup> polycyclophosphanes,<sup>21</sup> Zn<sub>3</sub><sup>+</sup> and Ge<sub>4</sub><sup>2+</sup> clusters,<sup>22,23</sup> lanthanum-doped boron clusters,<sup>24</sup> and unsaturated cyclopropametallapentalenes<sup>25,26</sup> have also been rationalized in terms of  $\sigma$ -aromaticity or surface delocalization.

**Received:** February 14, 2017

**Published:** April 27, 2017



Scheme 1. Structures<sup>a</sup> of Neutral Au<sub>m</sub> Clusters, Au<sub>3</sub><sup>+</sup>, Au<sub>2</sub>Zn<sup>1/2+</sup>, and Au<sub>5</sub>Zn<sup>+</sup>

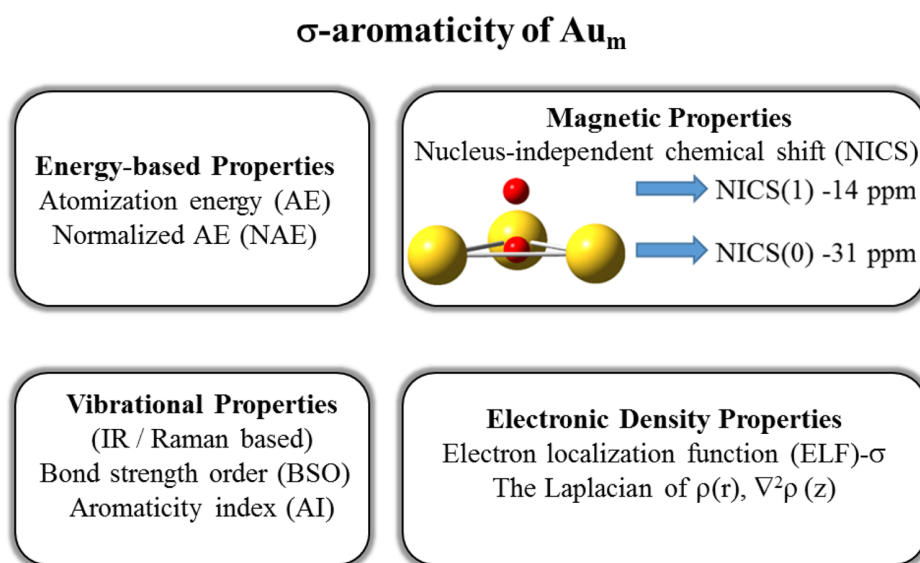
<sup>a</sup>The bond lengths (in Å) are given at the B3LYP/LANL2DZ level of theory.

To our knowledge, a systematic theoretical investigation of the stabilities of planar Au<sub>m</sub> (*m* = 4–7) clusters as an aggregation of Au<sub>3</sub>(2e) or Au<sub>3</sub>(3e) building blocks has not been performed so far. As becomes obvious from Scheme 1, the ground states of Au<sub>m</sub> clusters contain Au<sub>3</sub> units (Au<sub>3</sub> rings with 2 ≤ *p* ≤ 3 electrons), suggesting a simple structural principle for gold clusters. In this work, we will present an electronic structure description of the Au<sub>3</sub> units based on their energetic, geometric, vibrational, magnetic, and electron density properties and use the outcome of this analysis to discuss structure and stabilities of planar Au<sub>m</sub> clusters up to *m* = 7 for the purpose of obtaining a general building principle for Au<sub>m</sub> clusters. Apart from this, Au<sub>5</sub>Zn<sup>+</sup> will be analyzed, as it is an electronically interesting analogue of the Au<sub>6</sub> cluster and also a potential  $\sigma$ -aromatic cluster.<sup>27</sup>

## 2. COMPUTATIONAL DETAILS

Geometry optimizations and vibrational frequency calculations were performed for all Au<sub>m</sub> clusters shown in Scheme 1 utilizing DFT. Becke's three-parameter hybrid exchange-correlation functional (B3LYP)<sup>28,29</sup> was used in connection with the LANL2DZ basis set<sup>30–32</sup> (for Zn, the 6-31G(d) basis set was employed). Preliminary calculations were also performed with the CAM-B3LYP,<sup>33</sup> M06,<sup>34</sup> M06-2X,<sup>34</sup> LC- $\omega$ PBE,<sup>35–37</sup> and  $\omega$ B97XD<sup>38</sup> functionals. It turned out that B3LYP was more robust for the calculation of second-order response properties, and therefore most of the results were discussed for this hybrid functional. Each stationary point was verified to be a minimum on the potential energy surface with the help of the eigenvalues of the Hessian matrix of second derivatives. At the B3LYP/LANL2DZ level, the T<sub>d</sub>-symmetrical Au<sub>4</sub> and the D<sub>6h</sub>-symmetrical Au<sub>6</sub> clusters were located as stationary points with three and one imaginary frequencies, respectively, which was the reason why these two structures were not investigated in detail, although their relative stability was discussed in this work.

CCSD(T)<sup>39</sup> and PBEPBE-D3(BJ)<sup>40–42</sup> calculations with an aug-cc-pVTZ-PP basis set<sup>43,44</sup> were also performed to predict the atomization

Scheme 2. Overview of the Methods Used in This Work<sup>a</sup>

<sup>a</sup>The NICS(0) and NICS(1) values (in ppm) of  $Au_3^+$  are taken at pre-chosen positions indicated by the red dots: for NICS(0), the geometrical center (centroid) of the ring is taken, for NICS(1) the position 1 Å above the centroid of the  $Au_3^+$  ring.

energies (AE) and normalized AE (NAE or cohesive energy) of the planar clusters:  $NAE = AE/N$ , where  $N$  is the number of atoms in a molecule. In the case of the  $Au_3(3e)$  multireference system, CASSCF and broken-symmetry unrestricted DFT (BS-UDFT) calculations were performed to estimate its stability.

For the description of delocalization and potential aromaticity, we calculated the nucleus-independent chemical shift (NICS) parameters utilizing the Gauge-Independent Atomic Orbital (GIAO) method.<sup>45–49</sup> The NICS value gives the negative of the magnetic shielding computed at a prechosen position of the molecular geometry. In this work, NICS values are calculated at the centroids of the rings (denoted as NICS(0)) and 1.0 Å above the ring centroids (NICS(1)) to exclude to some extent the influence of the core electrons of Au (the atomic radius of Au is 1.35 Å) and to get a better description of  $\sigma$ -delocalization. Scheme 2 illustrates the NICS(0) and NICS(1) positions and their values for  $Au_3^+$ . The negative NICS(1) value means the existence of induced diatropic ring currents typical of an “aromatic” electron system, while a positive value suggests paratropic ring currents typical of an “antiaromatic” electron system.<sup>50</sup>

As a third aromaticity index, the electron localization function (ELF)- $\sigma$  was determined.<sup>51</sup> ELF- $\sigma$  is calculated at the bifurcation point of two ELF domains, which are dominated by the contributions of the  $\sigma$  orbitals. It reveals the degree of interaction between adjacent ELF domains: A larger ELF- $\sigma$  value suggests that the electrons more strongly delocalize between adjacent domains. Because NICS and ELF- $\sigma$  parameters are largely independent of method and basis set, we exclusively report here the B3LYP/LANL2DZ results.

To determine the intrinsic strength of an Au–Au bond, the vibrational modes of the  $Au_m$  clusters were analyzed. For this purpose, the  $3N - 6$  normal vibrational modes ( $N$ : number of atoms) of a cluster were converted into local vibrational modes using the Konkoli–Cremer method.<sup>52–54</sup> Then the local bond stretching force constants  $k^a$  were calculated, as these provided a quantitative and reliable measure of the intrinsic bond strength.<sup>55</sup> Accordingly,  $k^a$  values could be used to determine a bond strength order (BSO). For this purpose, we used as suitable references the  $Au_2$  dimer and the 3-ring  $Au_3^+$  with its 3c-2e bonding. The two molecules have Au–Au bond orders of 1.000 and 0.333 according to simple molecular orbital (MO) theory. This is a possible choice to convert local Au–Au stretching force constants into BSO values  $n$  with the help of the power relationship

$$n = a(k^a)^b \quad (1)$$

where the constants  $a$  and  $b$  are determined via the two reference molecules and the requirement that for  $k^a = 0$  the BSO value must be also zero.<sup>56</sup> Analysis of the relativistically corrected electron density obtained with the Dirac-exact Normalized Elimination of the Small Component (NESC) method<sup>57,58</sup> reveals that the MO-based assumption of bond orders given above underestimates bonding for  $Au_3^+$ . The more reliable Mayer bond orders<sup>59,60</sup> suggest  $n$ -values of 1.105 and 0.610 for  $Au_2$  and  $Au_3^+$ , respectively (for B3LYP/LANL2DZ,  $k^a$  values of 1.567 and 0.833 mdyne/Å were obtained), which lead to a power relationship (1) with  $a = 0.724$  and  $b = 0.941$ . All BSO values were calculated using eq 1 based on these constants.

Sometimes it is useful to scale BSO values so that the total number of valence electrons is reproduced. Although the scaled BSO values are no longer comparable with those of other molecules with different atoms, they provide an impression on the number of electrons in a 3-ring.

The charge distribution in the  $Au_m$  clusters was determined using the natural population analysis (NPA) by Weinhold and co-workers.<sup>61</sup> This approach was also employed to determine natural bond orders (NBOs) and to probe the possible existence of non-Lewis bonds with 3c-character.<sup>61</sup> The electron density analysis of Bader<sup>62</sup> was applied to find bond critical points (BCPs) and ring critical points (RCPs) of the electron density distribution  $\rho(\mathbf{r})$ . The Laplacian of  $\rho(\mathbf{r})$  in the  $z$ -direction (normal to the ring plane),  $\nabla^2\rho(z)$ , was used to investigate any density concentration in the center of the 3-ring. Larger density concentration is indicated by a more negative  $\nabla^2\rho(z)$  value.<sup>62</sup>

Cremer and co-workers have derived an aromaticity index (AI) from local stretching force constants and their associated BSO values  $n$ .<sup>63,64</sup> In this work, we extend the definition of AI to describe  $\sigma$ -delocalization and the nonclassical bonding character in  $Au_m$  clusters: For this purpose we use eq 2

$$AI = 1 - \frac{\gamma}{N_{\text{bonds}}} \sum (n_{\text{opt}} - n_i)^2 \quad (2)$$

where  $n_{\text{opt}} = 0.610$  gives the optimal BSO of  $Au_3^+$  at the B3LYP/LANL2DZ level of theory,  $n_i$  the BSO value of the  $i$ th bond,  $N_{\text{bonds}}$  is the number of bonds in an  $Au_m$  ring, and  $\gamma = 4.078$  is an adjustable parameter that sets the AI of the reference molecule  $Au_3^+$  equal to 1 (or 100%) thus identifying a completely delocalized 3c-2e system. Any

AI value smaller than 1 indicates a less delocalized  $\sigma$ -electron system. For AI = 0, classical covalent 2c-2e bonding is fully established as it is found in Au<sub>2</sub>.

Parameters such as AI can be used to determine  $\sigma$ -aromaticity (peripheral delocalization in a Au<sub>m</sub> ring), whereas  $\nabla^2\rho(z)$  measures the concentration of the energy density at the RCP, which reflects the degree of surface delocalization and is especially important in organic 3-rings and  $\pi$ -complexes.<sup>17,65</sup> One can weight  $\rho(\text{RCP})$  with  $\nabla^2\rho(z)$  to get  $\eta = |\rho(\text{RCP})/\nabla^2\rho(z)|$ , an area reflecting the extent of surface delocalization. If the concentration is large, the area becomes small as there is less delocalization; that is, concentration and delocalization of electrons are opposing properties. AI,  $\nabla^2\rho(z)$ , and  $\eta$  reflect the degree of electron delocalization, but they do not reflect other electronic factors such as ring strain or  $\pi$ -complex character of a 3-ring.<sup>17</sup> Therefore, the deviation  $d_i$  of the maximum electron density path (bond path) from the internuclear connection line at the BCP was calculated. Also, the extent of ring strain was evaluated by determining the deformation coordinates<sup>66</sup>  $R$  (breathing radius  $R$  of 3-ring;  $R - R_0 = t_0$  is the deviation from a suitable reference radius  $R_0$ ),  $t_1$  (deformation amplitude), and  $\phi_1$  (deformation phase angle). Once the deformation coordinates are known, the associated local deformation force constants<sup>66</sup> can be calculated that provide a direct measure of ring strain. Calculations were performed with Gaussian09,<sup>67</sup> Molpro,<sup>68</sup> and the COLOGNE2016 program.<sup>69</sup> ELF calculations were performed with the Multiwfn package.<sup>70</sup>

### 3. RESULTS AND DISCUSSIONS

The optimized planar structures of Au<sub>3</sub><sup>+</sup>, Au<sub>m</sub> ( $m = 4-7$ ), and cation Au<sub>5</sub>Zn<sup>+</sup> are displayed in Scheme 1 (for the Cartesian coordinates of the equilibrium geometries, see the Supporting Information). All structures calculated are planar or nearly planar. Their relative stabilities are determined via the corresponding AE and NAE values (Table 1 and Figure S1).

Table 1 and Figure S1 reveal that Au<sub>3</sub><sup>+</sup> represents (compared with Au<sub>6</sub>, Au<sub>2</sub>Zn<sup>2+</sup>, and Au<sub>5</sub>Zn<sup>+</sup>) a stable Au<sub>m</sub> cluster (NAE, PBEPBE-D3(BJ): 47.3 kcal/mol; CCSD(T): 42.5 kcal/mol) comparable in its stability with Au<sub>6</sub> (46.1; 43.1 kcal/mol) and Au<sub>7</sub> (45.3 kcal/mol, Table 1). Noteworthy is that all Au clusters

**Table 1.** Calculated Atomization Energies (AE) and Normalized AE (NAE)<sup>a</sup>

	B3LYP/ LANL2DZ <sup>a</sup>		PBEPBE- D3(BJ)/aug- VTZ-PP <sup>a</sup>		CCSD(T) <sup>b</sup> / aug-VTZ-PP	
	AE	NAE	AE	NAE	AE	NAE
Au <sub>2</sub> (D <sub>∞h</sub> ) → 2Au ( <sup>2</sup> S)	43.2	21.6	54.6	27.3	49.5	24.7
Au <sub>3</sub> <sup>+</sup> (2e)(D <sub>3h</sub> ) → 2Au ( <sup>2</sup> S) + 1Au <sup>+</sup> ( <sup>1</sup> S)	113.2	37.7	142.0	47.3	127.6	42.5
Au <sub>3</sub> (3e)(D <sub>3h</sub> ) → 3Au ( <sup>2</sup> S)	58.3	19.4	83.6	27.9	73.3	24.4
Au <sub>3</sub> (3e)(C <sub>2v</sub> ) → 3Au ( <sup>2</sup> S) <sup>c</sup>	63.5	21.2	86.7	28.9	72.5	24.2
Au <sub>4</sub> (D <sub>2h</sub> ) → 4Au ( <sup>2</sup> S)	107.5	26.9	147.1	36.8	134.6	33.6
Au <sub>4</sub> (C <sub>2h</sub> ) → 4Au ( <sup>2</sup> S)	102.0	25.5	136.7	34.2	118.2	29.5
Au <sub>5</sub> (C <sub>2v</sub> ) → 5Au ( <sup>2</sup> S)	147.7	29.5	202.1	40.4	184.6	36.9
Au <sub>6</sub> (D <sub>3h</sub> ) → 6Au ( <sup>2</sup> S)	208.1	34.7	276.5	46.1	258.6	43.1
Au <sub>7</sub> (C <sub>s</sub> ) → 7Au ( <sup>2</sup> S)	232.6	33.2	317.3	45.3	278.9	39.8
Au <sub>5</sub> Zn <sup>+</sup> (C <sub>2v</sub> ) → 2Au ( <sup>2</sup> S) + Zn <sup>+</sup> ( <sup>2</sup> S)	97.8	32.6	110.7	36.9	79.7	26.6
Au <sub>5</sub> Zn <sup>2+</sup> (C <sub>2v</sub> ) → 2Au ( <sup>2</sup> S) + Zn <sup>2+</sup> ( <sup>1</sup> S)	216.6	72.2	238.6	79.5	216.1	72.0
Au <sub>5</sub> Zn <sup>+</sup> (C <sub>2v</sub> ) → 5Au ( <sup>2</sup> S) + Zn <sup>+</sup> ( <sup>2</sup> S)	271.2	45.2	317.7	52.9	296.2	49.4

<sup>a</sup>In kilocalories per mole. <sup>b</sup>CCSD(T) energies at PBEPBE-D3(BJ)/aug-cc-pVTZ-PP geometries. <sup>c</sup>Broken symmetry solutions. UPBEPBE leads to an imaginary frequency of 210 i cm<sup>-1</sup>.

investigated have a larger NAE than Au<sub>2</sub> (27.3; 24.7 kcal/mol), which suggests that planar Au<sub>m</sub> rings gain a significant amount of stabilization, which obviously has to do with electron delocalization in the 3-ring units.

The energy differences between the frontier orbitals of Au<sub>3</sub><sup>+</sup>, Au<sub>m</sub>, and Au<sub>5</sub>Zn<sup>+</sup> calculated with different exchange-correlation (XC) functionals are shown in Figure 1 and Table S1. Although

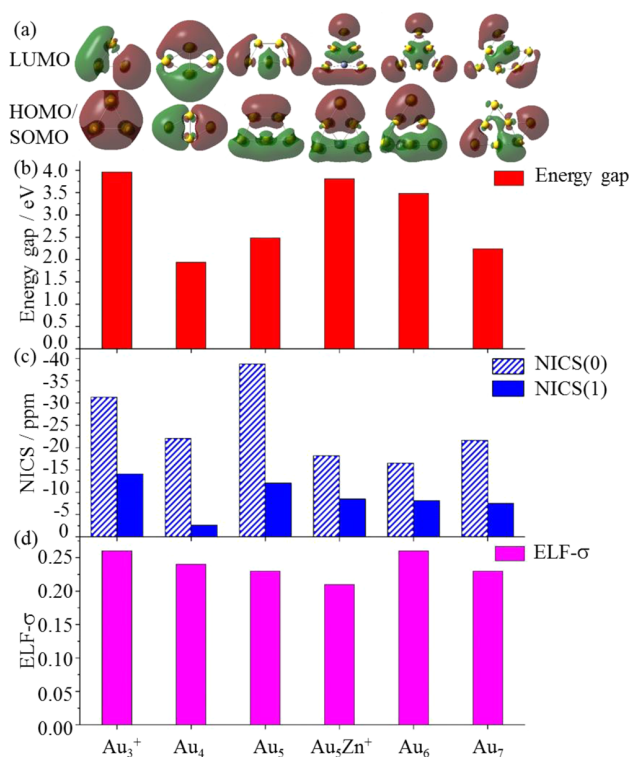


**Figure 1.** Comparison of some properties of Au<sub>3</sub><sup>+</sup>, Au<sub>m</sub> ( $m = 4-7$ ), and Au<sub>5</sub>Zn<sup>+</sup>. (a) Perspective drawings of the HOMO, singly occupied molecular orbital (SOMO), or LUMO. All MO drawings are obtained at the RHF (ROHF) level of theory. (b) Bar diagram of the corresponding energy gaps  $\Delta\epsilon$ . (c) Bar diagram of NICS(0) and NICS(1) values given for Au<sub>m</sub>. (d) Bar diagram of ELF- $\sigma$  values given for Au<sub>m</sub>. B3LYP/LANL2DZ calculations.

the magnitude of the highest occupied molecular orbital–lowest unoccupied molecular orbital (HOMO–LUMO) energy gaps,  $\Delta\epsilon$ , changes with the XC functional used, all XC functionals (with the exception of PBEPBE) predict the same order of  $\Delta\epsilon$  values: Au<sub>3</sub><sup>+</sup> > Au<sub>5</sub>Zn<sup>+</sup> > Au<sub>6</sub> > Au<sub>5</sub> > Au<sub>7</sub> > Au<sub>4</sub>. This trend does not exactly follow the trend of the calculated NAE in Table 1, but there are some similarities.

In addition to the energy gaps, the results of the NICS and ELF- $\sigma$  calculations are shown in Figure 1 and Table S1. The difference in the NICS(0) and NICS(1) values indicates that the  $\sigma$  frame has significant influence on NICS(0), which makes it advisable to base the analysis of the magnetic properties of the Au clusters investigated exclusively on NICS(1).

The NBO analysis of Au<sub>3</sub><sup>+</sup> confirms that the 6s orbitals of the Au atoms form an a<sub>1</sub>'-symmetrical, bonding 3c-orbital, that is, a fully delocalized orbital. Hence, it is justified to speak of a  $\sigma$ -aromatic 2e-ensemble that determines the stability and geometry of Au<sub>3</sub><sup>+</sup>. The scalar relativistic contraction of the 6s(Au) orbital and the positive charge both lead to a decrease of the energy of the 3c orbital, a shortening of the Au–Au

bonds, thereby an increase of the Au–Au bond strength, and an overall stabilization of the cation. Kalescky and co-workers<sup>71</sup> have coined in this connection the term electronegativity-driven increase of bond strength, which applies in the case of  $\text{Au}_3^+$  as the effective electronegativity of Au increases with regard to the 6s electrons. Scalar relativity also leads to an expansion of the 5d lone pair orbitals and to an increase of their energies, which leads to overall destabilizing contributions. The strong decrease of the  $a_1'$  HOMO relative to the  $e'$  LUMOs causes the increase in  $\Delta\varepsilon$  (Figure 1, Table S1). This observation causes two questions, which must be answered in the following: (i) Is  $\sigma$ -electron delocalization a typical phenomenon for Au clusters? (ii) The 3e system  $\text{Au}_3$  in its  ${}^2E'$  state does undergo a Jahn–Teller distortion from  $D_{3h}$  to  $C_{2v}$ <sup>72</sup> which leads to a bent  $\text{Au}_3({}^2A')$  structure. The question is whether  $\sigma$ -electron delocalization is also observed in this case.

Investigation of acyclic  $\text{Au}_3({}^2A')$  leads to a BSO value of 0.746 that suggests a 3e delocalization of the Au 6s electrons and a concomitant increase in the intrinsic bond strength from 0.610 ( $\text{Au}_3^+$ ) to 0.746 (reduction of the Au–Au bond lengths from 2.705 to 2.640 Å). At this point a caveat is needed regarding the Jahn–Teller unstable  $D_{3h}$ -symmetrical  $\text{Au}_3(3e)$ . Guo and co-workers<sup>6</sup> have performed for  $\text{Au}_3(3e)$  and its excited states multireference relativistic configuration interaction (CI) calculations, which explicitly include the effects of spin–orbit coupling (SOC). Their results reveal that (i) the Jahn–Teller distortion is relatively small and that (ii) SOC quenches the Jahn–Teller distortion so that the  $D_{3h}$  structure becomes more stable than the  $C_{2v}$  structure. Laser experiments confirm a  $D_{3h}$  symmetrical ground state.<sup>6</sup>

DFT in combination with an effective core potential such as LANL describes SOC only implicitly and in an averaged way so that its effect can be underestimated. At the BS-UB3LYP/LANL2DZ level of theory, the  $D_{3h}$  symmetrical form is a minimum (Table 1). Nevertheless, the acyclic  $\text{Au}_3({}^2A')$  form is somewhat more stable than the cyclic  $\text{Au}_3(3e)$  form, but both are much less stable than  $\text{Au}_3^+$  (PBEPBE, NAE: 28.9 and 27.9 vs 47.3 kcal/mol, Table 1). Strong SOC effects are only observed for open-shell systems with a fractional occupation of p, d, and f orbitals, whereas for closed-shell systems or open-shell systems with singly occupied s-orbitals, SOC effects are relatively small. Hence, the discussion of the electronic structure of the latter is reasonable.

SOC plays a role when comparing the  $D_{2h}$ -symmetrical  $\text{Au}_4$  gold cluster with the acyclic  $C_{2h}$ -symmetrical  $\text{Au}_4$ . The latter might be viewed as two  $\text{Au}_2$  units interacting via weak noncovalent interactions.  $\sigma$ -Delocalization changes this picture dramatically by establishing a relatively strong Au2–Au3 bond (BSO: 0.545; bond Au1–Au2: 1.028, Table 2).  $D_{2h}$ -Symmetrical  $\text{Au}_4$  is more stable than  $C_{2h}$ -symmetrical  $\text{Au}_4$  by 5.5 kcal/mol (or 1.4 kcal/mol per Au atom). Apart from these considerations, it is safe to say on the basis of the data shown in Tables 2, 3, and 4 that in acyclic and cyclic  $\text{Au}_m$  systems, there is a pronounced tendency for  $\sigma$ -electron delocalization that strongly influences the stability of the various clusters. Our results suggest that the formation of multiple  $\sigma$ -aromatic 2e  $\text{Au}_3^+$  units (or distorted  $\text{Au}_3(3e)$  units) within a polycyclic  $\text{Au}_m$  cluster lead to extra stability as will be discussed in the following in more detail.

Each of the gold clusters investigated is formed by 3-ring units (denoted as a, b, c, d, e from the core of an  $\text{Au}_m$  cluster to its periphery and in line with its symmetry properties; Figure 2). The NICS(1) values for each of the 3-ring units are listed in

**Table 2. Bond Distances  $r$  (Å), Local Force Constant  $k^a$  (mdyn/Å), and BSO Values  $n$  for the Gold Clusters Investigated**

molecule (sym)	bond	$r$	$k^a$	BSO $n$
$\text{Au}_3^+ (D_{3h})$	Au–Au	2.705	0.833	0.610
$\text{Au}_3 (D_{3h})$	Au–Au	2.750	0.785	0.577
$\text{Au}_3 (C_{2v})$	Au1–Au2	2.640	1.032	0.746
$\text{Au}_2\text{Zn}^+ (C_{2v})$	Zn–Au	2.640	0.230	0.182
	Au–Au	2.604	1.439	1.020
$\text{Au}_2\text{Zn}^{2+} (C_{2v})$	Zn–Au	2.532	0.753	0.555
	Au–Au	2.729	0.821	0.602
$\text{Au}_4 (D_{2h})$	Au1–Au2	2.771	0.462	0.350
	Au1–Au3	2.677	0.958	0.696
$\text{Au}_4 (C_{2h})$	Au1–Au2	2.589	1.452	1.028
	Au2–Au3	2.708	0.740	0.545
$\text{Au}_5 (C_{2v})$	Au1–Au2	2.752	0.634	0.472
	Au1–Au3	2.871	0.285	0.223
	Au1–Au5	2.778	0.593	0.443
	Au2–Au3	2.698	0.846	0.619
$\text{Au}_5\text{Zn}^+ (C_{2v})$	Au1–Au2	2.693	0.934	0.679
	Au2–Au3	2.717	0.844	0.618
	Au2–Zn4	2.620	0.568	0.425
	Au2–Au6	2.930	0.345	0.266
	Au3–Zn4	2.486	1.040	0.751
$\text{Au}_6 (D_{3h})$	Au1–Au2	2.704	0.855	0.625
	Au2–Au4	2.901	0.339	0.262
$\text{Au}_7 (C_s)$	Au1–Au2	2.694	0.909	0.662
	Au1–Au7	2.713	0.806	0.591
	Au2–Au3	2.714	0.798	0.586
	Au2–Au4	2.686	0.373	0.287
	Au2–Au7	2.846	0.420	0.320
	Au3–Au4	2.724	0.766	0.564
	Au4–Au5	2.717	0.802	0.589
	Au4–Au7	3.101	0.087	0.073
	Au5–Au6	2.770	0.560	0.420
	Au5–Au7	2.781	0.519	0.391
	Au6–Au7	2.756	0.592	0.442

Table 3. They reveal that NICS(1) values decrease with increasing annelation and decreasing positive charge of an  $\text{Au}_3$  ring. For the  $\text{Au}_3$  units in  $\text{Au}_3^+$ ,  $\text{Au}_5$ , and  $\text{Au}_6$  (in total five different  $\text{Au}_3$  rings in different clusters, called a@  $\text{Au}_5$ , etc.) an exponential decay of NICS(1) with the parameter of the number of shared edges in a polycyclic structure ( $n_{\text{share}}$ ) can be observed suggesting a decrease of aromatic  $\sigma$ -delocalization for the inner rings (Figure 3).

Free  $\text{Au}_3^+$  possesses the most negative NICS(1) value (−14.1 ppm) in line with its positive charge and the optimal 2e-delocalization. In  $\text{Au}_5$ , the central ring a shares one edge with each adjacent  $\text{Au}_3$  unit. In this case, the NICS(1) value of ring b is reduced to −11 ppm, whereas that of ring a is lowered to −9 ppm. Defining the number of the shared edges by the parameter  $n_{\text{share}}$ , the NICS(1) values vary from −9 ppm ( $n_{\text{share}}$ : 2) to −8 ppm ( $n_{\text{share}}$ : 3). This trend is qualitatively maintained for  $\text{Au}_7$  (Table 3) and reminds of the tendency of  $\pi$ -aromatic polybenzenoids to prefer the structure with the largest number of aromatic sextets according to the Clar's rule.<sup>63,73</sup> The Clar's rule has also been used for inorganic BN analogues of polybenzenoid hydrocarbon systems.<sup>74</sup>

In this sense, the value of  $n_{\text{share}}$  might be used to explain the relative low stability of isomers of the nonplanar  $\text{Au}_4$  and  $\text{Au}_7$  clusters. For  $\text{Au}_4 (T_d)$ ,  $n_{\text{share}}$  has a value of 6 that is larger than

Table 3. Results of NICS and the Electron Density Analysis

	a	b	c	d	e
NICS(1)/NICS(0) <sup>a</sup>					
Au <sub>3</sub> <sup>+</sup>	-14.08				
Au <sub>2</sub> Zn <sup>2+</sup>	-37.71/-14.32				
Au <sub>4</sub>	-2.48				
Au <sub>5</sub>	-9.03	-11.48			
Au <sub>5</sub> Zn <sup>+</sup>	-9.96	-12.60	-11.93		
Au <sub>6</sub>	-8.14	-11.41			
Au <sub>7</sub>	-6.27	-7.68	-8.52	-10.59	-8.64
electron density analysis <sup>b</sup>					
Au <sub>3</sub> <sup>+</sup>					
$\eta$	1.652				
$\nabla^2\rho(z)$	-0.023				
Au <sub>4</sub>					
$\eta$	1.619				
$\nabla^2\rho(z)$	-0.021				
Au <sub>5</sub>					
$\eta$	1.688	1.684			
$\nabla^2\rho(z)$	-0.016	-0.019			
Au <sub>5</sub> Zn <sup>+</sup>					
$\eta$	2.000	1.818	1.700		
$\nabla^2\rho(z)$	-0.009	-0.011	-0.020		
Au <sub>6</sub>					
$\eta$	1.714	-1.684			
$\nabla^2\rho(z)$	-0.014	-0.019			
Au <sub>7</sub>					
$\eta$	1.692	1.667	1.650	1.619	1.684
$\nabla^2\rho(z)$	-0.013	-0.015	-0.020	-0.021	-0.019

<sup>a</sup>In units of parts per million. <sup>b</sup>Given in form of the Laplacian at the RCP in *z*-direction,  $\nabla^2\rho(z)$ , and the relative electron density weighted by the Laplacian  $\rho/\nabla^2\rho(z)$  for the gold clusters investigated. B3LYP calculations. The symbol  $\eta = |\rho(\text{RCP})/\nabla^2\rho(z)|$  gives an area reflecting the extent of surface delocalization (see text). The Laplacian of  $\rho$  is given in e/bohr<sup>5</sup>, and  $\eta$  is in bohr<sup>2</sup>.

$n_{\text{share}} = 1$  for Au<sub>4</sub> (*D*<sub>2h</sub>) thus suggesting that the latter is more stable. The nonplanar Au<sub>4</sub> (*T*<sub>d</sub>) cluster turns out to be a saddle point of first order at the B3LYP level of theory. Similarly,  $n_{\text{share}}$  is 6 for Au<sub>7</sub> (*D*<sub>6h</sub>), whereas it is just 4 in Au<sub>7</sub> (*C*<sub>s</sub>), again explaining the lower stability of the former that is also a saddle point rather than a minimum. In other cases, the  $n_{\text{share}}$  value can be used to predict qualitative trends (see Table 3: Au<sub>7</sub>). It can be expected that the value of  $n_{\text{share}}$  increases when the size of planar Au<sub>*m*</sub> clusters becomes larger, suggesting the decrease of  $\sigma$ -aromaticity or instability of the planar structures of Au<sub>*m*</sub>. The energy difference between the planar and nonplanar structures will be decreased with the increasing of the cluster size, rationalizing the tendency that planar Au<sub>*m*</sub> clusters are no longer stable for larger *m*. The investigation of larger planar clusters is currently performed in our laboratories.

In general, both NAE and NICS(1) provide a measure too crude to correctly predict the relative stability of the neutral and cationic Au clusters investigated. The same holds for the energy gap  $\Delta\varepsilon$  and the ELF- $\sigma$  values. The latter are almost the same for all clusters (Figure 1). Therefore, other properties of the clusters were investigated, which relate to their electron density distribution and vibrational modes.

Listed in Tables 2, 3, and 4 are the calculated bond distances *r*, local stretching force constants  $k^a$ , their associated BSO values *n* (Table 2), the properties of the electron density distribution at the RCP in the form of the Laplacian of  $\rho(\mathbf{r})$  in

Table 4. Aromaticity Index (AI), Deformation Coordinates (Å), and Local Deformation Force Constants (mdyn/Å)<sup>a</sup>

cluster	AI	electrons <sup>b</sup>	R or <i>t</i> <sub>0</sub>	<i>k</i> <sup>a</sup> (R)	<i>q</i> ( <i>t</i> <sub>1</sub> )	<i>k</i> <sup>a</sup> ( <i>t</i> <sub>1</sub> )
Au <sub>3</sub> <sup>+</sup>						
a	1.000	2.000	1.561	8.880	0.000	3.477
Au <sub>2</sub> Zn <sup>2+</sup> <sup>c</sup>						
a	0.274	3.000	0.018	6.951	0.014	4.596
Au <sub>2</sub> Zn <sup>2+</sup> <sup>c</sup>						
a	0.992	2.000	1.499	8.062	0.077	3.666
Au <sub>4</sub>	0.725 (p)					
a	0.807	2.000	0.021	7.533	0.036	3.801
Au <sub>5</sub>	0.946 (p)					
a	0.553	1.084	0.079	4.213	0.036	2.135
b	0.770	1.958	0.040	5.172	0.059	1.592
Au <sub>6</sub>	0.999 (p)					
a	0.506	0.520	0.114	3.525	0.000	1.430
b	0.835	1.827	0.037	5.793	0.077	1.781
Au <sub>5</sub> Zn <sup>+</sup> <sup>c,d</sup>	0.891 (p)					
a	0.474	0.643	0.071	4.860	0.122	1.484
b	0.929	1.820	0.006	7.503	0.077	3.801
c	0.826	1.717	0.038	5.964	0.092	1.833
Au <sub>7</sub>	0.959 (p)					
a	0.352	0.484	0.134	2.049	0.095	0.469
b	0.542	1.166	0.091	2.174	0.140	0.512
c	0.848	1.502	0.038	6.024	0.008	2.257
d	0.882	2.010	0.027	6.512	0.056	2.152
e	0.854	1.838	0.037	5.912	0.058	1.880

<sup>a</sup>B3LYP calculations. The symbol (p) denotes the AI value based on the peripheral bonds. <sup>b</sup>Number of electrons in a ring unit based on scaled BSO values. <sup>c</sup>Values for *t*<sub>0</sub> were obtained with the *R* value of Au<sub>2</sub>Zn<sup>2+</sup> as reference. <sup>d</sup>The AI values obtained with Au<sub>2</sub>Zn<sup>2+</sup> as reference are given in the text (see also Supporting Information).

*z*-direction (Table 3), as well as the deformation coordinates and the associated force constants (Table 4). These properties will be discussed for each system in detail, where however some general remarks are first appropriate. (i) The analysis of the bond paths of the electron density distribution revealed only minor deviations from the internuclear connection lines, and therefore T-shaped or star-shaped structures can be excluded. However, it is relevant how strong RCPs are shifted away from the geometrical center of a ring toward one of the bonds. This is shown in Figure S2 in the Supporting Information. (ii) There is little evidence for surface delocalization in the center of the ring. Table 3 reveals that the  $\eta$  values decrease only slightly from an inner Au<sub>3</sub> unit to an outer one; that is, the inner unit has a somewhat larger degree of surface delocalization, but  $\eta$  ( $1.6 < \eta < 2$  bohr<sup>2</sup>) is in general too small because of a too small  $\rho(\mathbf{r})$ .

**Au<sub>4</sub>** (**1B<sub>1u</sub>**, **D<sub>2h</sub>**). The square form of Au<sub>4</sub> is Jahn–Teller unstable and can be stabilized either by rectangular or rhombic distortion.<sup>66</sup> The latter leads to a planar bicyclic form with two 3-rings in which the four 6s(Au) electrons avoid peripheral delocalization and Jahn–Teller destabilization as much as possible as documented by a peripheral AI of 0.725. *D*<sub>2h</sub>-Symmetrical Au<sub>4</sub> is best described as a central Au<sub>2</sub> unit that donates some negative charge to the two apical Au atoms (see NPA values in Figure 2). To avoid the less stable 3c-3e bonding situation of the 3-ring the apical bond lengths are weakened (BSO: 0.350, Table 2), and  $\sigma$ -delocalization is suppressed. Note that the AI(a) value of 0.807 is misleading insofar as both 3-rings compete for the electrons of the central bond. If these are

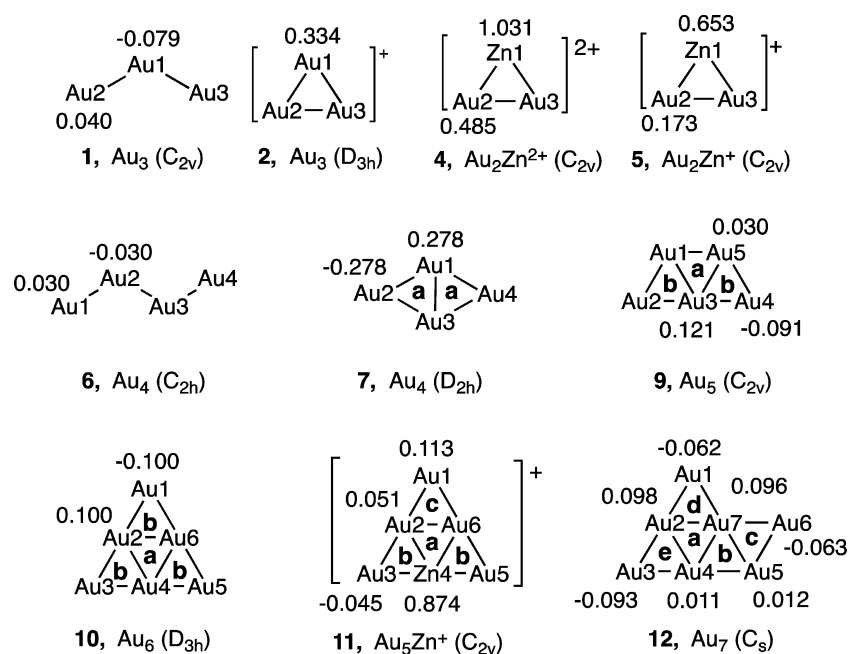


Figure 2. NPA charges for the clusters investigated, taken from B3LYP calculations. The 3-ring units are indicated by a letter code (a, b, c, etc.).

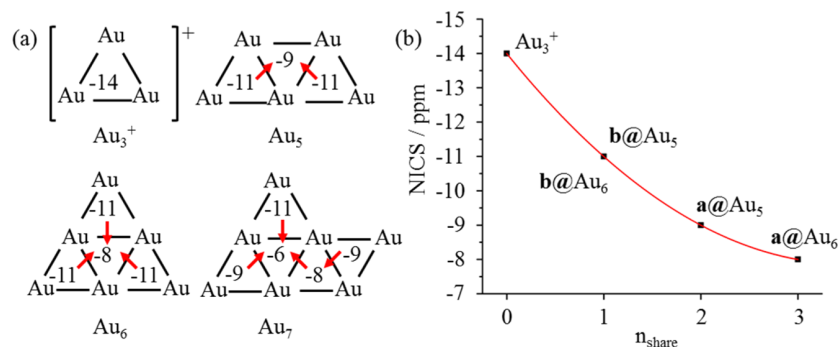


Figure 3. (a) The NICS(1) values of five Au<sub>3</sub> units. The red arrow points to less negative NICS(1) values. (b) The NICS(1) values of the Au<sub>3</sub> units in Au<sub>3</sub><sup>+</sup>, Au<sub>5</sub>, and Au<sub>6</sub> decrease in dependence of the parameter  $n_{\text{share}}$  that denotes the number of shared edges of a ring. The letters a and b indicate different 3-rings in Au<sub>5</sub> or Au<sub>6</sub> clusters (see Figure 2).

split up (by dividing the BSO value by 2), an AI value of just 0.722, like the peripheral delocalization of 0.725, is obtained.

Consequently, the absolute NICS(1) value of Au<sub>4</sub> is with  $-2.5$  ppm extremely low (Table 3). At the RCP (which is removed from the central bond; see Supporting Information) the degree of surface delocalization is small as indicated by a compact delocalization region ( $\eta = 1.619$  bohr<sup>2</sup>, smallest value for all 3-rings investigated, Table 3), which is typical of a slightly positively charged central bond attracting two apical negatively charged Au atoms. This is in line with a low NAE value of just 33.6 kcal/mol (CCSD(T), Table 1). Noteworthy is that the positive charge of the bridge atoms reduces their covalent radius so that the Au1–Au3 distance becomes shorter.

If one scales the BSO values so that they add up to the number of  $\sigma$ -type valence electrons of Au<sub>*m*</sub> (note that this leads to a loss of the comparability of local force constants and BSO values between different metal clusters), one obtains 2e for the Au–Au bridge of Au<sub>4</sub> and 2e for the four bonds connecting the apical Au atoms to the bridge. The four apical bonds have only slight concave character (i.e., there is no  $\pi$ -complex character<sup>54,55</sup>), which confirms that bonding in the Au<sub>*m*</sub> clusters

is different from what is known from organic systems having the possibility of involving  $p\pi$ -orbitals.

The analysis of the electronic structure of Au<sub>4</sub> reveals that the equilateral Au<sub>3</sub>(3e) units in a polycyclic system prefer to distort. In  $T_d$ -symmetrical Au<sub>4</sub>, symmetry and the polycyclic structure freeze the molecule in four unstable, equilateral 3c-3e units, which are prevented in the more stable rhombic  $D_{2h}$ -symmetrical form. Apart from this, the  $T_d$ -symmetrical Au<sub>4</sub> or the  $D_{6h}$ -symmetrical Au<sub>7</sub> cluster with its six destabilized 3c-3e units can only distort by ring breathing, that is, a concerted bond lengthening, and an overall weakening of the structure without effectively stabilizing the structure. This clarifies the chemical basis of the parameter  $n_{\text{share}}$ : polycyclic Au<sub>*m*</sub> structures with high symmetry and a large  $n_{\text{share}}$  parameter enforce equilateral Au<sub>3</sub>(3e) units and therefore cause instability.

In passing we note that the  $D_{2h}$ -symmetrical Au<sub>4</sub> cluster can be stabilized by opening one of the 3-rings and forming a more stable  $C_{2v}$ -symmetrical structure<sup>9</sup> for which it is easier to realize a 3c-2e unit.

**Au<sub>5</sub> (<sup>2</sup>A', C<sub>2v</sub>).** The ground state is a doublet radical with five 6s electrons that is characterized by a peripheral AI of 0.946,

whereas  $AI(a) = 0.553$  and  $AI(b) = 0.770$ .  $Au_5$  can be viewed as two overlapping  $Au_4$  units with a common central ring **a**, so that  $Au1$  and  $Au5$  are both apex atom and bridge atoms at the same time (Figure 2), which leads to an effective atomic charge close to zero (0.030e; Figure 2). The bridge bonds  $Au1-Au3$  and  $Au3-Au5$  become labialized (BSO 0.223) because of a strong electron deficiency resulting from the fact that seven  $Au-Au$  bonds must be formed with just five electrons corresponding to 65% electron deficiency (9e of 14e are missing;  $Au_4$ : 6e of 10e, i.e., 60% deficiency). Scaled BSO values reveal that there is effectively just one electron in ring **a** and two electrons in each ring **b** (Table 4). Peripheral electron delocalization involving somewhat more than 4.2e is preferred.

Aromatic  $\sigma$ -delocalization is stronger in ring **b** ( $AI = 0.770$ ) than in ring **a** ( $AI = 0.553$ , Table 4), in line with the Clar's rule for gold clusters (generation of largely independent 3c-2e units similar to the situation of 6c-6e  $\pi$ -units in phenanthrene<sup>63</sup>) and the NICS results. The surface delocalization values are comparable in **b** (1.684 bohr<sup>2</sup>) and in **a** (1.688 bohr<sup>2</sup>, Table 3). They are slightly larger than in the reference molecule  $Au_3^+$  thus indicating a somewhat increased tendency of surface delocalization because of the symmetry and topology of the bonding network.

The stability of two largely independent 3c-2e units in  $Au_5$  (topologically not possible in  $Au_4$ ) is confirmed by the increased NAE value (CCSD(T): 36.9 kcal/mol as compared to just 33.6 kcal/mol in  $Au_4$ ; Table 1). The extra stability of  $Au_5$  can also be documented by the breathing force constants  $k^a(R)$ , which for ring **b**@ $Au_5$  are significantly larger than those at ring **a**@ $Au_5$  but smaller compared to the corresponding  $Au_4$  value (breathing force constant, **b**@ $Au_5$ : 5.172 mdyn/Å;  $Au_4$ : 7.533 mdyn/Å, Table 4). Ring **b**@ $Au_5$  can easily be distorted to avoid the unstable 3c-3e situation (distortion amplitude  $t_1 = 0.059$  Å, distortion force constant  $k^a(t_1) = 1.592$  mdyn/Å, Table 4), which is more difficult for **a**@ $Au_4$  ( $t_1 = 0.036$  Å;  $k^a(t_1) = 3.801$  mdyn/Å, Table 4), as the latter has only the possibility of moving the apex atoms away from the bridge  $Au1-Au3$ , which leads to dissociation.

**$Au_6$  ( $^1A_g$ ,  $D_{3h}$ ).** If another Au atom is added to  $Au_5$  then the most stable structure of  $Au_6$  is formed as a planar  $D_{3h}$ -symmetrical cluster with three largely independent 3c-2e units and a central ring **a** that has a positive charge of +0.3 e (NBO value) and long, weak bonds (2.901 Å, BSO: 0.262). Scaled BSO values suggest that just 0.520e (Table 4) are forming the central ring. Its AI is relatively low (0.506) as is its breathing constant of 3.525 mdyn/Å (Table 4).

Ring **b** has stronger bonds (BSO: 0.625) and contains (after scaling) 1.827e in line with the ideal 3c-2e situation. Accordingly, both its AI and  $k^a(R)$  value are high: 0.835 and 5.793 mdyn/Å. The three rings **a** form a peripheral six-bond  $Au_6$  triangle with the perfect AI value of 0.999 (Table 4). Since the stabilities of the peripheral  $Au_6$  triangle and the three peripheral rings dominate the overall stability of the cluster, the NAE value of 43.1 kcal/mol is even somewhat larger than that of  $Au_3^+$  (42.5 kcal/mol; Table 1).

**$Au_7$  ( $^2A'$ ,  $C_3$ ).** Adding another Au atom to  $Au_6$  leads to  $Au_7$ , which in its most stable form has five different 3-rings. These can be viewed as being formed from a bicyclic  $Au_4$  unit (rings **a** and **b**) with three peripheral 3c-2e-rings **c**, **d**, and **e**. The AI values (0.352 (**a**), 0.542 (**b**), 0.848 (**c**), 0.882 (**d**), 0.854 (**e**)) are similarly ordered as the  $t_0 = R - R_0$  or  $k^a(R)$  values: 0.134 (**a**), 0.091 (**b**), 0.038 (**c**), 0.027 (**d**), 0.037 Å (**e**) and 2.049 (**a**), 2.174 (**b**), 6.024 (**c**), 6.512 (**d**), 5.912 mdyn/Å (**e**). This

suggests a decreased stability (increased breathing deformation) in the series  $d \approx e > c \gg b \gg a$  in line with the 3c-2e Clar's rule for  $Au_m$ .

For all  $Au_m$  investigated, bridge Au atoms have positive NPA charges, whereas apex atoms have negative charges (Figure 2). This is also the case for rings **d** (−0.062), **e** (−0.093), and **c** (−0.063 e) in  $Au_7$ . Scaled BSO values suggest that ring **d** is closest to the ideal 3c-2e situation (2.010 e), followed by rings **e** (1.838), **c** (1.502), **b** (1.166), and **a** (0.484 e). These observations are in line with the 3c-2e Clar's rule, the NICS values, and an NAE value of 45.3 kcal/mol (compared to 46.1 kcal/mol for  $Au_6$ ; PBEPBE-D3(BJ), Table 1), which results of course from the stability of three external relatively stable 3-rings.

**$Au_5Zn^+$  ( $^1A_1$ ,  $C_{2v}$ ).** This molecule has been previously described as a  $\sigma$ -aromatic system.<sup>27</sup> We have now the means to quantify this description by comparing with  $Au_2Zn^{2+}$  as a reference ion. The latter has an AI of 0.992; that is, it is also a  $\sigma$ -aromatic 3c-2e system. It is a suitable reference system to analyze  $Au_5Zn^+$ . For this purpose, eq 2 was reparametrized to obtain reasonable AI values (see Supporting Information). The three peripheral rings of  $Au_5Zn^+$  have AI values of 0.929 (**b**) and 0.826 (**c**), whereas ring **a** has an AI of just 0.474. This again indicates a large degree of  $\sigma$ -delocalization because of the positive charge, which is distributed over the atoms of rings **a** and **c**:  $Au1$  (0.113),  $Au2$  (0.051),  $Zn4$  (0.874e, Figure 2). The bonds involving Zn become stronger (BSO values of 0.751 and 0.425 vs 0.625 and 0.262 in  $Au_6$ , Table 2), which is because of the higher electronegativity of Zn (Pauling scale: 1.65 vs 1.42 for Au) especially in view of its high positive charge.

Theoretically, when splitting up charges always equally, the six valence electrons could be equally distributed among rings **c**,  $2 \times$  **b**, and **a**: 1.666; 1.666; 1.666; 1.000. The NPA charge distribution gives ratios of 1.519:1.737:1.737:1.007 thus suggesting that ring **c** loses charge that is drawn into the two rings **b** and to the more electronegative Zn atom (at Zn the charge is reduced from +1 to 0.874e) and  $Au3$  as well as  $Au5$  (−0.045e). The charge of ring **a** does not change much so that this ring is just a means for the charge flow from  $Au1$  to the base.

Since the covalent bonding radius of  $Zn^+$  is much smaller than that of Au or  $Au^+$ , the  $D_{3h}$ -symmetrical triangle of  $Au_6$  becomes a  $C_{2v}$ -symmetrical structure with inwardly bent  $Au3-Zn4-Au5$  unit (see bond path diagram in Supporting Information) so that  $Zn^+$  is "inside" the ring structure and bonds are much stronger. Both the AI (Table 4) and NICS(1) values (Table 3) confirm strong  $\sigma$ -delocalization: **b** (−12.6) < **c** (−11.9) < **a** (−10.0 ppm, Table 3).  $Au_5Zn^+$  is more stable than the valence isoelectronic  $Au_6$  as is confirmed by a high NAE value of 49.4 kcal/mol (CCSD(T), Table 1).

The optimal form of  $Au_5Zn^+$  must contain Zn in a central rather than apical position. Only in this way is the delocalization of some of the positive charge limited to rings **a** and **c** and leaves the apical atoms  $Au3$  and  $Au5$  negatively charged. The deformation force constants confirm the order of ring stabilities (Table 4) and, together with AI and NICS values, predict  $Au_5Zn^+$  as an exceptionally stable  $\sigma$ -aromatic cation.

## 4. CONCLUSIONS

Gold clusters have a strong tendency to adopt structures built from 3-ring units. This is a direct result of the extra stability of the  $Au_3^+(2e)$  unit, which benefits from  $\sigma$ -electron delocalization

partially caused by scalar relativistic effects. Adding another electron to obtain the neutral  $\text{Au}_3(3e)$  leads to a Jahn–Teller unstable system, which must distort to gain stability. This is most pronounced in polycyclic structures because of the difficulty of distorting a highly symmetric structure in an effective way. Examples are the  $T_d$ -symmetrical  $\text{Au}_4$  or the  $D_{6h}$ -symmetrical  $\text{Au}_7$  that are both stationary points of cluster rearrangements. The  $D_{2h}$ -symmetrical  $\text{Au}_4$  can better distort, however, for the price of a relatively small peripheral AI value leading to a central  $\text{Au}_2$  unit attracting two apical Au atoms.

AI, NICS, and deformation parameters suggest a simple building principle for small  $\text{Au}_m$  clusters that is closely connected to the relative stabilities of  $\text{Au}_3^+(2e)$  and  $\text{Au}_3(3e)$  systems. If a 3-ring can be converted into a unit adopting some features of the  $\text{Au}_3^+$ , stability will be achieved by  $\sigma$ -aromaticity. For the small  $\text{Au}_m$  clusters investigated, a distorted 3-ring is always possible if three-dimensional clusters are avoided. In the two-dimensional structures, the use of 3-rings as building blocks leads to a steep increase in the number of bonding interactions that require electron-deficient bonding. This in turn enforces electron sharing between 3-rings and a move of negative charge from the more central 3-rings to the peripheral 3-rings so that the latter can adopt 3c-2e units of larger stability with relatively strong bonding on the outside and weak (electron-deficient) Au–Au bonds on the inside. This is correctly predicted by the vibrational properties of these molecules in the form of the local stretching force constants, their associated BSO values, and the AI that measures the degree of  $\sigma$ -electron delocalization.

The results of this work can be a basis to predict the stability of larger gold clusters, which no longer might prefer a planar structure. Besides the Clar's rule for 3-rings, one must consider stabilization via peripheral electron delocalization and the avoidance of other highly destabilized subunits such as the tetracyclic and bicyclic  $\text{Au}_4$  or the hexacyclic  $\text{Au}_6$  unit. Work is in progress to provide a general rationale for the stability of larger gold clusters.

$\pi$ -Aromaticity has been described as a multidimensional problem,<sup>13</sup> which means that by measuring different properties of an aromatic molecule different manifestations of aromaticity are obtained. The same holds for  $\sigma$ -aromaticity: (i) Energetic properties reveal the impact of aromaticity on the molecular stability. (ii) The electron density distribution and its Laplacian provide an insight into the spatial extension of aromaticity (one-, two-, or three-dimensional delocalization). (iii) Vibrational force constants reflect via BSO and AI the bond strength and the degree of electron delocalization. (iv) Magnetic properties such as the NICS values are the basis for a hypersensitive measure of magnetic anisotropy and potential orbital currents. Since the energy is a robust but very insensitive measure and the magnetic properties are too sensitive indicating even the weakest delocalization effects, the AI based on local stretching force constants seems to be the most useful measure, especially if it is combined with electron or energy density properties: In this way, a sensitive but not too sensitive measure of electron delocalization is obtained, by which one can distinguish local and global electron delocalization.

## ■ ASSOCIATED CONTENT

### 📄 Supporting Information

The Supporting Information is available free of charge on the ACS Publications website at DOI: 10.1021/acs.inorgchem.7b00404.

Electron density paths and density critical points of the  $\text{Au}_m$  clusters; Cartesian coordinates; recalibration of the AI equation using 3c-2e  $\text{Au}_2\text{Zn}^{2+}$  as reference HOMO–LUMO orbital energy gaps (in eV), NICS(0), and NICS(1) values (in ppm) for the 3c-2e  $\text{Li}_3^+$  and  $\text{H}_3^+$  systems (PDF)

## ■ AUTHOR INFORMATION

### Corresponding Authors

\*E-mail: dieter.cremer@gmail.com. (D.C.)

\*E-mail: majing@nju.edu.cn. (J.M.)

### ORCID

Dieter Cremer: 0000-0002-6213-5555

Jing Ma: 0000-0001-5848-9775

### Author Contributions

§These authors equally contributed.

### Notes

The authors declare no competing financial interest.

## ■ ACKNOWLEDGMENTS

This work was supported by the National Natural Science Foundation of China (Grant Nos. 21290192 and 21673111) and the National Science Foundation of the USA (Grant No. CHE 1464906). We are grateful to the High Performance Computing Centers of Nanjing Univ. and SMU for providing sufficient computational resources. The authors acknowledge financial support by CAPES (Brazil); Fellowship Grant BEX 9534-13-0). One of the authors (C.L.) was also supported by the Program A for Outstanding Ph.D. Candidate of Nanjing Univ.

## ■ REFERENCES

- (1) Haruta, M.; Kobayashi, T.; Sano, H.; Yamada, N. Novel gold catalysts for the oxidation of carbon monoxide at a temperature far below 0 °C. *Chem. Lett.* **1987**, *16*, 405–408.
- (2) Schwerdtfeger, P. Gold goes nano - from small clusters to low-dimensional assemblies. *Angew. Chem., Int. Ed.* **2003**, *42*, 1892–1895.
- (3) Daniel, M. C.; Astruc, D. Gold nanoparticles: assembly, supramolecular chemistry, quantum-size-related properties, and applications toward biology, catalysis, and nanotechnology. *Chem. Rev. (Washington, DC, U. S.)* **2004**, *104*, 293–346.
- (4) Pyykkö, P. Structural properties: Magic nanoclusters of gold. *Nat. Nanotechnol.* **2007**, *2*, 273–274.
- (5) Johnston, P.; Carthey, N.; Hutchings, G. J. Discovery, development, and commercialization of gold catalysts for acetylene hydrochlorination. *J. Am. Chem. Soc.* **2015**, *137*, 14548–14557.
- (6) Guo, R.; Balasubramanian, K.; Wang, X.; Andrews, L. Infrared vibronic absorption spectrum and spin–orbit calculations of the upper spin–orbit component of the  $\text{Au}_3$  ground state. *J. Chem. Phys.* **2002**, *117*, 1614–1620.
- (7) Gruene, P.; Rayner, D. M.; Redlich, B.; van der Meer, A. F. G.; Lyon, J. T.; Meijer, G.; Fielicke, A. Structures of neutral  $\text{Au}_7$ ,  $\text{Au}_{19}$ , and  $\text{Au}_{20}$  clusters in the gas phase. *Science* **2008**, *321*, 674–676.
- (8) De, H. S.; Krishnamurthy, S.; Mishra, D.; Pal, S. Finite temperature behavior of gas phase neutral ( $3 \leq n \leq 10$ ) clusters: a first principles investigation. *J. Phys. Chem. C* **2011**, *115*, 17278–17285.

- (9) Zanti, G.; Peeters, D. Electronic structure analysis of small gold clusters  $Au_m$  ( $m \leq 16$ ) by density functional theory. *Theor. Chem. Acc.* **2013**, *132*, 1300.
- (10) Sergeeva, A. P.; Boldyrev, A. I. Rational design of small 3D gold clusters. *J. Cluster Sci.* **2011**, *22*, 321–329.
- (11) Xu, W. W.; Zhu, B.; Zeng, X. C.; Gao, Y. A grand unified model for liganded gold clusters. *Nat. Commun.* **2016**, *7*, 13574.
- (12) Gilb, S.; Weis, P.; Furche, F.; Ahlrichs, R.; Kappes, M. M. Structures of small gold cluster cations ( $Au_n^+$ ,  $n < 14$ ): Ion mobility measurements versus density functional calculations. *J. Chem. Phys.* **2002**, *116*, 4094–4101.
- (13) Cremer, D. Pros and cons of  $\sigma$ -aromaticity. *Tetrahedron* **1988**, *44*, 7427–7454.
- (14) Cremer, D.; Kraka, E.; Szabo, K. J. General and theoretical aspects of the cyclopropyl group. In *The Chemistry of Functional Groups: The Chemistry of the Cyclopropyl Group*; Rappoport, Z., Ed.; John Wiley: New York, NY, 1995; Vol. 2, p 43.
- (15) Dewar, M. J.  $\sigma$ -Conjugation and  $\sigma$ -aromaticity. *Bull. Soc. Chim. Belg.* **1979**, *88*, 957–967.
- (16) Cremer, D.; Gauss, J. Theoretical determination of molecular structure and conformation. 20. reevaluation of the strain energies of cyclopropane and cyclobutane—CC and CH bond energies, 1, 3 interactions, and  $\sigma$ -aromaticity. *J. Am. Chem. Soc.* **1986**, *108*, 7467–7477.
- (17) Cremer, D.; Kraka, E. Theoretical determination of molecular structure and conformation. 15. three-membered rings: bent bonds, ring strain, and surface delocalization. *J. Am. Chem. Soc.* **1985**, *107*, 3800–3810.
- (18) Cremer, D.; Kraka, E. Theoretical determination of molecular structure and conformation. 16. substituted cyclopropanes—an electron density model of substituent—ring interactions. *J. Am. Chem. Soc.* **1985**, *107*, 3811–3819.
- (19) Wu, W.; Ma, B.; Schleyer, P. V. R.; Mo, Y.; et al. Is cyclopropane really the  $\sigma$ -aromatic paradigm? *Chem. - Eur. J.* **2009**, *15*, 9730–9736.
- (20) Havenith, R. W.; De Proft, F.; Fowler, P. W.; Geerlings, P.  $\sigma$ -Aromaticity in: insights from ring-current maps. *Chem. Phys. Lett.* **2005**, *407*, 391–396.
- (21) Ma, J.; Hozaki, A.; Inagaki, S. Pentagon stability: cyclic delocalization of lone pairs through  $\sigma$  conjugation and design of polycyclophosphanes. *Inorg. Chem.* **2002**, *41*, 1876–1882.
- (22) Freitag, K.; Gemel, C.; Jerabek, P.; Opperl, I. M.; Seidel, R. W.; Frenking, G.; Banh, H.; Dilchert, K.; Fischer, R. A. The  $\sigma$ -aromatic clusters  $[Zn_3]^+$  and  $[Zn_2Cu]$ : embryonic brass. *Angew. Chem., Int. Ed.* **2015**, *54*, 4370–4374.
- (23) Diaz-Cervantes, E.; Poater, J.; Robles, J.; Swart, M.; Solà, M. Unraveling the origin of the relative stabilities of group 14  $M_2N_2^{2+}$  ( $M = C, Si, Ge, Sn, Pb$ ) isomer clusters. *J. Phys. Chem. A* **2013**, *117*, 10462–10469.
- (24) Cheng, S. B.; Berkdemir, C.; Castleman, A. W. Observation of d–p hybridized aromaticity in lanthanum-doped boron clusters. *Phys. Chem. Chem. Phys.* **2014**, *16*, 533–539.
- (25) Zhu, C.; Zhou, X.; Xing, H.; An, K.; Zhu, J.; Xia, H.  $\sigma$ -Aromaticity in an unsaturated ring: osmapentalene derivatives containing a metallocyclopropene unit. *Angew. Chem., Int. Ed.* **2015**, *54*, 3102–3106.
- (26) Hao, Y.; Wu, J.; Zhu, J.  $\sigma$  Aromaticity dominates in the unsaturated three-membered ring of cyclopropametallapentalenes from groups 7–9: A DFT study. *Chem. - Eur. J.* **2015**, *21*, 18805–18810.
- (27) Tanaka, H.; Neukermans, S.; Janssens, E.; Silverans, R. E.; Lievens, P.  $\sigma$  Aromaticity of the bimetallic  $Au_3Zn^+$  cluster. *J. Am. Chem. Soc.* **2003**, *125*, 2862–2863.
- (28) Becke, A. D. Density-functional thermochemistry. III. The role of exact exchange. *J. Chem. Phys.* **1993**, *98*, 5648–5652.
- (29) Lee, C.; Yang, W.; Parr, R. G. Development of the Colle-Salvetti correlation-energy formula into a functional of the electron density. *Phys. Rev. B: Condens. Matter Mater. Phys.* **1988**, *37*, 785.
- (30) Hay, P. J.; Wadt, W. R. Ab initio effective core potentials for molecular calculations. Potentials for the transition metal atoms Sc to Hg. *J. Chem. Phys.* **1985**, *82*, 270–283.
- (31) Wadt, W. R.; Hay, P. J. Ab initio effective core potentials for molecular calculations. Potentials for main group elements Na to Bi. *J. Chem. Phys.* **1985**, *82*, 284–298.
- (32) Hay, P. J.; Wadt, W. R. Ab initio effective core potentials for molecular calculations. Potentials for K to Au including the outermost core orbitals. *J. Chem. Phys.* **1985**, *82*, 299–310.
- (33) Yanai, T.; Tew, D. P.; Handy, N. C. A new hybrid exchange-correlation functional using the Coulomb-attenuating method (CAM-B3LYP). *Chem. Phys. Lett.* **2004**, *393*, 51–57.
- (34) Zhao, Y.; Truhlar, D. G. The M06 suite of density functionals for main group thermochemistry, thermochemical kinetics, non-covalent interactions, excited states, and transition elements: two new functionals and systematic testing of four M06-class functionals and 12 other functionals. *Theor. Chem. Acc.* **2008**, *120*, 215–241.
- (35) Vydrov, O. A.; Scuseria, G. E. Assessment of a long-range corrected hybrid functional. *J. Chem. Phys.* **2006**, *125*, 234109.
- (36) Vydrov, O. A.; Heyd, J.; Krukau, A. V.; Scuseria, G. E. Importance of short-range versus long-range Hartree-Fock exchange for the performance of hybrid density functionals. *J. Chem. Phys.* **2006**, *125*, 074106.
- (37) Vydrov, O. A.; Scuseria, G. E.; Perdew, J. P. Tests of functionals for systems with fractional electron number. *J. Chem. Phys.* **2007**, *126*, 154109.
- (38) Chai, J. D.; Head-Gordon, M. Long-range corrected hybrid density functionals with damped atom–atom dispersion corrections. *Phys. Chem. Chem. Phys.* **2008**, *10*, 6615–6620.
- (39) Raghavachari, K.; Trucks, G. W.; Pople, J. A.; Head-Gordon, M. A fifth-order perturbation comparison of electron correlation theories. *Chem. Phys. Lett.* **1989**, *157*, 479–483.
- (40) Perdew, J. P.; Burke, K.; Ernzerhof, M. Generalized gradient approximation made simple. *Phys. Rev. Lett.* **1996**, *77*, 3865–3868.
- (41) Grimme, S.; Antony, J.; Ehrlich, S.; Krieg, H. A consistent and accurate ab initio parametrization of density functional dispersion correction (DFT-D) for the 94 elements H–Pu. *J. Chem. Phys.* **2010**, *132*, 154104.
- (42) Grimme, S.; Ehrlich, S.; Goerigk, L. Effect of the damping function in dispersion corrected density functional theory. *J. Comput. Chem.* **2011**, *32*, 1456–1465.
- (43) Peterson, K.; Puzzarini, C. Systematically convergent basis sets for transition metals. II. Pseudopotential-based correlation consistent basis sets for the group 11 (Cu, Ag, Au) and 12 (Zn, Cd, Hg) elements. *Theor. Chem. Acc.* **2005**, *114*, 283–296.
- (44) Balabanov, N. B.; Peterson, K. A. Systematically convergent basis sets for transition metals. I. All-electron correlation consistent basis sets for the 3d elements Sc–Zn. *J. Chem. Phys.* **2005**, *123*, 064107.
- (45) London, F. Théorie quantique des courants interatomiques dans les combinaisons aromatiques. *J. Phys. Radium* **1937**, *8*, 397–409.
- (46) McWeeny, R. Perturbation theory for the Fock-Dirac density matrix. *Phys. Rev.* **1962**, *126*, 1028.
- (47) Ditchfield, R. Self-consistent perturbation theory of diamagnetism: I. A gauge-invariant LCAO method for NMR chemical shifts. *Mol. Phys.* **1974**, *27*, 789–807.
- (48) Wolinski, K.; Hinton, J. F.; Pulay, P. Efficient implementation of the gauge-independent atomic orbital method for NMR chemical shift calculations. *J. Am. Chem. Soc.* **1990**, *112*, 8251–8260.
- (49) Cheeseman, J. R.; Trucks, G. W.; Keith, T. A.; Frisch, M. J. A comparison of models for calculating nuclear magnetic resonance shielding tensors. *J. Chem. Phys.* **1996**, *104*, 5497–5509.
- (50) Chen, Z.; Wannere, C. S.; Corminboeuf, C.; Puchta, R.; Schleyer, P. v. R. Nucleus-independent chemical shifts (NICS) as an aromaticity criterion. *Chem. Rev. (Washington, DC, U. S.)* **2005**, *105*, 3842–3888.
- (51) Santos, J.; Tiznado, W.; Contreras, R.; Fuentealba, P. Sigma-pi separation of the electron localization function and aromaticity. *J. Chem. Phys.* **2004**, *120*, 1670–1673.

- (52) Konkoli, Z.; Cremer, D. A new way of analyzing vibrational spectra. I. Derivation of adiabatic internal modes. *Int. J. Quantum Chem.* **1998**, *67*, 1–9.
- (53) Zou, W.; Kalescky, R.; Kraka, E.; Cremer, D. Relating normal vibrational modes to local vibrational modes with the help of an adiabatic connection scheme. *J. Chem. Phys.* **2012**, *137*, 084114.
- (54) Zou, W.; Cremer, D. Properties of local vibrational modes: the infrared intensity. *Theor. Chem. Acc.* **2014**, *133*, 1–15.
- (55) Zou, W.; Cremer, D. C2 in a box: determining its intrinsic bond strength for the  $X1\Sigma_g^+$  ground state. *Chem. - Eur. J.* **2016**, *22*, 4087–4099.
- (56) Kraka, E.; Larsson, J. A.; Cremer, D. Generalization of the Badger rule based on the use of adiabatic vibrational modes. *Vibrational Modes in Computational IR Spectroscopy*; Wiley: New York, 2010, 105–149.
- (57) Zou, W.; Filatov, M.; Cremer, D. An improved algorithm for the normalized elimination of the small-component method. *Theor. Chem. Acc.* **2011**, *130*, 633–644.
- (58) Cremer, D.; Zou, W.; Filatov, M. Dirac-exact relativistic methods: the normalized elimination of the small component method. *WIREs Comput. Mol. Sci.* **2014**, *4*, 436–467.
- (59) Mayer, I. Bond orders and valences from ab initio wave functions. *Int. J. Quantum Chem.* **1986**, *29*, 477–483.
- (60) Mayer, I. Bond order and valence indices: A personal account. *J. Comput. Chem.* **2007**, *28*, 204–221.
- (61) Weinhold, F.; Landis, C. R. *Valency and Bonding, A Natural Bond Orbital Donor–Acceptor Perspective*; Cambridge University Press: New York, 2005.
- (62) Bader, R. F. W. *Atoms in Molecules: A Quantum Theory*; Oxford University Press: Oxford, England, 1994.
- (63) Kalescky, R.; Kraka, E.; Cremer, D. Description of aromaticity with the help of vibrational spectroscopy: anthracene and phenanthrene. *J. Phys. Chem. A* **2014**, *118*, 223–237.
- (64) Setiawan, D.; Kraka, E.; Cremer, D. Quantitative assessment of aromaticity and antiaromaticity utilizing vibrational spectroscopy. *J. Org. Chem.* **2016**, *81*, 9669–9686.
- (65) Cremer, D. New ways of analyzing chemical bonding. *Modell. Struct. Prop. Mol.* **1987**, 128–144.
- (66) Zou, W.; Izotov, D.; Cremer, D. New way of describing static and dynamic deformations of the Jahn-Teller type in ring molecules. *J. Phys. Chem. A* **2011**, *115*, 8731–8742.
- (67) Frisch, M. J.; Trucks, G. W.; Schlegel, H. B.; Scuseria, G. E.; Robb, M. A.; Cheeseman, J. R.; Scalmani, G.; Barone, V.; Mennucci, B.; Petersson, G. A.; Nakatsuji, H.; Caricato, M.; Li, X.; Hratchian, H. P.; Izmaylov, A. F.; Bloino, J.; Zheng, G.; Sonnenberg, J. L.; Hada, M.; Ehara, M.; Toyota, K.; Fukuda, R.; Hasegawa, J.; Ishida, M.; Nakajima, T.; Honda, Y.; Kitao, O.; Nakai, H.; Vreven, T.; Montgomery, J. A., Jr.; Peralta, J. E.; Ogliaro, F.; Bearpark, M.; Heyd, J. J.; Brothers, E.; Kudin, K. N.; Staroverov, V. N.; Kobayashi, R.; Normand, J.; Raghavachari, K.; Rendell, A.; Burant, J. C.; Iyengar, S. S.; Tomasi, J.; Cossi, M.; Rega, N.; Millam, J. M.; Klene, M.; Knox, J. E.; Cross, J. B.; Bakken, V.; Adamo, C.; Jaramillo, J.; Gomperts, R.; Stratmann, R. E.; Yazyev, O.; Austin, A. J.; Cammi, R.; Pomelli, C.; Ochterski, J. W.; Martin, R. L.; Morokuma, K.; Zakrzewski, V. G.; Voth, G. A.; Salvador, P.; Dannenberg, J. J.; Dapprich, S.; Daniels, A. D.; Farkas, Ö.; Foresman, J. B.; Ortiz, J. V.; Cioslowski, J.; Fox, D. J. *Gaussian09, Revision D.01*; Gaussian Inc.: Wallingford, CT, 2013.
- (68) Werner, H.-J.; Knowles, P. J.; Knizia, G.; Manby, F. R.; Schütz, M. Molpro: a general-purpose quantum chemistry program package. *WIREs Comput. Mol. Sci.* **2012**, *2*, 242–253.
- (69) Kraka, E.; Zou, W.; Filatov, M.; Gräfenstein, J.; Gauss, J.; He, Y.; Wu, A.; Konkoli, Z.; He, Z.; Cremer, D. *COLOGNE16*; Southern Methodist University: Dallas, TX, 2016.
- (70) Lu, T.; Chen, F. Multiwfn: a multifunctional wavefunction analyzer. *J. Comput. Chem.* **2012**, *33*, 580–592.
- (71) Kalescky, R.; Kraka, E.; Cremer, D. Identification of the strongest bonds in chemistry. *J. Phys. Chem. A* **2013**, *117*, 8981–8995.
- (72) Bersuker, I. B. *The Jahn-Teller Effect*; Cambridge University Press: Cambridge, England, 2006.
- (73) Clar, E.; Schoental, R. *Polycyclic Hydrocarbons*; Academic Press: London, England, 1964; Vols. 1 & 2.
- (74) Wu, J.; Zhu, J. The Clar structure in inorganic BN analogues of polybenzenoid hydrocarbons: Does it exist or not? *ChemPhysChem* **2015**, *16*, 3806–3813.